PACIFIC EARTHQUAKE ENGINEERING RESEARCH CENTER

Seismic Evaluation and Analysis of 230-kV Disconnect Switches

Amir S. J. Gilani
Andrew S. Whittaker
Gregory L. Fenves
Chun-Hao Chen
University of California, Berkeley

Henry Ho
Eric Fujisaki
Pacific Gas & Electric Company

PEER 2000/06
JULY 2000

Seismic Evaluation and Analysis of 230-kV Disconnect Switches

Amir S. J. Gilani
Andrew S. Whittaker
Gregory L. Fenves
Chun-Hao Chen
University of California, Berkeley

Henry Ho
Eric Fujisaki
Pacific Gas & Electric Company

PEER Report 2000/06
Pacific Earthquake Engineering Research Center
College of Engineering
University of California, Berkeley

July 2000

ABSTRACT

Five 230-kV disconnect switches were selected for testing and evaluation. Switches of this rating were known to be vulnerable to the effects of earthquake shaking. The class of the switches selected included two horizontal-break and three vertical-break switches. Switches with both porcelain and composite polymer insulators, and switches with both cast aluminum and welded steel base hardware were tested. First, an individual pole (out of three) of each switch was mounted directly on the simulator platform. Static and resonance search tests were conducted to determine the dynamic properties of the posts and to assist in preparing simple analytical models of the posts. Earthquake tests were then conducted to see if the poles were robust. Following these tests, three-pole (phase) switches were mounted on a stiff, low-profile frame, similar to a frame proposed by PG&E for new construction, and tested. Static and resonance search tests were conducted to determine the dynamic properties of the switch posts.

Triaxial earthquake tests were used to qualify the switches on the frame. Two sets of part spectrum-compatible ground motion records were derived from the near-field motions recorded during the 1978 Tabas, Iran, earthquake for the earthquake-simulator studies. Neither of the horizontal-break switches was qualified to the High Level on the stiff frame. The vertical-break switches were qualified to the High Level on a stiff frame provided that welded steel spacers were used at the base of the insulators. The most vulnerable components in the switches were the cast aluminum spacers at the base of the switch posts, the welded post-blade connection, and the bolted connections at the base of the posts.

Single-degree-of-freedom models of the switch insulator posts were developed using experimental data. These models predicted reasonably well the displacement response of the switches mounted on the test frame. These models were then used to evaluate the likely amplification of response of switches when mounted on frames of different heights and stiffnesses. Four frames were selected for study: two in-service (one tall and one short), and two proposed for new construction (one tall and one short). The short braced frame proposed for new construction was stiff and did not amplify the response of the switches significantly. For the other three frames, amplification factors of greater than 2 were recorded. The tall braced frame proposed for new construction produced the largest amplification factors, and consideration should be given to stiffening this frame.

ACKNOWLEDGMENTS

The work described in this report was undertaken by the Pacific Earthquake Engineering Research Center (PEER) with funding from the Pacific Gas and Electric (PG&E) Company. This financial support is gratefully acknowledged. The 230-kV disconnect switches used in the testing program were supplied by the ABB Power T&D Company, Inc., Components Division (ABB) of Bland, Virginia.

The authors wish to thank the following individuals for their significant technical contributions to this project: Messrs. Ed Matsuda and Eric Fujisaki, and Dr. Norman Abrahamson of PG&E, and Messrs. Ken Harless and Durand Stacy of ABB. Thanks are also due to Mr. Don Clyde (PEER) who made significant contributions to the experimental program and Ms. Janine Hannel (PEER) who edited this report.

This work was supported in part by the Pacific Earthquake Engineering Research Center through the Earthquake Engineering Research Centers Program of the National Science Foundation under Award Number EEC-9701568.

CONTENTS

LIST OF TABLES

LIST OF FIGURES

1 Introduction

1.1 Overview

Disconnect switches are a key component of power transmission and distribution (T&D) systems. They are used to control the flow of electricity between all types of substation equipment and are used to isolate all types of substation equipment for maintenance. Figure 1-1 shows an elevated three-phase (pole) vertical-break disconnect switch. At one end, the switch is connected to a transformer bushing by stiff aluminum tubes. Heavy standard cables connect the other end of the switch to the high-voltage lines. The aluminum tubes and cables can be seen in the figure.

Disconnect switches consist of three poles (or phases), each consisting of two or three posts (insulators). For the switches tested as part of this study, the posts were mounted on base hardware attached to double-channel framing. The switch blade mounted at top of the posts provides control over the electrical connection between the posts. A crank and inter-pole linkages operate the blade and synchronize the operation of the three poles. The blade opens either in-plane of the switch (vertical-break) or out-of-plane of the switch (horizontal-break). The insulators are fabricated from either porcelain or composite polymers. Cast aluminum is used for most of the base and operation-mechanism hardware.

Disconnect switches are typically mounted on support structures. For most applications, the switch is installed upright in the vertical position. The frames are classified by the utilities as either low-profile (typical height of 12 ft or 4 m) or high-profile (typical height of 60 ft or 18 m). Mounting frames in service at the time of this writing are typically not braced and rely on the channel at the base of the disconnect switches to provide stiffness in the short direction of the frame. New low-profile frames will be fully braced.

Recent major earthquakes in the United States (e.g., Northridge, California, 1994) and other parts of the world (e.g., Taiwan 1999) have demonstrated that the reliability of a power transmission and distribution system in a seismically active region is dependent upon the seismic response of its individual components. Porcelain disconnect switches have suffered two types of failures in past earthquakes: structural damage (e.g., fracture of brittle components) and loss of functionality (e.g., switch blades not operating correctly). Since disconnect switches form an integral part of power T&D systems, their structural and electrical integrity are critical to maintaining power.

To mitigate the vulnerability of new disconnect switches and other electrical substation equipment in the United States, the Institute for Electrical and Electronics Engineers, (IEEE) developed guidelines for seismic testing and qualification of disconnect switches. These guidelines are described in *IEEE Recommended Practices for Seismic Design of Substations*, IEEE 693-1997. The key IEEE 693-1997 requirements for seismic qualification tests are paraphrased in Appendix A.

1.2 Literature Survey

The literature contains no information on the seismic performance of disconnect switches except for a report by Wyle Laboratories (Thornberry and Hardy 1997) on the qualification of a switch. The scope of the Wyle work was limited to switch testing and qualification. No fragility data were collected and no conclusions were drawn regarding the seismic performance of the switch.

For the Wyle tests, the elevated switch was attached to the biaxial simulator using bolted connections. The specimen was tested initially along its longitudinal and vertical axes. It was then rotated 90 degrees and tested along its lateral and vertical axes. Resonant-search, sine-beat, and bidirectional seismic simulation tests were conducted to characterize the switch. Random motions and not earthquake histories were used for the earthquake-simulation tests. The switch had a fundamental frequency of between 5 and 6 Hz and a damping ratio of between 2 and 4 percent of critical.

1.3 Objectives of the Current Study

The lack of information on disconnect switches motivated the research project described in this report. The work outlined in this report is summarized in the flowchart presented in Figure 1-2. The five objectives of the research project were to:

1. Develop earthquake ground motion records suitable for the seismic evaluation, qualification, and fragility testing of 230-kV disconnect switches.

2. Conduct resonant-search and triaxial earthquake tests of single poles of porcelain and composite disconnect switches mounted directly on the simulator platform to determine the dynamic properties of the poles and to evaluate the seismic response of the poles.

3. Conduct resonant-search and triaxial earthquake tests of porcelain and composite disconnect switches mounted on an elevated frame to determine the dynamic properties of the switches, to qualify the switches to the High Level if possible, and to determine the modes of failure for the switches.

4. Analyze the data acquired from the earthquake-simulator tests to develop single degree-of-freedom mathematical models for switch poles.

5. Estimate the response of switches mounted on elevated support frames of different flexibility, using the switch models of item 4, for the purpose of improving qualification procedures for disconnect switches.

1.4 Report Organization

This report comprises eight chapters, a reference list, and two appendices. Chapter 2 provides information on the mounting frame and disconnect switches tested on the U.C. Berkeley simulator. Chapter 3 discusses the earthquake motions developed for the earthquake tests. Chapter 4 describes the test setup and the results from the earthquake testing of components of disconnect switches mounted on the simulator platform. Chapter 5 reports the test setup and the results from the earthquake testing of disconnect switches mounted on an elevated frame. Chapter 6 presents the analytical modeling for the switches. Chapter 7 examines the analytical response of switches mounted on elevated support structures. Chapter 8 includes a summary of the key findings and conclusions drawn from the research project. References are listed following Chapter 7. The IEEE 693-1997 recommended practice for earthquake testing of disconnect switches is summarized in Appendix A. Appendix B describes the procedure for preparing mathematical models of switch posts. Raw data and video images from all earthquake tests were supplied to Pacific Gas & Electric under separate cover.

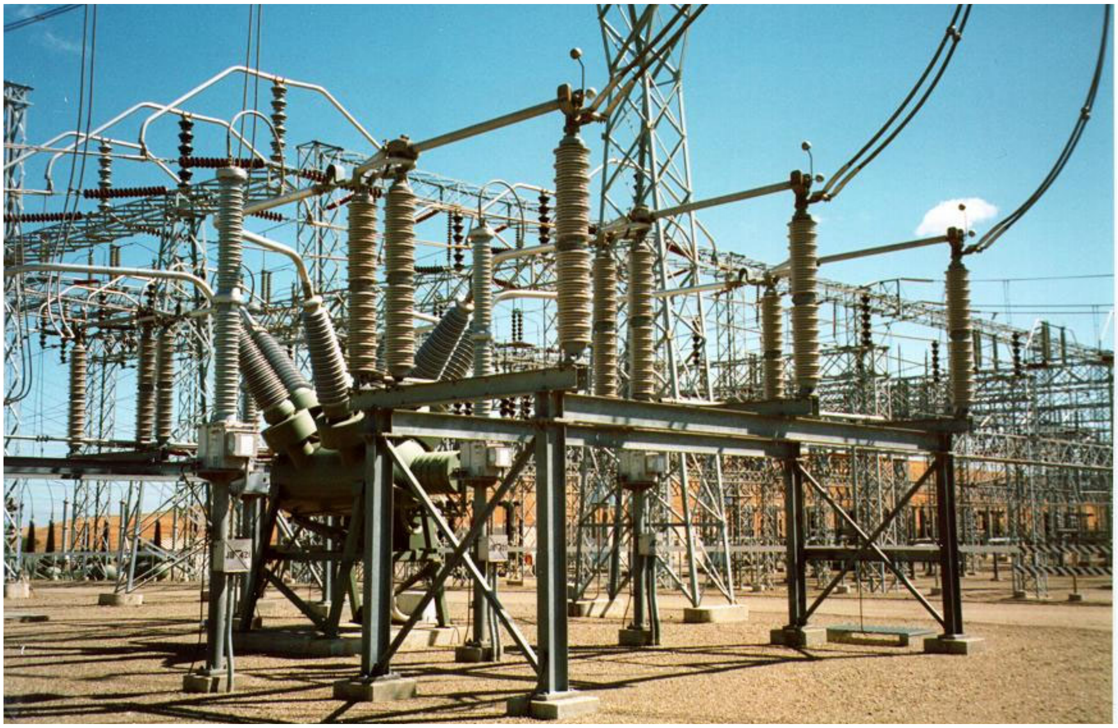

Figure 1-1 Three-phase vertical-break disconnect switch mounted on a low-rise frame

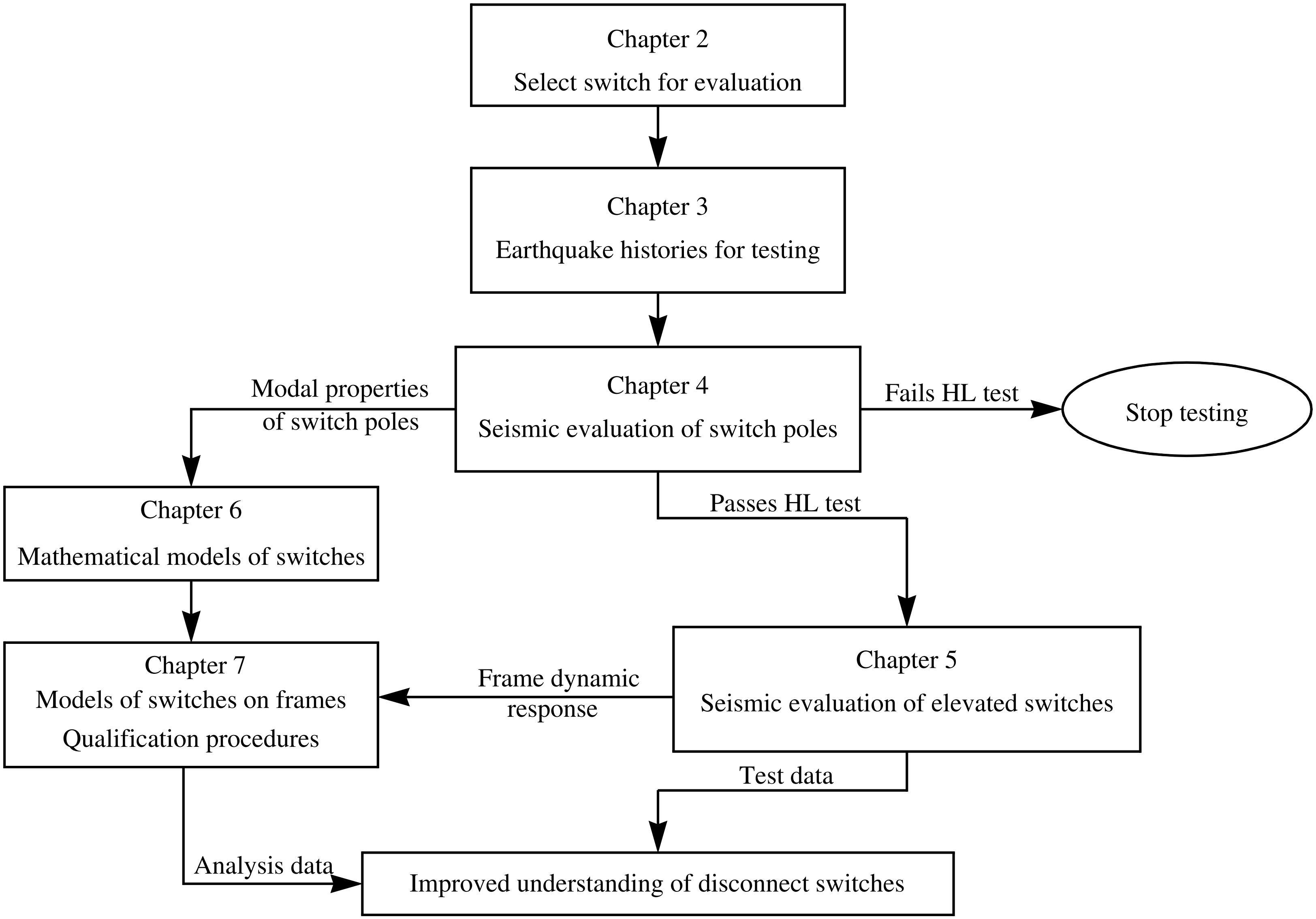

Figure 1-2 Flowchart for the seismic evaluation of disconnect switches

2 Earthquake Simulator Testing

2.1 Introduction

Triaxial earthquake simulator testing was used to evaluate the seismic behavior of the 230-kV disconnect switches. The earthquake testing protocol for disconnect switches set forth in IEEE 693-1997 (IEEE 1998) was adopted for this study. Section 2.2 describes the earthquake simulator used for testing. Section 2.3 describes the test protocol and Section 2.4 outlines the test configuration including the mounting frame. Section 2.5 describes the disconnect switches tested.

2.2 Earthquake Simulator

The earthquake simulator at the Pacific Earthquake Engineering Research (PEER) Center at the University of California at Berkeley was used for the seismic evaluation and qualification studies described in this report. The simulator, also known as a shaking table, measures 20 ft by 20 ft (6.1 by 6.1 m) in plan. The maximum payload is 140 kips (623 kN). Models up to 40 ft (12.2 m) in height can be tested. The six-degree-of-freedom simulator can be programmed to reproduce any waveform (e.g., sinusoidal, white noise, earthquake history). The maximum stroke and velocity of the simulator are 5 in. (127 mm) and 25 in./sec (635 mm/sec), respectively.

2.3 Experimental Program

IEEE 693-1997 specifies that disconnect switches must be qualified while mounted on a support frame similar to in-service supports. To evaluate the seismic performance of a proposed frame and qualify the 230-kV disconnect switches, a two-step experimental program was developed.

First, the seismic response of a single pole from each of three disconnect switches (SW1, SW2, and SW3) was evaluated by testing the poles when mounted directly on the simulator platform. The objective was to seismically evaluate the individual poles in the absence of support flexibility.

Second, the complete (three-pole) switches (SW1, SW2, SW2a, and SW3) and an individual pole of a fifth switch (SW4) were mounted and tested on an elevated frame that is similar to a frame proposed by PG&E for new construction.

2.4 Support Frames for Switch Components

2.4.1 Introduction

Disconnect switches are typically mounted atop unbraced steel frames in the field. The lateral stiffness of these frames can vary widely. The base of each pole of a typical switch is generally supported on a double-channel steel beam. The toes of the channels are turned toward each other to form a tubular-type member. The flanges of the double-channels are connected by intermittent steel lacing. The double-channels are routinely supplied by the switch manufacturer and are considered part of the switch assembly. The double-channel base is bolted to the steel frame in the field using W, TS, and angle sections.

2.4.2 Support frame for the tests of single poles

To simulate the field mounting of the poles, the double-channel beams were bolted at each end to short lengths of W8x31 beams for tests of single poles mounted directly on the simulator platform. The connection of the double-channel to the W8x31 beams was identical to the field connection, and utilized four 1/2 in. (13 mm) diameter galvanized steel bolts. The W8x31 beams were welded to 2 in. (51 mm) thick steel base plates measuring 24 by 48 in. (0.6 by 1.2 m) in plan, which were post-tensioned to the simulator platform using 1 in. (25 mm) diameter high-strength rods. To provide lateral stiffness, 0.75 in. (19 mm) thick stiffeners were welded to the W8x31 beams. Figure 2-1 shows the mounting configuration. The coordinate system used for the studies described in this chapter and Chapter 4 is shown in the figure.

2.4.3 Elevated support frame for tests of switches

Disconnect switches are mounted on the top of elevated supports in the field. The frames are classified either as short (typical height of 8 to 12 ft or 2.0 to 3.7 m) or tall (typical height of 60 ft or 18.3 m). Older mounting frames are not braced and rely on the double-channels at the base of the disconnect switches to provide stiffness in the transverse direction. The frames proposed for use by Pacific Gas and Electric (PG&E) for new construction are fully braced.

One objective of the studies reported herein was to evaluate the performance of disconnect switches mounted on a low-rise braced frame. This frame, hereafter referred to as the PG&E frame, will be used by PG&E for future installations of 230-kV disconnect switches. Figure 2-2 is a line drawing showing the member sizes and dimensions. The double-channel members for the switches are bolted to the top of the W8x31 beams.

The PG&E frame was designed to be stiff to reduce the amplification of ground motion that is characteristic of the older unbraced frames. SAP2000 (CSI 1996) was used to estimate the dynamic properties of the PG&E frame. Table 2-1 reports the computed analytical modal properties of the frame alone, and the frame including the mass of a 230-kV three-phase disconnect switch. In these models, the frame was assumed to be 12 ft (3.7 m) tall; see Figure 2-2a.

Table 2-1 Modal properties of the PG&E frame by analysis

		Frequency (Hz)	
Mode	*Predominant direction*	*Frame only*	*Frame and switch*
1	longitudinal	45	43
2	transverse	24	24
3	vertical	54	52

The footprint of the PG&E frame is 26.7 ft by 8.7 ft (8.2 m by 2.7 m). In the longitudinal direction, the frame dimension exceeds the simulator-platform plan dimension of 20 ft (6.1 m). To test switches on this frame, the investigators would have had to have constructed an outrigger frame on which to mount the frame. A number of potential designs were developed for the outrigger frame. The design objective was to not substantially change the frequencies of the PG&E frame, but this objective was difficult to achieve. Only extremely heavy and stiff braced outriggers could limit the change in the outrigger-mounted PG&E frame frequency to within 20 percent of the frequency of the PG&E frame. For outriggers composed of more reasonable member sizes, the longitudinal frequency of the outrigger-mounted frame was nearly halved.

Because of the difficulty and expense of constructing an outrigger, an alternative frame, hereafter referred to as the PEER frame was designed to replicate the dynamic properties of the PG&E frame and fit on the simulator platform. Figure 2-3 presents the member sizes and dimensions of the PEER frame. The footprint of the frame was 18 ft by 8.7 ft (5.5 m by 2.7 m) and the frame was 12 ft (3.6 m) tall. The transverse braces in the PEER frame were reduced from L4x3x1/4” to L3x3x1/4” to duplicate the fundamental frequencies of the PG&E frame.

SAP2000 (CSI 1996) was used to compute the dynamic properties of the PEER frame. Table 2-2 reports the modal properties of the frame alone, and the frame including the mass of a 230-kV three-phase disconnect switch.

Table 2-2 Modal properties of the PEER frame by analysis

		Frequency (Hz)	
Mode	*Predominant direction*	*Frame only*	*Frame and switch*
1	longitudinal	44	42
2	transverse	26	25
3	vertical	98	90

Since the PEER frame and the PG&E frames were designed to have nearly identical dynamic properties, switches qualified on the PEER frame would have been qualified on the PG&E frame. Figure 2-4 shows the PEER frame on the Berkeley earthquake-simulator platform.

Prior to installing the switches on the PEER frame, pull-back, quick-release tests where conducted to determine the modal frequencies of the frame. The measured frequencies of the

PEER frame were nearly identical to the frequencies computed by analysis and are summarized in Table 2-3.

Table 2-3 Modal properties of the PEER frame alone by experimentation

Mode	*Predominant direction*	*Frequency, Hz*
1	longitudinal	44
2	transverse	24
3	torsional	50

2.5 Disconnect Switches

2.5.1 Introduction

Five disconnect switches (three poles) and components thereof (single pole) were evaluated by analysis and experimentation. The key properties of the switches are tabulated in Table 2-4.

Table 2-4 Disconnect switches

Switch[1]	*Break*	*No. of posts per pole*	*No of stacks per post*	*Insulator*[2]	*Base hardware*[3]
SW1	horizontal	2	2	porcelain	a
SW2	vertical	3	2	porcelain	a
SW2a	vertical	3	2	porcelain	b
SW3	vertical	3	1	composite	a, b
SW4	horizontal	2	2	porcelain	a

1. For SW1, SW2, SW2a, and SW3, all three poles were tested on the PEER frame. For SW4, only an individual pole was tested on the PEER frame.
2. Insulator manufacturers: Locke for SW1, SW2, and SW2a; Sediver for SW3; and Lapp for SW4.
3. a = cast aluminum, b = welded steel.

The designations used for the switch posts and poles in this report are shown in Figure 2-5. Pole A of switches SW1, SW2, and SW3 were tested while mounted directly on the simulator platform (see Chapter 4). Three-pole switches, SW1, SW2, SW2a, and SW3, and a single pole of switch SW4 were mounted on the PEER frame for testing (see Chapter 5). For all switches, the operating mechanism was attached to pole B. The switches were adjusted mechanically prior to testing to ensure synchronization of operation between the three poles. The following subsections briefly describe the switches.

2.5.2 *Horizontal-break switches (SW1 and SW4)*

Switches SW1 and SW4 were Type DR9 porcelain horizontal-break 230-kV switches. One pole of the horizontal-break switch is shown in Figure 2-6. The poles were approximately 90.5 in. (2.3 m) long and spaced 94 in. (2.4 m) apart. The operation of the switch was controlled by a crank handle at the base of post 2. Figure 2-7 shows details of blades and the operating crank attached to post 2.

Each post consisted of two porcelain insulators. Figure 2-8 shows the high-strength porcelain insulators used for SW1. The insulators were each 40 in. (1.0 m) long and together weighed 280 lbs (1.3 kN). Figure 2-9 shows the high-strength porcelain insulators used for SW4. The insulators were each 40 in. (1.0 m) long and together weighed 380 lbs (1.7 kN). Three-quarter (19 mm) bolts were used to attach the blades to the upper insulator and the upper insulator to the lower insulator.

The insulator posts were mounted on welded steel spacers (see Figure 2-10), which in turn were bolted to cast aluminum rotor bearings (see Figure 2-11). The bearings were attached to a C8x11.5 double-channel beam that was connected to the W8x31 beams by 5x5x1/4” angles using 3/4 in. (19 mm) bolts. Figure 2-12 shows details for double-channel beams.

2.5.3 *Vertical-break switches (SW2, SW2a, and SW3)*

Switches SW2, SW2a, and SW3 were Type TTR-8 vertical-break 230-kV switches. One pole of these switches is shown in Figure 2-13. The poles were approximately 95.5 in. (2.4 m) long. A counterweight was attached at the tip of posts 2 and 3 to which the blade arm was attached. The operation of the switch was controlled through a crank handle at the base of post 2. Figure 2-14 shows the operating mechanism attached to the top of posts 2 and 3.

Each post of porcelain switches SW2 and SW2a consisted of two porcelain insulators (see Figure 2-8). The posts for switch SW3 were single composite polymer insulators (see Figure 2-15), 80 in. (2.0 m) long and weighed approximately 110 lbs (0.5 kN).

The insulators for posts 1 and 3 were mounted on spacers. For switch SW2, cast aluminum spacers (see Figure 2-16) were used; for switch SW2a, welded steel spacers (see Figure 2-17) were used. Both aluminum and steel spacers were used for switch SW3. Post 2 of all three switches was attached to the cast aluminum rotor bearings (see Figure 2-11). The posts were bolted to C8x11.5 double-channel beams.

2.5.4 *Operating mechanism*

Both the vertical-break and horizontal-break switches were operated (opened and closed) manually. The operating mechanism shown in Figure 2-18 consisted of a crank attached to the mounting frame. Galvanized steel pipes and clamps linked the crank to the control unit at the base of post 2 of pole B. Galvanized steel pipes were used to connect the rotor bearing attachments of pole B to those of poles A and C. The bolts in the rotor bearing of each pole (see Figure 2-11) were mechanically adjusted to obtain the full operation range for individual poles, and the aluminum pipes were sized to synchronize the operation of the three poles.

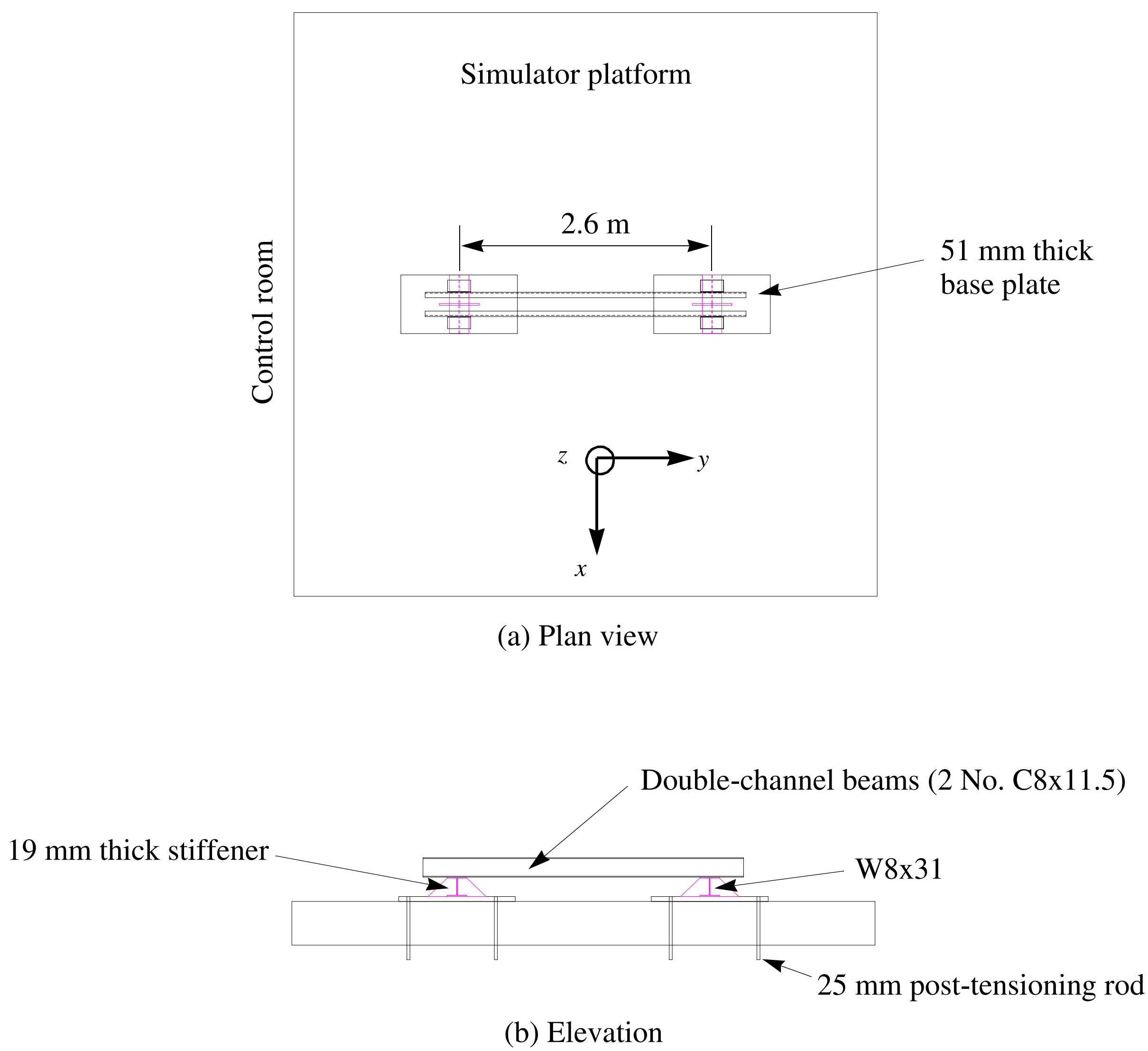

Figure 2-1 Support for poles mounted on the simulator platform

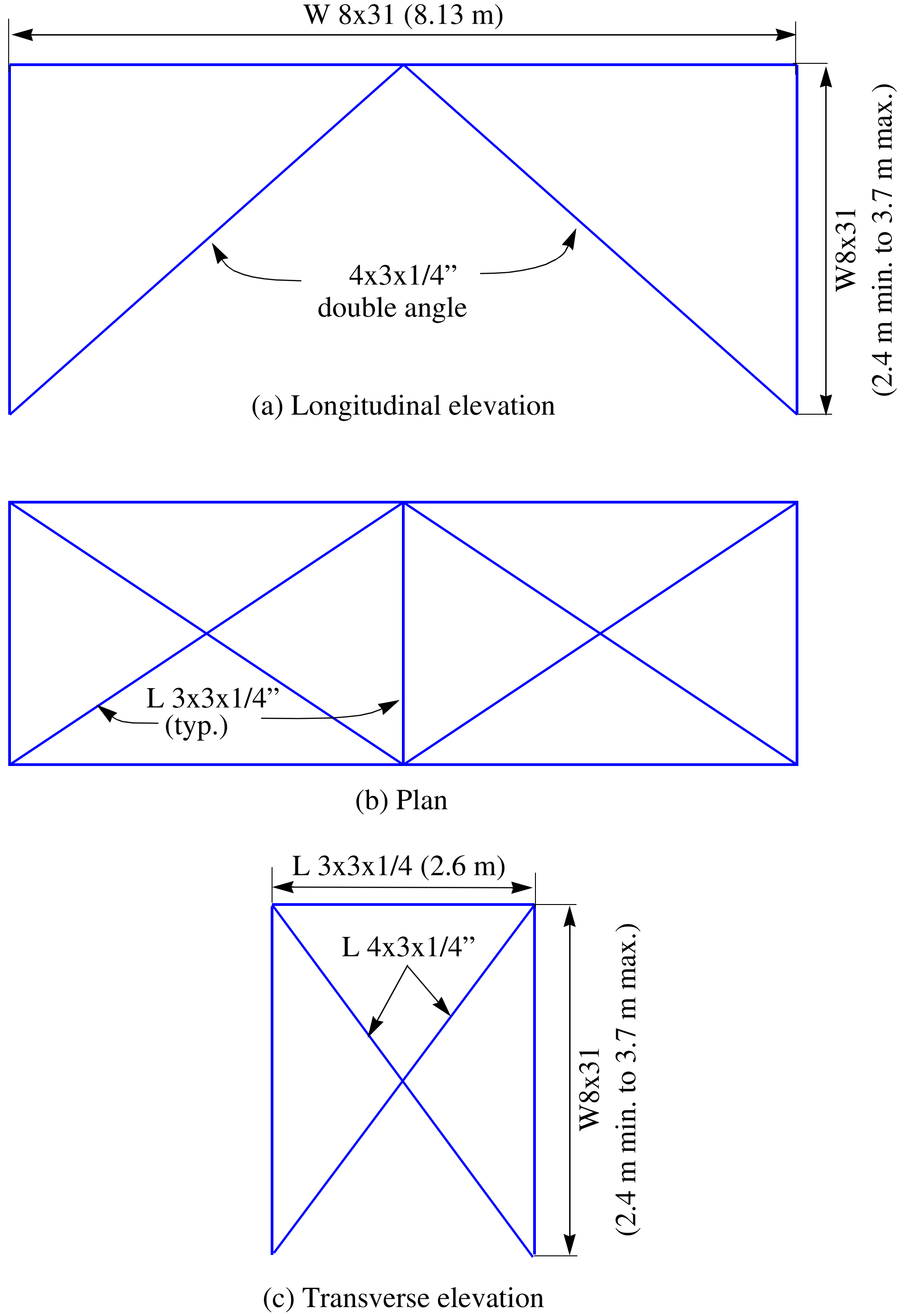

Figure 2-2 Line drawing of the PG&E frame

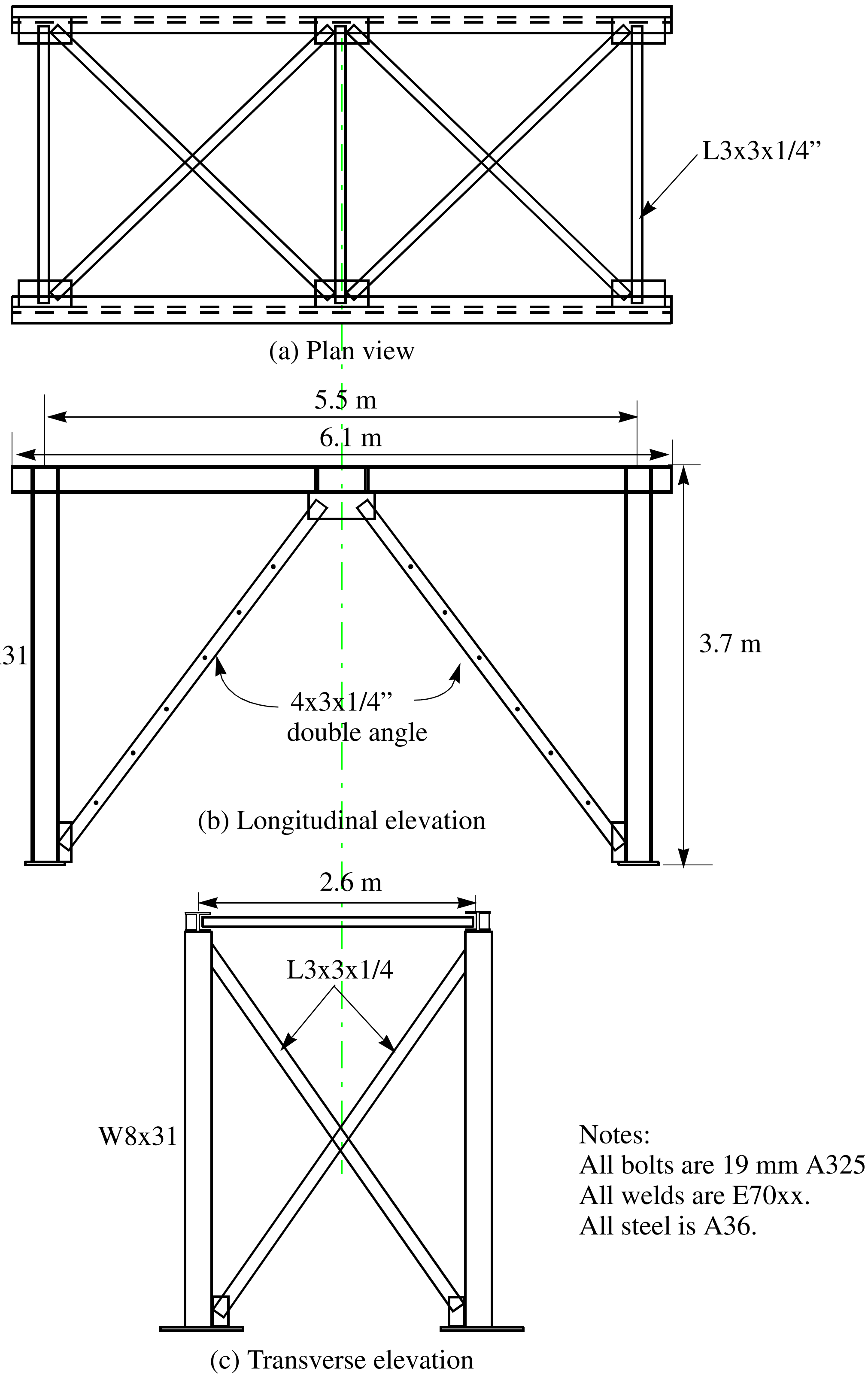

Figure 2-3 Line drawing of the PEER frame

Figure 2-4 PEER frame

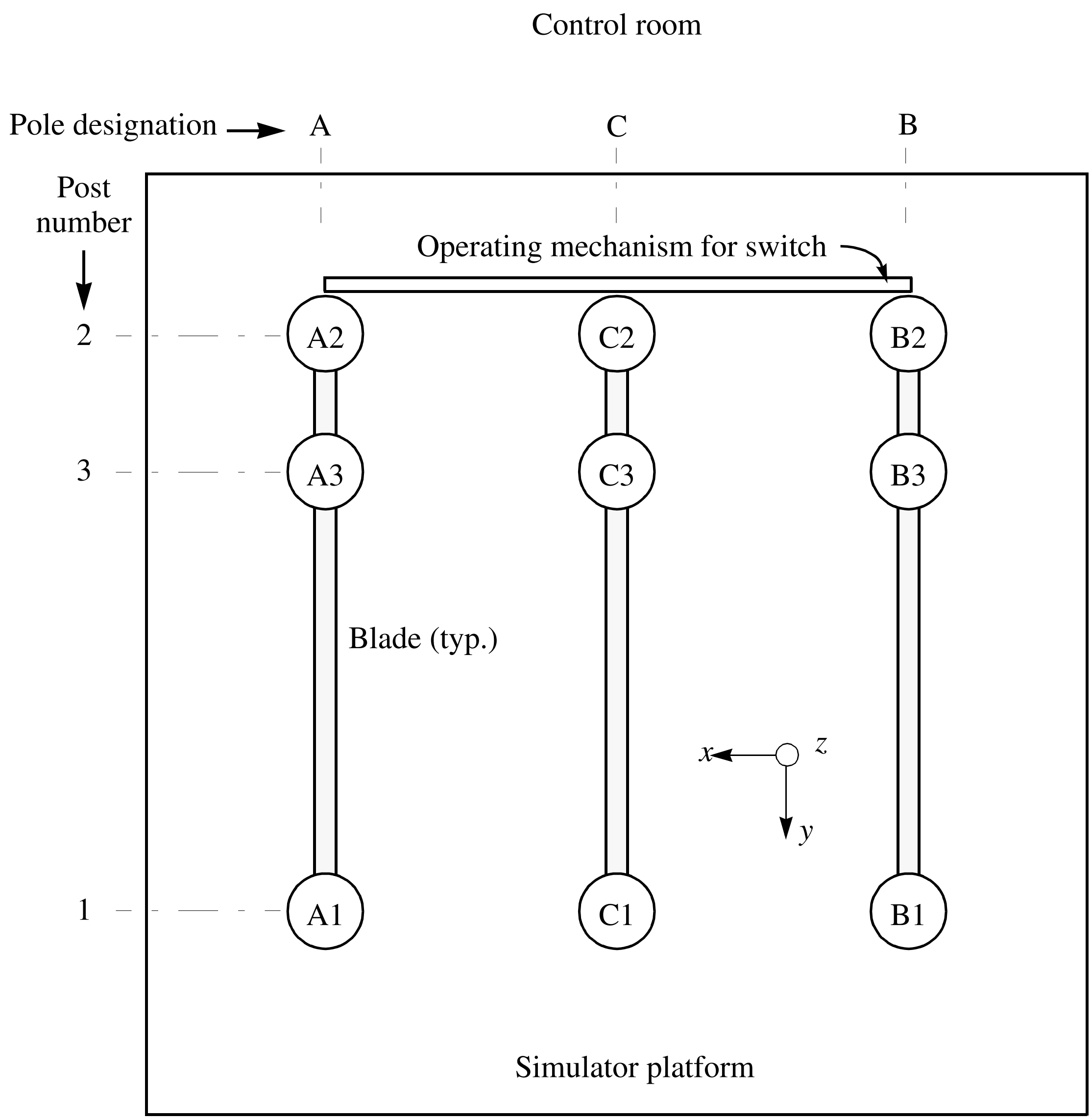

Figure 2-5 Layout of 230-kV disconnect switches on the Berkeley earthquake simulator platform

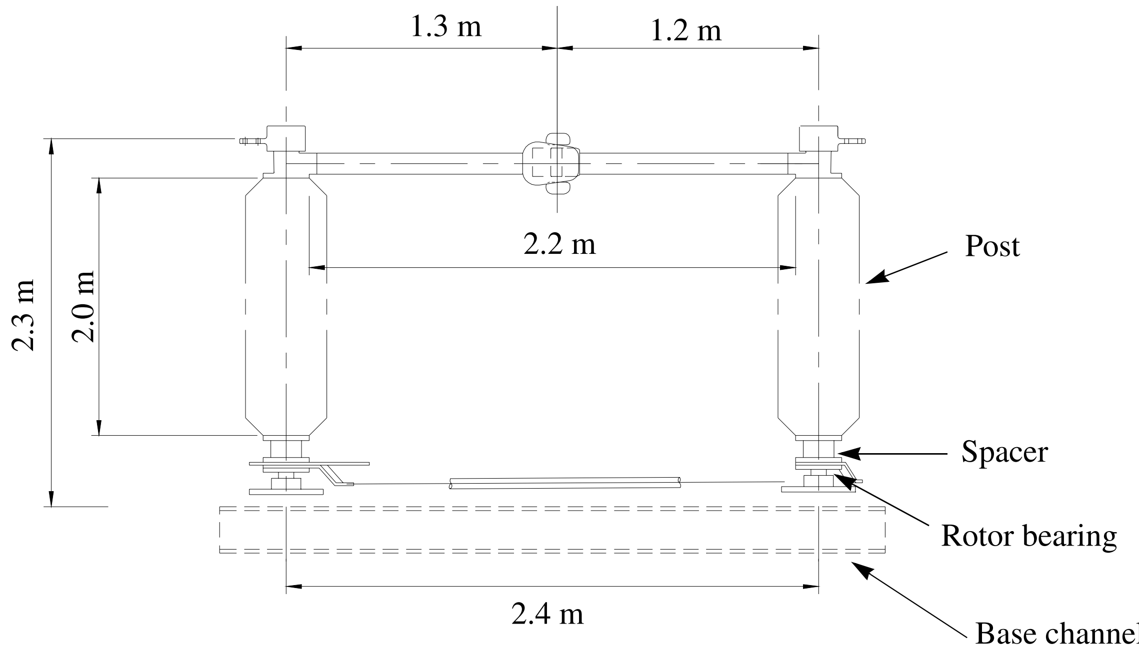

Figure 2-6 Horizontal-break switches (courtesy of ABB)

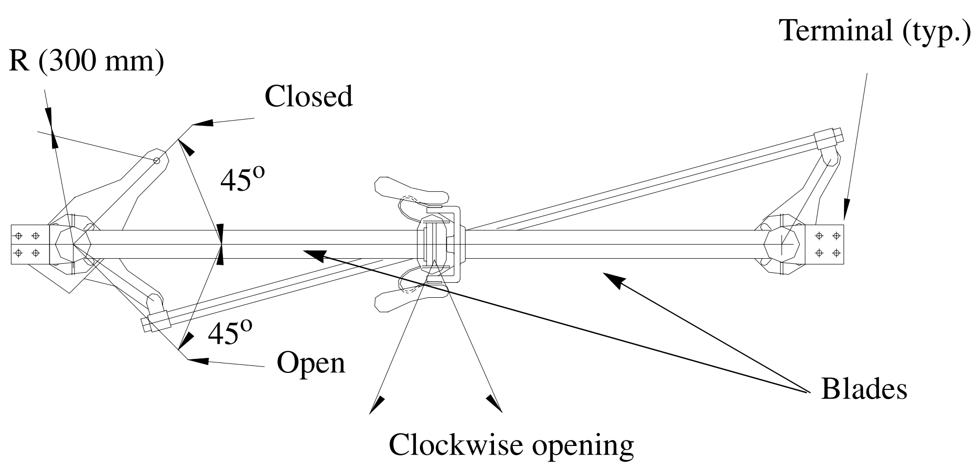

Figure 2-7 Operating mechanism for horizontal-break switches (courtesy of ABB)

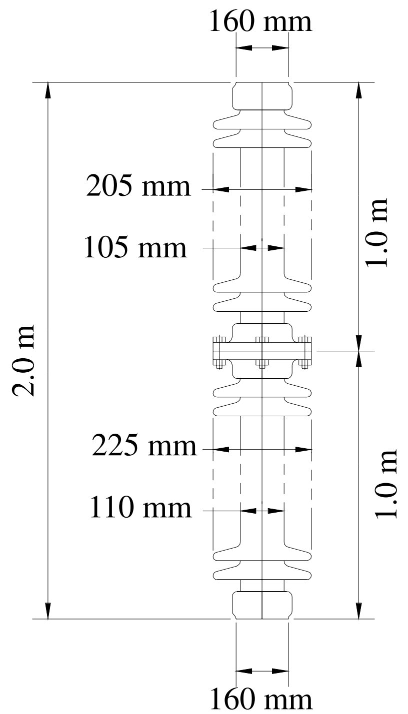

Figure 2-8 Porcelain insulators for switch SW1 (courtesy of Locke Insulators Inc.)

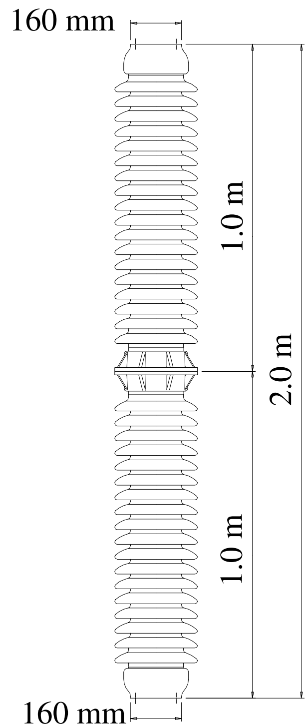

Figure 2-9 Porcelain insulators for switch SW4 (courtesy of Lapp Insulator Company)

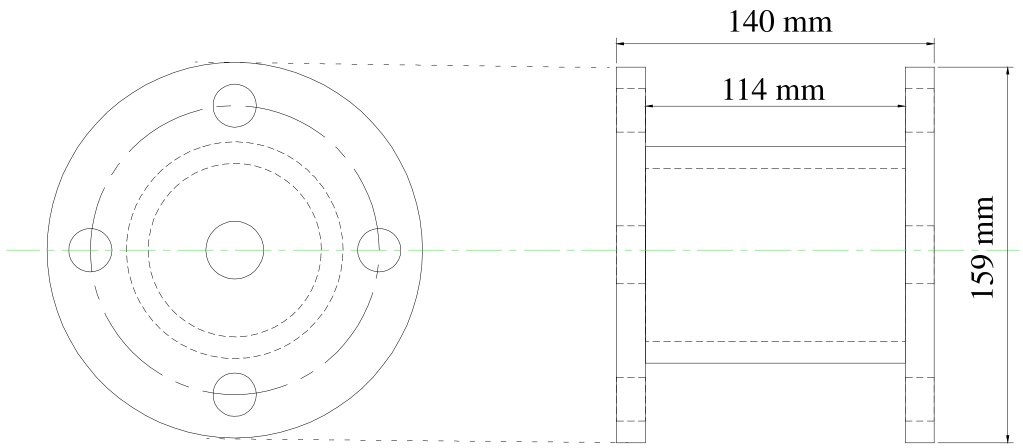

Figure 2-10 Spacer for horizontal-break switches (courtesy of ABB)

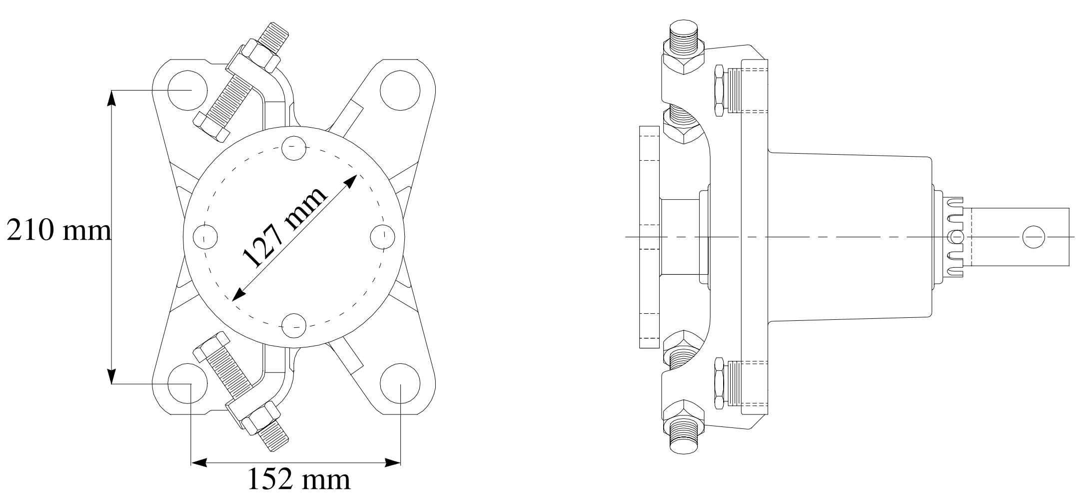

Figure 2-11 Cast aluminum rotor bearing housing for all switches (courtesy of ABB)

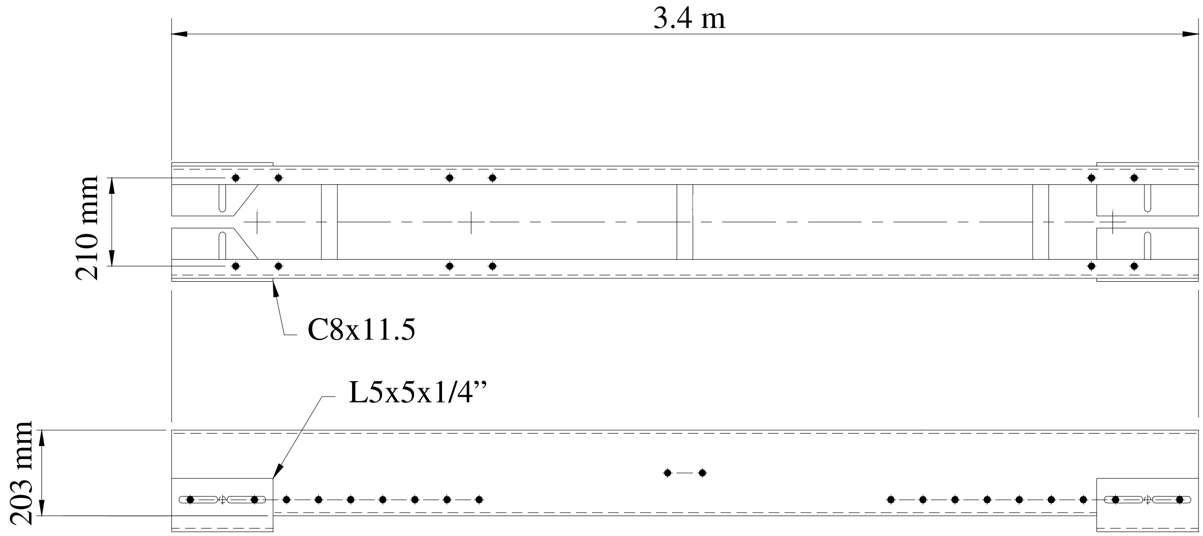

Figure 2-12 Double-channel connection (courtesy of ABB)

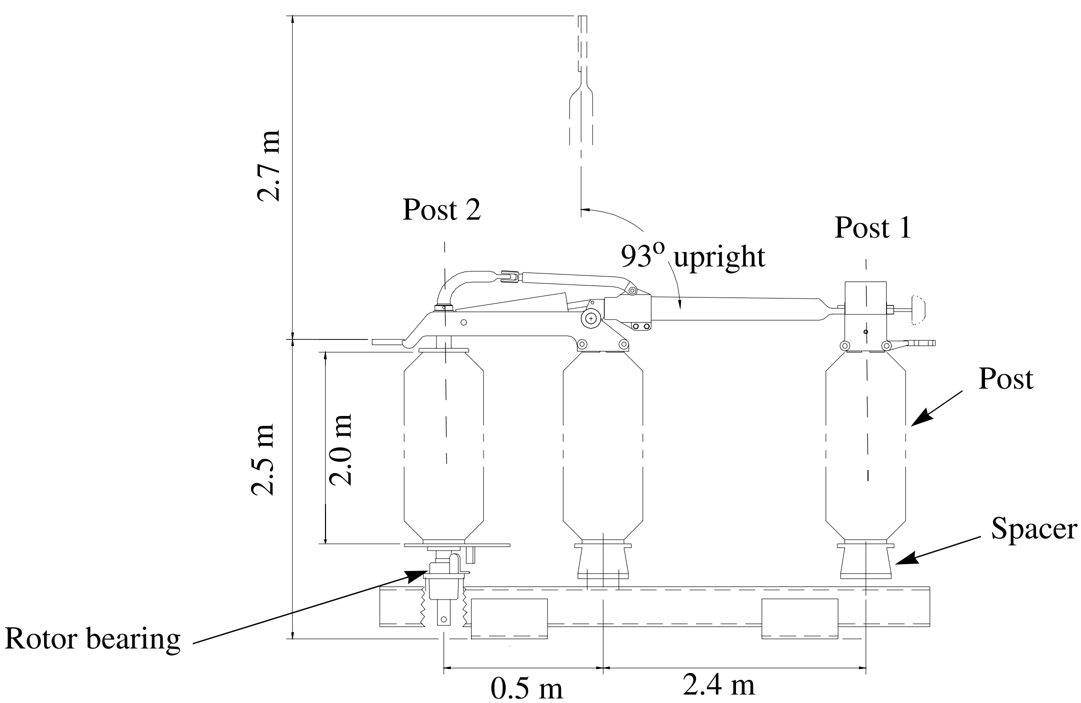

Figure 2-13 Vertical-break switches (courtesy of ABB)

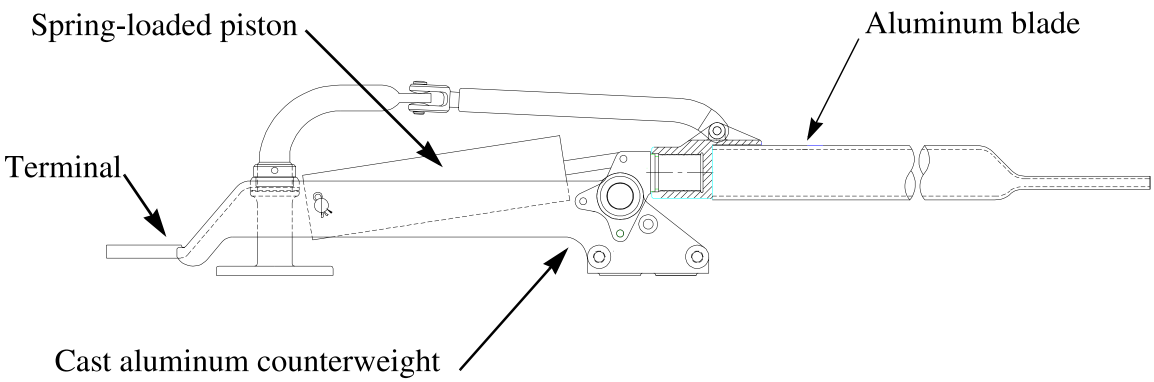

Figure 2-14 Operating mechanism for vertical-break switches (courtesy of ABB)

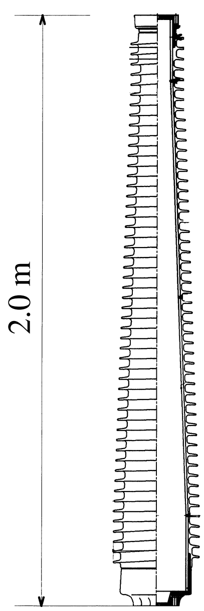

Figure 2-15 Composite polymer insulators for switch SW3 (courtesy of Sediver Insulators)

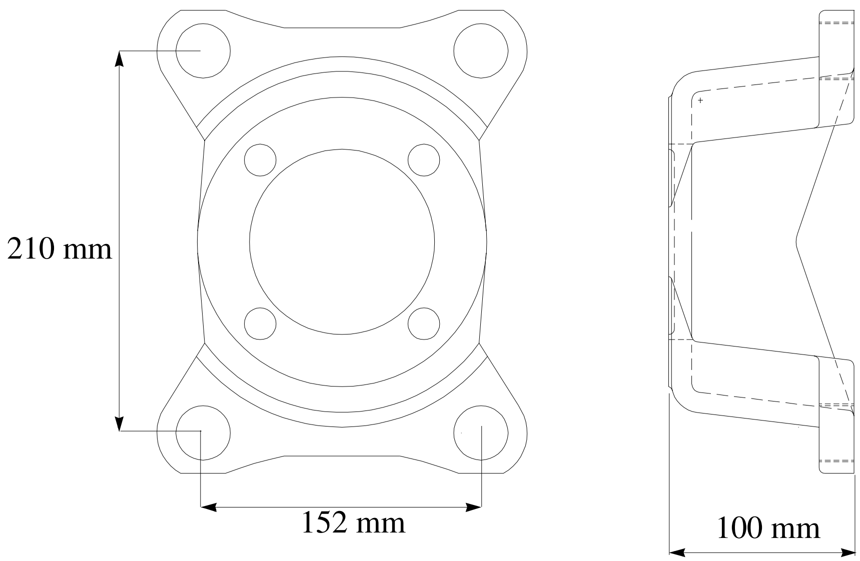

Figure 2-16 Cast aluminum spacer for posts 1 and 3 of vertical-break switches (courtesy of ABB)

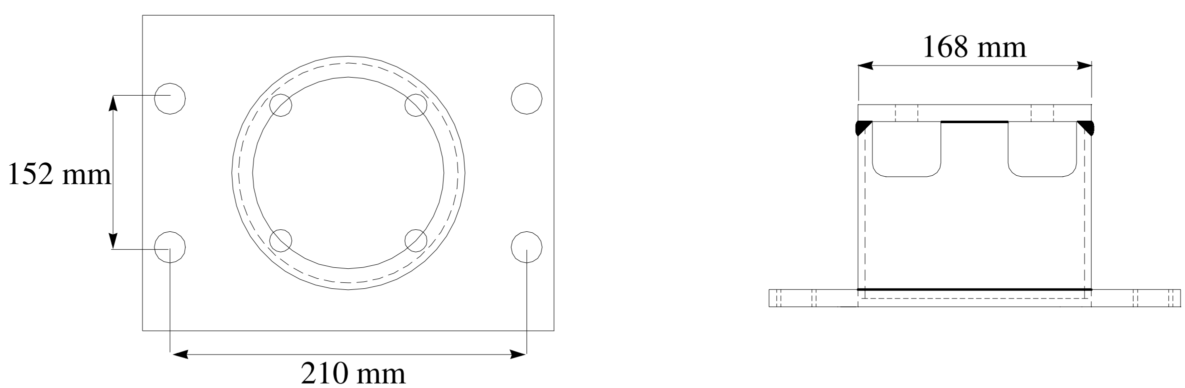

Figure 2-17 Welded steel spacer for posts 1 and 3 of vertical-break switches (courtesy of ABB)

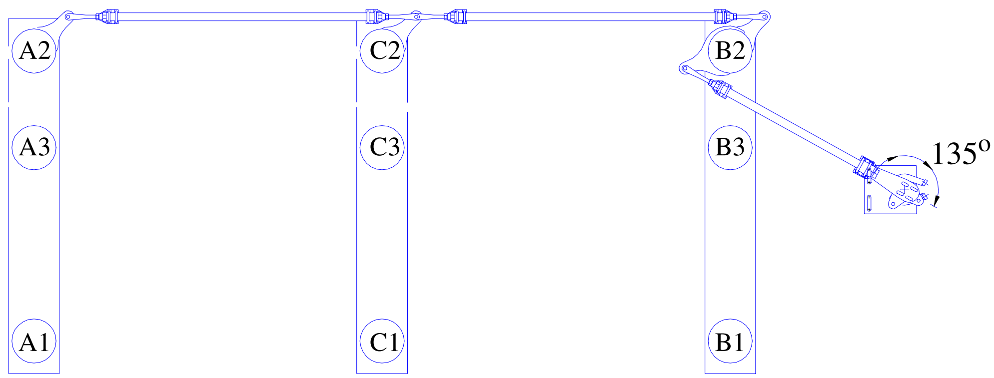

(a) Plan

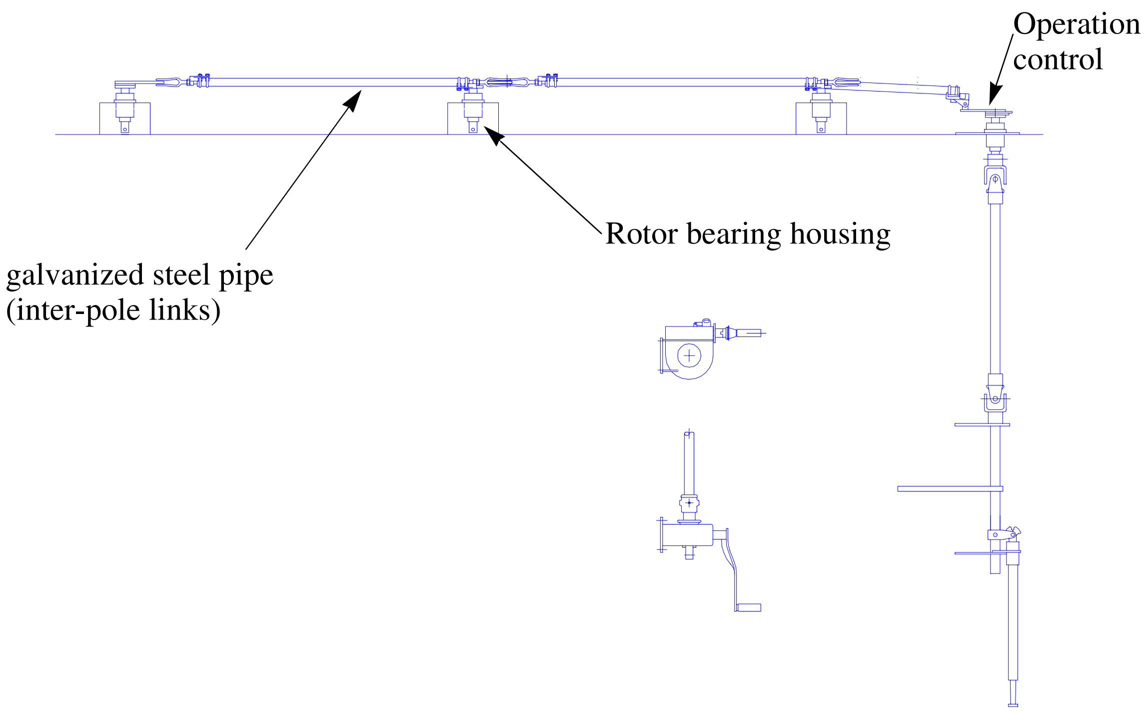

(b) Elevation

Figure 2-18 Operating mechanism for 230-kV disconnect switches (courtesy of ABB)

3 Earthquake Histories and Qualification

3.1 Introduction

Recorded earthquake ground motion histories were used to evaluate the seismic response of five 230-kV disconnect switches: SW1, SW2, SW2a, SW3, and SW4. The following section describes the requirements of IEEE 693-1997 (IEEE 1998) for the qualification of disconnect switches and the procedures used to develop earthquake histories for testing.

3.2 IEEE 693-1997 Requirements for Qualification of Disconnect Switches

Three types of earthquake-simulator testing are identified in IEEE 693-1997 for the seismic qualification of switches: frequency resonant-search, sine-beat, and earthquake ground motion tests. Resonant frequency tests and earthquake ground motion tests (termed *time-history shake table tests* in IEEE 693-1997) are mandatory. Additional information on these two tests follow.

3.2.1 Resonant search tests

Unidirectional sine-sweep or broadband white-noise tests are used to establish dynamic characteristics (natural frequencies and damping ratios) of disconnect switches. IEEE 693-1997 specifies that the input level for the resonant-search tests be between 0.05 and 0.1g. If only sine-sweep tests are used, IEEE 693-1997 specifies that the resonant search be conducted at a rate not exceeding one octave per minute in the range for which the equipment has resonant frequencies. Frequency searching below 1 Hz or above 33 Hz is not required. Because both sine-sweep and white-noise tests were used in this testing program to identify the modal properties of the switches, the recommendations of IEEE 693-1997 were not followed exactly.

The history for the banded white-noise tests was prepared using a random signal generator. The sine-sweep history was developed using a rate of two octaves per minute. (At two octaves per minute, the input frequency doubles every 30 sec.) A continuous frequency function was used to develop the sine-sweep function

$$x(t) = x_0 \sin\left(2\pi\left[\frac{30}{\log 2}\right]2^{t/30}\right) \tag{3-1}$$

where x is the displacement, and x_0 is the maximum displacement. For both sine-sweep and white-noise tests, a simulator input acceleration amplitude of 0.1g was used.

3.2.2 Earthquake test response spectrum

For earthquake simulator testing, IEEE 693-1997 states that the response spectrum for each horizontal earthquake input motion must envelope (match or exceed) the target spectrum and that the response spectrum for vertical earthquake input motion be no less than 80 percent of target spectrum. IEEE 693-1997 recommends that 2-percent damping be used for spectral matching and requires at least 20 sec of strong motion shaking be present in each earthquake record. Earthquake motions can be established using either synthetic or recorded histories. Recorded motions formed the basis of the earthquake histories used to test the 230-kV switches.

IEEE 693-1997 identifies several response spectra of identical shape but different amplitudes for the qualification of disconnect switches. These spectra are described below. A more detailed description is presented in Appendix A.

Performance Level (PL). IEEE 693-1997 represents a PL for substation equipment by a response spectrum. The PL represents the expected level of performance when a piece of equipment is qualified to the Required Response Spectrum (RRS) and allowable stresses are not exceeded. The two PLs relevant to California are *Moderate* and *High*. The target PL set by Pacific Gas and Electric (PG&E) for the disconnect switches described in this report was the High Level. Figure 3-1 shows the High Seismic Performance Level spectrum.

Required Response Spectrum (RRS). It is often neither practical nor cost effective to test components to the PL. As such, IEEE 693-1997 permits equipment to be tested using a reduced level of shaking called the RRS. The shapes of the RRS and the PL are identical, but the ordinates of the PL (referred to as performance factor in IEEE 693-1997) are twice that of the RRS. Equipment tested or analyzed using the RRS is expected to have acceptable performance at the PL. This assumption is checked by measuring the stresses obtained from testing at the RRS, and (a) comparing the stresses to 50 percent (equal to the inverse of the performance factor) of the ultimate strength of the brittle (e.g., porcelain and cast aluminum) components; (b) using a factor of safety against yield combined with an allowance for ductility for steel, ductile aluminum, and other ductile materials; and (c) checking composite components for damage and large residual deflections (deviating by more than 5 percent from pre-deflected position).

Test Response Spectrum (TRS). IEEE 693-1997 specifies a test acceleration spectrum with ordinates identical to that of the RRS for testing disconnect switches mounted on frames that replicate in-service structures. The target peak horizontal acceleration for this TRS is 0.5g for High Level qualification For this level of shaking, IEEE 693-1997 writes that the stresses in the brittle (porcelain and cast aluminum) components must be less than 50 percent of the ultimate stress.

It is often impractical to instrument brittle components to ensure that the measured stresses comply with this requirement. An alternate approach that is identified in IEEE 693-1997 was used for the studies reported herein. Namely, earthquake histories with spectral ordinates twice those of the RRS were used for testing and the target peak horizontal acceleration for High Level qualification was 1.0g. For qualification to the High Level using this method, the stresses in porcelain and other brittle components are required to be less than or equal to the ultimate value and there is to be no damage to the other components of the switch. Figure 3-2 shows the target spectra of the horizontal acceleration histories used for High Level qualification testing of disconnect switches.

3.2.3 Earthquake ground motions

The earthquake histories used for the qualification and fragility testing of the 230-kV disconnect were developed using the three-component set of near-field earthquake motions recorded during the 1978 Tabas earthquake. Figures 3-3 through 3-5 present the acceleration history, power spectrum, and pseudo-acceleration response spectra for the three components of the Tabas record. The amplitude of each history (*X-*, *Y-*, and *Z-*) was normalized to a peak acceleration of 1.0g. The power spectrum for each history has moderate bandwidth. The 2-percent and 5-percent damped IEEE spectra for High Level qualification, anchored to a peak ground acceleration (PGA) of 1.0g, are also shown in the figures. The response-spectrum ordinates for each normalized earthquake history typically exceed the target IEEE values for frequencies between 4 to 10 Hz and drop below the target values for other frequencies.

To obtain IEEE 693-1997 spectrum-compatible normalized histories, the original Tabas acceleration records were modified using a non stationary response-spectrum matching technique developed by Abrahamson (Abrahamson 1996). In Abrahamson's time-domain algorithm, short-duration wavelets are added to the original earthquake history at optimal times in the history to match the spectral amplitude at each frequency to the target value. The modified history generally resembles the original earthquake history in time and spectral context.

Testing of 196-kV ABB bushings (Gilani, et al., 1998) at Berkeley conducted prior to the work described in this report utilized spectrum-compatible earthquake histories developed using the Abrahamson technique. The spectrum-compatible motions were high-pass filtered (removal of low-frequency content) to reduce the peak displacements and velocities of the simulator platform below 5 in. (127 mm) and 25 in./sec (635 mm/sec), respectively. Although the resulting spectra matched the target spectra across a broad frequency range (0.1 Hz to 100 Hz), the power spectra of the filtered histories were narrow banded and not particularly representative of strong earthquake ground motion. As such, PG&E and the Berkeley research team studied alternative procedures to improve the quality of the earthquake histories.

IEEE 693-1997 presents a broadband response spectrum that envelopes the effects of earthquakes in different areas considering site conditions ranging from rock to soft soil. One feature of this response spectrum is an extended plateau of constant spectral acceleration between 1 and 8 Hz. Recorded ground motions typically have a moderate to broadband power spectrum and small constant spectral acceleration plateau. Figure 3-6 shows 5-percent damped spectra for hard rock (S_B) (dash-dot line) and soft soil sites (S_E) (dashed line) that are presented in the Uniform Building Code [UBC] (ICBO 1997) for seismic zone 4. For these spectra, the near-source coefficients are set equal to unity. Also shown in the figure is the 5-percent damped IEEE spectrum anchored to the same zero-period acceleration as the UBC rock spectrum. The IEEE spectrum approximately envelopes acceleration spectra for S_B through S_E sites: sites with shear wave velocities ranging from 5000 ft/sec (1500 m/sec) to less than 600 ft/sec (180 m/sec). Ground motion histories with a spectrum compatible with that of IEEE likely will not be representative of recorded earthquake histories.

To examine the relationship between the smoothed response spectrum and the corresponding power spectrum, the technique developed by Keshishian (Der Kiureghian et al. 1998) was used to generate a power spectrum. Figure 3-7 is the normalized power spectrum generated using the IEEE 693-1997 2-percent damped High Level spectrum of Figure 3-2. There is significant energy between 1 and 2 Hz but the ordinates of power spectrum decline rapidly for frequencies greater than 2 Hz. As such, the power spectrum is relatively narrow banded. Accordingly, acceleration records that match the entire IEEE 693-1997 spectrum will likely be somewhat narrow banded.

To obtain spectrum-compatible histories with frequency contents more representative of recorded ground motions (i.e., moderate to broadband power spectrum), only a segment of IEEE spectrum was matched with individual histories. This approach was used to develop input histories for testing of the 230-kV disconnect switches. Two independent sets of three earthquake histories (Tabas-1 and Tabas-2) were generated to envelope collectively the entire IEEE spectrum. The part spectrum-compatible Tabas-1 set of histories was developed using the Abrahamson method and matched the IEEE spectrum above 3.5 Hz. As such, Tabas-1 could be used to qualify equipment at stiff soil or rock sites. The Tabas-2 set of histories matched the IEEE spectrum below 3.5 Hz and could be used to qualify equipment at soft soil sites. The 5-percent damped response spectra for the longitudinal components of these records are shown in Figure 3-8.

For purpose of qualifying and characterizing the disconnect switches, an *envelope* acceleration spectrum was developed using the Tabas-1 and Tabas-2 histories. This procedure is outlined here and illustrated in Figure 3-9 for the longitudinal components of the Tabas histories. The dash-dot and dashed lines in the figure represent the 2-percent damped acceleration response spectra calculated from the recorded Tabas-1 and Tabas-2 histories, respectively. The *envelope* spectrum is shown with a solid line. At each frequency, the ordinate of the *envelope* spectrum is the larger of the ordinates of the Tabas-1 and Tabas-2 spectral ordinates.

The part spectrum-compatible motions were high-pass filtered to limit the maximum displacement and velocity of the simulator platform to 5 in. (127 mm) and 25 in./sec (635 mm/sec), respectively. The cut-off frequencies (0.3 Hz for motions with peak accelerations less than or equal to 1.0g, and 0.5 Hz for other motions) of the filters were much less than the resonant frequencies of the 230-kV disconnect switches that were known to vary between 3 and 8 Hz. Removal of such low-frequency components from the input signals to the simulator would have negligible impact on the dynamic response of the switches. Figures 3-10 through 3-12 present the acceleration history, power spectrum, and response spectra for the three part spectrum-compatible Tabas-1 records. Figures 3-13 through 3-15 present the same information for Tabas-2 records. The power spectra for the three components of the filtered Tabas-1 and Tabas-2 records are broadbanded and collectively have significant input energy up to 10 Hz.

3.3 Seismic Qualification of Disconnect Switches

In the field, disconnect switches are typically mounted on frames. These frames vary in height, geometry, and flexibility. IEEE 693-1997 specifies that the disconnect switches must be qualified on frames similar to those used for field installation. Since it is impractical to qualify the switches on all possible mounting frames, the research team proposed to test the switches on two frames, one stiff and one flexible whose dynamic properties enveloped those of frames in service in California.

For the tests described in this report, the switches were mounted on a stiff mounting frame (termed the PEER frame in Section 2.4) that is similar to a low-profile braced frame proposed for new construction by PG&E. The switches were tested on the frame with open and closed blades using the Tabas-1 and Tabas-2 histories. The qualification procedure for each disconnect switch included four separate tests as listed in Table 3-1. A switch was qualified to the High Level, if (a) it passed the IEEE general and functional (electrical and operational) requirements following all four tests, and (b) the spectrum provided by the envelope of the Tabas-1 and Tabas-2 spectra exceeded the IEEE 693-1997 spectrum.

Instead of testing the switches on a flexible frame with the earthquake histories of Figures 3-10 through 3-15, an alternative approach was used. When equipment is installed on supports that are different than those used for qualification, IEEE 693-1997 writes that the supports should be *dynamically equivalent*. IEEE 693-1997 presents three definitions for *dynamic equivalency* of supports of which one is "...conservatively estimate the acceleration that the equipment would experience on the support structure during the required earthquake shaking and then qualify the equipment to the estimated or more severe motion..." At time of this study, such an estimate was not available and an alternate IEEE procedure for qualification of transformer bushings was used instead. For the seismic qualification of bushings on rigid frames, IEEE increases the ordinates of the Performance Level by a factor of 2 to account for the flexibility of the transformer tank. This strategy was adopted for the qualification of the switches, namely, test the switches on a stiff or rigid frame and double the ordinates of the target spectrum to account for frame flexibility.

Table 3-1 Qualification tests for disconnect switches

Test	*Blade*	*Input motion*[1, 2]
1	Closed	Tabas-1
2	Closed	Tabas-2
3	Open	Tabas-1
4	Open	Tabas-2

1. PGA equal to 1.0g for High Level qualification on stiff frame;
2. PGA equal to at 2.0g for High Level qualification on flexible frame.

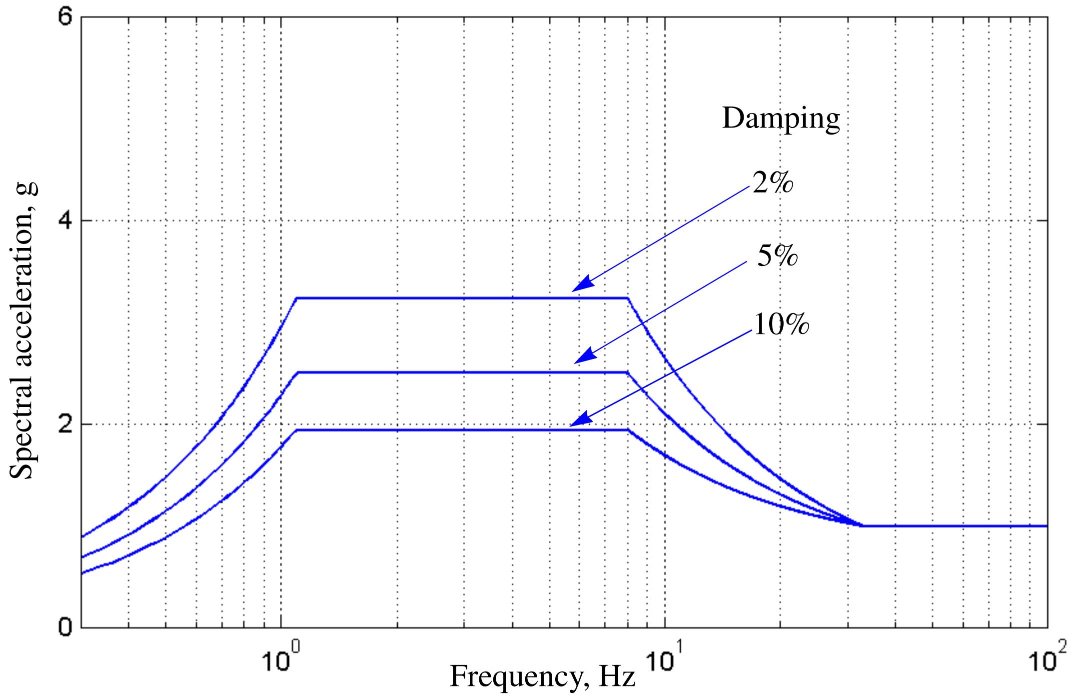

Figure 3-1 IEEE Spectra for the High Seismic Performance Level (PL)

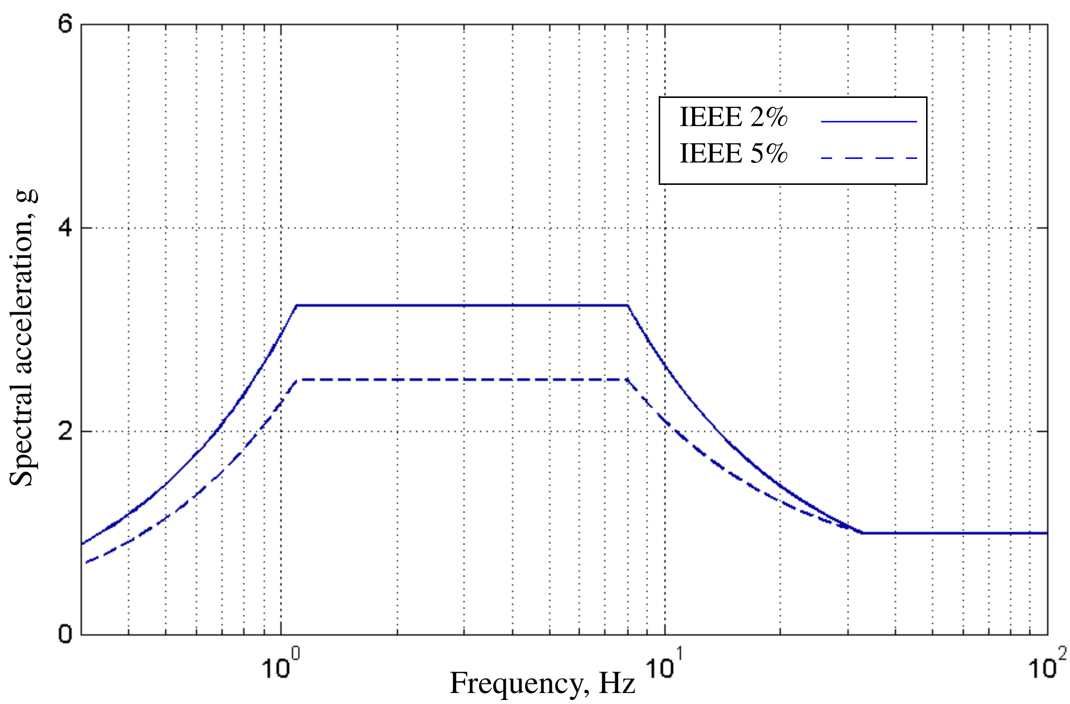

Figure 3-2 Target spectra for High Level qualification of disconnect switches

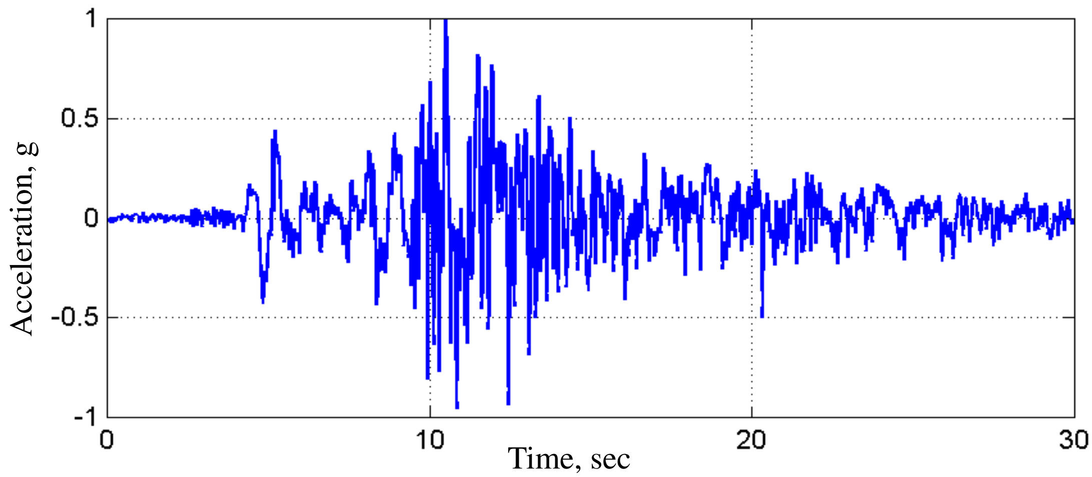

(a) Acceleration history

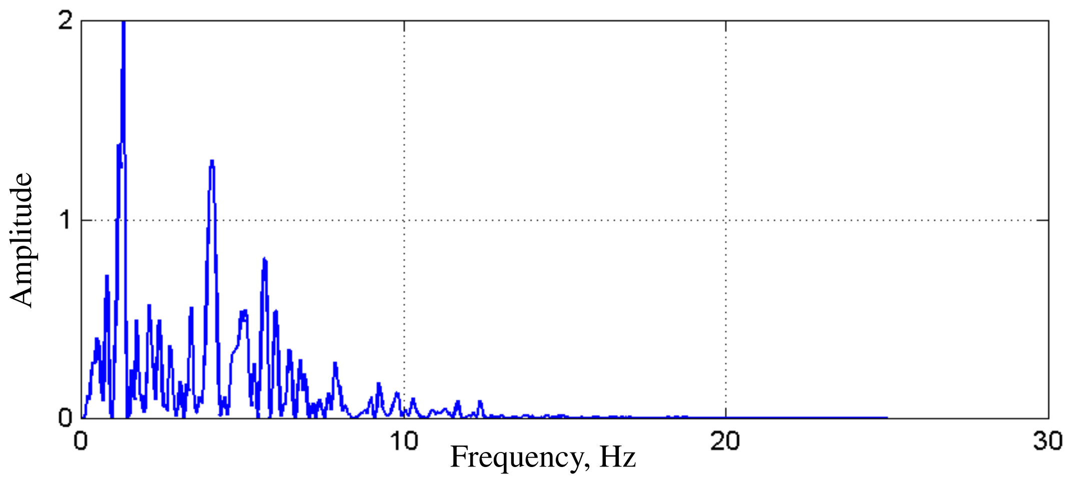

(b) Power spectrum

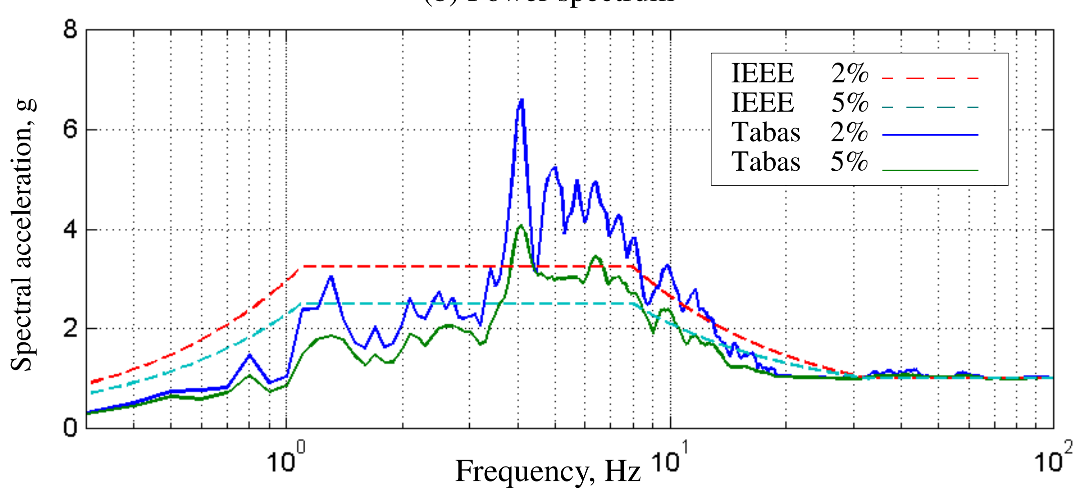

(c) Response spectrum

Figure 3-3 Acceleration history, power spectrum, and response spectra for the normalized longitudinal (*X*-) component of the original Tabas record

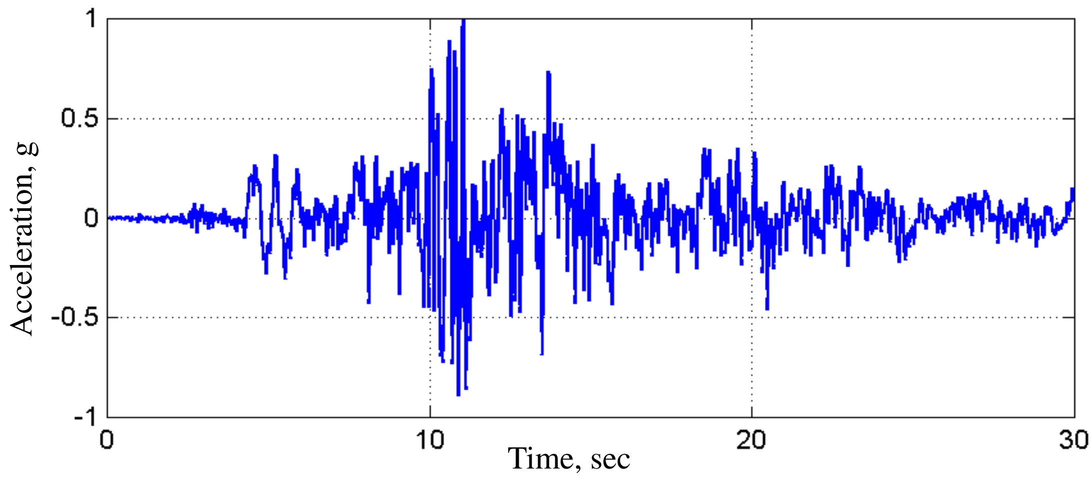

(a) Acceleration history

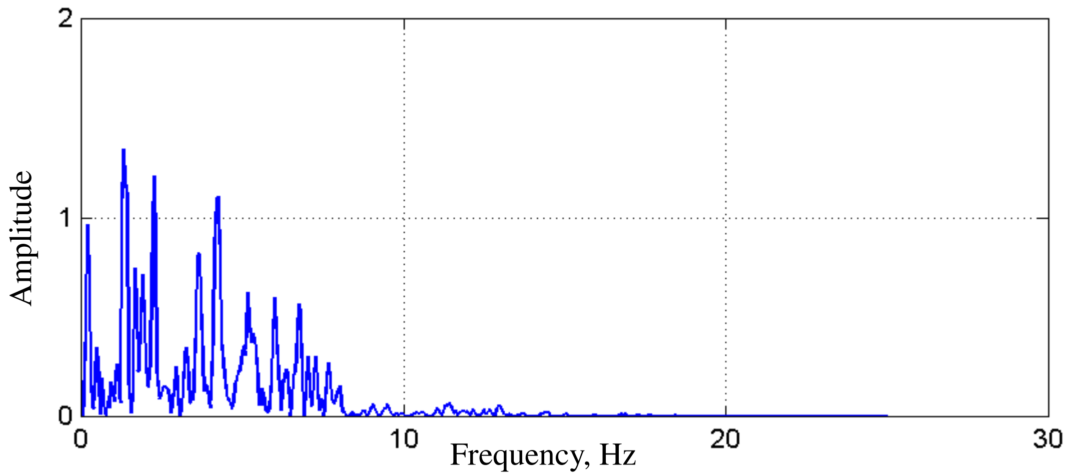

(b) Power spectrum

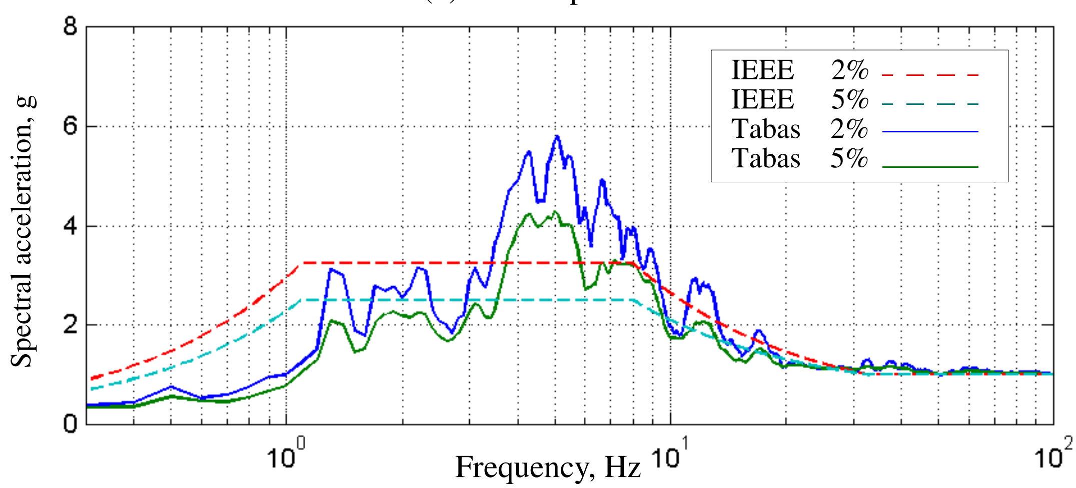

(c) Response spectrum

Figure 3-4 Acceleration history, power spectrum, and response spectra for the normalized lateral (Y-) component of the original Tabas record

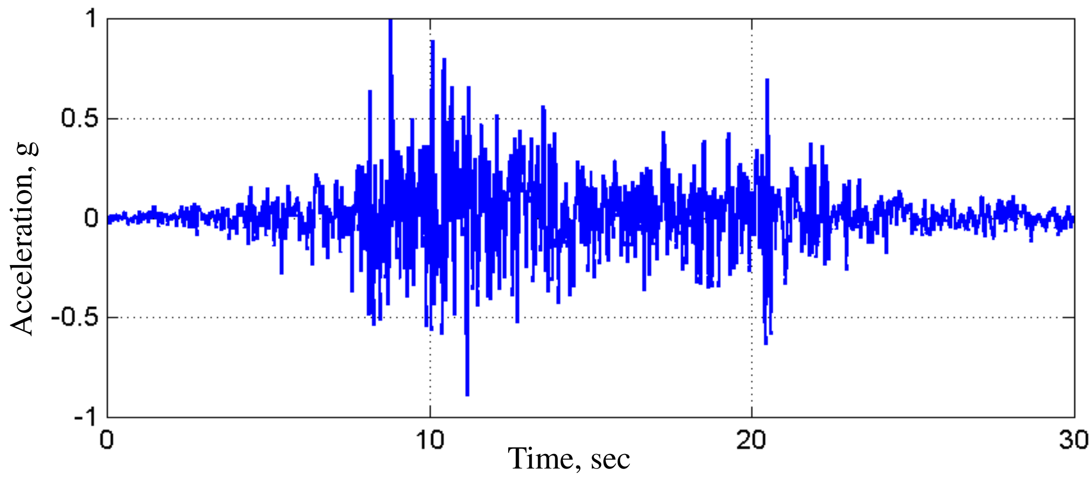

(a) Acceleration history

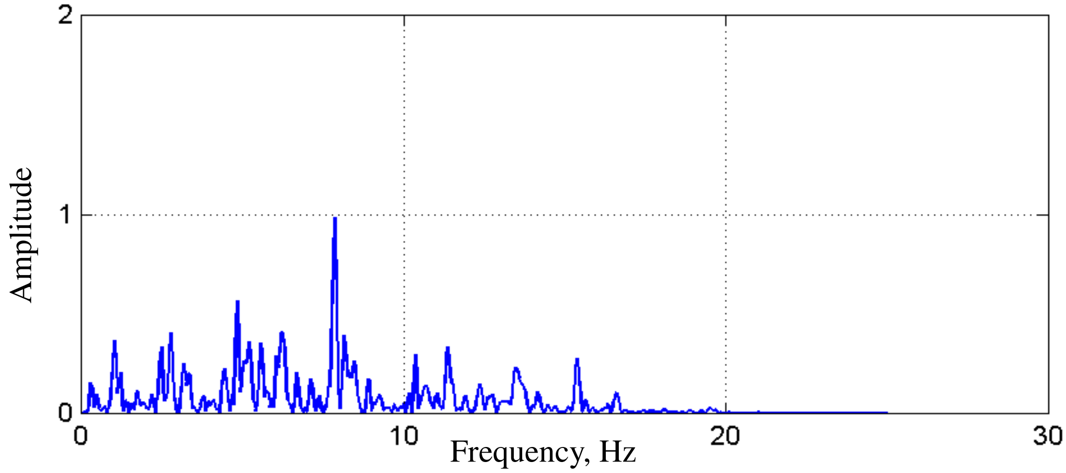

(b) Power spectrum

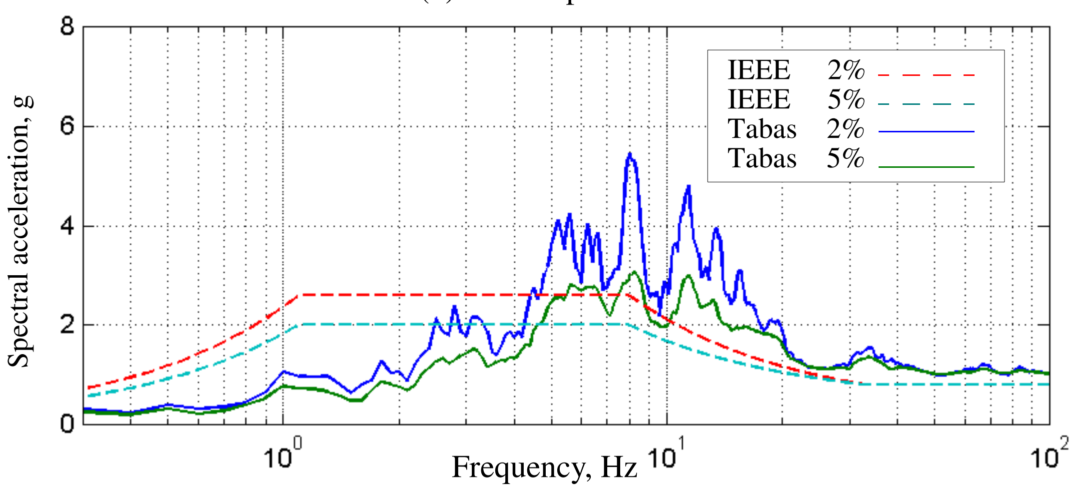

(c) Response spectrum

Figure 3-5 Acceleration history, power spectrum, and response spectra for the normalized vertical (*Z*-) component of the original Tabas record

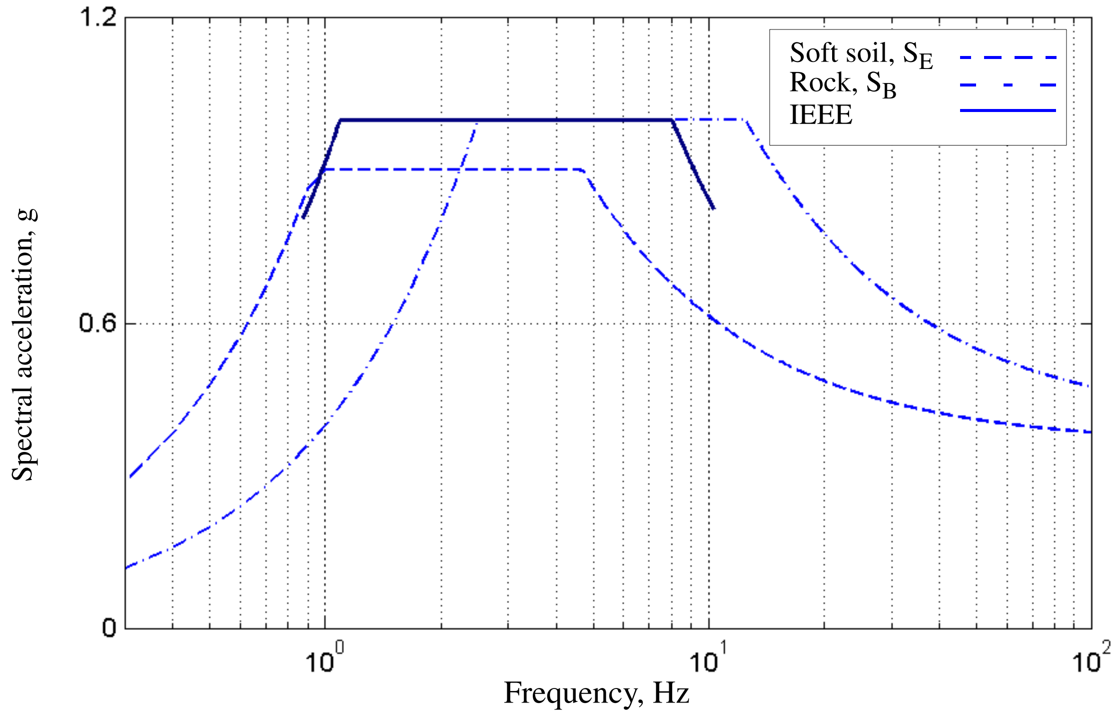

Figure 3-6 Five-percent damped spectra for rock and soft soil sites (ICBO 1997)

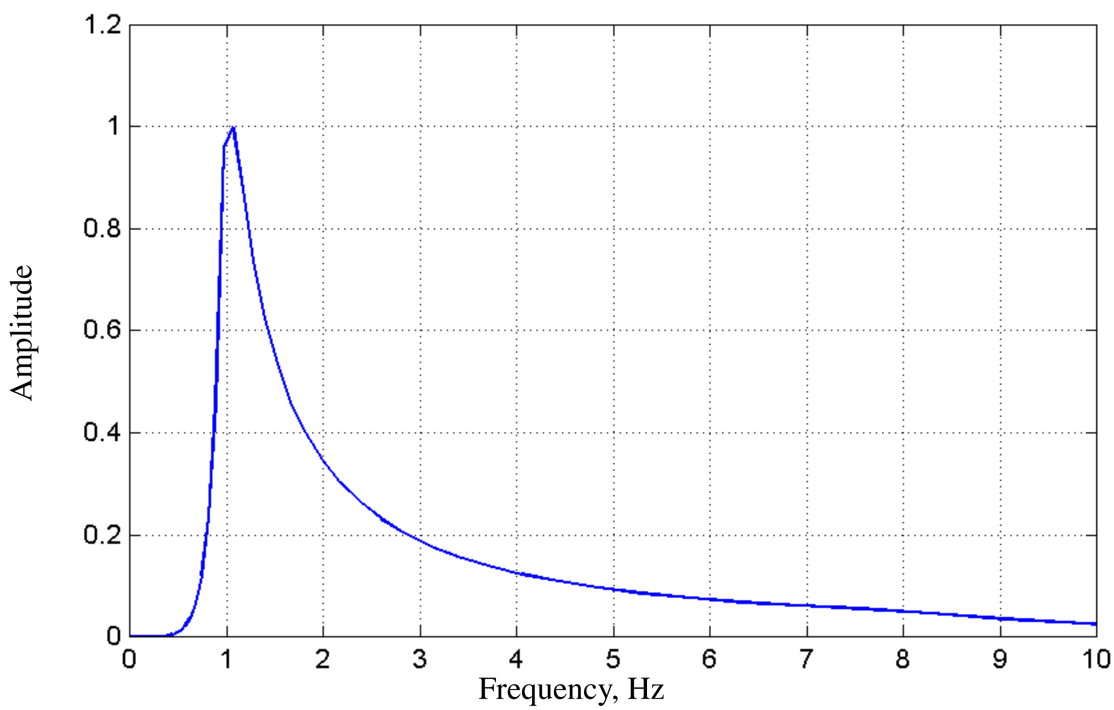

Figure 3-7 Acceleration power spectrum corresponding to the IEEE 2-percent damped spectrum

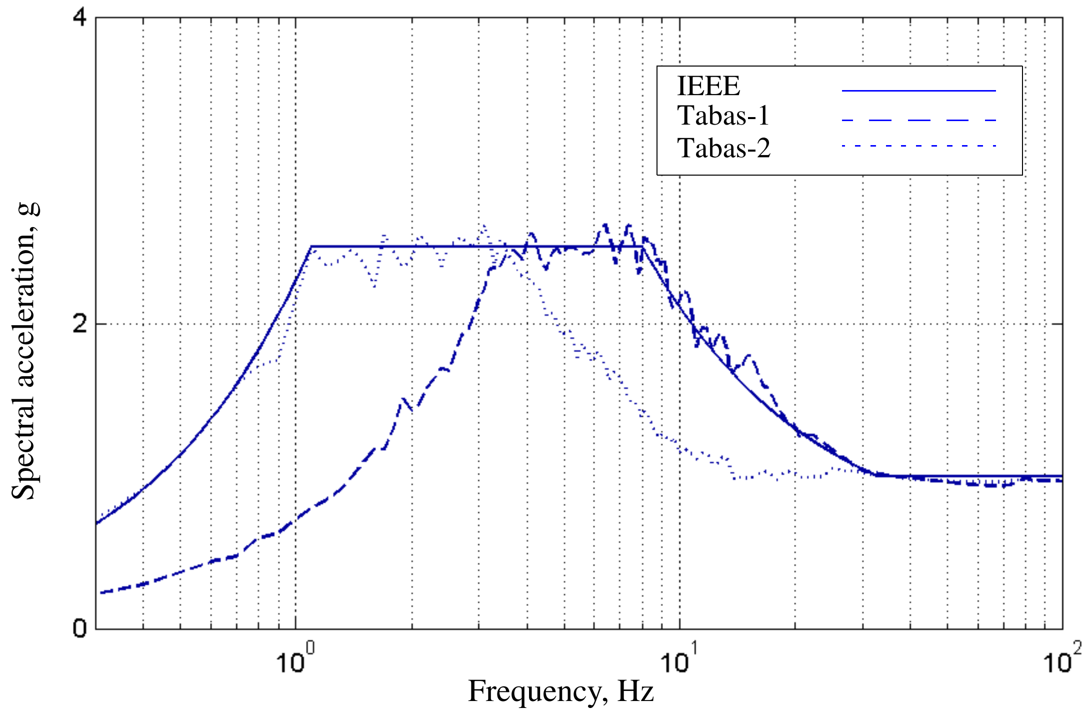

Figure 3-8 IEEE and Tabas 5-percent damped High Level response spectrum

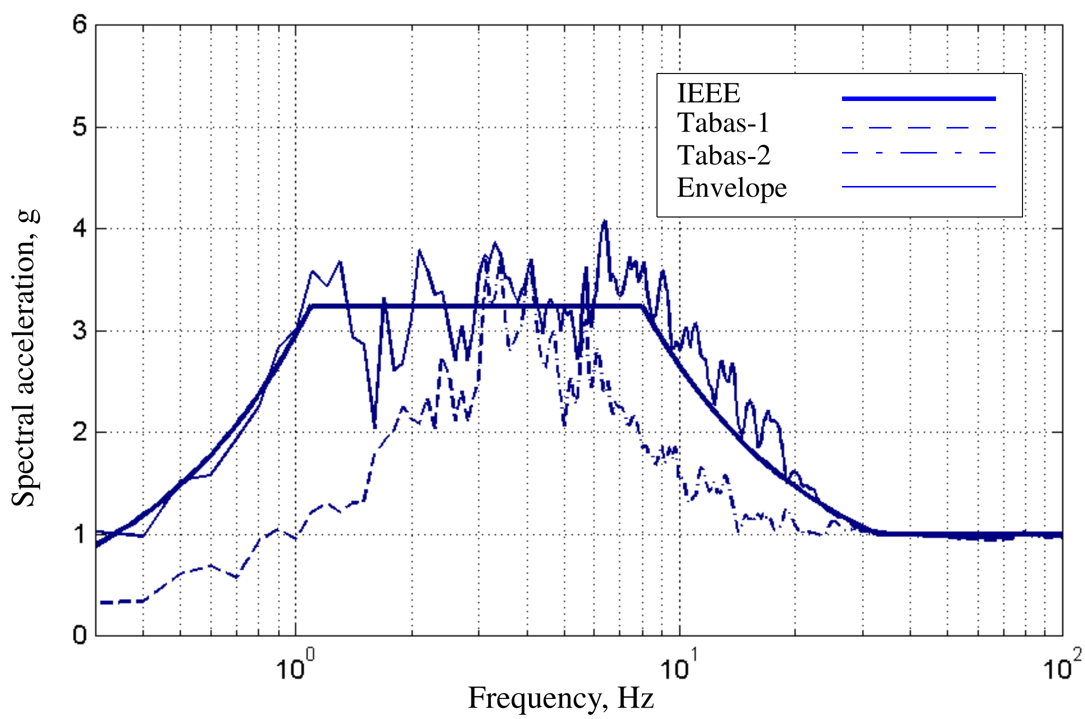

Figure 3-9 Envelope response spectrum for 2-percent damped Tabas motions

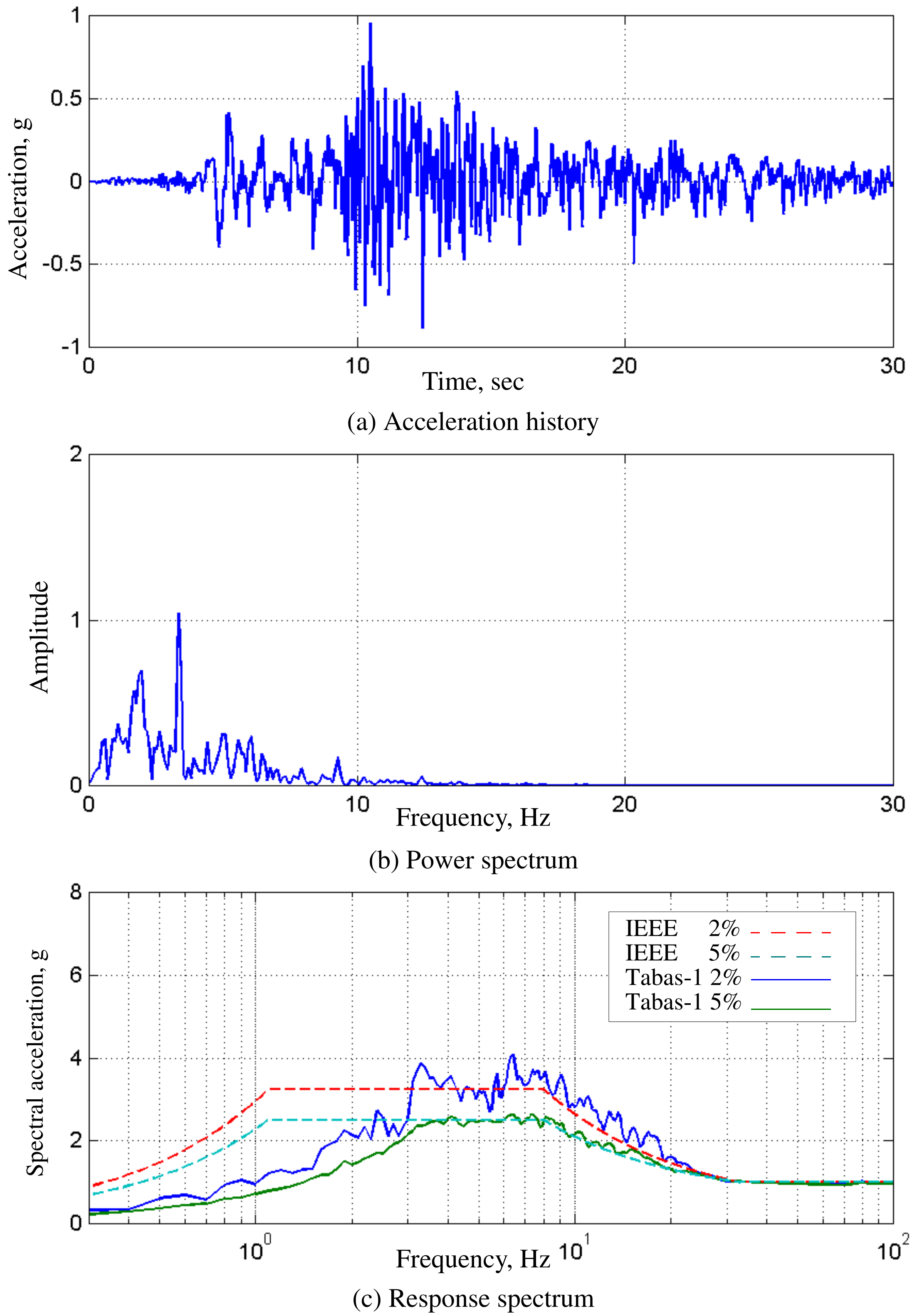

Figure 3-10 Acceleration history, power spectrum, and response spectra for the longitudinal (*X*-) component of the Tabas-1 record

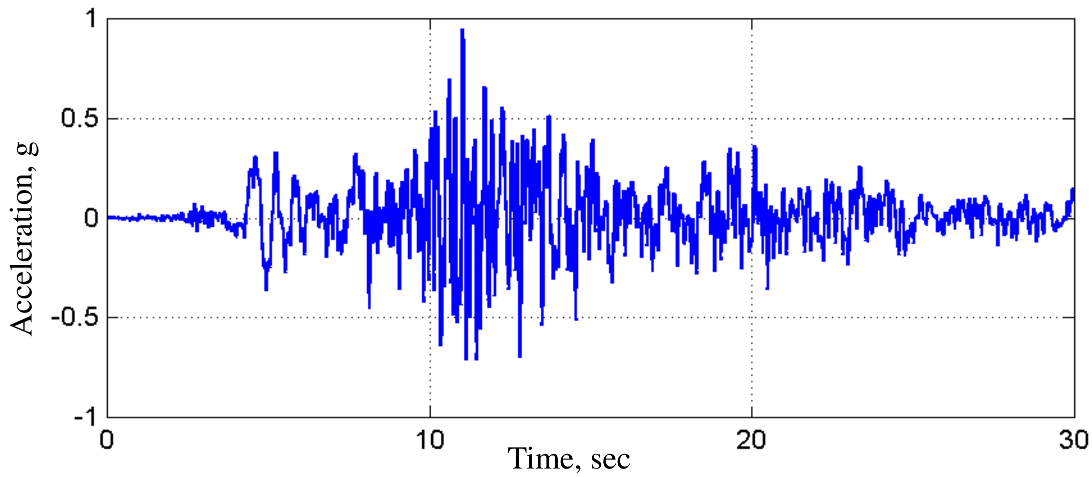

(a) Acceleration history

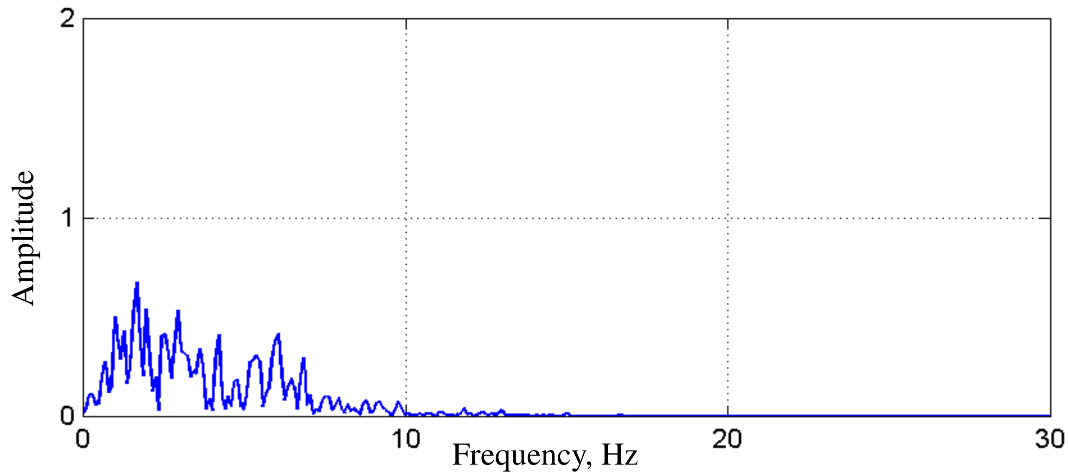

(b) Power spectrum

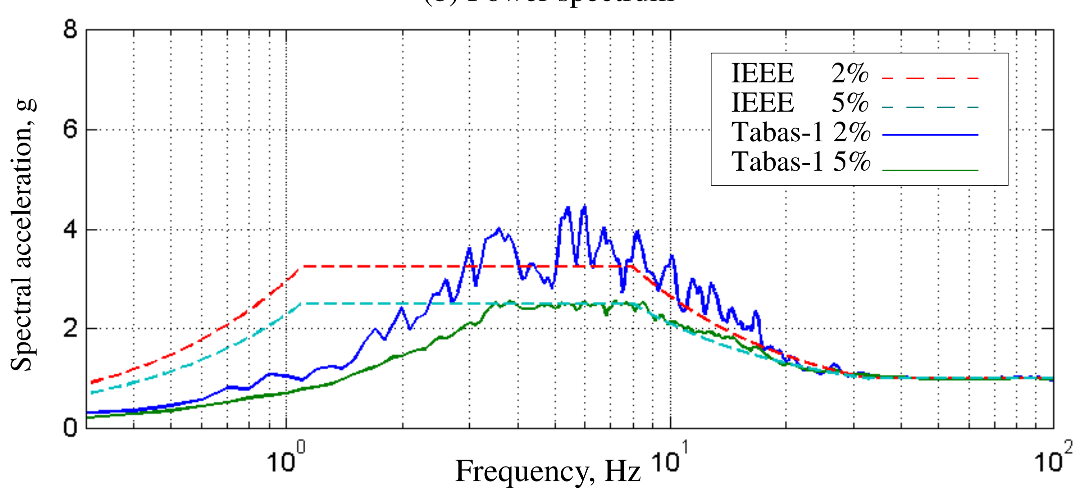

(c) Response spectrum

Figure 3-11 Acceleration history, power spectrum, and response spectra for the lateral (*Y*-) component of the Tabas-1 record

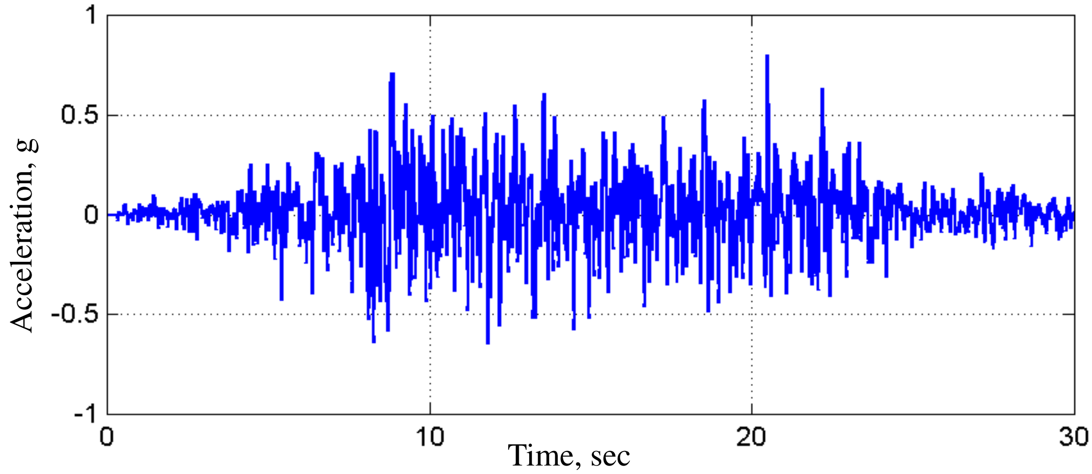

(a) Acceleration history

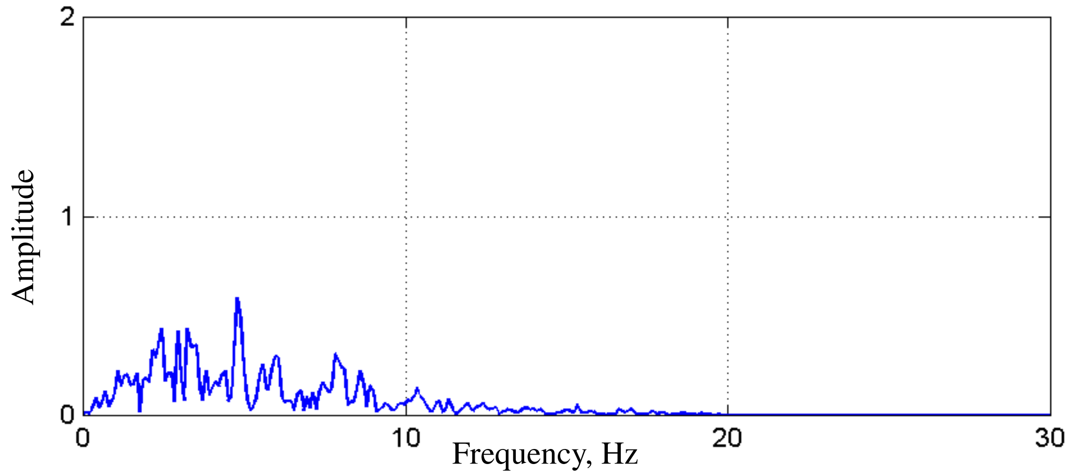

(b) Power spectrum

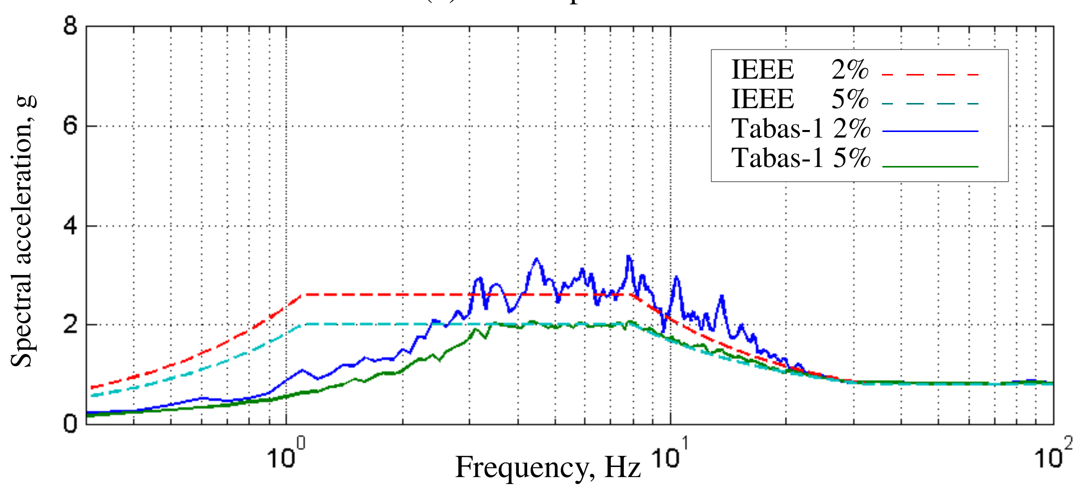

(c) Response spectrum

Figure 3-12 Acceleration history, power spectrum, and response spectra for the vertical (*Z*-) component of the Tabas-1 record

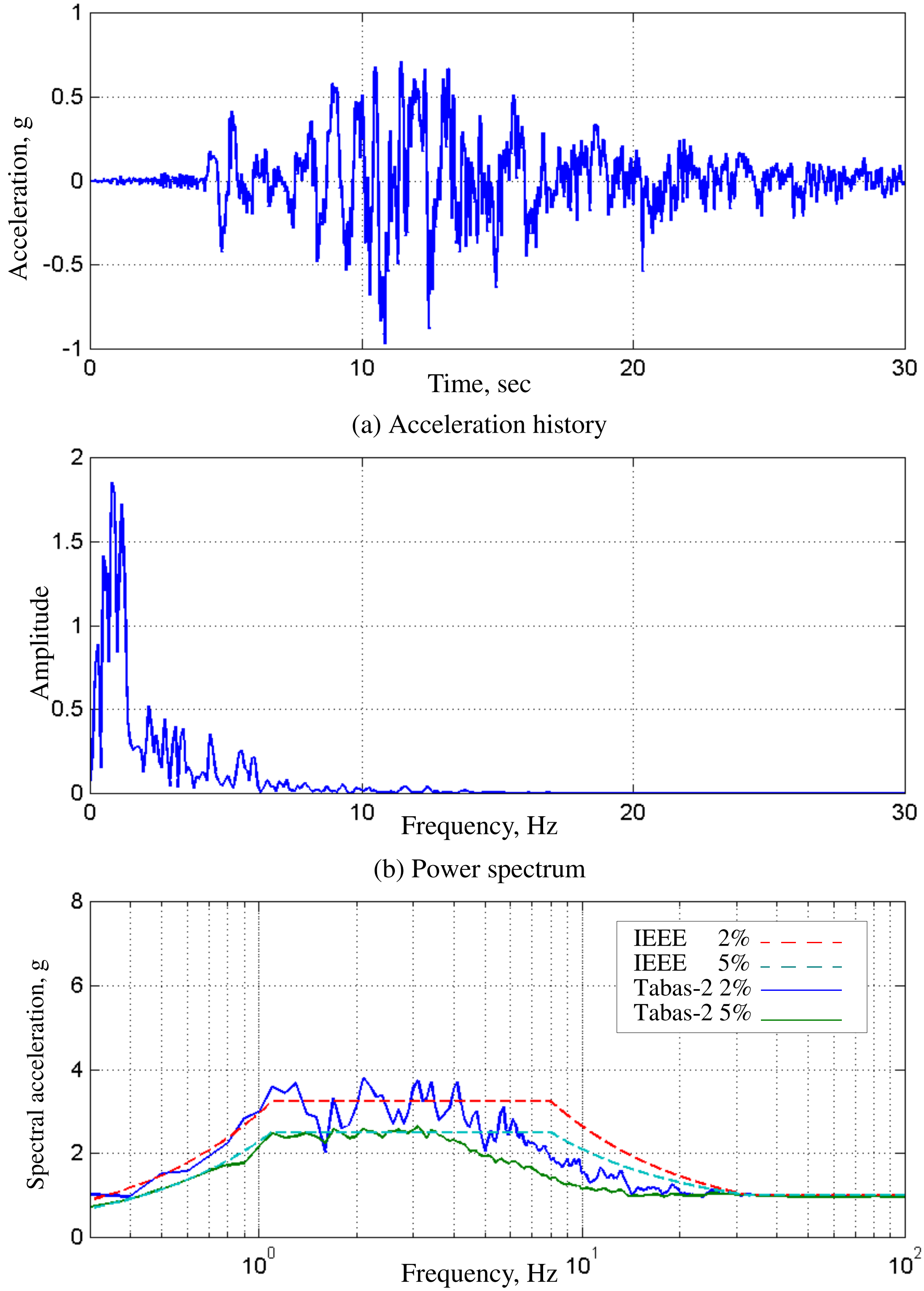

(a) Acceleration history

(b) Power spectrum

(c) Response spectrum

Figure 3-13 Acceleration history, power spectrum, and response spectra for the longitudinal (*X*-) component of the Tabas-2 record

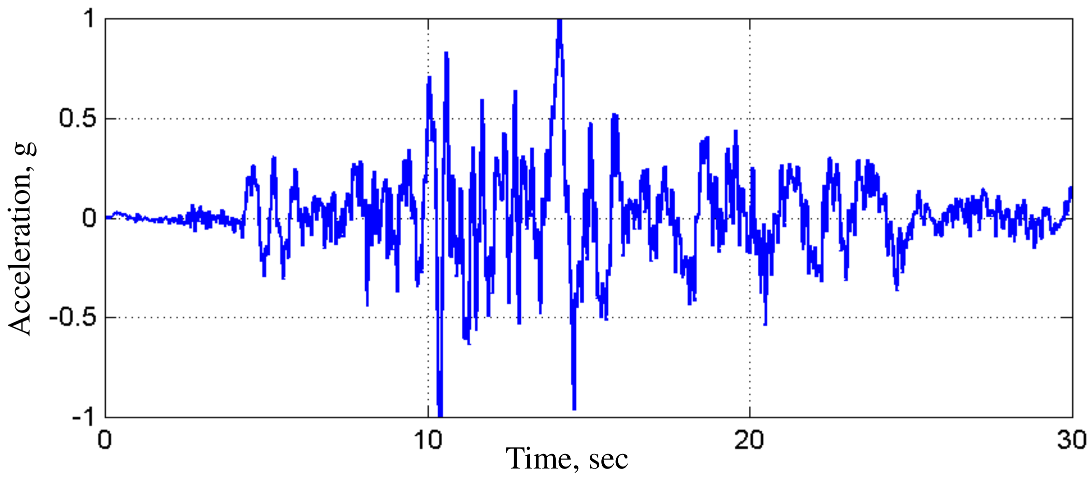

(a) Acceleration history

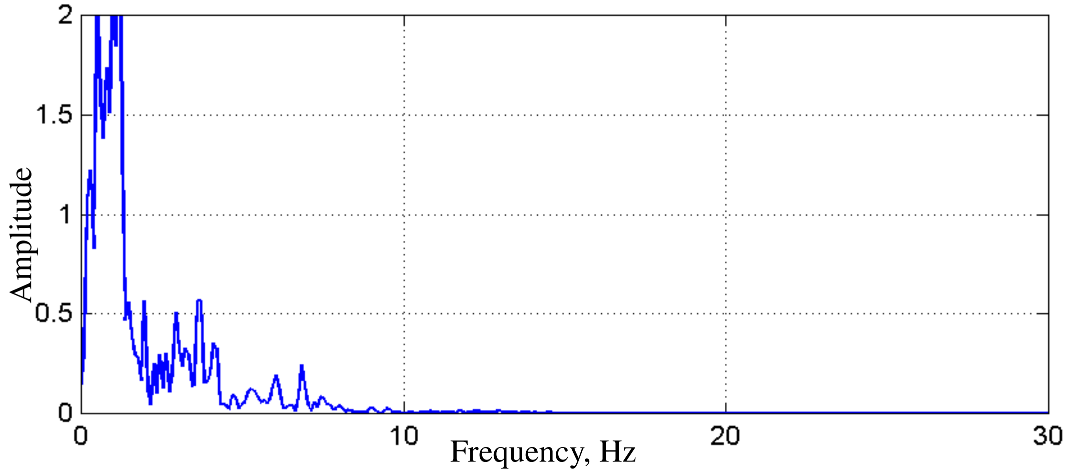

(b) Power spectrum

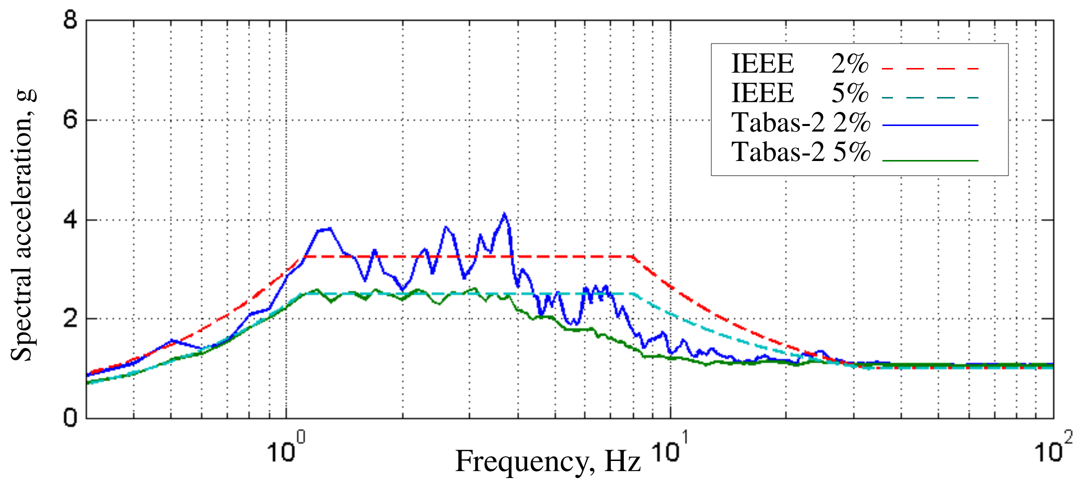

(c) Response spectrum

Figure 3-14 Acceleration history, power spectrum, and response spectra for the lateral (*Y*-) component of the Tabas-2 record

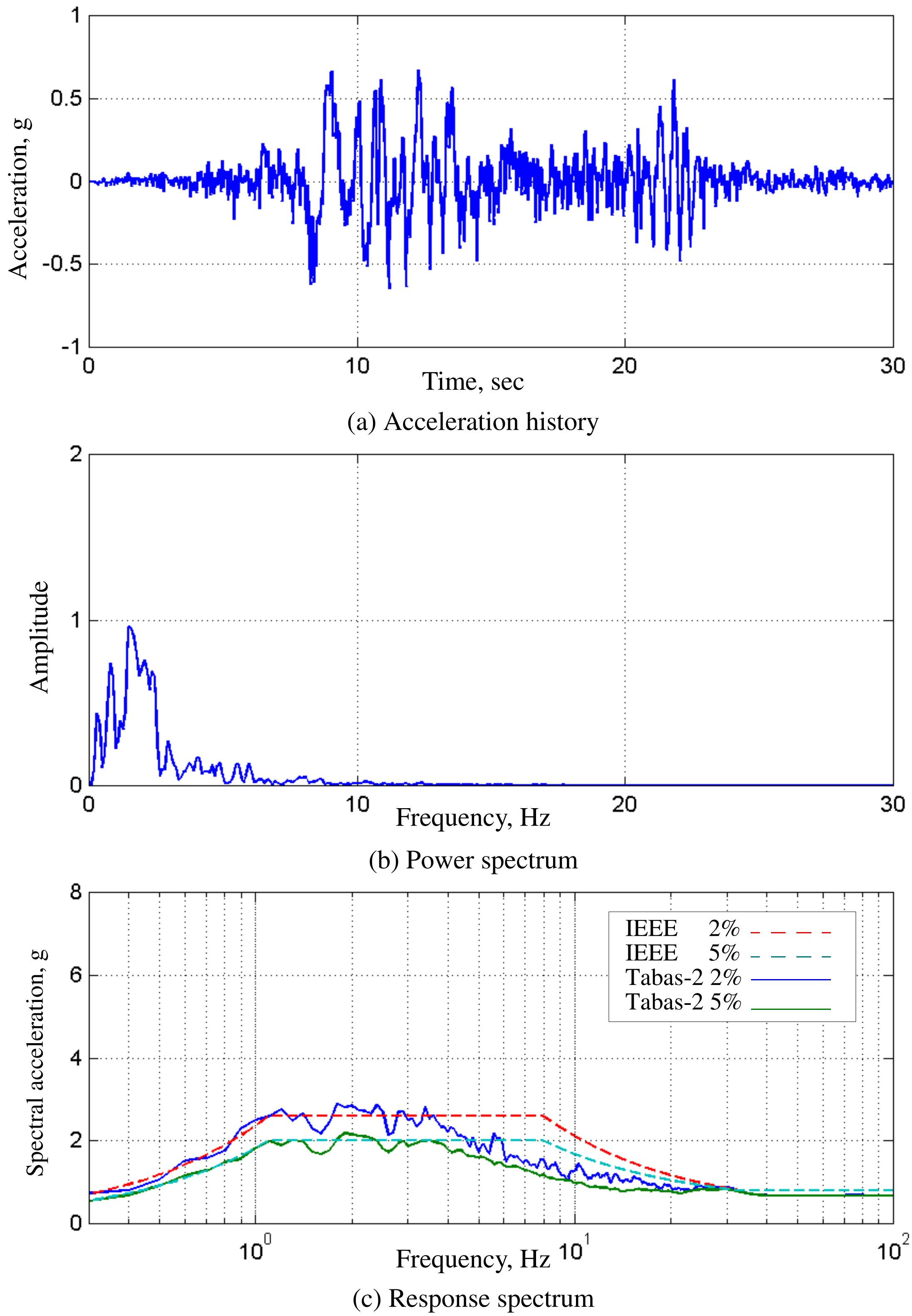

Figure 3-15 Acceleration history, power spectrum, and response spectra for the vertical (*Z*-) component of the Tabas-2 record

4 Seismic Evaluation of Switch Poles

4.1 Introduction

One pole of each of the three separate switches was first mounted directly on the simulator platform and tested prior to earthquake simulator testing of three-phase disconnect switches on the PEER frame. Poles from switches SW1 (a two-post porcelain horizontal-break switch), SW2 (a three-post porcelain vertical-break pole), and SW3 (a three-post composite vertical-break pole) were tested.

For testing, the double-channel beams at the base of switch poles were mounted directly on the simulator platform. Static, resonant-search, and triaxial earthquake simulator tests were used to evaluate the response of the poles. A description of the test setup, the instrumentation, and the earthquake motions used for the seismic tests, and a discussion of selected test results follow.

4.2 Experimental program

4.2.1 Overview

Tests of the three 230-kV switch poles were conducted using the U.C. Berkeley earthquake simulator. Two sets of three-component spectrum-compatible input motions were developed for testing. For seismic testing, IEEE 693-1997 states that the switches must be instrumented to record (a) maximum vertical and horizontal accelerations at the top of the insulators, at the end of the switch blade, and at the top of the earthquake simulator platform, (b) maximum displacement at the top of the insulator and at the top of the blade, and (c) maximum stresses at the base of the posts and at the base of the opposite legs of the support frame. The displacements at the tip of the blades were computed by double integration of the accelerations recorded at the tip. Since the poles were not mounted on an elevated support, strain gages were placed only at the base of the insulator posts. The instrumentation scheme developed for the tests described in this chapter exceeded the requirements of IEEE 693-1997. IEEE 693-1997 also writes that the correct operation (full opening and full closing) must be verified prior to testing, and that testing shall be performed with the switches both closed and open. These requirements were followed exactly in the testing program.

4.2.2 Mounting configuration

Individual poles of switches were assembled prior to placement on the simulator platform. The bolts at the base of the rotor bearings (Figure 2-11) were adjusted to obtain the full range of operation for the switch blades. The double-channel beams at the base of the poles were bolted to W8x31 sections as described in Chapter 2. The connection was identical to the field connection and utilized four 1/2 in. (13 mm) diameter galvanized steel bolts.

4.2.3 Testing program

4.2.3.1 Introduction

IEEE 693-1997 requires that experimental testing of disconnect switches and switch components include: (a) static tests to 50 percent of the specified mechanical load (SML) to measure the deflection of composite insulators, (b) uniaxial resonant-search tests to identify the dynamic properties of the switches, and (c) triaxial earthquake history tests for switch qualification. Comments on the static and uniaxial tests follow. Information on triaxial earthquake history testing is presented in Chapter 3.

4.2.3.2 Static tests

Prior to earthquake-simulator testing, pull-back and quick-release tests were undertaken to characterize the static (stiffness) and dynamic (frequency) properties of the poles. Although IEEE 693-1997 requires only cantilever tests for composite posts, such tests were conducted for both porcelain and composite insulators. IEEE 693-1997 recommends static tests to be conducted to 50% of the SML of the insulators. The value of SML for composite and porcelain insulators was measured by manufacturers to be approximately 0.6 kips (2.5 kN). For the static tests reported in this chapter, the maximum applied force was approximately 0.2 kips (0.9 kN).

The test setup for the static tests, shown in Figure 4-1, consisted of a nylon rope connecting the top of post A1 (Figure 2-5) to reaction points in-line with a turnbuckle, a load cell, and a machined bolt. During the pull-back stage of the tests, the insulator was gradually loaded to approximately 0.2 kips (0.9 kN). The applied force and displacement at top of the insulator were monitored and recorded using the in-line load cell and displacement transducers. The applied force was then released by cutting the machined bolt, and the free vibration response was recorded. The tests were repeated in both the x- and y- directions, with the blade both open and closed. The pull-back segment of the tests was repeated three times to improve the accuracy of the acquired data in accordance with IEEE 693-1997.

4.2.4 Resonant-search tests

Sine-sweep and white-noise tests were used to establish the dynamic characteristics (resonant frequencies and damping ratios) of the poles. These so-called resonant-search tests were undertaken using unidirectional excitation along each axis of the earthquake simulator platform. An IEEE-specified simulator acceleration amplitude of 0.1g was used for both the sine-sweep and white-noise tests.

4.2.5 Instrumentation

The instrumentation scheme developed for the tests described in this chapter included 54 transducers and 56 channels of data. Table 4-1 lists the channel number, instrument type, response quantity, orientation, and location for each transducer. Figures 4-2 through 4-4 present information on the instrumentation of the earthquake simulator platform, acceleration of insulators and blade(s), post displacements, and porcelain strains for the base of insulators or at the blade-post connection for the composite switch. The coordinate system used in this chapter and the post designation (posts 1, 2, and 3) are also shown in the figures. Figure 4-5 shows the accelerometers at the blade tips for switch SW1. Figure 4-6 shows the instrumentation at the top of posts 2 and 3 for switch SW2.

4.3 Experimental Results

4.3.1 Overview

The objectives of the testing program described in this chapter were to conduct static, resonance-search, and triaxial seismic tests to estimate the dynamic properties of and to evaluate the seismic performance of individual poles of three disconnect switches. The poles were assembled by the research team, but representatives from PG&E and ABB completed the mechanical adjustment of the poles prior to testing. To simulate field conditions, the operating mechanism for the poles was locked by attaching it to the simulator platform using a turnbuckle to ensure that its position (open or closed) did not change during the tests. Figures 4-7 through 4-9 show the assembled pole of the switches SW1 through SW3 prior to testing. The list of static, resonant-search, and earthquake tests, and the key observations are presented in Table 4-2. The test sequence for all three poles was the same. The x, y, and z directions specified in the table denote the lateral, longitudinal, and vertical axes of the switches, respectively. The longitudinal axis of the double-channel beams at the base of the poles coincided with the y-axis of the simulator (see Figure 2-1).

For all tests, the transducer response histories were processed using the computer program Matlab (Mathworks 1999). Experimental histories were low-passed filtered using a rectangular filter with a cut-off frequency of 30 Hz and then zero-corrected. After each earthquake test, the response data were analyzed, the pole was inspected for damage and the bolts were checked for tightness. All bolts were found to be tight after all tests. The following sections summarize the dynamic properties and the seismic response of the switch poles. Section 4.3.2 through 4.3.4 present the results from the static, resonant-search, and earthquake tests.

Table 4-1 Instrumentation for seismic tests of 230-kV switch poles

Channel No	*Transducer*[1]	*Response Quantity*	*Orientation*[2,3]	*Transducer Location*[4]		
				SW1	SW2	SW3
1	-	date	-	-		
2	-	time	-	-		
3	LVDT	displacement	*x*	simulator platform		
4	LVDT	displacement	*y*	simulator platform		
5	LVDT	displacement	*x*	simulator platform		
6	LVDT	displacement	*y*	simulator platform		
7	LVDT	displacement	*z*	simulator platform		
8	LVDT	displacement	*z*	simulator platform		
9	LVDT	displacement	*z*	simulator platform		
10	LVDT	displacement	z	simulator platform		
11	A	acceleration	*x*	simulator platform		
12	A	acceleration	*x*	simulator platform		
13	A	acceleration	*y*	simulator platform		
14	A	acceleration	*y*	simulator platform		
15	A	acceleration	*z*	simulator platform		
16	A	acceleration	*z*	simulator platform		
17	A	acceleration	*z*	simulator platform		
18	A	acceleration	z	simulator platform		
19	A	acceleration	*x*	base of post 1		
20	A	acceleration	*y*	base of post 1		
21	A	acceleration	*z*	base of post 1		
22	A	acceleration	*x*	base of post 2		
23	A	acceleration	*y*	base of post 2		
24	A	acceleration	*z*	base of post 2		
25	A	acceleration	*x*	midheight of post 1		not used
26	A	acceleration	*y*	midheight of post 1		not used
27	A	acceleration	*z*	midheight of post 1		not used
28	A	acceleration	*x*	midheight of post 1		base of post 3
29	A	acceleration	*y*	midheight of post 1		base of post 3
30	A	acceleration	*z*	midheight of post 1		base of post 3
31	A	acceleration	*x*	top of post 1		

Table 4-1 Instrumentation for seismic tests of 230-kV switch poles

Channel No	*Transducer*[1]	*Response Quantity*	*Orientation*[2,3]	*Transducer Location*[4]		
				SW1	SW2	SW3
32	A	acceleration	*y*	top of post 1		
33	A	acceleration	*z*	top of post 1		
34	A	acceleration	*x*	top of post 2		
35	A	acceleration	*y*	top of post 2		
36	A	acceleration	*z*	top of post 2		
37	A	acceleration	*x*	tip of blade 1		
38	A	acceleration	*y*	tip of blade 1		
39	A	acceleration	*z*	tip of blade 1		
40	A	acceleration	*x*	tip of blade 2	top of post 3	
41	A	acceleration	*y*	tip of blade 2	top of post 3	
42	A	acceleration	*z*	tip of blade 2	top of post 3	
43	LP	displacement	*x*	base of post 1		
44	LP	displacement	*x*	base of post 2		
45	LP	displacement	*x*	midheight of post 1		
46	LP	displacement	*y*	midheight of post 1		
47	LP	displacement	*x*	midheight of post 2		
48	LP	displacement	*y*	midheight of post 2		
49	LP	displacement	*x*	top of post 1		
50	LP	displacement	*y*	top of post 1		
51	LP	displacement	*x*	top of post 2		
52	LP	displacement	*y*	top of post 2		
53	SG	strain	-	base of post 1		base of blade
54	SG	strain	-	base of post 1		base of blade
55	SG	strain	-	base of post 1		base of blade
56	SG	strain	-	base of post 1		base of blade

1. A = accelerometer; LVDT = displacement transducer; LP = linear potentiometer; SG = strain gage.
2. For the global (*x*-, *y*-, *z*-) coordinate systems, see Figures 4-2 through 4-4.
3. The specified directions for the accelerometers mounted on the insulators and blades are for the closed position; the accelerometers were rotated 90 degrees when the switch was in the open position.
4. For the location of posts, see Figures 4-2 through 4-4.

Table 4-2 Sequence of tests for a single pole of disconnect switches SW1, SW2, and SW3

No.	*Description*[1]	*PGA*[2] *(g)*	*Blade position*	*Comments*
1	ST-x	-	Closed	
2	ST-y	-	Closed	
3	ST-x	-	Open	
4	ST-y	-	Open	
5	WN-x	0.1	Closed	
6	WN-y	0.1	Closed	
7	WN-z	0.1	Closed	
8	SS-x	0.1	Closed	
9	SS-y	0.1	Closed	
10	SS-z	0.1	Closed	
11	Tabas-1	0.1	Closed	
12	Tabas-2	0.1	Closed	
13	Tabas-1	0.5	Closed	Spectrum equivalent to Moderate Level qualification.
14	Tabas-2	0.5	Closed	
15	Tabas-1	1.0	Closed	Spectrum equivalent to High Level qualification.
16	Tabas-2	1.0	Closed	
17	WN-x	0.1	Open	
18	WN-y	0.1	Open	
19	WN-z	0.1	Open	
20	SS-x	0.1	Open	
21	SS-y	0.1	Open	
22	SS-z	0.1	Open	
23	Tabas-1	0.1	Open	
24	Tabas-2	0.1	Open	
25	Tabas-1	0.5	Open	Spectrum equivalent to Moderate Level qualification.
26	Tabas-2	0.5	Open	
27	Tabas-1	1.0	Open	Spectrum equivalent to High Level qualification.
28	Tabas-2	1.0	Open	

1. ST = static, WN = white-noise, SS = sine-sweep; *-x, -y*, and *-z* denote direction of testing; Tabas-1 and Tabas-2 = part spectrum-compatible earthquake histories.
2. PGA = target peak acceleration of the simulator platform.

4.3.2 Static tests

Static pull-back, and quick-release tests of post A1 (see Figure 2-5) of the three switch poles were undertaken to determine stiffness and frequency of the poles. The computed stiffness and resonant frequency of the posts are presented in Table 4-3 for each pole with the blade(s) in the open and closed positions. The stiffness of the post was computed using the measured forces and displacements during the pull-back segment of the tests. The acceleration records at the tip of post 1 following the quick-release of the applied load was used to compute the resonant frequencies of the pole.

Table 4-3 Stiffness and frequency properties of poles from static tests

		Stiffness (kN/m)		*Frequency (Hz)*	
Switch	*Blade*[1]	x-direction	y-direction	x-direction	y-direction
SW1	Closed	34	74	3	5
SW1	Open	28	39	3	3
SW2	Closed	58	160	5, 6[2]	7
SW2	Open	49	74	5	6
SW3	Closed	44	150	6, 7[2]	8
SW3	Open	39	58	7	8

1. Data from Tests 1 and 2 (see Table 4-2) were used to compute properties for the closed blade; data from Tests 3 and 4 were used to compute properties for the open blade.
2. Two modal frequencies were present for these tests.

Several observations can be made using the data presented in Table 4-3: (1) the stiffness and frequency of the SW1 post was less than that of SW2 because the detail used to connect the base of insulators to the double-channel beams was more flexible for SW1; (2) the fundamental frequencies of SW3 are greater than those of SW2 because the composite insulators of SW3 are lighter than the porcelain insulators of SW2; (3) for each post, the deformation in fundamental mode is primarily due to the flexibility of the double-channel beams and other attachments; (4) the frequency in the y-direction (coinciding with the longitudinal axis of the double-channel beam) is greater than the frequency in the x-direction because the double-channel beam is much stiffer in flexure than in torsion; (5) when the blade is closed, the frequency in the y-direction is greater than the frequency in the x-direction because the connectivity of the posts produces frame-type action (see Figure 2-13); and (6) when the blade is closed, the blade of vertical blade poles introduces an additional mode (out-of-phase motion of posts), this type of mode is not present for horizontal-break pole SW1 because the connection of the two blades for this pole acts as a pin (see Figure 2-7).

The stiffness of the composite posts mounted on a rigid base was measured by the manufacturer to be approximately 0.72 k/in. (125 kN/m). The open blade stiffnesses of SW3 listed in Table 4-3 are less than 125 kN/m because the data in Table 4-3 includes the flexibility of the double-channel beam at the base of the post.

4.3.3 Resonance-search tests

Sine-sweep and white-noise tests were used to calculate the modal frequencies and damping ratios for the poles. Figures 4-10 through 4-15 present the power spectra for the tip of post 1 from the sine-sweep tests for SW1 through SW3 with closed and open blades. The power spectra were normalized to a maximum ordinate of unity. Post tip acceleration data were used to calculate frequency and damping values for the poles. The modal frequencies were taken from the peaks in the power spectrum and the damping ratios were computed using the half-power method.

Table 4-4 summarizes the measured dynamic properties of the switches in the *x*- and *y*-directions. Modal data could not be determined for the local *z*-direction. The modal data obtained from the resonant-search tests were consistent with the modal properties computed from the pull-back, quick-release tests.

Table 4-4 Modal properties of poles from resonance-search tests

		Frequency (Hz)		*Damping Ratio (% critical)*	
Switch	*Blade*[1]	*x*-direction	*y*-direction	*x*-direction	*y*-direction
SW1	Closed	3	5	3	4
SW1	Open	3	3	3	4
SW2	Closed	5, 6[2]	6	3, 2	2
SW2	Open	5	6	3	2
SW3	Closed	6, 7[2]	8	2, 2	2
SW3	Open	7	8	2	2

1. Data from Tests 5 through 10 (see Table 4-2) were used to compute properties for the closed blade; data from Tests 17 through 22 were used to compute properties for the open blade.
2. Two modal frequencies were present for these tests.

Examination of the data listed in Table 4-4 leads to observations similar to those of Section 4.3.2. The resonant frequency for the poles ranged between 3 and 5 Hz for SW1, 5 and 6 Hz for SW2, and 5 and 8 Hz for SW3. For all poles, the damping ratio was between 2 and 4 percent of critical. Two-percent damping was therefore used to generate the spectrum-compatible earthquake histories for the experimental studies described in the remainder of this chapter.

4.3.3.1 Earthquake testing of poles

The following paragraphs present the peak responses of the poles measured during the tests with target peak accelerations equal to or greater than 0.5 g, and an evaluation of the seismic response of the poles for Tests 15 and 16, and 27 and 28 (target peak acceleration equal to 1.0g).

Peak acceleration and relative displacement of the poles, and stresses in the poles are presented in Table 4-5. Only the peak responses at the top of the insulator posts are reported. The peak absolute accelerations for the posts were defined as the maximum of the vector sum of acceleration components in the *x*- and *y*-directions, evaluated from acceleration histories. The vector summation was limited to the horizontal components, as these are the critical components that introduce flexural stresses at the base of the insulators. The displacement in an insulator was computed by subtracting the *x*-displacement at the base of the insulator from the *x*-displacement at the top of the post. Data were not recorded in the *y*-direction at the base of the posts. The peak absolute acceleration for the blades was defined as the maximum of the vector sum of the acceleration components in the *x*- and *z*-directions. The vector summation was limited to these components because only the *x*- and *z*-components contribute to the flexural stresses at the blade-post connection. The maximum stress was computed from the measured porcelain or aluminum strains (channels 53 through 56). Values of stress were computed by multiplying the measured strains by the Young's modulus, assumed to equal 97,000 MPa for porcelain insulators and 69,000 MPa for the aluminum blade.

The global responses of poles SW1, SW2, and SW3 were assessed by analysis of data from Tests 15 and 27, (Tabas-1, target PGA equal to 1.0g) and Tests 16 and 28 (Tabas-2, target PGA equal to 1.0g). The peak responses for these tests are listed in Table 4-5. The envelope response spectrum for the poles was obtained using the procedure described in Section 3.2. Figures 4-16 through 4-18 present the 2-percent damped acceleration response spectra for the *x*- and *y*-components of Tabas-1 (Test 15) and Tabas-2 (Test 16) tests of poles SW1, SW2, and SW3, respectively. The spectra are presented for the closed blade tests only because the spectra for the tests with the open blade were nearly identical to those of the closed blade. For all poles, the ordinates of the envelope spectrum exceeded the IEEE 693-1997 target spectrum for a zero-period acceleration of 1.0g in the range of frequencies of the poles in the *y*-direction; the envelope spectrum fell below the target spectrum between 5 and 6 Hz in the *x*-direction; the porcelain strains were less than the ultimate value and no structural damage was observed; the pole was fully operational (closed to open and open to closed) following each test; and electrical connectivity was maintained throughout the tests with the blade closed.

Table 4-5 Peak responses of the switches

		Acceleration (g)			*Acceleration (g)*		*Displacement (mm)*		*Stress (MPa)*	
Switch	*Test*[2]	*Post 1*	*Post 2*	*Post 3*	*Blade 1*	*Blade 2*	*Post 1*	*Post 2*	*Por.*[1]	*Al.*[1]
SW1	13	0.7	0.7	-	1.1	1.1	9	9	3	-
SW1	14	2.2	2.7	-	3.8	3.6	25	33	9	-
SW1	15	3.6	4.6	-	5.7	6.9	49	60	14	-
SW1	16	4.7	4.3	-	5.6	6.7	57	55	17	-
SW1	25	2.8	3.4	-	4.5	5.5	43	41	14	-
SW1	26	3.2	3.4	-	4.4	5.6	37	35	15	-
SW1	27	4.3	4.7	-	6.2	6.5	73	62	21	-
SW1	28	4.7	4.5	-	7.6	7.0	55	54	24	-
SW2	13	2.6	3.1	2.5	2.6	-	16	33	12	-
SW2	14	2.1	3.1	2.6	2.2	-	16	34	10	-
SW2	15	4.5	4.1	3.6	4.5	-	29	61	24	-
SW2	16	4.4	4.5	3.6	4.1	-	36	61	24	-
SW2	25	3.9	3.1	1.8	8.0	-	26	32	14	-
SW2	26	2.8	2.9	1.9	7.0	-	22	34	11	-
SW2	27	4.9	3.9	2.6	8.2	-	35	48	20	-
SW2	28	5.0	4.0	2.8	8.4	-	38	64	25	-
SW3	13	3.5	4.3	4.2	3.6	-	23	30	-	5
SW3	14	3.0	3.9	3.5	3.4	-	20	26	-	4
SW3	15	5.3	5.3	6.1	5.4	-	31	36	-	9
SW3	16	4.7	4.3	5.3	4.0	-	23	30	-	14
SW3	25	5.7	2.9	3.6	4.7	-	25	17	-	53
SW3	26	3.4	2.7	2.1	4.4	-	16	15	-	48
SW3	27	6.6	4.5	5.9	7.6	-	37	26	-	137
SW3	28	6.9	5.2	7.9	5.3	-	32	38	-	131

1. Por. = porcelain, Al. = aluminum.
2. Refer to Table 4-2 for information on the test numbers.

4.4 Summary Remarks

Pole A of three disconnect switches was evaluated by static and dynamic testing. Poles from a two-post porcelain horizontal break switch (SW1) a three-post porcelain vertical-break switch (SW2), and a three-post composite vertical break switch (SW3) were studied. The three poles were assembled by members of the project team with assistance from ABB Power T&D Company, Inc., Components Division (ABB), and Pacific Gas and Electric (PG&E) Company engineering staff. Much care was taken in the assembly and mechanical adjustment of the poles and similar care must be taken in the field if the laboratory results presented above are to be used to judge the likely field performance during a severe earthquake.

Modal frequencies in the range of 3 to 8 Hz were recorded for the three poles; damping ratios ranged between 2 and 4 percent of critical. All three poles were tested using earthquake histories with spectra compatible with the IEEE 693-1997 spectra for High Level qualification. No structural damage was observed during these tests and the poles complied with the IEEE 693-997 electrical and functional requirements throughout the testing program.

Figure 4-1 Pull-back testing of pole SW1

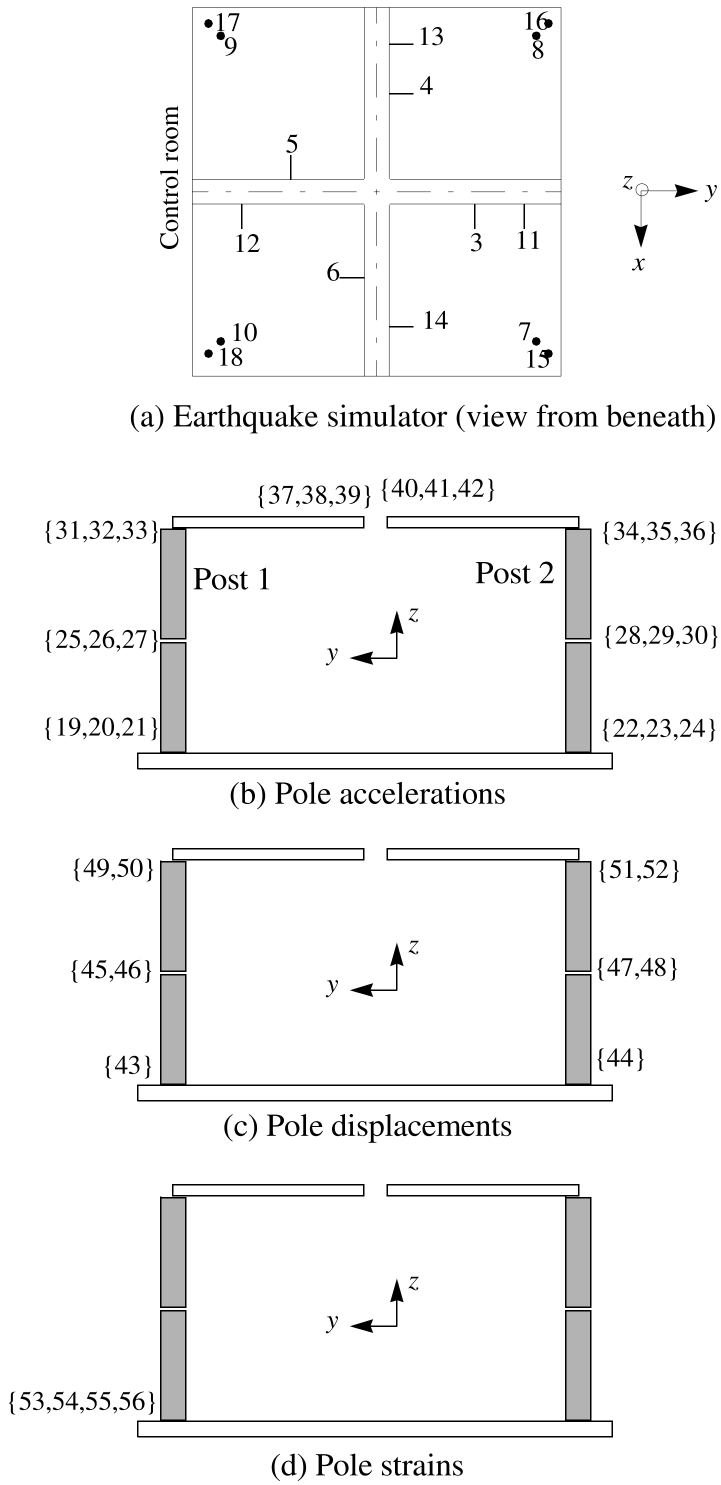

Figure 4-2 Instrumentation for pole SW1

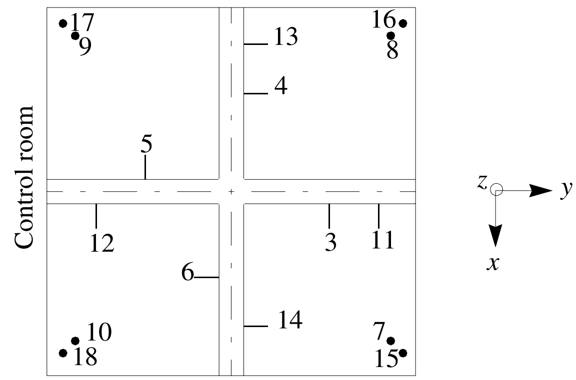

(a) Earthquake simulator (view from beneath)

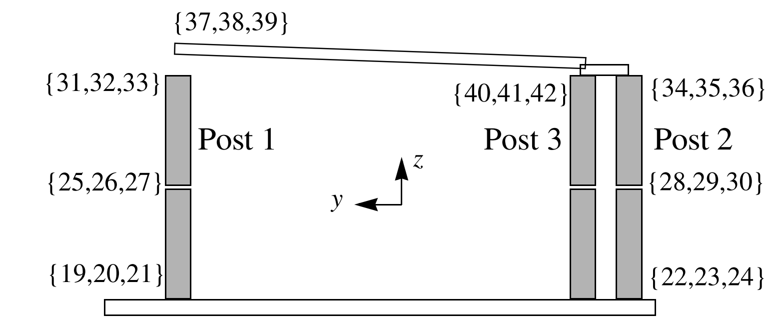

(b) Pole accelerations

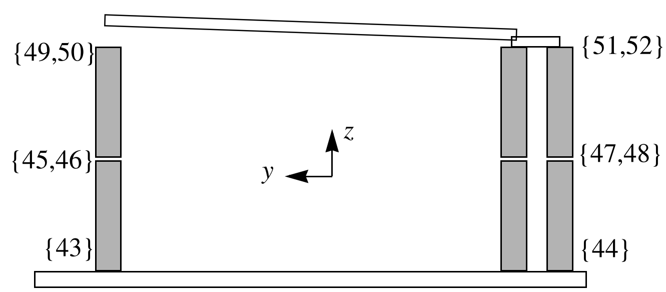

(c) Pole displacements

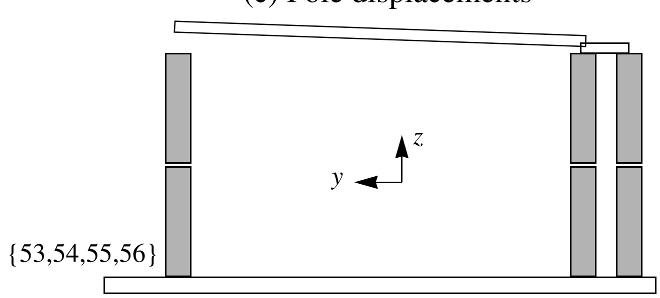

(d) Pole strains

Figure 4-3 Instrumentation for pole SW2

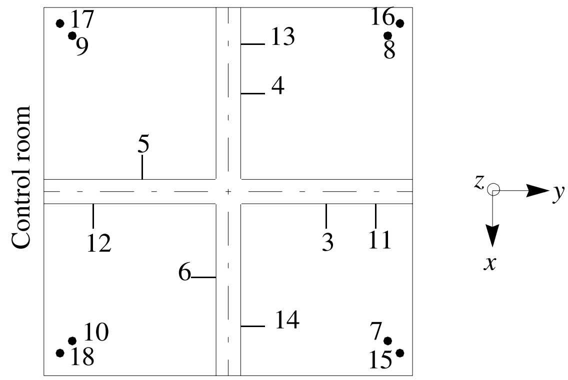

(a) Earthquake simulator (view from beneath)

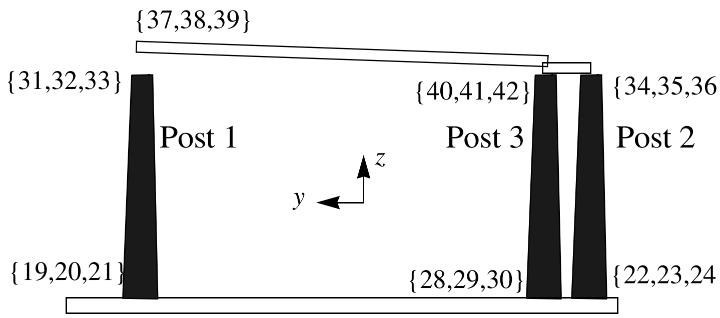

(b) Pole accelerations

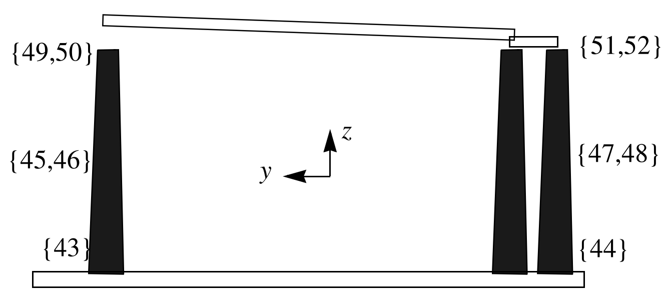

(c) Pole displacements

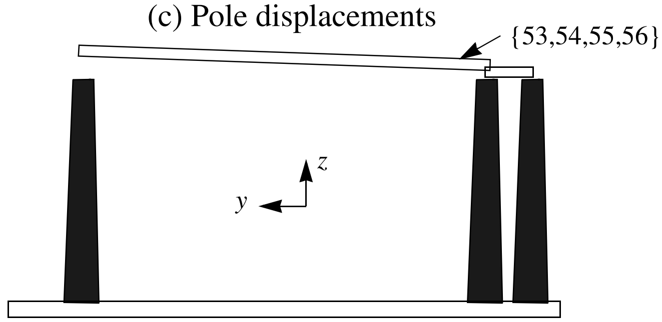

(d) Pole strains

Figure 4-4 Instrumentation for pole SW3

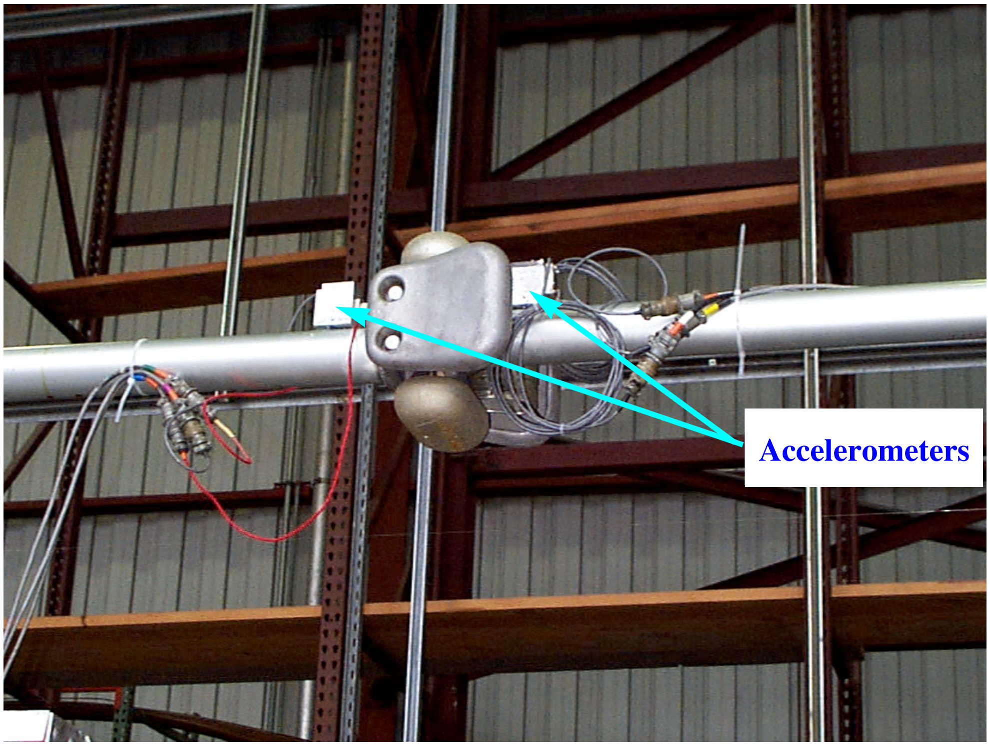

Figure 4-5 Instrumentation of blade tips for pole SW1

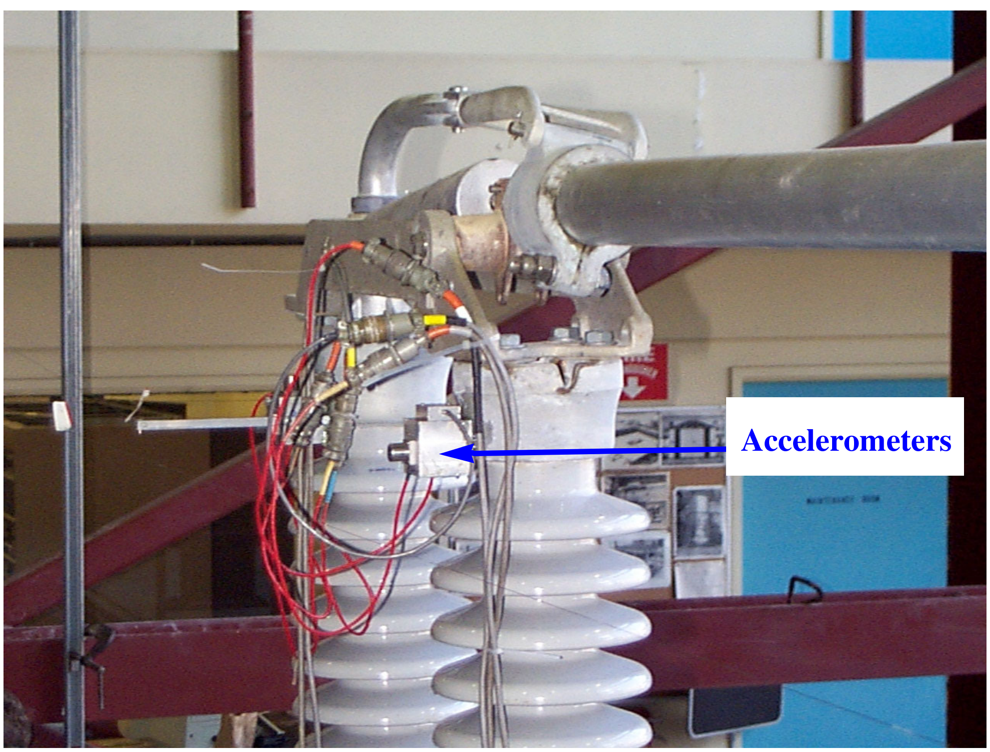

Figure 4-6 Instrumentation of top of posts 2 and 3 for pole SW2

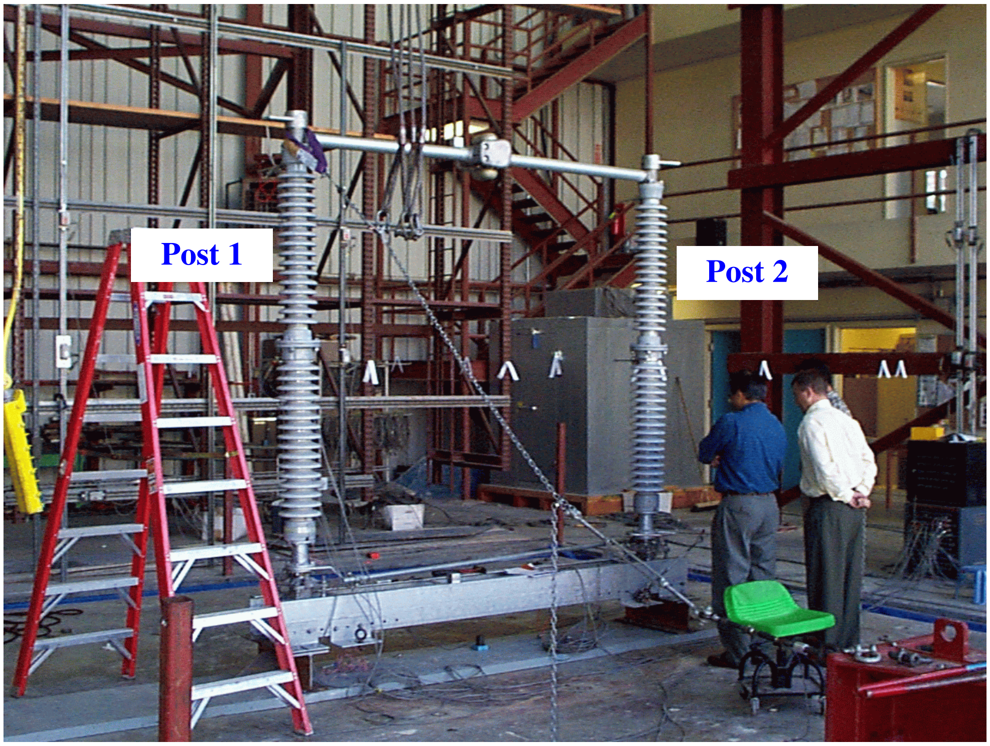

Figure 4-7 Pole A of switch SW1 mounted on the simulator platform

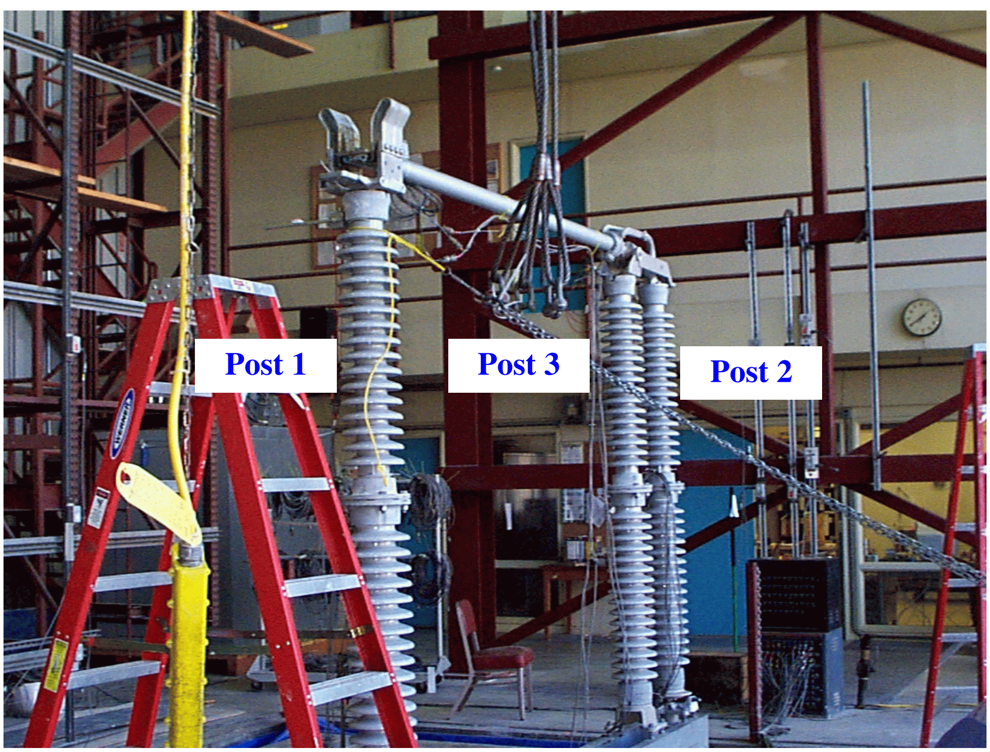

Figure 4-8 Pole A of switch SW2 mounted on the simulator platform

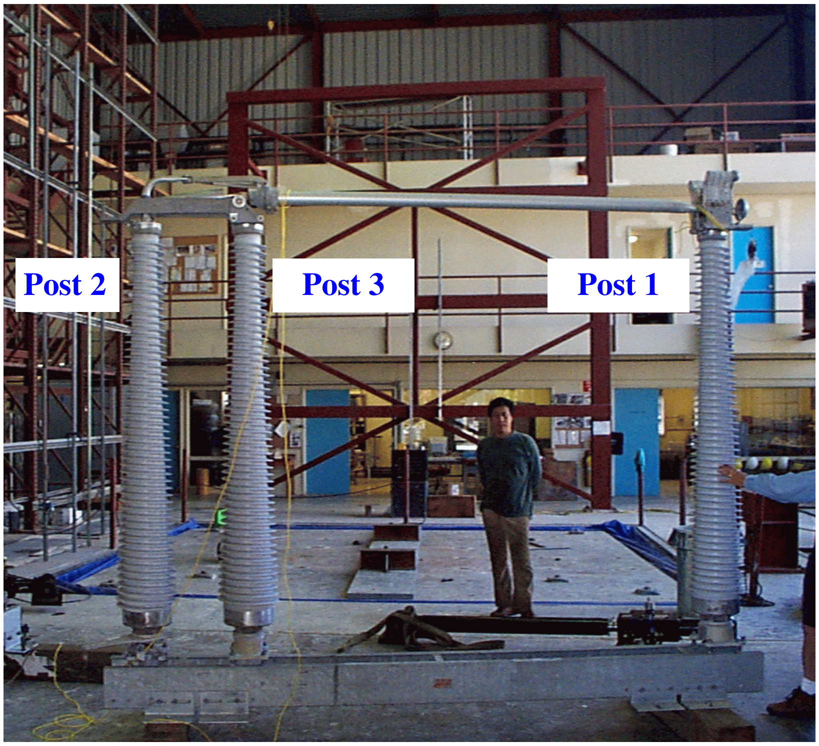

Figure 4-9 Pole A of switch SW3 prior to mounting on the simulator platform

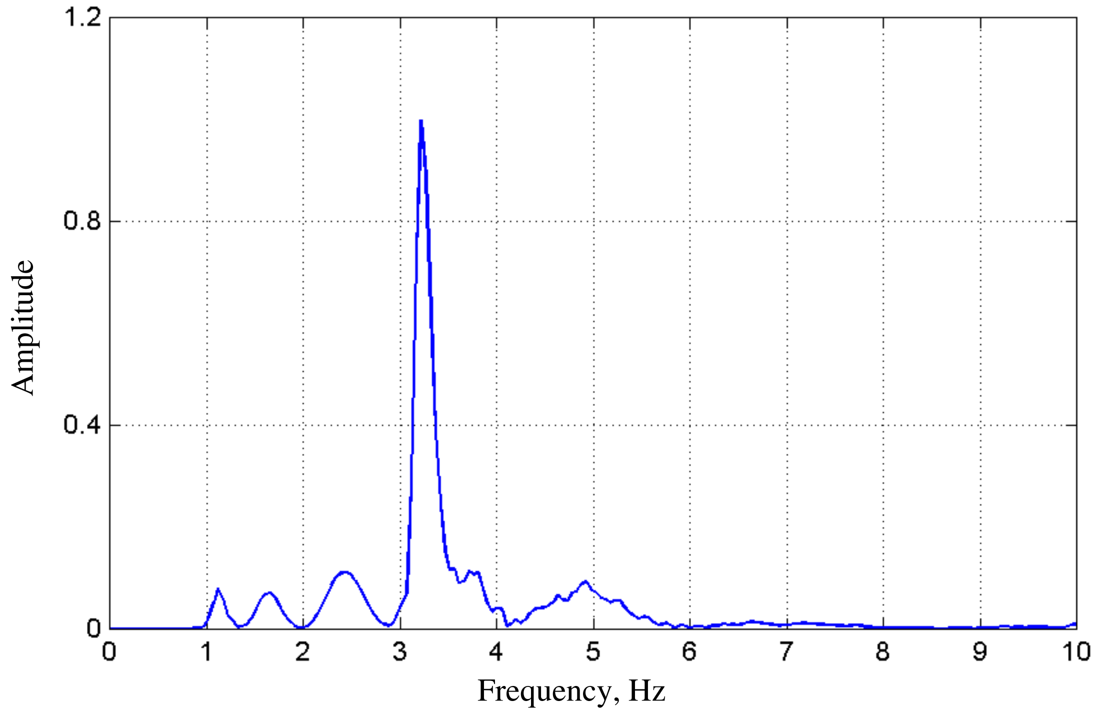

(a) *x*-direction

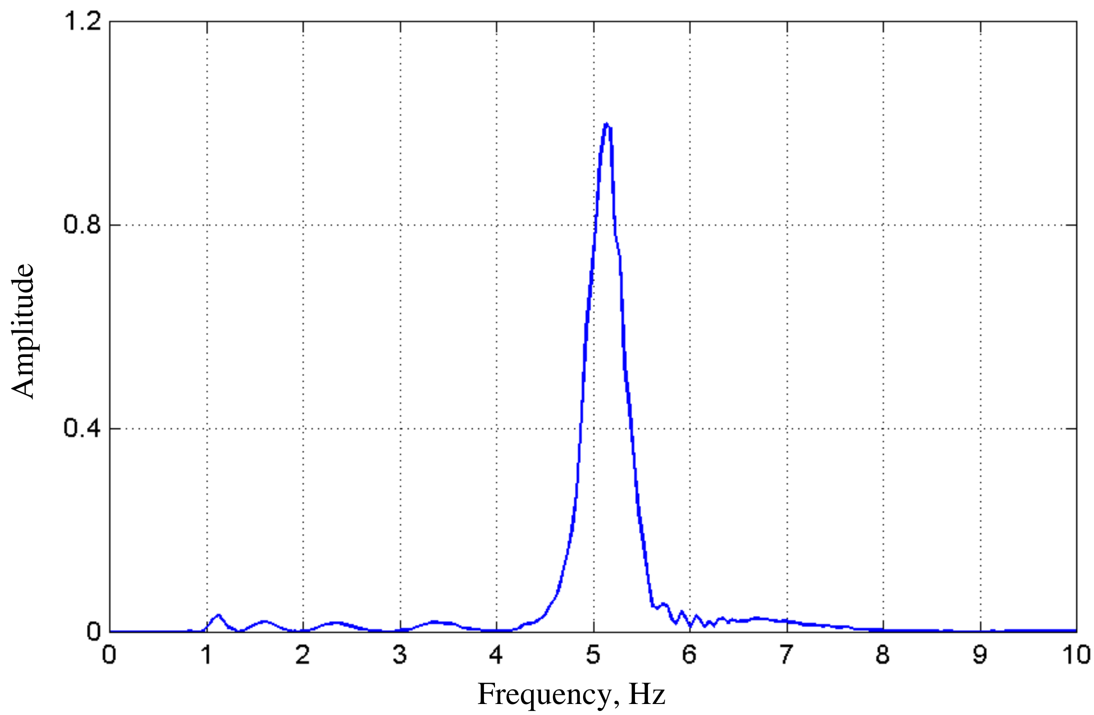

(b) *y*-direction

Figure 4-10 Normalized power spectrum for the top of post 1, SW1, closed blade

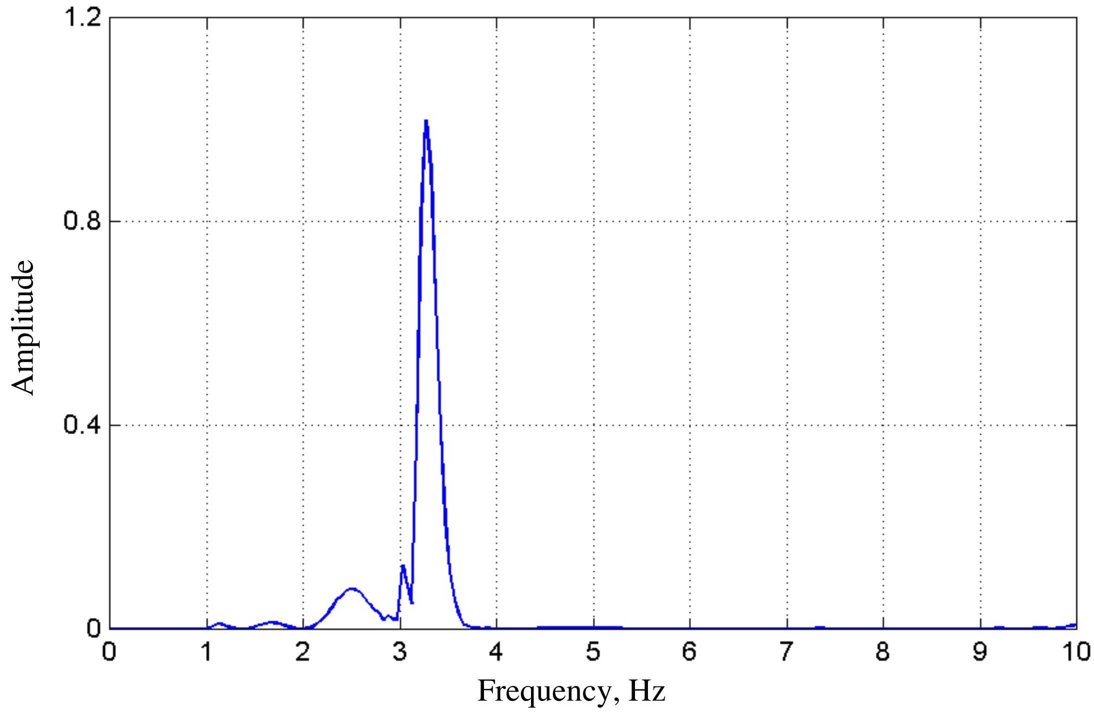

(a) *x*-direction

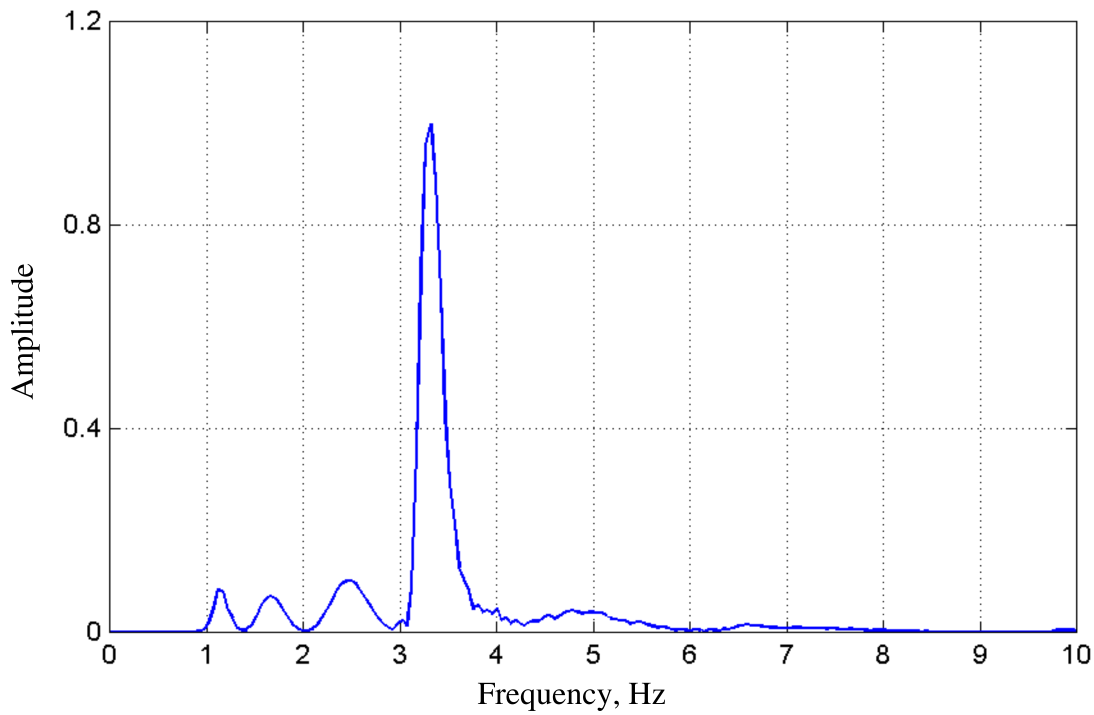

(b) *y*-direction

Figure 4-11 Normalized power spectrum for the top of post 1, SW1, open blade

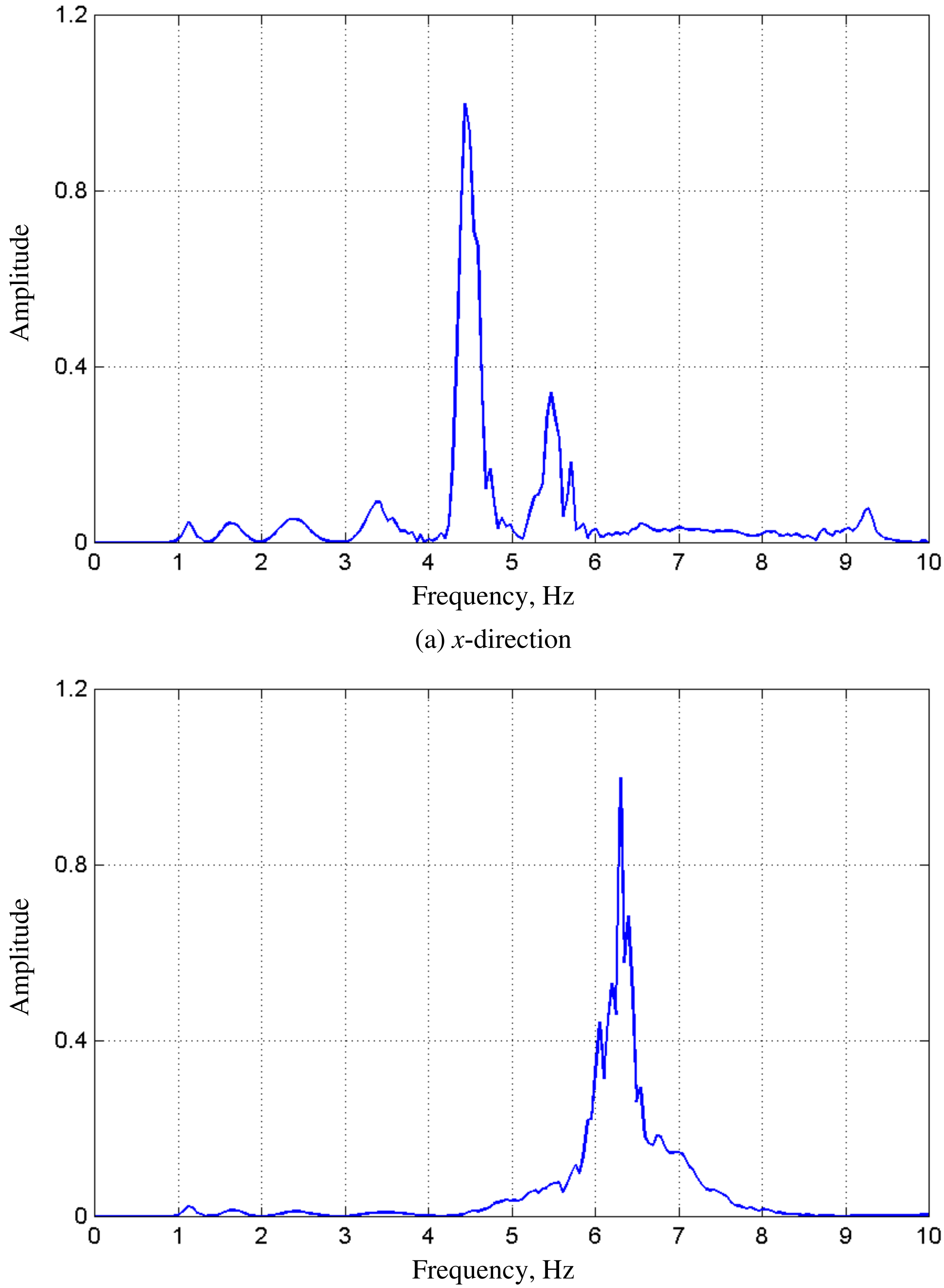

(a) *x*-direction

(b) *y*-direction

Figure 4-12 Normalized power spectrum for the top of post 1, SW2, closed blade

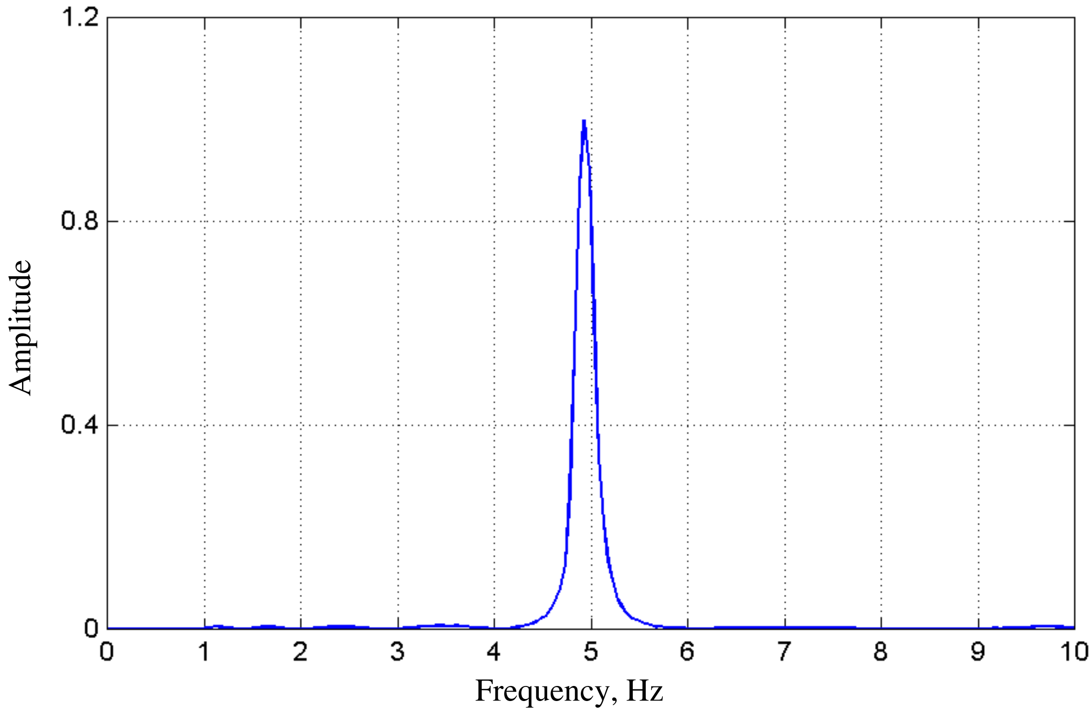

(a) *x*-direction

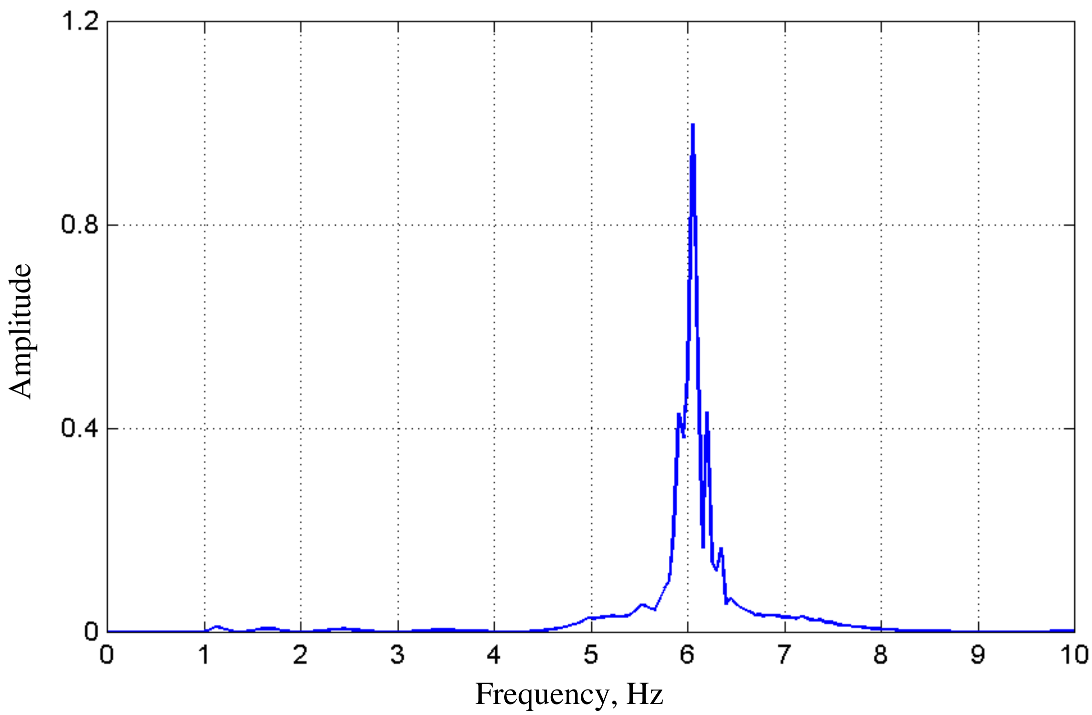

(b) *y*-direction

Figure 4-13 Normalized power spectrum for the top of post 1, SW2, open blade

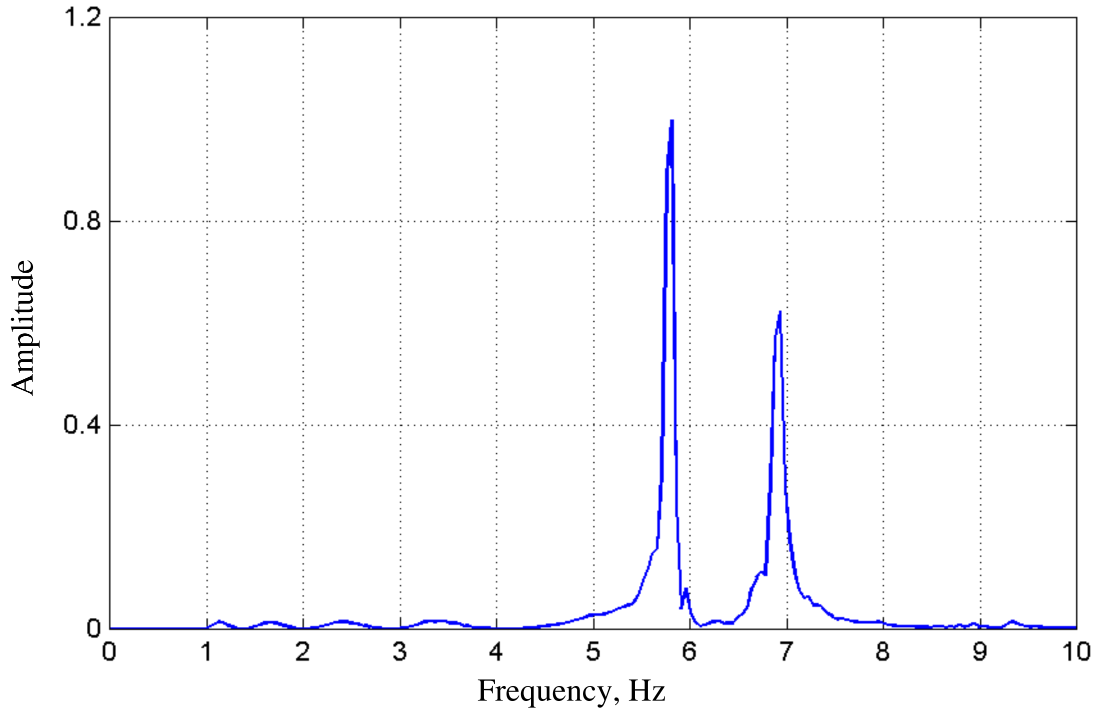

(a) *x*-direction

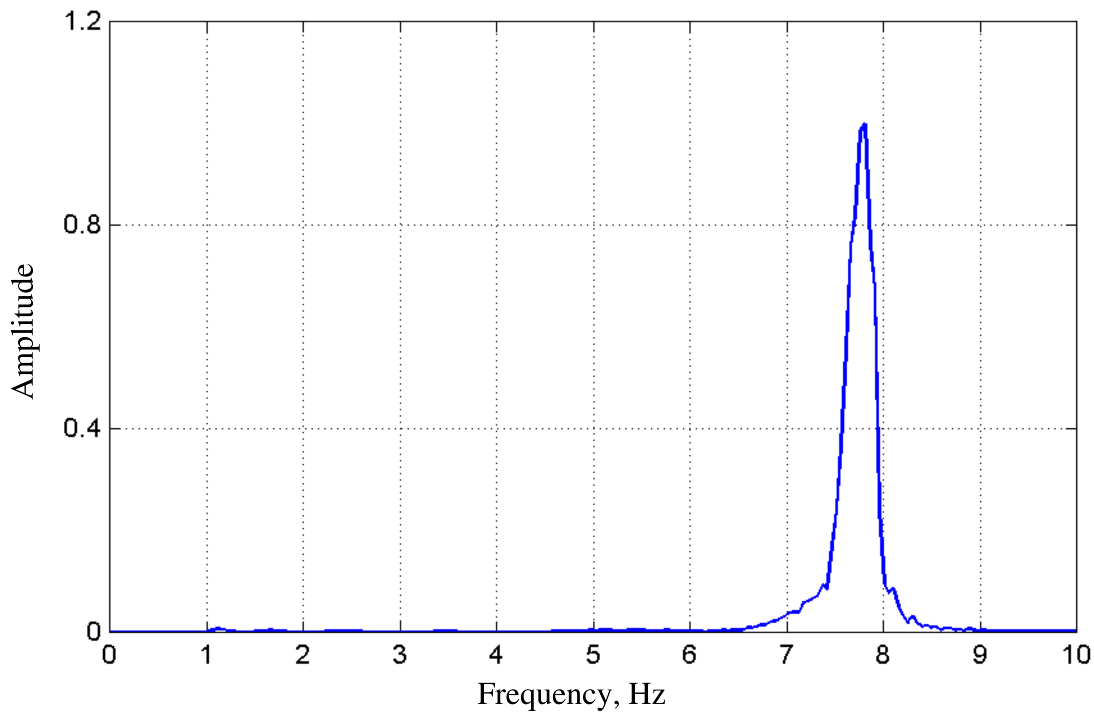

(b) *y*-direction

Figure 4-14 Normalized power spectrum for the top of post 1, SW3, closed blade

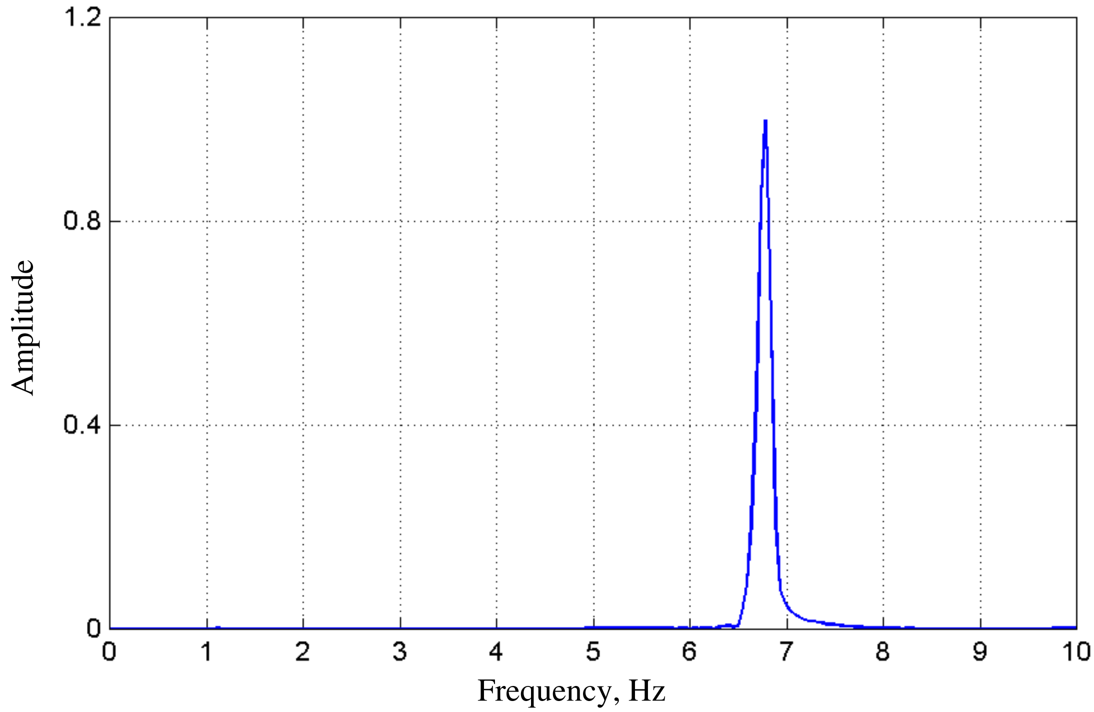

(a) *x*-direction

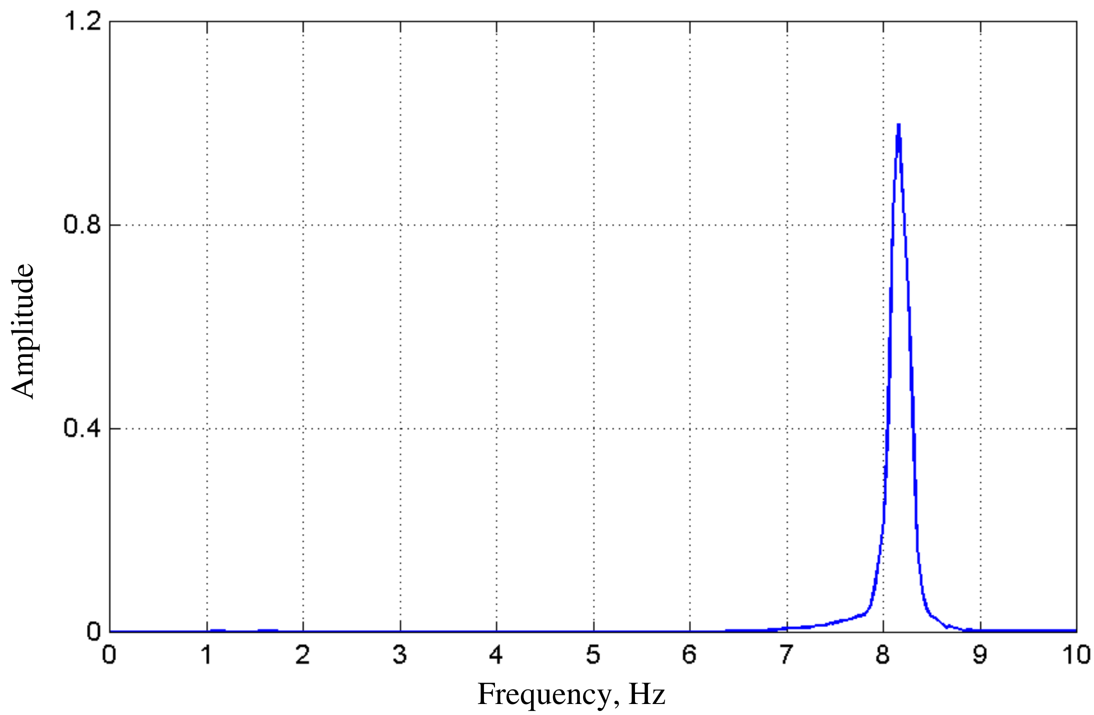

(b) *y*-direction

Figure 4-15 Normalized power spectrum for the top of post 1, SW3, open blade

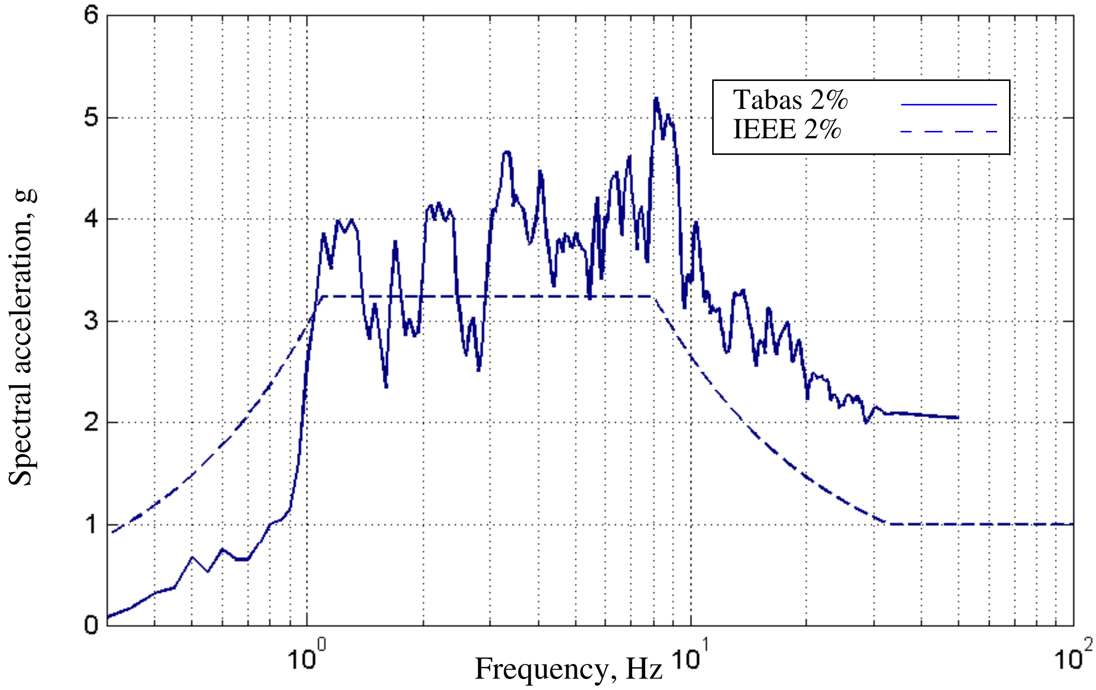

(a) *x*-direction

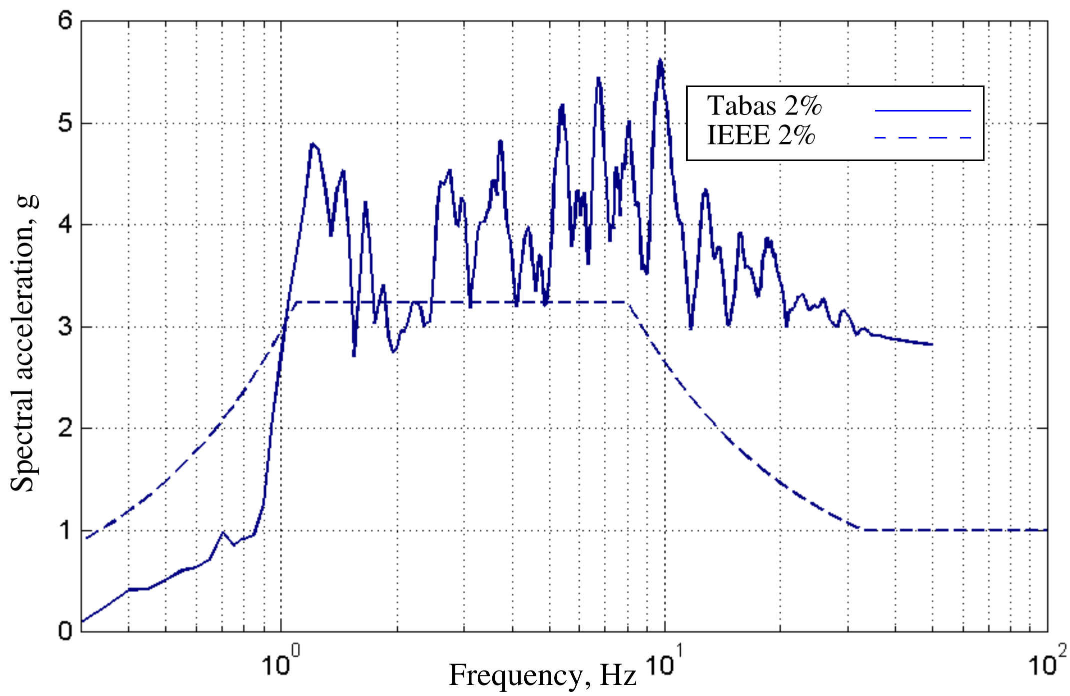

(b) *y*-direction

Figure 4-16 Response spectra for SW1, Tests 15 and 16, closed blade (target PGA equal to 1g)

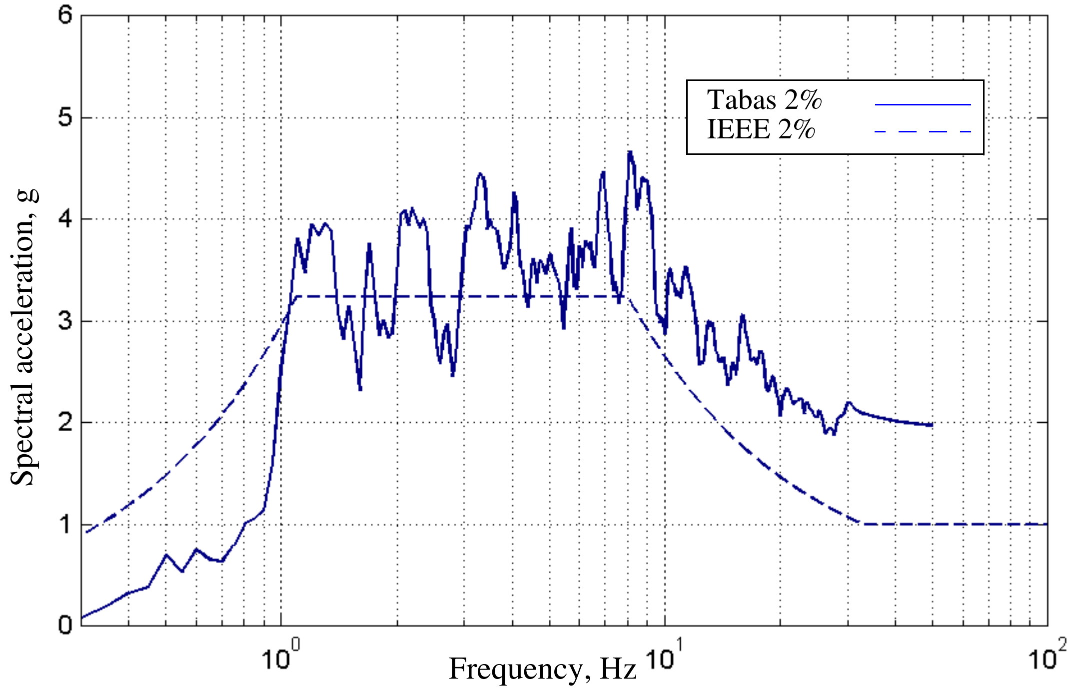

(a) *x*-direction

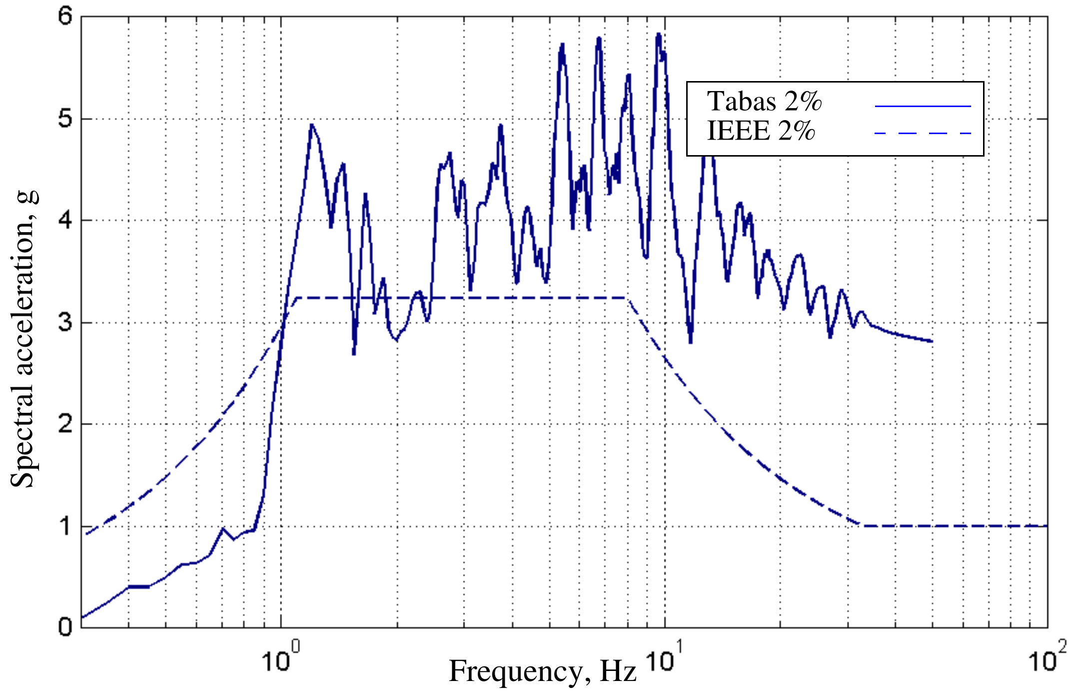

(b) *y*-direction

Figure 4-17 Response spectra for SW2, Tests 15 and 16, closed blade (target PGA equal to 1g)

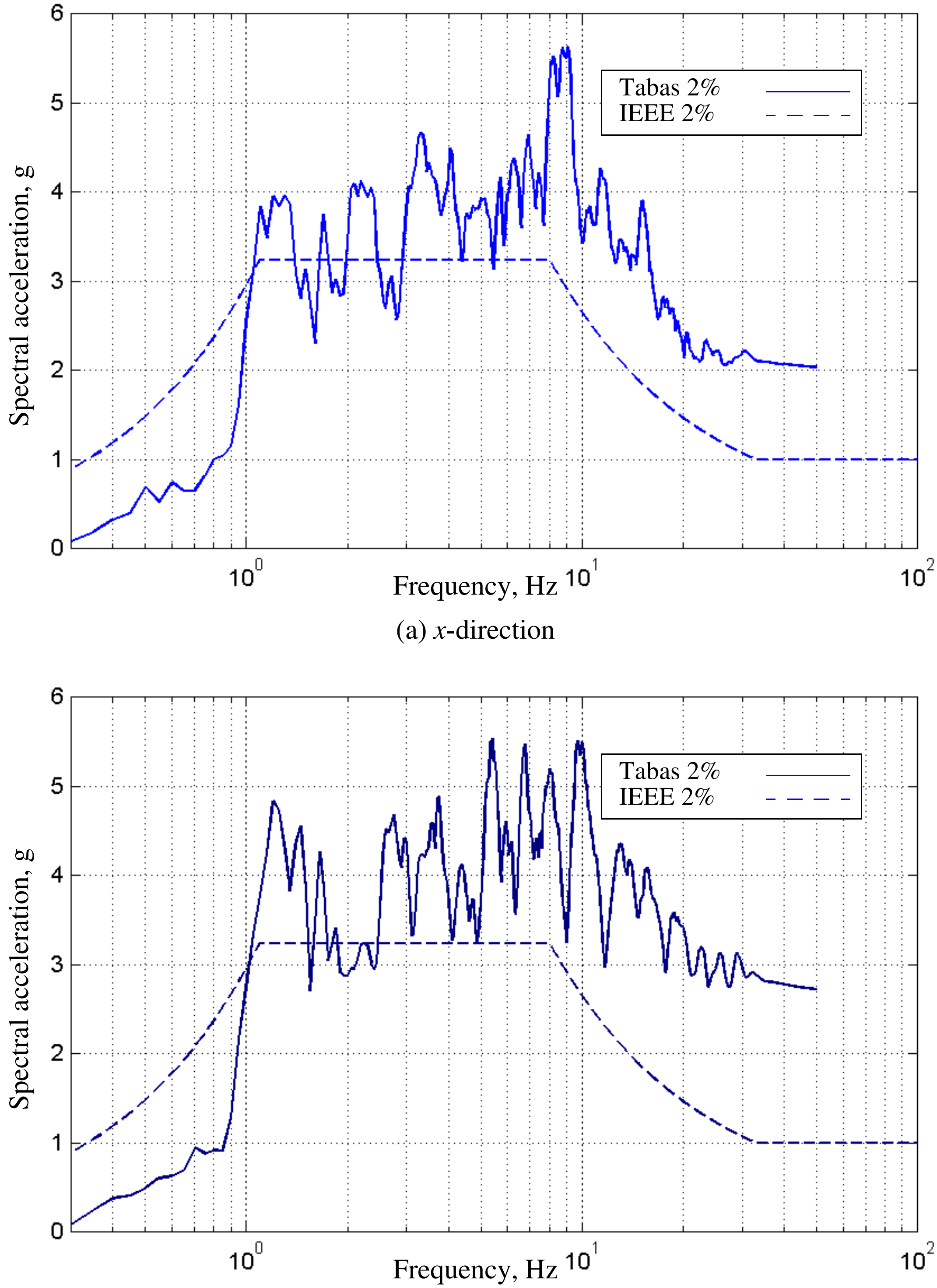

(a) *x*-direction

(b) *y*-direction

Figure 4-18 Response spectra for SW3, Tests 15 and 16, closed blade (target PGA equal to 1g)

5 Seismic Evaluation of Disconnect Switches

5.1 Introduction

Static, harmonic, uniaxial resonant-search, and triaxial earthquake simulator tests were used to evaluate the seismic response of five 230-kV disconnect switches (SW1, SW2, SW2a, SW3, and SW4) and to qualify the switches to the High Level, if possible, per the requirements of IEEE 693-1997. For testing, the switches were mounted on a low-profile braced frame similar to those proposed for new construction. This frame, termed the PEER frame, is described in detail in Chapter 2. Section 5.2 describes the test setup including the instrumentation and the earthquake motions developed for simulator testing. Summary of experimental results and key observations are presented in Section 5.3. A detailed description of the experimental results including response of the PEER frame and the results from the seismic qualification tests are presented in Section 5.4. Section 5.5 provides a summary of key findings.

5.2 Experimental program

5.2.1 Test specimens

Five disconnect switches were evaluated by experimentation. Figures 5-1 through 5-5 show switches SW1, SW2, SW2a, SW3, and SW4 mounted on the PEER frame atop the earthquake simulator. The designation used for the various posts and poles of the disconnect switches, and the coordinate system used in this chapter are shown in Figure 5-6. The key properties of the switches and the base hardware used for each post are tabulated in Table 5-1.

For all switches, the operation of each individual pole (e.g., pole A) was controlled by a crank that was attached to a rotor bearing at the base of post 2. The operation of the switch was controlled by a mechanism that was attached to the double-channel beams at the base of pole B.

Table 5-1 Disconnect switch base hardware

Switch[1]	*Break*	*Insulator*[2]	*Base hardware for posts*[3,4]								
			A1	*A2*	*A3*	*B1*	*B2*	*B3*	*C1*	*C2*	*C3*
SW1	horizontal	porcelain	a	a	-	a	a	-	a	a	-
SW2	vertical	porcelain	b	c	b	b	c	b	b	c	b
SW2a	vertical	porcelain	d	c	d	d	c	d	d	c	d
SW3	vertical	composite	b	c	b	d	c	d	d	c	d
SW4	horizontal	porcelain	a	a	-	a	a	-	a	a	-

1. For SW1, SW2, SW2a, and SW3 all three poles were tested; one pole was tested for SW4.
2. Insulator manufacturers: Locke for SW1, SW2, and SW2a; Sediver for SW3; and Lapp for SW4.
3. a = welded steel spacer mounted on cast aluminum rotor bearing housing, b = cast aluminum spacer, c = cast aluminum rotor bearing housing, d = welded steel spacer. (see Chapter 2 for drawings of various units.)
4. For post designation, see Figure 5-6.

5.2.2 Mounting frame

Disconnect switches are typically mounted on elevated supports in the field. One objective of the studies reported in this chapter was to evaluate the performance of 230-kV disconnect switches mounted on a low-profile braced frame.

The PEER frame was designed to replicate the dynamic properties of a braced frame proposed for future use by PG&E. Similar to in-service frames, the double-channel beams at the base of the switch poles were bolted to the top of W8x31 beams that spanned the short dimension of the PEER frame. Since the PEER and the PG&E frames had nearly identical dynamic properties (see Chapter 2), switches qualified on the PEER frame would be qualified on the PG&E frame.

5.2.3 Testing program

The testing program for switches installed on the PEER frame included static, uniaxial resonant-search tests, triaxial earthquake ground motion tests, and single-frequency harmonic tests. Tests were conducted on switches in open and closed blade configurations. Information on the static, uniaxial resonant-search, and single-frequency harmonic tests follow. Information on the triaxial earthquake history testing is presented in Chapter 3.

Static tests of single poles of switches SW1, SW2, and SW3 were described in Chapter 4. Prior to earthquake-simulator testing of switch SW4, pull-back, quick-release tests were undertaken to characterize the static (stiffness) and dynamic (frequency) of the switch. For the static tests reported in this chapter, the maximum applied force was approximately 0.2 kips (0.9 kN).

The test setup for the static tests consisted of a nylon rope, a load cell, and a machined bolt. During the pull-back stage of the tests, the applied force and displacement at the top of the insulator were monitored. The applied force was then released by cutting the machined bolt. The free vibration response was then recorded. The tests were repeated in both *x*- and *y*- directions with the blade in both the open and closed positions.

Sine-sweep and broadband white-noise tests were used to compute the natural frequencies and damping ratios of the five disconnect switches. These so-called resonant-search tests were undertaken using unidirectional excitation along each global axis of the earthquake-simulator platform. For both sine-sweep and white-noise tests, a simulator input acceleration amplitude of 0.1g was used.

Unidirectional single-frequency harmonic tests were conducted to investigate the response of the switches to harmonic loading. Each test consisted of 40 cycles of sinusoidal motion. The amplitude of the motion was between 0.1 and 0.4g at frequencies of 2, 4, 6, and 8 Hz.

5.2.4 Instrumentation

For seismic testing, IEEE 693-1997 states that the switches must be instrumented to record (a) maximum vertical and horizontal accelerations at the top of the insulators, at the end of the switch blade, and at the top of the earthquake simulator platform, (b) maximum displacement at the top of the insulator and top of the blade, and (c) maximum stresses at the base of the posts and at the base of the support frame. The blades were not instrumented for the tests reported in this chapter. The requirements of (c) assume that the spectra for the qualification tests will match the RRS and that stresses will be compared with 50% of the ultimate values. For the tests described in this chapter, the spectra for the qualification tests were matched to the PL, eliminating the formal requirement to check stresses. See Section 3.2 for more details.

The instrumentation scheme developed for the complete switch tests described in this chapter varied considerably from switch to switch, but consisted of 78 transducers and 80 channels of data. Following the tests of switches SW1 and SW2 and the failures of some cast aluminum components, selected cast aluminum components were instrumented for the tests of switches SW2a, SW3, and SW4. Table 5-2 lists the channel number, instrument type, response quantity, coordinate system, and location for each transducer.

Figure 5-7 presents information on the instrumentation of the earthquake simulator platform (Figure 5-7a), the elevated support (Figure 5-7b), and the switches (Figure 5-7c). The coordinate system adopted for the tests described in this chapter is also shown in the figure. Sixteen channels (channels 3 through 18) recorded the acceleration and displacement of the earthquake simulator platform. The accelerations of the PEER frame (channels 19 through 30) and the absolute displacements of the PEER frame (channels 43 through 47), the accelerations of the switch posts (channels 31 through 42), and absolute displacements of the posts (channels 48 through 59), and the electrical continuity for the three poles (channels 68 through 70) were recorded. The stresses in the porcelain posts, the cast aluminum rotor bearing housings, and the steel spacers were also measured as noted in the table.

Figure 5-8 is a photograph of the instrumentation at the top of the PEER frame. Figure 5-9 shows the instrumentation at top of one of the posts. Figures 5-10 and 5-11 shows the strain gages placed on a porcelain insulator and a cast aluminum rotor bearing housing, respectively.

5.2.5 Preparation of Switches

The switch poles were assembled by the research team. Representatives from PG&E and ABB completed the mechanical adjustment of the switches prior to testing. The bolts at the base of the rotor bearings (Figure 2-11) were adjusted to obtain the full operating range for the individual poles.

The double-channel beams at the base of the poles were bolted to W8x31 beams in the long direction of the PEER frame with four 1/2 in. (13 mm) diameter galvanized steel bolts: a connection identical to in-service connection. Prior to the seismic tests, the length of the inter-pole links were adjusted to synchronize the operation of the poles. To simulate field conditions, the operating mechanism for the poles was locked at the handle (see Figure 5-6) to ensure that its position (open or closed) did not change during the tests.

Much care was taken in the assembly and mechanical adjustment of the switches and similar care must be taken in the field if the laboratory test results presented in this chapter are to be used to judge the likely seismic performance of in-service switches.

5.3 Summary of Test Results

5.3.1 Switch SW1

Switch SW1 was subjected to 35 tests with target peak *ground* accelerations (PGAs) of up to 1.75g. The sequence of tests for switch SW1 and key observations are tabulated in Table 5-3. After Test 24, it was observed that some of the posts were no longer vertical. The nuts in the rotor bearings and the bolts connecting the posts to the double-channel beams were retightened and the posts were realigned. During Test 29 (Tabas-1, target PGA equal to 1.50g), the attachment at the tip of blade and the welded post-blade connection for post B2 fractured (see Figure 5-12). During Test 31 (Tabas-1, target PGA equal to 1.50g), the cast aluminum rotor bearing housings at the base of posts B1 and B2 fractured (see Figure 5-13) causing the posts to tilt (see Figure 5-14). At the conclusion of this test, Pole B was removed and testing was continued with poles A and C only. During Test 34 (Tabas-2, target PGA equal to 1.75g), the attachment at the tip of blade and the welded post-blade connection for post A2 fractured. The cast aluminum rotor bearing housings at the base of post A1, A2, and C2 fractured and post C2 tilted during Test 35 (Tabas-1, target PGA equal to 1.75g).

Table 5-2 Instrumentation for seismic tests of 230-kV switches

No	*Transducer*[1]	*Response*	*Orientation*[2,3]	*Transducer Location*[4]				
				SW1	*SW2*	*SW2a*	*SW3*	*SW4*
1	-	-	-	-				
2	-	-	-	-				
3	LVDT	displacement	*x*	simulator platform				
4	LVDT	displacement	*y*	simulator platform				
5	LVDT	displacement	*x*	simulator platform				
6	LVDT	displacement	*y*	simulator platform				
7	LVDT	displacement	*z*	simulator platform				
8	LVDT	displacement	*z*	simulator platform				
9	LVDT	displacement	*z*	simulator platform				
10	LVDT	displacement	z	simulator platform				
11	A	acceleration	*x*	simulator platform				
12	A	acceleration	*x*	simulator platform				
13	A	acceleration	*y*	simulator platform				
14	A	acceleration	*y*	simulator platform				
15	A	acceleration	*z*	simulator platform				
16	A	acceleration	*z*	simulator platform				
17	A	acceleration	*z*	simulator platform				
18	A	acceleration	z	simulator platform				
19	A	acceleration	*x*	support frame, base of A1				
20	A	acceleration	*y*	support frame, base of A1				
21	A	acceleration	*x*	support frame, base of A2				
22	A	acceleration	*y*	support frame, base of A2				
23	A	acceleration	*x*	support frame, base of B1				
24	A	acceleration	*y*	support frame, base of B1				
25	A	acceleration	*x*	support frame, base of B2				
26	A	acceleration	*y*	support frame, base of B2				
27	A	acceleration	*x*	support frame, base of C1				
28	A	acceleration	*y*	support frame, base of C1				
29	A	acceleration	*x*	support frame, base of C2				
30	A	acceleration	*y*	support frame, base of C2				
31	A	acceleration	*x*	top of post A1				-
32	A	acceleration	*y*	top of post A1				-

Table 5-2 Instrumentation for seismic tests of 230-kV switches

No	*Transducer*[1]	*Response*	*Orientation*[2,3]	*Transducer Location*[4]				
				SW1	*SW2*	*SW2a*	*SW3*	*SW4*
33	A	acceleration	x	top of post A2				-
34	A	acceleration	y	top of post A2				-
35	A	acceleration	x	top of post B1				-
36	A	acceleration	y	top of post B1				-
37	A	acceleration	x	top of post B2				-
38	A	acceleration	y	top of post B2				-
39	A	acceleration	x	top of post C1				
40	A	acceleration	y	top of post C1				
41	A	acceleration	x	top of post C2				
42	A	acceleration	y	top of post C2				
43	LP	displacement	x	support frame, base of A1				
44	LP	displacement	x	support frame, base of A2				
45	LP	displacement	y	support frame, base of A2				
46	LP	displacement	y	support frame, base of B2				
47	LP	displacement	y	support frame, base of C2				
48	LP	displacement	x	top of post A1				-
49	LP	displacement	y	top of post A1				-
50	LP	displacement	x	top of post A2				-
51	LP	displacement	y	top of post A2				-
52	LP	displacement	x	top of post B1				-
53	LP	displacement	y	top of post B1				-
54	LP	displacement	x	top of post B2				-
55	LP	displacement	y	top of post B2				-
56	LP	displacement	x	top of post C1				
57	LP	displacement	y	top of post C1				
58	LP	displacement	x	top of post C2				
59	LP	displacement	y	top of post C2				
60	SG	strain-p[5]	-	bottom of post A1			-	
61	SG	strain-p	-	bottom of post A1			-	
62	SG	strain-p	-	bottom of post A1			-	
63	SG	strain-p	-	bottom of post A1			-	
64	SG	strain-p	-	bottom of post B2			-	

Table 5-2 Instrumentation for seismic tests of 230-kV switches

<table>
<tr><th rowspan="2">No</th><th rowspan="2">Transducer[1]</th><th rowspan="2">Response</th><th rowspan="2">Orientation[2,3]</th><th colspan="5">Transducer Location[4]</th></tr>
<tr><th>SW1</th><th>SW2</th><th>SW2a</th><th>SW3</th><th>SW4</th></tr>
<tr><td>65</td><td>SG</td><td>strain-p</td><td>-</td><td colspan="3">bottom of post B2</td><td colspan="2">-</td></tr>
<tr><td>66</td><td>SG</td><td>strain-p</td><td>-</td><td colspan="3">bottom of post B2</td><td colspan="2">-</td></tr>
<tr><td>67</td><td>SG</td><td>strain-p</td><td>-</td><td colspan="3">bottom of post B2</td><td colspan="2">-</td></tr>
<tr><td>68</td><td>DM</td><td>current</td><td>-</td><td colspan="4">electrical connectivity for pole A</td><td>-</td></tr>
<tr><td>69</td><td>DM</td><td>current</td><td>-</td><td colspan="4">electrical connectivity for pole B</td><td>-</td></tr>
<tr><td>70</td><td>DM</td><td>current</td><td>-</td><td colspan="5">electrical connectivity for pole C</td></tr>
<tr><td>71</td><td>SG</td><td>strain-a[5]</td><td>-</td><td>-</td><td colspan="3">base of post A2</td><td></td></tr>
<tr><td>72</td><td>SG</td><td>strain-a</td><td>-</td><td>-</td><td colspan="3">base of post A2</td><td></td></tr>
<tr><td>73</td><td>SG</td><td>strain-a</td><td>-</td><td>-</td><td colspan="3">base of post B2</td><td></td></tr>
<tr><td>74</td><td>SG</td><td>strain-a</td><td>-</td><td>-</td><td colspan="3">base of post B2</td><td></td></tr>
<tr><td>75</td><td>SG</td><td>strain-a</td><td>-</td><td>-</td><td colspan="4">base of post C2</td></tr>
<tr><td>76</td><td>SG</td><td>strain-a</td><td>-</td><td>-</td><td colspan="4">base of post C2</td></tr>
<tr><td>77</td><td>SG</td><td>strain-s[5]</td><td>-</td><td colspan="2">-</td><td>B3</td><td>A3</td><td>C2</td></tr>
<tr><td>78</td><td>SG</td><td>strain-s</td><td>-</td><td colspan="2">-</td><td>B3</td><td>A3</td><td>C2</td></tr>
<tr><td>79</td><td>SG</td><td>strain-s</td><td>-</td><td colspan="2">-</td><td>B3</td><td>A3</td><td>C2</td></tr>
<tr><td>80</td><td>SG</td><td>strain-s</td><td>-</td><td colspan="2">-</td><td>B3</td><td>A3</td><td>C2</td></tr>
</table>

1. A = accelerometer; LVDT = displacement transducer; LP = linear potentiometer; SG = strain gage; DM = digital meter.
2. For the global (x-, y-, and z-) coordinate systems, see Figure 5-6
3. The specified directions for the accelerometers mounted on the insulators and blades are for the closed blade position. The accelerometers at top of all the posts for horizontal-break switches, and at top of post 2 for vertical-break switches rotated 90 degrees when the switch was opened. Switch displacements were not recorded for open position.
4. For post locations, see Figure 5-6.
5. Strain-p denotes strain gages at the base of porcelain insulators (see Figure 5-10); Strain-a denotes strain gages placed on the cast aluminum rotor bearing housings (see Figure 5-11); Strain-s denotes strain gages placed on the welded steel spacers.

5.3.2 Switch SW2

Switch SW2 was subjected to 24 tests with target PGAs of up to 1.0g. The sequence of tests for switch SW2 and key observations are tabulated in Table 5-4. During Test 23 (Tabas-1, target PGA equal to 1.0g), the cast aluminum spacer at the base of post B3 cracked (see Figure 5-15). The spacer was removed and a new cast aluminum spacer was installed. Test 23 was repeated (and designated Test 24). The cast aluminum spacer at the base of posts B3 and C3 fractured (see Figure 5-16) during this test. Testing of SW2 was terminated at that time. New welded steel spacers were fabricated by ABB and shipped to U.C. Berkeley as substitutes for the cast aluminum spacers. The retrofitted switch SW2 was designated SW2a.

5.3.3 Switch SW2a

Switch SW2a was subjected to 53 tests with target PGAs of up to 2.0g. The sequence of tests for switch SW2a and key observations are tabulated in Table 5-5. During Test 47 (Tabas-1, target PGA equal to 1.75g), the cast aluminum counterweight at the top of post C3 fractured (see Figure 5-17). The counterweight was removed, a new cast aluminum counterweight was installed, and the test was repeated. During Tests 50 through 53 (target PGA equal to 2.0g), there was large deformation in the flanges of the double-channel beams and the angles connecting the poles to the PEER frame. Post-test inspection of these connections showed that many of the attachment bolts were badly damaged as seen in Figure 5-18.

5.3.4 Switch SW3

Switch SW3 was subjected to 58 tests with target PGAs of up to 2.0g. The sequence of tests for switch SW3 and key observations are tabulated in Table 5-6. During Test 18 (Tabas-1, target PGA equal to 0.5g), the pin connecting the piston to the counterweight at the top of post B dislodged, as seen in Figure 5-19. The pin was reinstalled, a cotter pin was used to secure the pin, and the test was repeated.

During Tests 39 through 42, the inter-pole links and the aluminum pipe connecting post B2 to the switch operation hardware (see Figure 5-6) were disconnected and the poles were individually locked in position using turnbuckles attached to the double-channel beams at the base of the poles (see Figure 5-20). Tests at a target PGA of 0.5g were then repeated to investigate the effect of the switch operation mechanism on the response.

There was no visible structural damage to the switch during testing. However, post-test inspections following Test 58 revealed that the cast aluminum spacers at base of poles B3 and C3 had fractured (see Figure 5-21).

5.3.5 Switch SW4

Switch SW4 was subjected to 36 tests with target PGAs of up to 3.0g. The sequence of tests for switch SW4 and key observations are tabulated in Table 5-7. During Test 25 (Tabas-2, target PGA equal to 1.0g), the welded post-blade connection for post C2 fractured (see Figure 5-22). Testing was continued but the blade was not replaced. The cast aluminum rotor bearing at base of post C2 fractured (see Figure 5-23) during Test 36 (Tabas-2, target PGA equal to 3.0g).

Table 5-3 Sequence of tests for disconnect switch SW1

Test	*Description*[1]	*PGA*[2] *(g)*	*Blade position*	*Comments*
1	WN-*x*	0.1	Closed	
2	WN-*y*	0.1	Closed	
3	SS-*x*	0.1	Closed	
4	SS-*y*	0.1	Closed	
5	Tabas-1	0.1	Closed	
6	Tabas-2	0.1	Closed	
7	Tabas-1	0.5	Closed	
8	Tabas-2	0.5	Closed	
9	OS2-*x*	0.4	Closed	
10	OS2-*y*	0.4	Closed	
11	WN-*x*	0.1	Open	
12	WN-*y*	0.1	Open	
13	SS-*x*	0.1	Open	
14	SS-*y*	0.1	Open	
15	Tabas-1	0.1	Open	
16	Tabas-2	0.1	Open	
17	Tabas-1	0.5	Open	
18	Tabas-2	0.5	Open	
19	OS2-*x*	0.4	Open	
20	OS2-*y*	0.4	Open	
21	Tabas-1	1.0	Closed	Target spectrum equivalent to High Level qualification on stiff frame.
22	Tabas-2	1.0	Closed	
23	Tabas-1	1.0	Open	
24	Tabas-2	1.0	Open	
25	Tabas-1	1.25	Closed	
26	Tabas-2	1.25	Closed	Filter points and simulator span settings adjusted following Test 26.
27	Tabas-1	1.25	Open	
28	Tabas-2	1.25	Open	
29	Tabas-1	1.50	Closed	Failure of welded connections at the blade tip and blade-post for post B2; see Figure 5-12.
30	Tabas-2	1.50	Closed	

Table 5-3 Sequence of tests for disconnect switch SW1

31	Tabas-1	1.50	Open	Fracture of cast aluminum rotor bearings at base of posts B1 and B2; see Figure 5-13.
33	Tabas-1	1.75	Closed	
34	Tabas-2	1.75	Closed	Failure of welded connections at the blade tip and blade-post for post A2.
35	Tabas-1	1.75	Open	Fracture of cast aluminum rotor bearings at base of posts A1, A2, and C2.

1. WN = white-noise, SS = sine-sweep; *-x, -y*, and *-z* denote direction of testing; Tabas-1 and Tabas-2 = part spectrum-compatible earthquake histories; OSn = single-frequency harmonic test at frequency of n Hz.
2. PGA = target peak acceleration of the simulator platform.

5.4 Experimental Results

5.4.1 General

For all tests, the transducer response histories were processed using the computer program Matlab (Mathworks 1999). Experimental histories were low-pass filtered using a rectangular filter with a cut-off frequency of 30 Hz and then zero-corrected. After each earthquake test, the response data were analyzed, the switch was inspected for damage, and the bolts were checked for tightness. The following sections summarize the dynamic properties and the seismic response of the PEER frame and the switches.

5.4.2 Response of the PEER frame

The response of the PEER frame was evaluated by analyzing the data from the resonant-search tests and an earthquake test with target PGA equal to 1.0g. Data from sine-sweep tests of the PEER frame alone were used to compute the frequencies of the PEER frame. Modal properties could not be computed in the longitudinal direction of the PEER frame (coinciding with the *x*-direction of the simulator of Figure 5-6) because the frequency of the frame in this direction exceeded the maximum resonant-search frequency (33 Hz). The frequency of the frame in the lateral direction of the PEER frame (coinciding with the *y*-direction of the simulator of Figure 5-6) was 22 Hz and was similar to the analytical and quick-release frequencies of 26 and 24 Hz, respectively, that were presented in Table 2-3.

Data from Test 21 of switch SW1 (Tabas-1, target PGA equal to 1.0g) were used to characterize the amplification of the earthquake shaking from the simulator platform to the base of the switches. Figure 5-24 shows the acceleration response of the PEER frame and the simulator platform for a two-second response segment. Although the PEER frame does not amplify the simulator platform acceleration in the *x*-direction, it appears that there is significant amplification of input acceleration in the *y*-direction. However, this amplification occurs at high frequencies close to the resonant frequency of the frame. Figure 5-25 shows the displacement response of the frame and the simulator platform for a 10 sec response segment. The deformation in the PEER

Table 5-4 Sequence of tests for disconnect switch SW2

Test	*Description*[1]	*PGA*[2] *(g)*	*Blade position*	*Comments*
1	WN-*x*	0.1	Closed	
2	WN-*y*	0.1	Closed	
3	SS-*x*	0.1	Closed	
4	SS-*y*	0.1	Closed	
5	Tabas-1	0.1	Closed	
6	Tabas-2	0.1	Closed	
7	Tabas-1	0.5	Closed	Filter points and simulator span settings used for Tabas-1.
8	Tabas-2	0.5	Closed	
9	OS2-*x*	0.4	Closed	
10	OS2-*y*	0.4	Closed	
11	WN-*x*	0.1	Open	
12	WN-*y*	0.1	Open	
13	SS-*x*	0.1	Open	
14	SS-*y*	0.1	Open	
15	Tabas-1	0.1	Open	
16	Tabas-2	0.1	Open	
17	Tabas-1	0.5	Open	
18	Tabas-2	0.5	Open	
19	OS2-*x*	0.4	Open	
20	OS2-*y*	0.4	Open	
21	Tabas-1	1.0	Closed	
22	Tabas-2	1.0	Closed	
23	Tabas-1	1.0	Open	Fracture of cast aluminum spacer at base of post B3; see Figure 5-15.
24	Tabas-1	1.0	Open	Fracture of cast aluminum spacer at base of posts B3 and C3; see Figure 5-16.

1. WN = white-noise, SS = sine-sweep; *-x, -y*, and *-z* denote direction of testing; Tabas-1 and Tabas-2 = part spectrum-compatible earthquake histories; OSn = single-frequency harmonic test at frequency of n Hz.
2. PGA = target peak acceleration of the simulator platform.

Table 5-5 Sequence of tests for disconnect switch SW2a

Test	*Description*[1]	*PGA*[2] *(g)*	*Blade position*	*Comments*
1	WN-*x*	0.1	Closed	
2	WN-*y*	0.1	Closed	
3	SS-*x*	0.1	Closed	
4	SS-*y*	0.1	Closed	
5	Tabas-1	0.1	Closed	
6	Tabas-2	0.1	Closed	
7	Tabas-1	0.5	Closed	
8	Tabas-2	0.5	Closed	
9	OS2-*x*	0.1	Closed	
10	OS2-*y*	0.1	Closed	
11	WN-*x*	0.1	Open	
12	WN-*y*	0.1	Open	
13	SS-*x*	0.1	Open	
14	SS-*y*	0.1	Open	
15	Tabas-1	0.1	Open	
16	Tabas-2	0.1	Open	
17	Tabas-1	0.5	Open	
18	Tabas-2	0.5	Open	
19	OS2-*x*	0.1	Open	
20	OS2-*y*	0.1	Open	
21	Tabas-1	1.0	Closed	Target spectrum equivalent to High Level qualification on stiff frame.
22	Tabas-2	1.0	Closed	
23	Tabas-1	1.0	Open	
24	Tabas-1	1.0	Open	
25	OS4-*x*	0.1	Closed	
26	OS4-*y*	0.1	Closed	
27	OS6-*x*	0.1	Closed	
28	OS6-*y*	0.1	Closed	
29	OS8-*x*	0.1	Closed	
30	OS8-*y*	0.1	Closed	
31	OS4-*x*	0.1	Open	
32	OS4-*y*	0.1	Open	

Table 5-5 Sequence of tests for disconnect switch SW2a

33	OS6-*x*	0.1	Open	
34	OS6-*y*	0.1	Open	
35	OS8-*x*	0.1	Open	
36	OS8-*y*	0.1	Open	
37	Tabas-1	1.25	Closed	The filter points and span settings for Tabas-1 input histories were changed following Test 37.
38	Tabas-2	1.25	Closed	
39	Tabas-1	1.25	Open	
40	Tabas-2	1.25	Open	
41	Tabas-1	1.50	Closed	
42	Tabas-2	1.50	Closed	
43	Tabas-1	1.50	Open	
44	Tabas-2	1.50	Open	
45	Tabas-1	1.75	Closed	
46	Tabas-2	1.75	Closed	
47	Tabas-1	1.75	Open	Fracture of cast aluminum counterweight at top of post C3; see Figure 5-17.
48	Tabas-1	1.75	Open	
49	Tabas-2	1.75	Open	
50	Tabas-1	2.0	Closed	Deformation in the flanges of the double-channel beams and the connection angles, and damage to the attachment bolts; see Figure 5-18.
51	Tabas-2	2.0	Closed	
52	Tabas-1	2.0	Open	
53	Tabas-2	2.0	Open	

1. WN = white-noise, SS = sine-sweep; *-x*, *-y*, and *-z* denote direction of testing; Tabas-1 and Tabas-2 = part spectrum-compatible earthquake histories; OSn = single-frequency harmonic test at frequency of n Hz.
2. PGA = target peak acceleration of the simulator platform.

frame is small in both the longitudinal (*x*-) and lateral (*y*-) directions. The horizontal in-plane rigidity of the PEER frame was examined by comparing the displacement responses of the frame as shown in Figure 5-26. Both the *x*- and *y*-components of displacement are identical at different locations on the frame, indicating that there is no significant torsion of the frame. Accordingly, the lateral and torsional stiffness in the PEER frame were sufficiently large so that (1) the input motions at the bases of the switches were not amplified in the range of switch frequencies, and (2) the individual poles and posts were subjected to identical excitation during testing.

Table 5-6 Sequence of tests for disconnect switch SW3

Test	*Description*[1]	*PGA*[2] *(g)*	*Blade position*	*Comments*
1	WN-*x*	0.1	Closed	
2	WN-*y*	0.1	Closed	
3	SS-*x*	0.1	Closed	
4	SS-*y*	0.1	Closed	
5	Tabas-1	0.1	Closed	
6	Tabas-2	0.1	Closed	
7	Tabas-1	0.5	Closed	
8	Tabas-1	0.5	Closed	Spectral amplitudes for Test 7 were below the target values, test repeated.
9	Tabas-2	0.5	Closed	
10	OS2-*x*	0.1	Closed	
11	OS2-*y*	0.1	Closed	
12	WN-*x*	0.1	Open	
13	WN-*y*	0.1	Open	
14	SS-*x*	0.1	Open	
15	SS-*y*	0.1	Open	
16	Tabas-1	0.1	Open	
17	Tabas-2	0.1	Open	
18	Tabas-1	0.5	Open	The pin connecting the piston to the counterweight of pole B dislodged; see Figure 5-19; new pin inserted; test repeated.
19	Tabas-1	0.5	Open	
20	Tabas-2	0.5	Open	
21	OS2-*x*	0.1	Open	
22	OS2-*y*	0.1	Open	
23	Tabas-1	1.0	Closed	Target spectrum equivalent to High Level qualification on stiff frame.
24	Tabas-2	1.0	Closed	
25	Tabas-1	1.0	Open	
26	Tabas-1	1.0	Open	
27	OS4-*x*	0.1	Closed	
28	OS4-*y*	0.1	Closed	
29	OS6-*x*	0.1	Closed	

Table 5-6 Sequence of tests for disconnect switch SW3

30	OS6-*y*	0.1	Closed	
31	OS8-*x*	0.1	Closed	
32	OS8-*y*	0.1	Closed	
33	OS4-*x*	0.1	Open	
34	OS4-*y*	0.1	Open	
35	OS6-*x*	0.1	Open	
36	OS6-*y*	0.1	Open	
37	OS8-*x*	0.1	Open	
38	OS8-*y*	0.1	Open	
39	Tabas-1	0.5	Closed	The inter-pole links were disconnected, the poles were attached to the double-channel beams by a turnbuckle similar to the setup used for testing individual poles of Chapter 4; see Figure 5-20.
40	Tabas-2	0.5	Closed	
41	Tabas-1	0.5	Open	
42	Tabas-2	0.5	Open	
43	Tabas-1	1.25	Closed	
44	Tabas-2	1.25	Closed	
45	Tabas-1	1.25	Open	
46	Tabas-2	1.25	Open	
47	Tabas-1	1.50	Closed	
48	Tabas-2	1.50	Closed	
49	Tabas-1	1.50	Open	
50	Tabas-2	1.50	Open	
51	Tabas-1	1.75	Closed	The bolts connecting the double-channel beams to the rotor bearings and spacers were retightened.
52	Tabas-2	1.75	Closed	
53	Tabas-1	1.75	Open	
54	Tabas-2	1.75	Open	
55	Tabas-1	2.0	Closed	Cracking of cast aluminum spacers at base of posts B3 and C3; see Figure 5-21.
56	Tabas-2	2.0	Closed	
57	Tabas-1	2.0	Open	
58	Tabas-2	2.0	Open	

1. WN = white-noise, SS = sine-sweep; *-x*, *-y*, and *-z* denote direction of testing; Tabas-1 and Tabas-2 = part spectrum-compatible earthquake histories; OSn = single-frequency harmonic test at frequency of n Hz.
2. PGA = target peak acceleration of the simulator platform.

Table 5-7 Sequence of tests for disconnect switch SW4

Test	*Description*[1]	*PGA*[2] *(g)*	*Blade position*	*Comments*
1	ST-*x*	-	closed	
2	ST-*x*	-	open	
3	ST-*y*	-	open	
4	ST-*y*	-	closed	
5	ST-*y*	-	open	Test 4 repeated.
6	WN-*x*	0.1	Closed	
7	WN-*x*	0.1	Closed	Test 6 repeated.
8	WN-*y*	0.1	Closed	
9	SS-*x*	0.1	Closed	
10	SS-*y*	0.1	Closed	
11	Tabas-1	0.1	Closed	
12	Tabas-1	0.1	Closed	Test 11 repeated.
13	Tabas-2	0.1	Closed	
14	WN-*x*	0.1	Open	
15	WN-*y*	0.1	Open	
16	SS-*x*	0.1	Open	
17	SS-*y*	0.1	Open	
18	Tabas-1	0.1	Open	
19	Tabas-2	0.1	Open	
20	Tabas-1	0.5	Closed	
21	Tabas-2	0.5	Closed	
22	Tabas-1	0.5	Open	
23	Tabas-2	0.5	Open	
24	Tabas-1	1.0	Closed	
25	Tabas-2	1.0	Closed	Fracture of the welded blade-post connection for post C2; see Figure 5-22.
26	Tabas-1	1.0	Open	
27	Tabas-1	1.0	Open	
28	Tabas-1	1.25	Open	Continue testing for open blade only.
29	Tabas-2	1.25	Open	
30	Tabas-1	1.50	Open	

Table 5-7 Sequence of tests for disconnect switch SW4

31	Tabas-2	1.50	Open	
32	Tabas-1	1.75	Open	
33	Tabas-2	1.75	Open	
34	Tabas-1	2.0	Open	
35	Tabas-2	2.0	Open	
36	Tabas-2	3.0	Open	Fracture of the cast aluminum rotor bearing at base of post C2, see Figure 5-23.

1. ST = static tests, WN = white-noise, SS = sine-sweep; *-x, -y*, and *-z* denote direction of testing; Tabas-1 and Tabas-2 = part spectrum-compatible earthquake histories; OSn = single-frequency harmonic test at frequency of n Hz.
2. PGA = target peak acceleration of the simulator platform.

Since the resonant frequencies of the switches are much less than that of the PEER frame, and because there is no amplification of simulator-platform motions around the of frequencies of the switches, the PEER frame was classified as stiff for the purpose of switch qualification. As such, seismic tests on the PEER frame with a target PGA of 1.0g were deemed equivalent to High Level qualification on a stiff frame.

5.4.3 Static tests

Static pull-back, and quick-release tests of post C2 (see Figure 2-5) of the switch SW4 were undertaken to determine the stiffness and frequency of the switch pole when installed on the PEER frame. The stiffness of the post was computed using the measured forces and displacements during the pull-back segment of the tests. The accelerations at the tip of post C2 recorded following the quick-release of the applied load were used to compute the resonant frequencies of the pole. The computed stiffnesses and resonant frequencies of the switch are presented in Table 5-8 with the blades in the open and closed positions. For comparison, the results of static testing of switch SW1 listed in Table 4-3 are also presented in Table 5-8. The data for switch SW1 were acquired with the switch pole mounted directly on the simulator platform whereas SW4 was tested atop the PEER frame. However, because the PEER frame was stiff, a direct comparison of the data is possible

Examination of the data listed in Table 5-8 revealed that the poles of SW4 and SW1 have similar stiffness, even though the insulators of SW4 are larger. Much of the flexibility in the posts is in the double-channel beam and the attachment hardware at the base of the posts. As such, characterization of the dynamic properties of the switches for qualification and analysis must include the flexibility of the switch base. The fundamental frequencies of SW4 are less than those of SW1 because the porcelain insulators of SW4 are heavier than the porcelain insulators of SW1. When the blade is closed, the value of stiffness and frequency in the *y*-direction are greater than those in the *x*-direction due to the frame action between the posts and because the double-channel beams at the base are stiffer in flexure than in torsion.

Table 5-8 Stiffness and frequency properties of horizontal-break switches from static tests

		Stiffness (kN/m)		*Frequency (Hz)*	
Switch	*Blade*	x-direction	y-direction	x-direction	y-direction
SW1	Closed	34	74	3	5
SW1	Open	28	39	3	3
SW4	Closed	30	77	2	4
SW4	Open	28	41	2	2

5.4.4 Resonance-search tests

5.4.4.1 Introduction

Post tip acceleration data from sine-sweep tests were used to calculate the modal frequencies and damping ratios for the switches on the PEER frame. Figures 5-27 through 5-37 present the power spectra for the tip of post 1 from the sine-sweep tests. The power spectra are normalized to a maximum ordinate of unity. The modal frequencies were taken from the peaks in the power spectrum and the damping ratios were computed using the half-power method (Chopra 1996).

5.4.4.2 Switch SW1

Figures 5-27 and 5-29 present the normalized power spectra for posts 1 of switch SW1. The data were obtained from sine-sweep tests of the switch in x- and y-directions with closed and open blades (Tests 3, 4, 13, and 14 of Table 5-3). Switch SW1 had a fundamental frequency of 3 to 4 Hz and its damping ratio ranged from 2 to 4 percent of critical. These values are in general agreement with those computed from resonant-search testing of pole A mounted directly on the simulator platform (see Table 4-4).

Posts 1 and 2 have similar dynamic properties because the posts have similar insulators and blade masses. The frequency in the y-direction is larger than in the x-direction (see Section 5.4.3). Table 5-9 summarizes the measured dynamic properties of the posts in the x- and y-directions for switch SW1.

5.4.4.3 Switch SW2

Figures 5-29 and 5-31 present the normalized power spectra for posts 1 of switch SW2. The data were obtained from sine-sweep tests of the switch in x- and y-directions with closed and open blades (Tests 3, 4, 13, and 14 of Table 5-4). Switch SW2 had a fundamental frequency of 5 to 6 Hz and its damping ratio ranged from 2 to 4 percent of critical. These values are in good agreement with those computed from resonant-search testing of pole A of switch SW2 mounted directly on the simulator platform (see Table 4-4).

The fundamental frequency for post 2 was slightly less than that of post 1 because the cast aluminum connection for the blade is mounted atop posts 2 and 3 and the additional mass reduces the frequency of this post. The dynamic properties were substantially independent of blade position (open or closed). Table 5-10 summarizes the measured dynamic properties of the switches in the *x*- and *y*-directions of the switch posts.

Table 5-9 Modal properties of switch SW1 on the PEER frame from resonance-search tests

	Closed Blade				*Open Blade*			
	Frequency (Hz)		*Damping ratio (% critical)*		*Frequency (Hz)*		*Damping ratio (% critical)*	
Post[1]	*x-direction*	*y-direction*	*x-direction*	*y-direction*	*x-direction*	*y-direction*	*x-direction*	*y-direction*
A1	3	5	5	2	3	3	3	4
A2	3	5	5	3	3	3	3	4
B1	4	5	3	2	4	4	3	4
B2	4	5	3	3	4	4	3	4
C1	3	5	3	2	3	3	3	4
C2	3	5	3	3	3	3	3	4

1. For post designation, refer to Figure 5-6.

Table 5-10 Modal properties of switch SW2 on the PEER frame from resonance-search tests

	Closed Blade				*Open Blade*			
	Frequency (Hz)		*Damping ratio (% critical)*		*Frequency (Hz)*		*Damping ratio (% critical)*	
Post[1]	*x-direction*	*y-direction*	*x-direction*	*y-direction*	*x-direction*	*y-direction*	*x-direction*	*y-direction*
A1	6	6	3	2	6	6	2	2
A2	5	6	4	2	6	5	2	2
B1	6	6	3	2	6	7	2	2
B2	5	6	4	2	6	5	2	2
C1	6	6	3	2	6	6	2	2
C2	5	6	4	2	6	5	2	2

1. For post designation, refer to Figure 5-6.

5.4.4.4 Switch SW2a

Figures 5-31 and 5-33 present the normalized power spectra for posts 1 of switch SW2a. The data were obtained from sine-sweep tests of the switch in *x*- and *y*-directions with closed and open blades (Tests 3, 4, 13, and 14 of Table 5-5). Switch SW2a had a fundamental frequency of 5 to 6 Hz and its damping ratio ranged from 3 to 4 percent of critical.

The fundamental frequency for post 2 was slightly less than that of post 1 (see Section 5.4.4.3). The dynamic properties of switch SW2a were similar to those of switch SW2, implying that the use of steel spacers, instead of cast aluminum spacers, at base of posts 1 and 3 did not change the frequency of the switch. Table 5-11 summarizes the measured dynamic properties of the switches in the *x*- and *y*-directions of the switch posts.

Table 5-11 Modal properties of switch SW2a on the PEER frame from resonance-search tests

	Closed blade				*Open blade*			
	Frequency (Hz)		*Damping Ratio (% critical)*		*Frequency (Hz)*		*Damping Ratio (% critical)*	
Post[1]	*x-direction*	*y-direction*	*x-direction*	*y-direction*	*x-direction*	*y-direction*	*x-direction*	*y-direction*
A1	6	6	3	3	6	6	3	3
A2	5	6	4	3	6	5	3	4
B1	6	6	3	3	6	6	3	3
B2	5	6	4	3	5	5	3	4
C1	6	6	3	3	6	6	3	3
C2	5	6	4	3	6	5	3	4

1. For post designation, refer to Figure 5-6.

5.4.4.5 Switch SW3

Figures 5-33 and 5-35 present the normalized power spectra for posts 1 of switch SW3. The data were obtained from sine-sweep tests of the switch in *x*- and *y*-directions with closed and open blades (Tests 3, 4, 14, and 15 of Table 5-6). Switch SW3 had a fundamental frequency of 6 to 8 Hz and its damping ratio ranged from 2 to 3 percent of critical. These values are in good agreement with those computed from resonant-search testing of pole A of switch SW3 directly mounted on the simulator platform (see Table 4-4).

When the blade was open, the fundamental frequency for post 2 was noticeably less than that of post 1 because the cast aluminum connection for the blade is mounted atop posts 2 and 3 and this additional mass reduces the frequency of these posts. The difference between frequencies of posts 1 and 2 for switch SW3 was larger than the difference between the same posts for switch SW2 because the effect of the additional mass was more significant for switch SW3, which had lighter composite insulators. Although the insulators on poles A and C were mounted on cast aluminum spacers and the insulators on pole B were mounted on steel spacers, the poles had similar frequencies. Table 5-12 summarizes the measured dynamic properties of the switches in the *x*- and *y*-directions of switch SW3.

Table 5-12 Modal properties of switch SW3 on the PEER frame from resonance-search tests

	Closed blade				*Open blade*			
	Frequency (Hz)		*Damping Ratio (% critical)*		*Frequency (Hz)*		*Damping Ratio (% critical)*	
Post[1]	*x-direction*	*y-direction*	*x-direction*	*y-direction*	*x-direction*	*y-direction*	*x-direction*	*y-direction*
A1	8,6[2]	6	2,2[2]	2	8	8	2	2
A2	8,6	6	2,2	3	6	6	2	2
B1	8,6	8	2,2	2	8	8	2	2
B2	8,6	8	2,2	3	6	6	2	2
C1	8,6	8	2,2	2	8	8	2	2
C2	8,6	8	2,2	3	6	6	2	2

1. For post designation, refer to Figure 5-6.
2. Two modal frequencies were identified in these tests.

5.4.4.6 Switch SW4

Figures 5-35 and 5-37 present the normalized power spectra for post 1 of switch SW4. The data were obtained from sine-sweep tests of the switch in *x*- and *y*-directions with closed and open blades (Tests 9, 10, 16, and 17 of Table 5-7). Switch SW4 had a fundamental frequency of 2 to 4 Hz and its damping ratio ranged from 2 to 4 percent of critical. The frequencies of switch SW4 computed from sine-sweep tests were similar to those obtained from static tests (see Table 5-8).

The frequencies and damping ratios for posts 1 and 2 are similar because the posts have similar insulators and blade masses.When the blade was closed, the frequency in the *y*-direction was larger than in the *x*-direction (see Section 5.4.3). Table 5-13 summarizes the measured dynamic properties in the *x*- and *y*-directions of switch SW4.

Table 5-13 Modal properties of switch SW4 on the PEER frame from resonance-search tests

	Closed blade				*Open blade*			
	Frequency (Hz)		*Damping Ratio (% critical)*		*Frequency (Hz)*		*Damping Ratio (% critical)*	
Post[1]	*x-direction*	*y-direction*	*x-direction*	*y-direction*	*x-direction*	*y-direction*	*x-direction*	*y-direction*
C1	3	4	4	4	2	3	4	2
C2	3	4	3	4	2	3	4	2

1. For post designation, refer to Figure 5-6.

5.4.5 Peak responses

5.4.5.1 Introduction

Peak accelerations and displacements are reported herein for tests with target PGA equal to or greater than 0.5g. Peak absolute accelerations for switch posts were calculated as the maximum of the vector sum of acceleration components in the *x*- and *y*-directions, evaluated at every time increment.

Peak relative displacements in the switches were computed as the maximum of the vector sum of relative displacement components in the *x*- and *y*-directions, evaluated by subtracting the *x*- and *y*-displacements at the top of the posts from the *x*- and *y*-displacements at the top of the PEER frame at every time increment. Post displacements were not recorded when the blade was open.

5.4.5.2 Switch SW1

Peak acceleration and relative displacement data for switch SW1 are presented in Table 5-14. Only the peak response at the top of the insulator posts are reported. For this switch, a maximum post acceleration of close to 13g was computed using equation (5-1). In the tests just prior to the fracture of the blade-post connection and cast aluminum rotor bearings, the post displacements were very large. The maximum acceleration and displacement relative to the frame were typically recorded at pole B: the operational hardware of the switch is attached to the base of this pole. For pole B, the response at post B2, the post at which the pole crank was mounted, was larger than the response at post B1.

5.4.5.3 Switch SW2

Peak acceleration and post relative displacement data for switch SW2 are listed in Table 5-15. For this switch, the maximum post acceleration was 8.5g. The recorded switch deformations for switch SW2 were significantly smaller than the corresponding values for switch SW1 because switch SW2 used a stiffer base hardware to attach the insulators to the double-channel beams. The maximum responses were typically recorded at post B2 (see Section 5.4.5.2).

5.4.5.4 Switch SW2a

Peak acceleration and post relative displacement data for switch SW2a are listed in Table 5-16. For this switch, the maximum post acceleration was 14g. The maximum accelerations were recorded at post B2 (see Section 5.4.5.2). The recorded switch deformations and accelerations were similar to those for switch SW2 because the use of welded steel spacers in place of cast aluminum spacers did not alter the dynamic properties (and hence maximum response) of the poles.

Table 5-14 Peak response of switch SW1

Test[1]	*PGA*[2] *(g)*	*Post Acceleration*[3] *(g)*						*Post Displacement*[4] *(mm)*					
		A1	*A2*	*B1*	*B2*	*C1*	*C2*	*A1*	*A2*	*B1*	*B2*	*C1*	*C2*
7	0.5	3.5	3.9	3.9	4.9	4.5	5.3	41	41	41	52	56	41
8	0.5	3.6	4.4	4.6	3.9	4.0	4.8	42	49	45	47	51	40
17	0.5	4.0	4.2	3.7	4.4	4.2	4.5	-[5]	-	-	-	-	-
18	0.5	3.8	4.9	3.1	4.7	4.1	5.1	-	-	-	-	-	-
21	1.0	5.9	6.0	6.8	8.3	-	7.3	55	60	69	90	79	70
22	1.0	6.6	6.4	6.6	9.8	-	7.9	72	72	83	81	84	67
23	1.0	6.6	6.8	5.9	11.3	-	6.9	-	-	-	-	-	-
24	1.0	7.1	7.9	6.3	10.3	-	8.3	-	-	-	-	-	-
25	1.25	6.6	6.7	7.4	8.0	-	10.0	64	66	90	80	70	70
26	1.25	5.6	6.4	7.5	9.9	-	7.8	59	55	79	90	68	61
27	1.25	5.7	7.5	5.9	12.7	-	8.4	-	-	-	-	-	-
28	1.25	7.5	9.7	7.2	12.3	9.7	10.3	-	-	-	-	-	-
29	1.5	8.9	7.8	7.6	11.7	9.4	8.5	71	73	148	165	91	88
30	1.5	7.2	6.9	7.9	11.4	10.3	9.8	93	100	180	277	135	156
31	1.5	6.0	9.0	*[6]	*	6.6	8.1	-	-	-	-	-	-
33	1.75	10.0	7.4	-	-	11.1	8.3	94	94	-	-	101	93
34	1.75	10	11	-	-	11.9	10.2	202	192	-	-	151	103
35	1.75	*	*	-	-	9.1	*	-	-	-	-	-	-

1. Refer to Table 5-3 for test list.
2. PGA designates the target peak acceleration of the simulator platform.
3. For post designation, refer to Figure 5-6.
4. Post displacements were not recorded when the blade was open.
5. Data were not recorded.
6. Posts or blades broke during the test.

Table 5-15 Peak response of switch SW2

Test[1]	*PGA*[2] *(g)*	*Post Acceleration*[3] *(g)*						*Post Displacement*[4] *(mm)*					
		A1	*A2*	*B1*	*B2*	*C1*	*C2*	*A1*	*A2*	*B1*	*B2*	*C1*	*C2*
7	0.5	4.2	4.7	3.4	4.4	3.9	4.4	34	41	23	28	28	37
8	0.5	3.8	3.8	2.9	3.2	3.3	3.4	24	35	23	32	21	36
17	0.5	3.0	5.0	3.3	5.2	3.4	-	-[5]	-	-	-	-	-
18	0.5	3.7	4.6	3.4	4.7	3.0	-	-	-	-	-	-	-
21	1.0	5.7	6.2	5.1	7.8	7.3	7.2	51	79	47	81	52	82
22	1.0	5.3	5.8	6.0	8.5	5.8	7.2	49	73	56	80	43	90
23	1.0	5.0	5.6	5.7	7.6	4.8	5.9	-	-	-	-	-	-
24	1.0	5.2	6.2	6.4	9.4	5.4	7.2	-	-	-	-	-	-

1. Refer to Table 5-3 for test list.
2. PGA designates the target peak acceleration of the simulator platform.
3. For post designation, refer to Figure 5-6.
4. Post displacements were not recorded when the blade was open.
5. Data were not recorded.

5.4.5.5 Switch SW3

Peak acceleration and relative displacement data for switch SW3 are listed in Table 5-17. For this switch, the maximum post acceleration was 15g. The maximum accelerations were typically recorded at post B2, although post C2 also had large accelerations. When the poles were individually locked and the inter-pole links were disconnected during Tests 39 through 42, the accelerations of post B2 were significantly reduced and were similar to those both of the other posts in the switch and to the values measured during the tests of single pole of switch SW3 (see Table 4-5).

5.4.5.6 Switch SW4

Peak acceleration and relative displacement data for switch SW4 are listed in Table 5-18. For this switch, the maximum post acceleration was 8.3g. The measured accelerations for switch SW4 were less than those of switch SW1 for similar tests. Although the switches had similar dynamic properties and were subjected to similar input histories, the operational hardware for the two switches were different. For switch SW1, the inter-pole links and hand crank that were used to open and close the switch were in place and such hardware amplified the acceleration response of the posts. No links and cranks were attached to switch SW4. Switch SW4 was locked using a turnbuckle attached to the double-channel beams.

Table 5-16 Peak response of switch SW2a

Test[1]	*PGA*[2] *(g)*	*Post Acceleration*[3] *(g)*						*Post Displacement*[4] *(mm)*					
		A1	*A2*	*B1*	*B2*	*C1*	*C2*	*A1*	*A2*	*B1*	*B2*	*C1*	*C2*
7	0.5	3.3	3.2	6.0	6.8	3.3	3.6	23	46	51	62	23	50
8	0.5	3.7	3.8	4.0	5.5	3.0	3.1	27	44	43	54	25	48
17	0.5	3.8	5.1	4.4	7.9	4.4	5.1	-	-	-	-	-	-
18	0.5	3.7	5.7	4.1	5.3	3.2	3.4	27	43	40	46	23	41
21	1.0	4.6	5.9	7.0	7.8	4.5	8.0	41	87	67	84	38	85
22	1.0	5.2	5.8	6.4	7.3	6.5	7.0	35	71	59	78	41	90
23	1.0	4.1	5.7	5.9	10.0	5.0	6.3	-	-	-	-	-	-
24	1.0	6.1	6.0	6.7	8.1	7.2	7.6	-	-	-	-	-	-
37	1.25	5.7	6.1	7.0	9.5	5.9	6.2	44	43	72	69	41	44
38	1.25	5.6	6.0	6.7	10.2	6.0	6.1	38	53	83	90	43	61
39	1.25	5.0	8.4	7.3	10.3	6.0	8.4	-	-	-	-	-	-
40	1.25	4.8	6.2	6.7	10.2	5.7	6.1	-	-	-	-	-	-
41	1.50	6.0	6.4	6.9	9.3	6.8	8.3	55	66	75	83	49	96
42	1.50	5.9	7.7	7.6	12.0	7.5	8.9	67	102	94	163	58	119
43	1.50	5.3	6.8	7.0	10.0	6.2	9.0	-	-	-	-	-	-
44	1.50	5.5	6.4	6.8	11.6	6.7	8.4	-	-	-	-	-	-
45	1.75	6.1	6.2	7.2	10.4	7.2	7.0	52	71	83	96	52	104
46	1.75	6.7	8.4	7.3	13.8	10.0	11.2	79	136	111	184	73	176
48	1.75	5.8	7.0	7.1	11.8	6.2	8.6	-	-	-	-	-	-
49	1.75	7.0	8.2	7.8	14.0	9.1	8.7	-	-	-	-	-	-
50	2.0	5.9	7.1	6.8	9.6	7.7	10.3	56	114	116	125	72	158
51	2.0	6.8	10.7	9.0	11.2	11.0	10.1	74	186	107	157	105	107
52	2.0	6.9	8.6	7.1	9.7	8.6	9.2	-	-	-	-	-	-
53	2.0	7.1	11.2	8.7	13.3	10.4	10.3	-	-	-	-	-	-

1. Refer to Table 5-3 for test list.
2. PGA designates the target peak acceleration of the simulator platform.
3. For post designation, refer to Figure 5-6.
4. Post displacements were not recorded when the blade was open.
5. Data were not recorded.

Table 5-17 Peak response of switch SW3

Test[1]	*PGA*[2] *(g)*	*Post Acceleration*[3] *(g)*						*Post Displacement*[4] *(mm)*					
		A1	*A2*	*B1*	*B2*	*C1*	*C2*	*A1*	*A2*	*B1*	*B2*	*C1*	*C2*
8	0.5	3.2	4.3	3.1	4.0	3.0	4.2	20	24	17	28	14	22
9	0.5	3.8	4.1	3.6	4.4	3.3	4.6	22	22	20	24	16	19
19	0.5	4.3	5.8	3.8	7.0	4.6	4.5	-[5]	-	-	-	-	-
20	0.5	3.7	5.2	3.2	5.5	3.6	4.4	-	-	-	-	-	-
39	0.5	3.4	3.7	3.1	4.2	4.1	5.3	26	28	17	22	19	22
40	0.5	3.5	3.9	2.9	3.8	4.2	4.8	22	25	18	23	16	20
41	0.5	5.0	4.4	4.1	4.1	3.9	4.2	-	-	-	-	-	-
42	0.5	4.4	3.9	4.2	4.7	4.0	3.9	-	-	-	-	-	-
23	1.0	6.9	7.6	5.6	9.3	6.4	6.9	37	53	29	45	29	32
24	1.0	8.8	9.0	6.6	8.4	7.3	7.7	45	50	34	34	30	31
25	1.0	7.2	7.1	7.1	8.8	8.6	8.6	-	-	-	-	-	-
26	1.0	9.7	8.8	7.1	13.1	7.8	7.5	-	-	-	-	-	-
43	1.25	8.0	8.0	7.0	8.3	8.1	8.3	43	49	35	41	33	44
44	1.25	5.0	5.8	6.4	9.3	7.7	9.4	31	47	32	39	34	37
45	1.25	6.7	7.9	7.2	7.9	9.8	8.8	-	-	-	-	-	-
46	1.25	7.7	7.9	6.8	9.4	7.9		-	-	-	-	-	-
47	1.50	7.5	7.3	6.9	8.9	8.0	8.0	41	52	38	49	39	45
48	1.50	7.2	8.8	7.7	11.5	10.0	9.8	36	98	40	53	45	70
49	1.50	7.9	7.7	7.2	9.2	10.4	7.9	-	-	-	-	-	-
50	1.50	8.8	7.8	8.7	10.2	9.7	11.0	-	-	-	-	-	-
51	1.75	9.9	9.4	7.3	9.6	8.4	8.2	47	58	37	51	38	49
52	1.75	10.2	10.0	7.7	10.6	11.0	11.9	46	81	45	69	52	94
53	1.75	8.7	7.0	8.0	9.0	9.3	8.8	-	-	-	-	-	-
54	1.75	11.8	11.8	8.3	12.5	11.0	12.8	-	-	-	-	-	-
55	2.0	9.9	9.9	8.0	13.5	11.4	9.5	51	53	43	59	51	61
56	2.0	11.7	11.5	8.3	12.8	12.3	12.0	51	100	61	82	58	133
57	2.0	9.2	8.9	8.2	13.4	11.0	9.9	-	-	-	-	-	-
58	2.0	8.8	11.0	8.8	14.7	11.9	15.0	-	-	-	-	-	-

1. Refer to Table 5-3 for test list.
2. PGA designates the target peak acceleration of the simulator platform.
3. For post designation, refer to Figure 5-6.
4. Post displacements were not recorded when the blade was open.
5. Data were not recorded.

Table 5-18 Peak response of switch SW4

Test[1]	*PGA*[2] *(g)*	*Post Acceleration*[3] *(g)*		*Post Displacement*[4] *(mm)*	
		C1[7]	*C2*	*C1*	*C2*
20	0.5	1.7	3.1	89	88
21	0.5	2.5	3.2	112	90
22	0.5	1.8	3.0	-[5]	-
23	0.5	2.4	3.1	-	-
24	1.0	4.8	5.8	121	155
25	1.0	4.6	5.5	197	174
26	1.0	2.2	4.5	-	-
27	1.0	3.0	5.2	-	-
28	1.25	2.0	4.8	-	-
29	1.25	2.2	5.0	-	-
30	1.50	3.1	5.4 *[6]	-	-
31	1.50	3.0	6.1	-	-
32	1.75	3.1	5.6	-	-
33	1.75	4.1	7.1	-	-
34	2.0	4.4	6.3	-	-
35	2.0	4.0	6.8	-	-
36	3.0	6.8	8.3	-	-

1. Refer to Table 5-3 for test list.
2. PGA designates the target peak acceleration of the simulator platform.
3. For post designation, refer to Figure 5-6.
4. Post displacements were not recorded when the blade was open.
5. Data were not recorded.
6. Posts or blades broke during the test.
7. The *y*-component of acceleration was not recorded; maximum acceleration in *x*-direction.

5.4.6 *Earthquake response of switches*

5.4.6.1 Introduction

For qualification of switches to the High Level, the IEEE 693-1997 response spectrum shape of Figure 3-8 was used. The spectrum was anchored to a PGA of 1.0g for qualification of switches on a stiff frame. For qualification of switches on a flexible frame, the identical spectral shape was used but with spectral ordinates equal to twice those of the IEEE 693-1997 spectrum of Figure 3-8. Two-percent damped spectra were used for evaluation since the damping ratios of switches ranged between 2 and 5 percent. The qualification program included the four tests listed in Table 3-1. For qualification, an *envelope* spectrum was developed using the procedure described in Section 3.2.3.

The earthquake responses of the switches were evaluated using a set of four tests of the same target peak acceleration (1) that had the largest computed acceleration spectrum and (2) for which there was no structural failure. For example, for switch SW1, tests with target PGA of 1.0g were used for evaluation. These tests produced the response spectrum with the largest acceleration ordinates for which there were no component failures. Table 5-19 lists the tests used to characterize the seismic response of the five switches.

Table 5-19 Selected tests for seismic evaluation of switches

Switch	*Tests*[1]	*PGA*[2]
SW1	21, 22, 23, 24	1.0
SW2	7, 8, 17, 18	0.5
SW2a	50, 51, 52, 53	2.0
SW3	55, 56, 57, 58	2.0
SW4	20, 21, 22, 23	0.5

1. Refer to Tables 5-3 through 5-7.
2. PGA denotes target peak acceleration of the simulator platform.

A switch would be qualified to the High Level if it passed the IEEE 693-1997 general, functional, and operational requirements (see Appendix A) following all four tests with earthquake histories whose envelope spectrum exceeded the IEEE 693-1997 spectrum. Discussion regarding the seismic qualification of the five switches follows.

5.4.6.2 Earthquake response of switch SW1

The earthquake response of switch SW1 was assessed by analysis of data from Tests 21 and 23, (Tabas-1, target PGA equal to 1.0g) and Tests 22 and 24 (Tabas-2, target PGA equal to 1.0g). The peak response values for these tests are listed in Table 5-14. The maximum porcelain stress measured during these four tests was 9 ksi (63 MPa). Figures 5-37 and 5-38 present the 2-percent damped envelope of acceleration response spectra for these four tests. The ordinates of the envelope spectra in both *x*- and *y*-directions exceeded the ordinates of the IEEE 693-1997 spectrum anchored at 0.6g, which is larger than the IEEE 693-1997 spectrum for the Moderate Level qualification (anchored at 0.5g). The ordinates of the envelope spectra in *x*- and *y*-directions fell below the ordinates of the IEEE 693-1997 spectrum for high level qualification. As such, this switch did not meet the requirements for High Level qualification on a stiff frame.

5.4.6.3 Earthquake response of switch SW2

The earthquake response of switch SW2 was assessed by analysis of data from Tests 7 and 17, (Tabas-1, target PGA equal to 0.5g) and Tests 8 and 18 (Tabas-2, target PGA equal to 0.5g). The peak response values for these tests are listed in Table 5-15. The maximum porcelain stress measured during these four tests was 3 ksi (20 MPa). Figures 5-39 and 5-40 present the 2-percent damped envelope of acceleration response spectra for these four tests. The ordinates of the envelope spectra fell below the ordinates of the IEEE 693-1997 spectrum and this switch did not meet the requirements for High Level qualification on a stiff frame.

5.4.6.4 Earthquake response of switch SW2a

The earthquake response of switch SW2a was assessed by analysis of data from Tests 50 and 52, (Tabas-1, target PGA equal to 2.0g) and Tests 51 and 53 (Tabas-2, target PGA equal to 2.0g). The peak response values for these tests are listed in Table 5-16. The maximum porcelain stress measured during these four tests was 5 ksi (34 MPa). Figures 5-41 and 5-42 present the 2-percent damped envelope of acceleration response spectra for these four tests. During these tests, the switch was fully operational, and the electrical connections for all three poles were maintained throughout the tests with closed blades. The ordinates of the envelope spectra in both *x*- and *y*-directions exceeded the ordinates of the IEEE 693-1997 spectrum for High Level qualification and this switch was qualified to the High Level on a stiff frame.

5.4.6.5 Earthquake response of switch SW3

The earthquake response of switch SW3 was assessed by analysis of data from Tests 55 and 57, (Tabas-1, target PGA equal to 2.0g) and Tests 56 and 58 (Tabas-2, target PGA equal to 2.0g). The peak response values for these tests are listed in Table 5-17. Figures 5-43 and 5-44 present the 2-percent damped envelope of acceleration response spectra for the tests. During these tests, there was no structural damage for the posts mounted on steel spacers, the switch was fully operational, and the electrical connections for all three poles were maintained during the tests with closed blades. The ordinates of the envelope spectra exceeded the ordinates of the IEEE 693-1997 spectrum for High Level qualification. Switch SW3 was therefore qualified to the High Level when mounted on a stiff frame provided that steel spacers are used to attach the switch to the double-channel beams.

5.4.6.6 Earthquake response of switch SW4

The earthquake response of switch SW4 was assessed by analysis of data from Tests 20 and 22, (Tabas-1, target PGA equal to 0.5g) and Tests 21 and 23 (Tabas-2, target PGA equal to 0.5g). The peak response values for these tests are listed in Table 5-18. Figures 5-45 and 5-46 present the 2-percent damped envelope of acceleration response spectra for these tests. The ordinates of the envelope spectra fell below the ordinates of the IEEE 693-1997 spectrum for High level qualification and this switch did not meet the requirements for High Level qualification on stiff frame.

5.5 Summary Remarks

Five disconnect switches were evaluated by static and dynamic testing. A two-post porcelain horizontal-break switch (SW1), a three-post porcelain vertical-break switch with cast aluminum spacers (SW2), a three-post porcelain vertical-break switch with welded steel spacers (SW2a), a three-post composite vertical-break switch (SW3), and a two-post porcelain horizontal-break switch (SW4) were studied. The switches were assembled by members of the project team with assistance from ABB and PG&E engineering staff. The switches were mounted and tested on the PEER frame.

The fundamental frequency of the PEER frame in the lateral direction was approximately 22 Hz. No resonant frequency was computed in the longitudinal direction because a resonant search above 33 Hz was not conducted. In the longitudinal and transverse directions, the PEER frame did not amplify the displacement response of the simulator platform. The PEER frame was also torsionally stiff.

Modal frequencies in the range of 2 to 8 Hz were recorded for the five switches; damping ratios ranged between 2 and 5 percent of critical. These values were in good agreement with those computed when single poles of the switches were tested. For the vertical-break switches, the fundamental frequency of post 2 was less than that of post 1 because of the added mass of the cast aluminum counterweight directly mounted on top of posts 2 and 3.

For the horizontal-break switches, switch failure was caused by either the fracture of the welded blade-post connection or the fracture of the cast aluminum rotor bearings at the base of the posts. For the vertical-break switches, the cast aluminum spacers at the base of posts 2 and 3 were the most vulnerable components. When welded steel spacers were substituted for the cast aluminum spacers, the vertical-break switches were able to withstand more severe shaking. However, for the larger levels of shaking, there was significant deformation in the flanges of the double-channel beams and angles at the base of the poles, and the bolts in these connections were severely damaged in some cases.

When subjected to severe shaking, the switch posts experienced large accelerations which frequently exceeded 10.0g. Post B2 typically experienced the largest accelerations. (The operation hardware of the switch was bolted to the double-channel beam at the base of pole B and the inter-pole links were also attached to post B2, see Figure 5-6b). When the links between the poles were disconnected, the accelerations of post B2 significantly reduced. The effect of the switch operating mechanism and hardware on the response of the switches warrants further examination. To reduce the large accelerations for pole B of the switches, strategies to isolate the operation mechanism from the switches in the field should be explored. Otherwise, experimentation and analysis must include all the attachment hardware for the switch poles and posts. The inclusion of such hardware will make numerical analysis of switches very difficult.

Neither of the horizontal-break switches met the IEEE 693-1997 requirements for High Level qualification. The vertical-break switches were qualified to the High Level when mounted on a stiff frame provided that welded steel spacers were used to attach the posts to the double-channel beams. Because the spectral accelerations were below twice that of the IEEE 693-1997 ordinates for High Level qualification, no statements regarding the likely qualification of these switches on flexible frames can be made.

Figure 5-1 Switch SW1 (open blade) prior to testing

Figure 5-2 Switch SW2 (closed blade) prior to testing

Figure 5-3 Switch SW2a (open blade) prior to testing

Figure 5-4 Switch SW3 (closed blade) prior to testing

Figure 5-5 Switch SW4 (closed blade) prior to testing

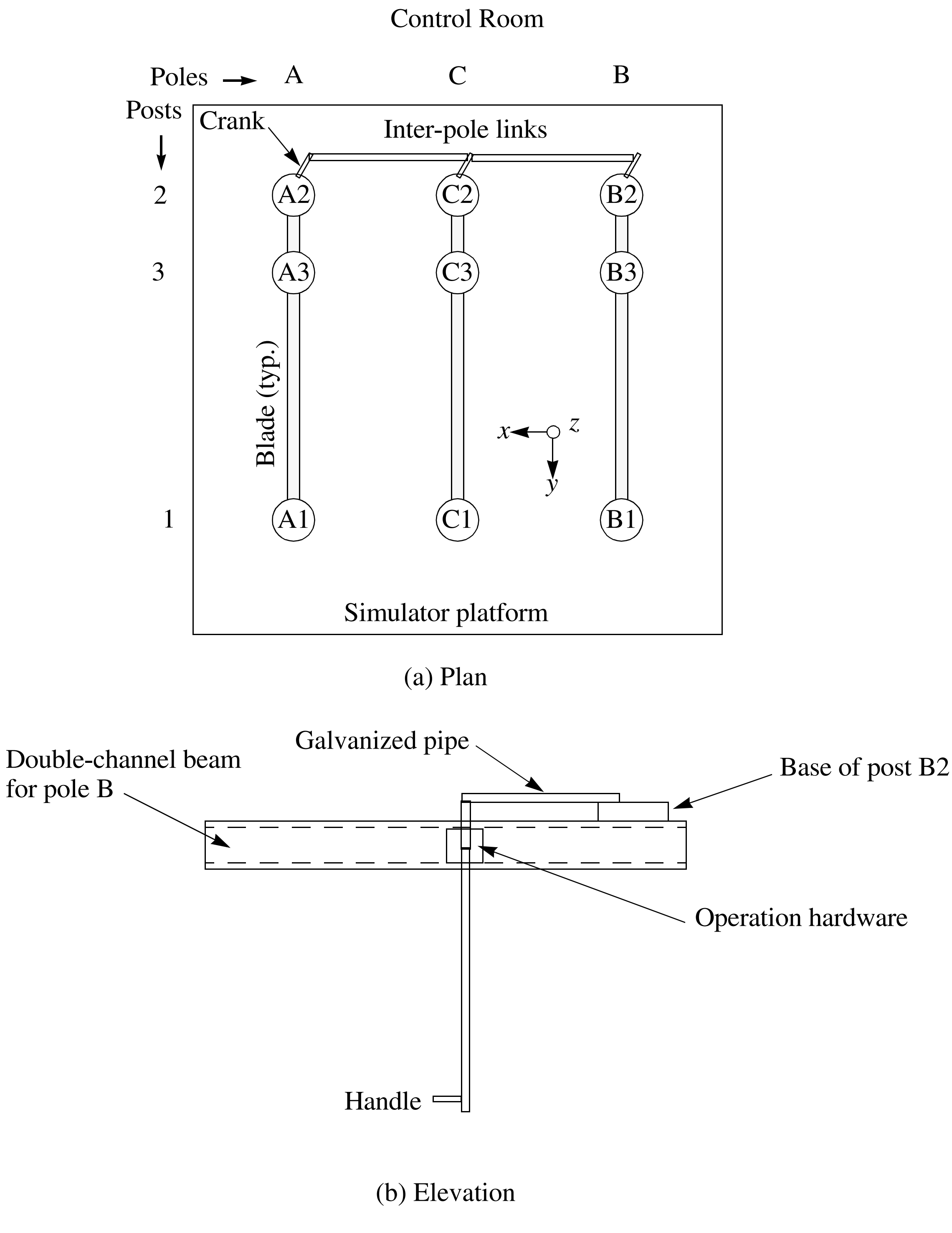

Figure 5-6 Post and pole designation, and operation of disconnect switches

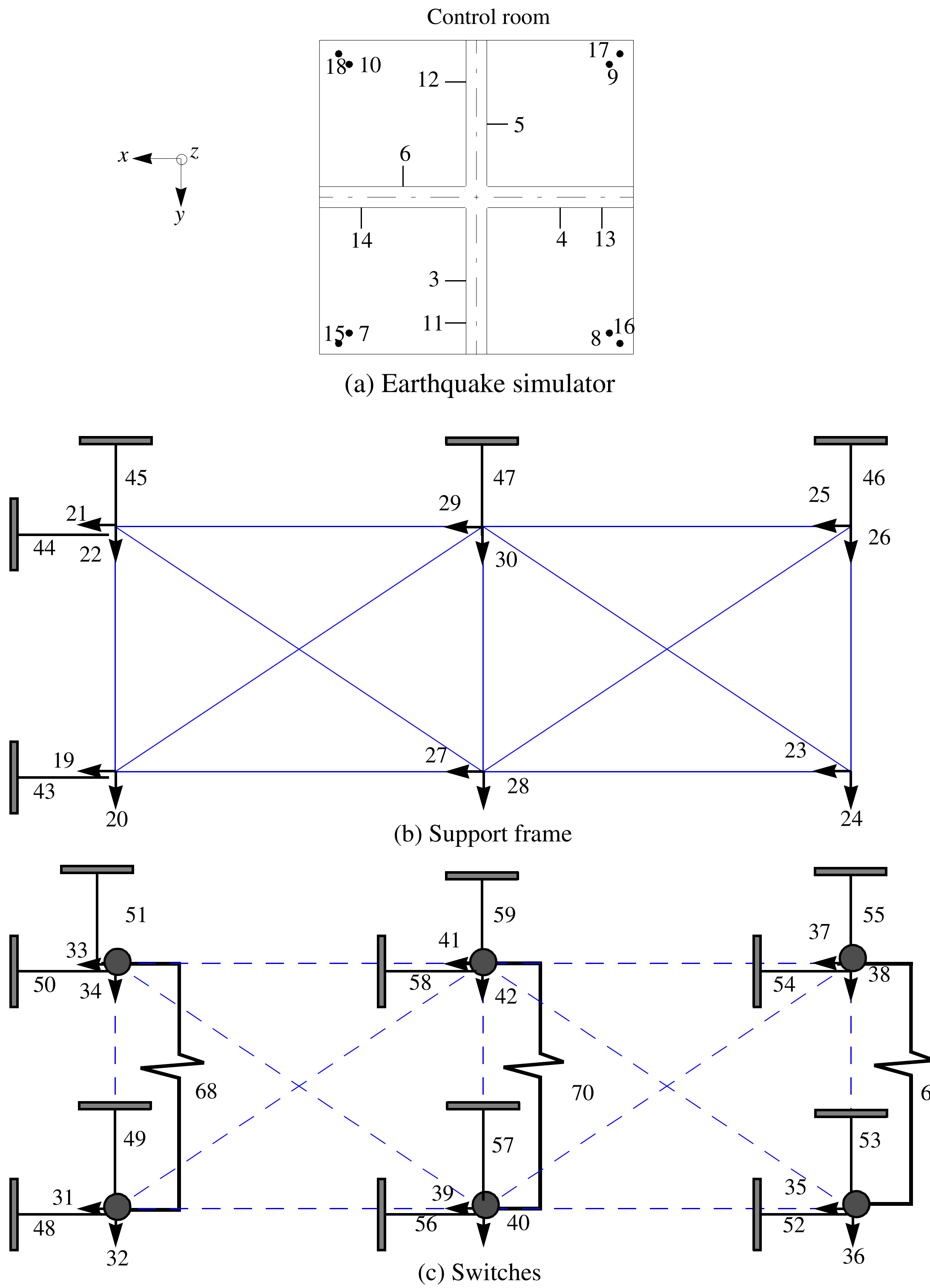

Figure 5-7 Instrumentation for switches

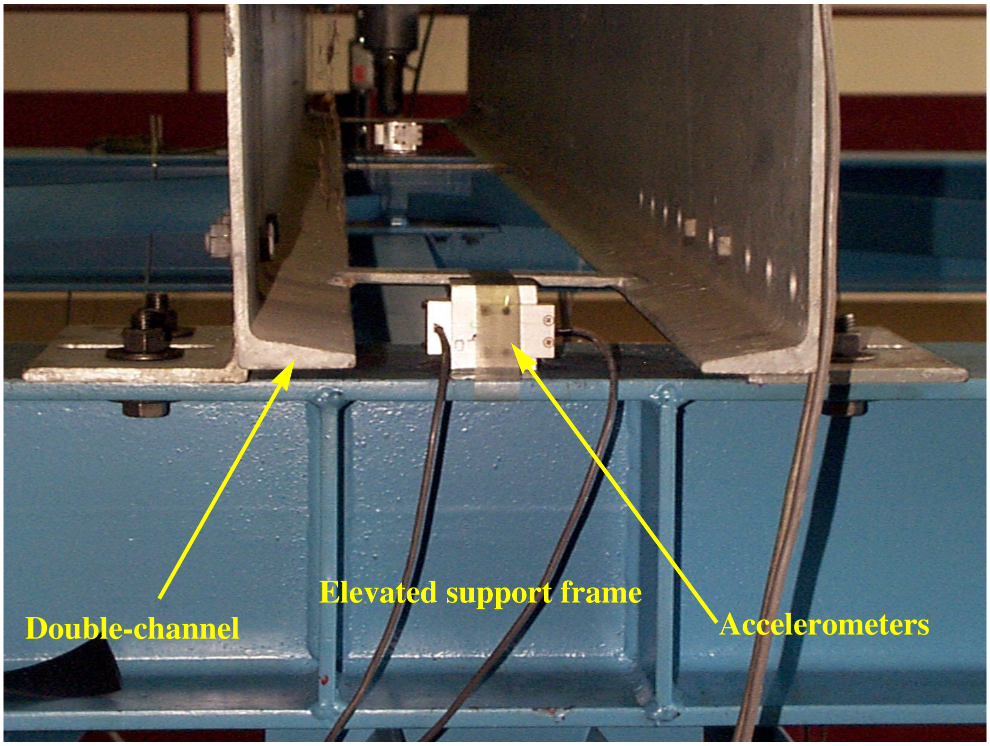

Figure 5-8 Instrumentation of the support frame

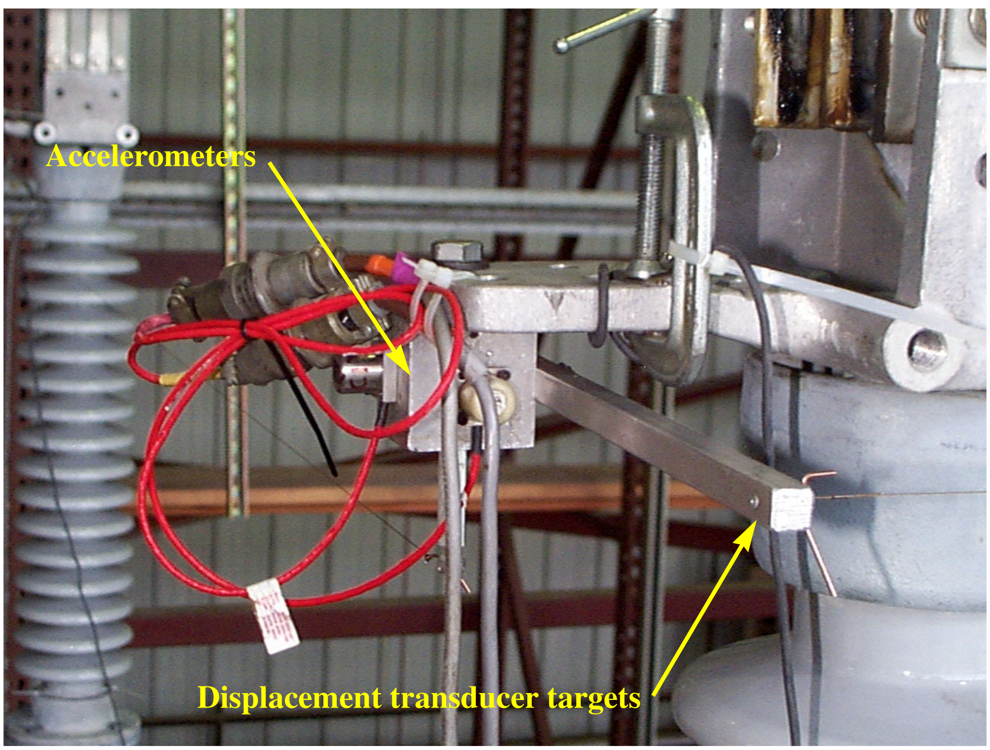

Figure 5-9 Instrumentation at top of switch posts

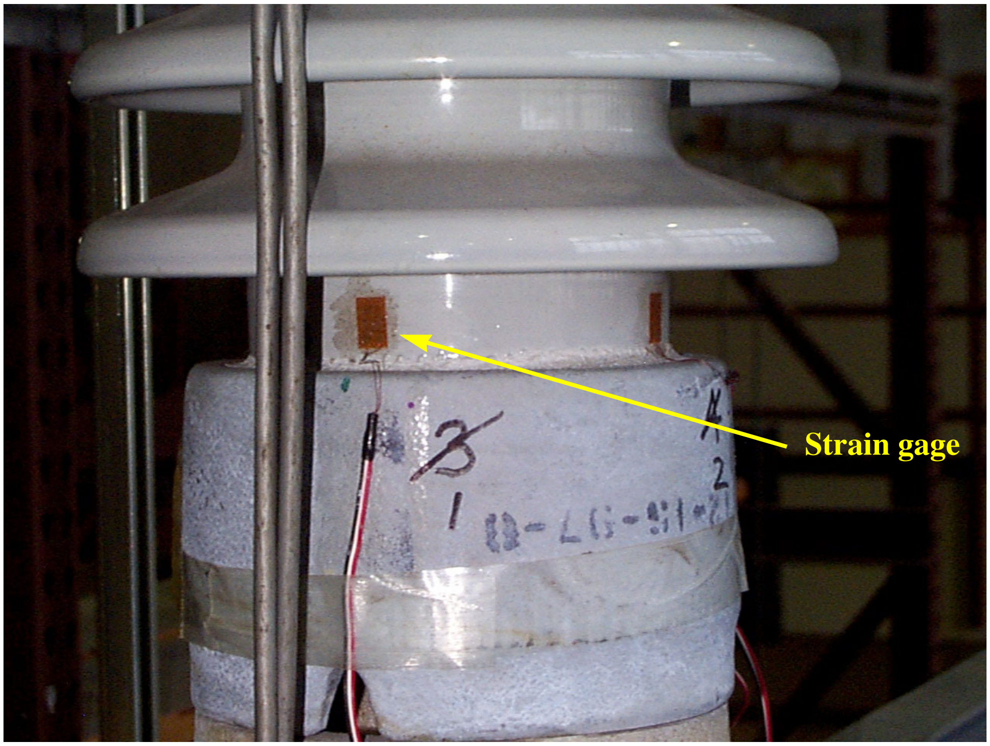

Figure 5-10 Instrumentation at the base of porcelain insulators

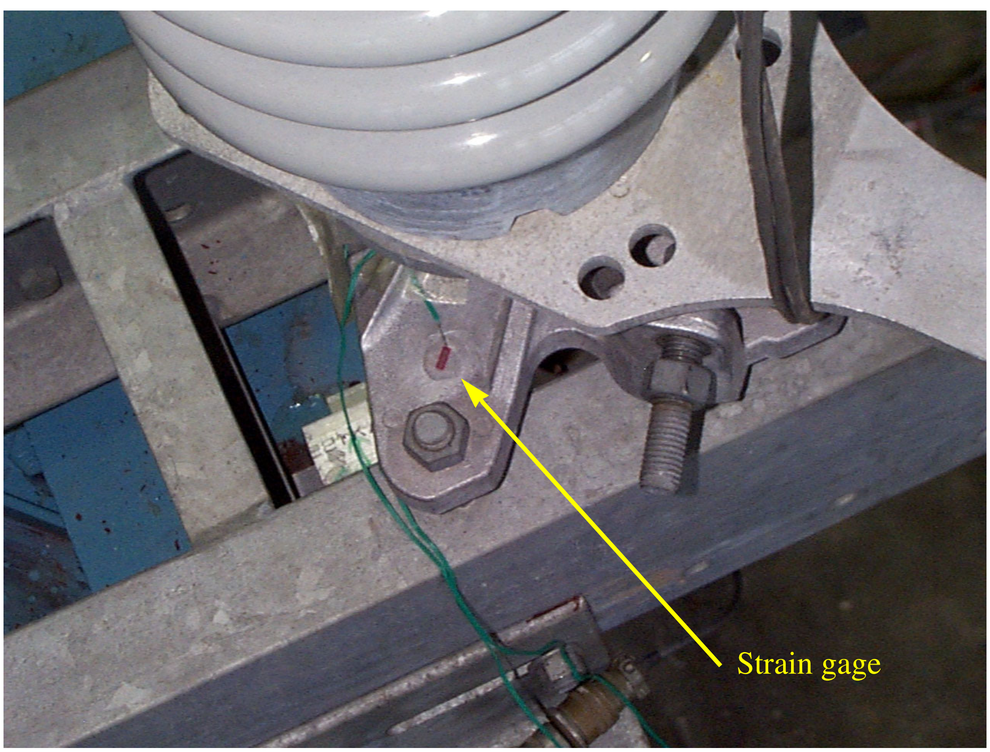

Figure 5-11 Instrumentation for the cast aluminum rotor bearing housing

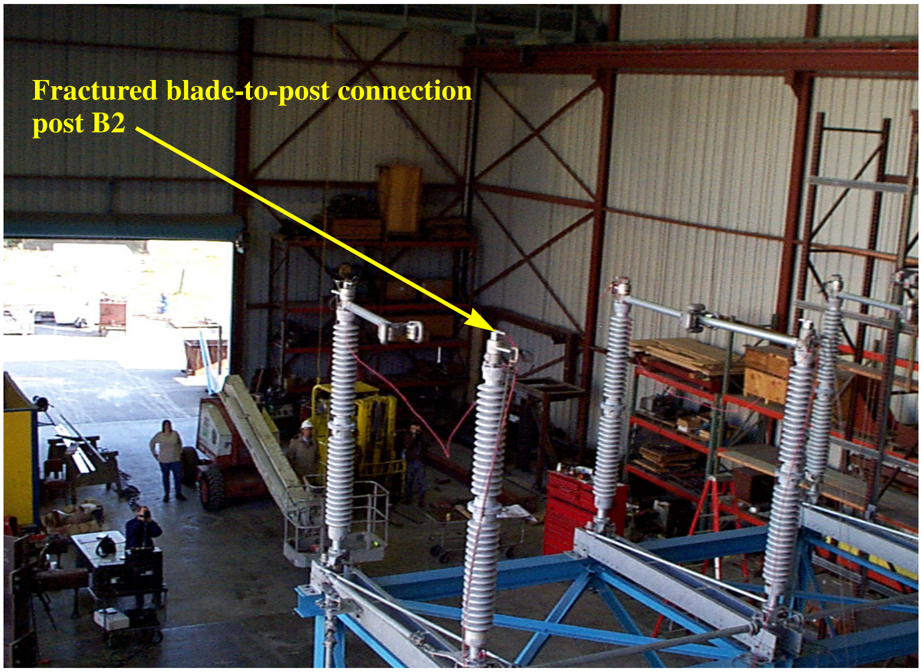

Figure 5-12 Missing blade due to fracture of the weld at the blade-to-post connection, switch SW1, closed blade, after Test 29 (Tabas-1, target PGA = 1.5g)

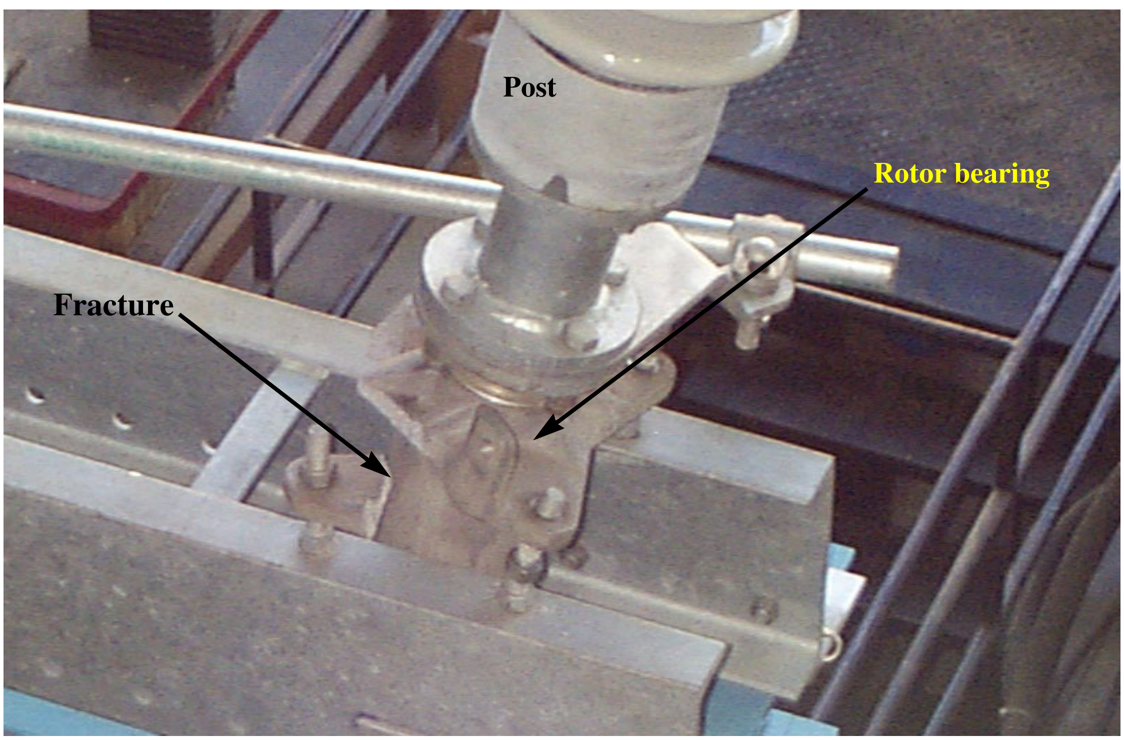

Figure 5-13 Fracture of cast aluminum rotor bearing housing for post B1, switch SW1, open blade, after Test 31 (Tabas-1, target PGA = 1.5g)

Figure 5-14 Tilting of posts due to fracture of cast aluminum rotor bearing housings, switch SW1, open blade, after Test 31 (Tabas-1, target PGA = 1.5g)

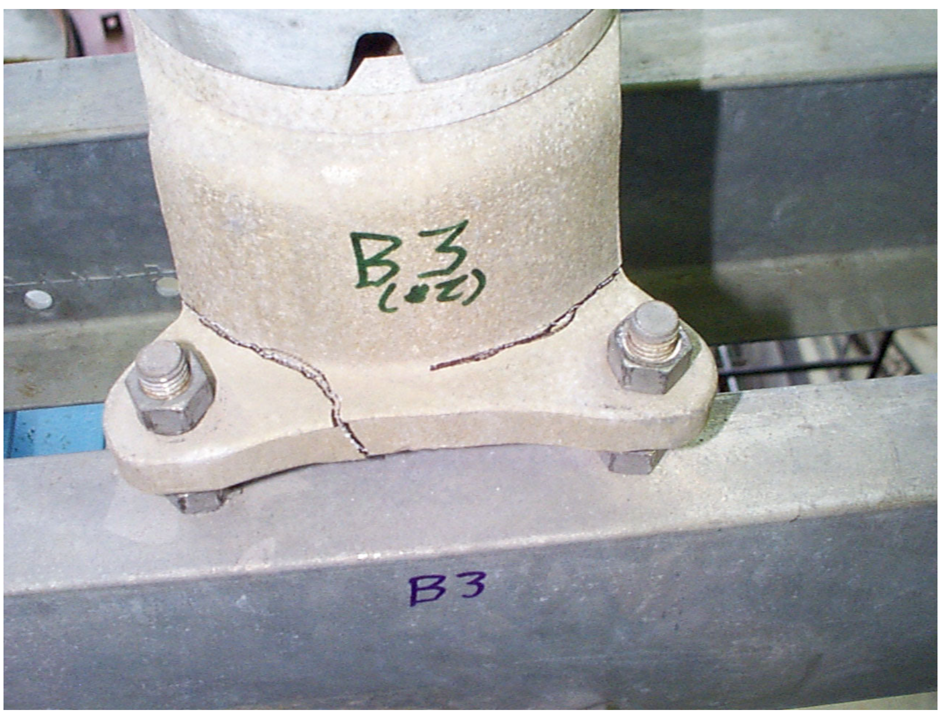

Figure 5-15 Cracking of cast aluminum spacer for post B3, switch SW2, open blade, after Test 23 (Tabas-1, target PGA = 1.0g)

Figure 5-16 Fractured cast aluminum spacer for post C3, switch SW2, open blade, after Test 24 (Tabas-1, target PGA = 1.0g)

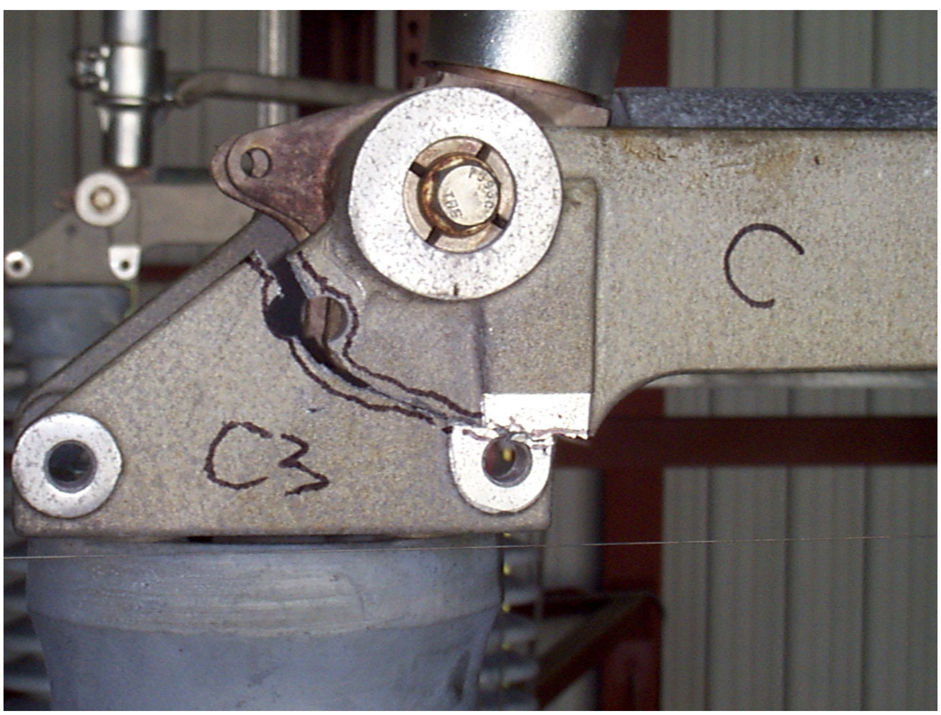

Figure 5-17 Fracture of cast aluminum counterweight atop post C3, switch SW2a, open blade, after Test 47 (Tabas-1, target PGA = 1.75g)

Figure 5-18 Damage to the bolts connecting the double-channel beams to the support frame for switch SW2a, after completion of tests

Figure 5-19 Dislodged piston atop pole B, switch SW3, open blade, after Test 18 (Tabas-1, target PGA = 0.5g)

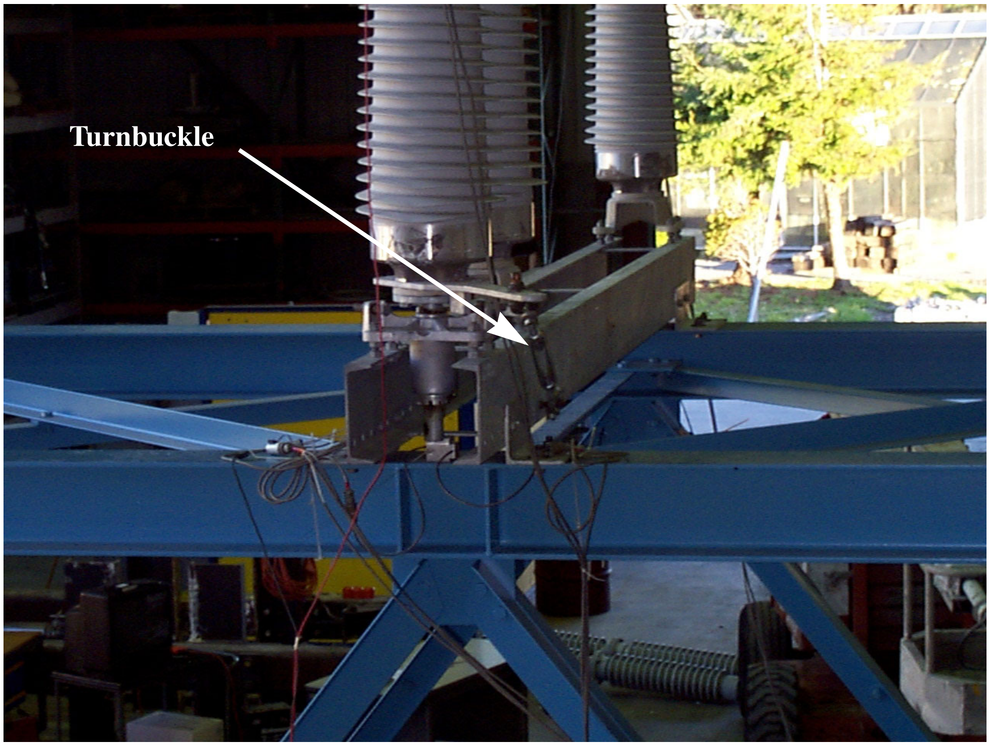

Figure 5-20 Alternative attachment of poles to the support frame, switch SW3

Figure 5-21 Cracking of cast aluminum spacer at the base of post B3, switch SW3, open blade, after Test 58 (Tabas-2, target PGA = 2.0g)

Figure 5-22 Fracture of welded blade-to-post connection for post C2, switch SW4, closed blade, after Test 25 (Tabas-2, target PGA = 1.0g)

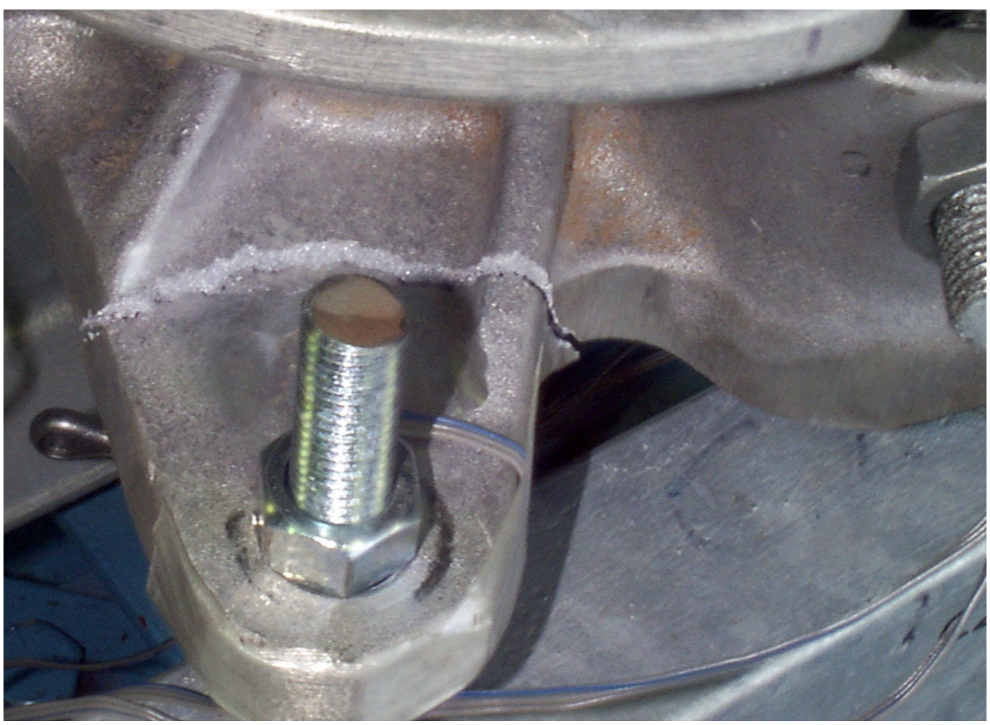

Figure 5-23 Fracture of cast aluminum rotor bearing housing for post C2, switch SW4, open blade, after Test 36 (Tabas-2, target PGA = 3.0g)

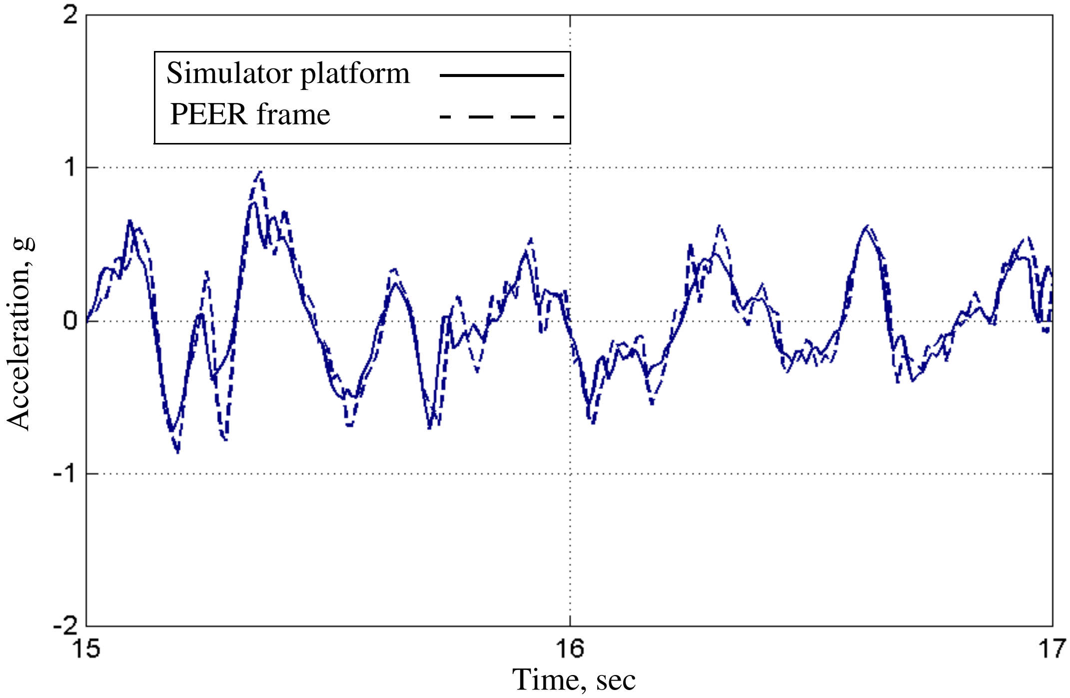

(a) *x*-direction

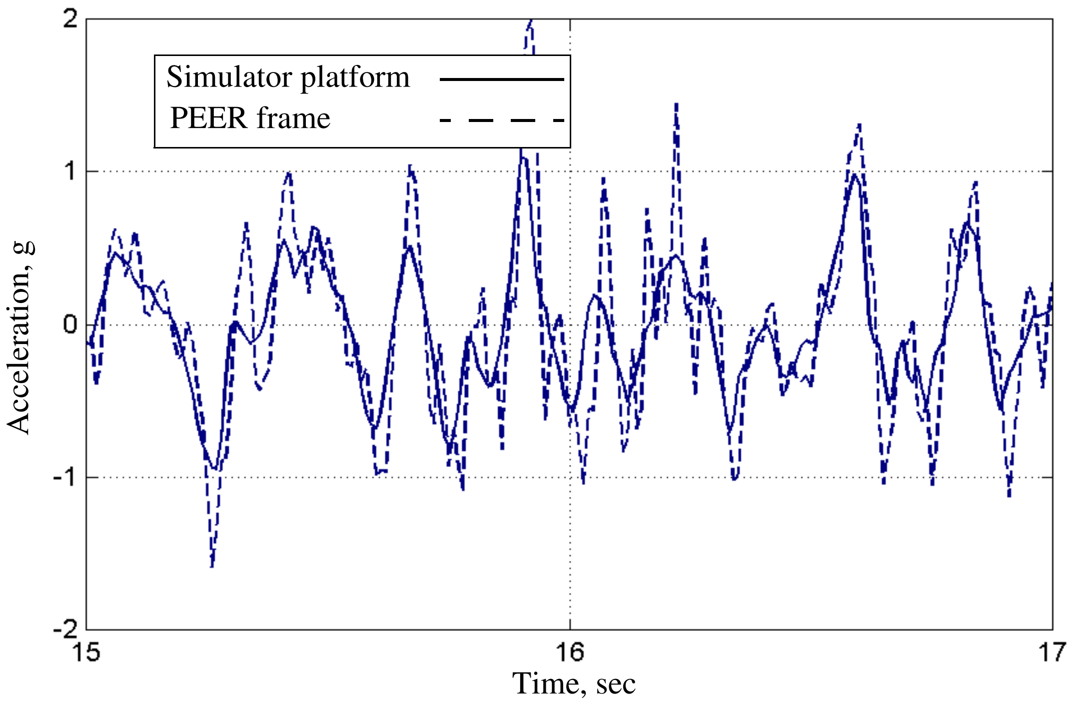

(b) *y*-direction

Figure 5-24 Acceleration response of the PEER frame

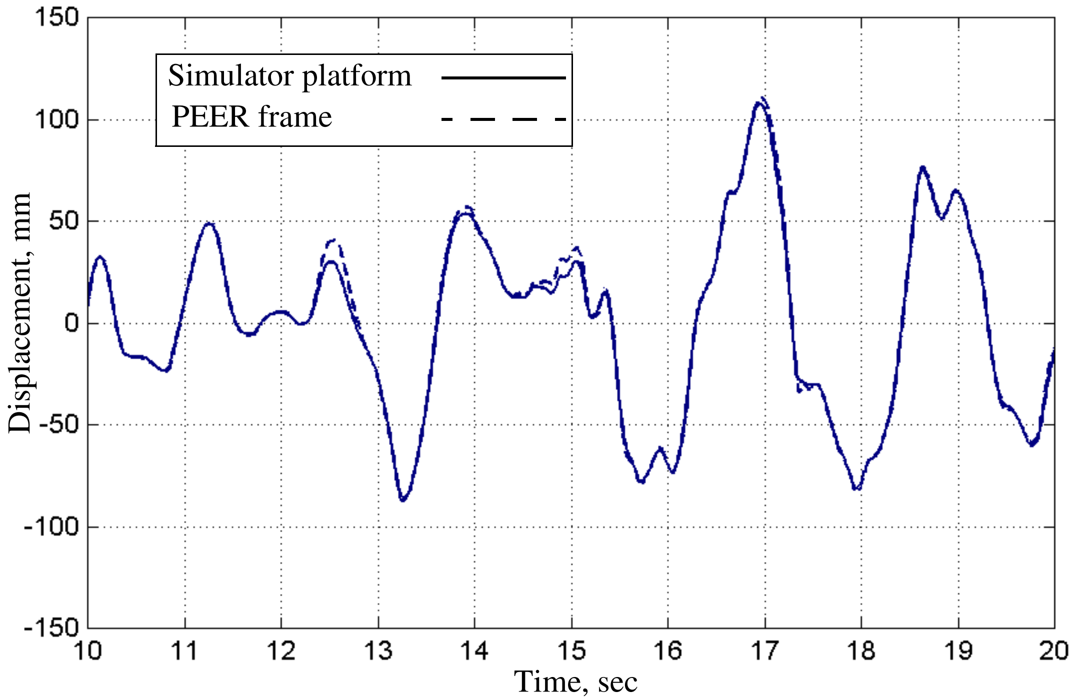

(a) *x*-direction

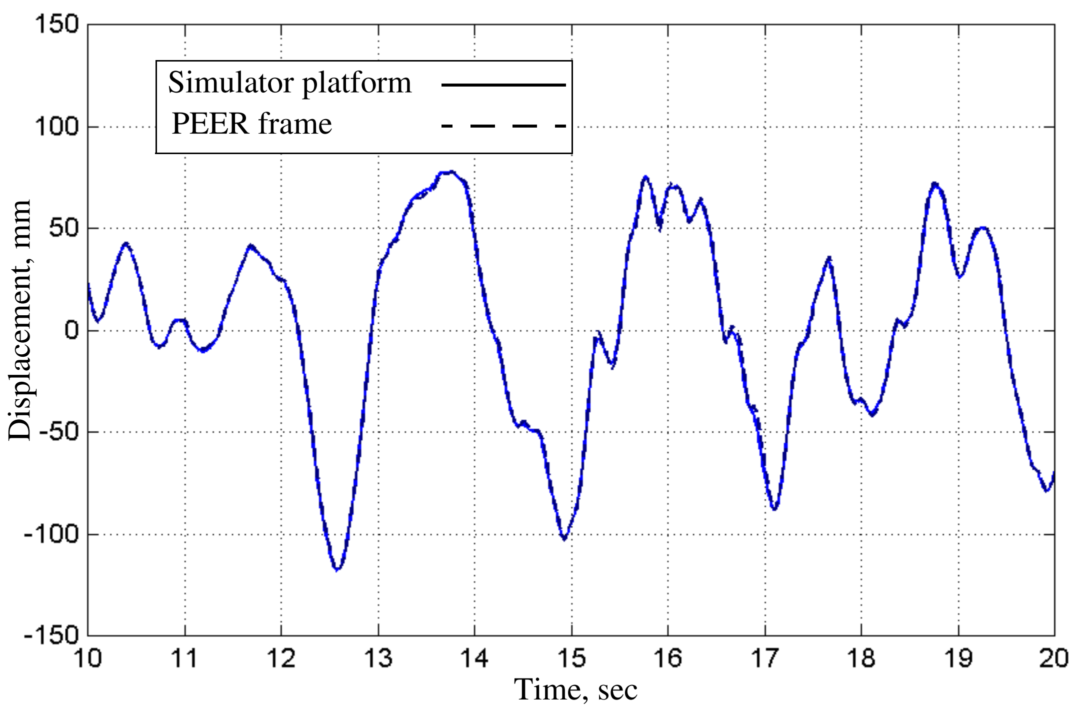

(b) *y*-direction

Figure 5-25 Displacement response of the PEER frame with respect to the simulator platform

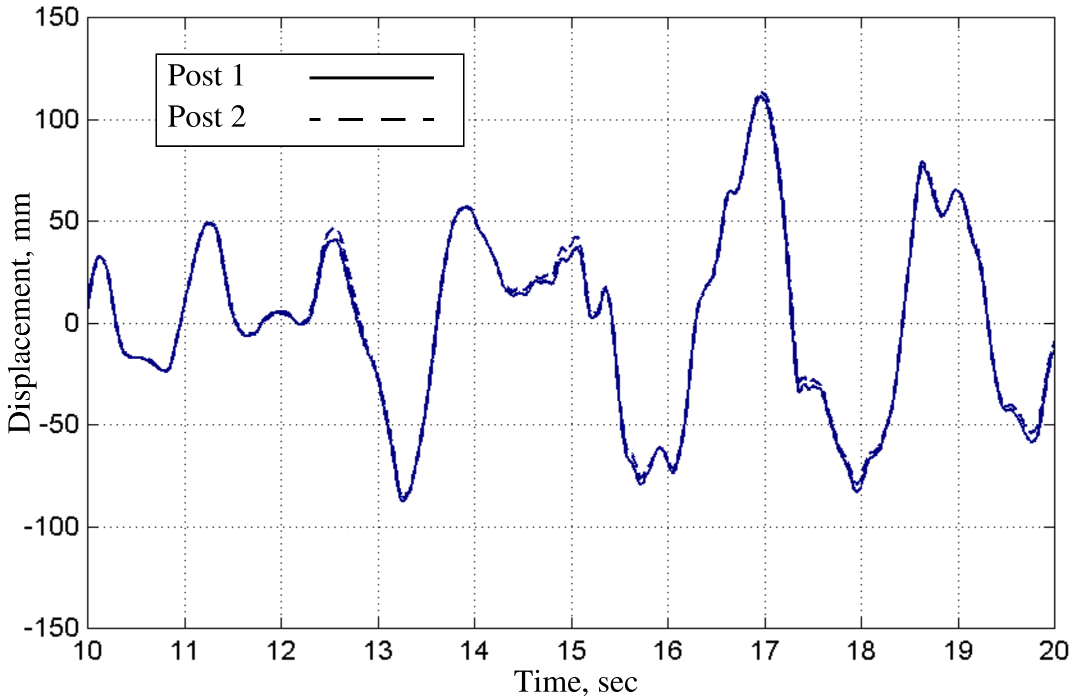

(a) *x*-direction

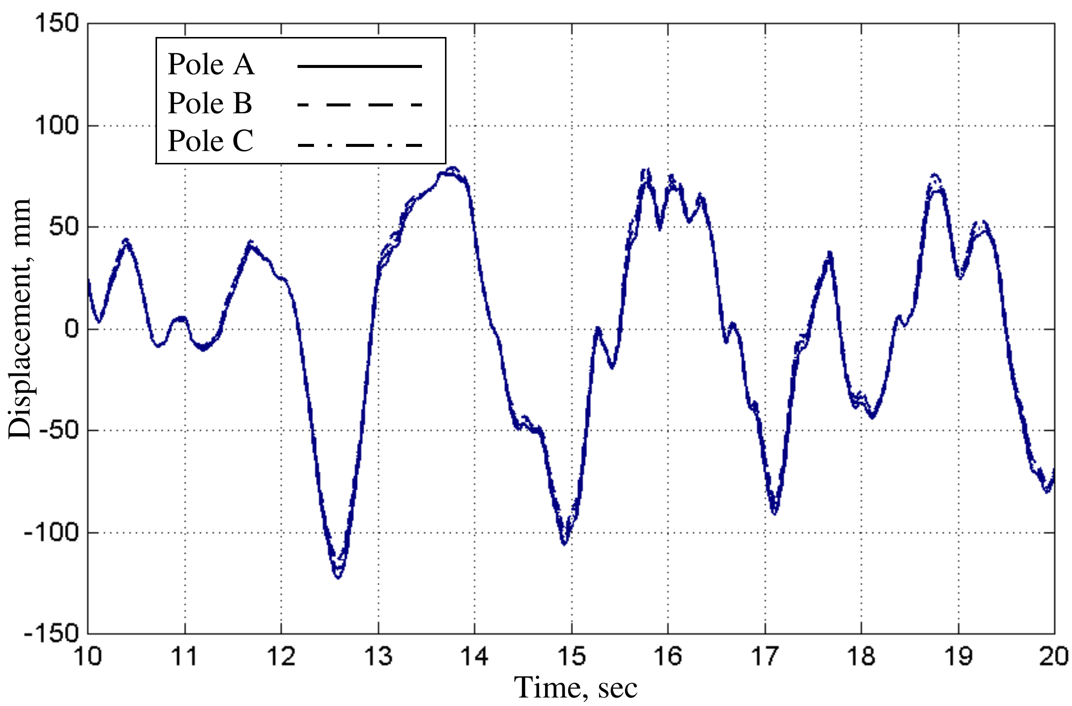

(b) *y*-direction

Figure 5-26 Displacement histories at base of switch posts

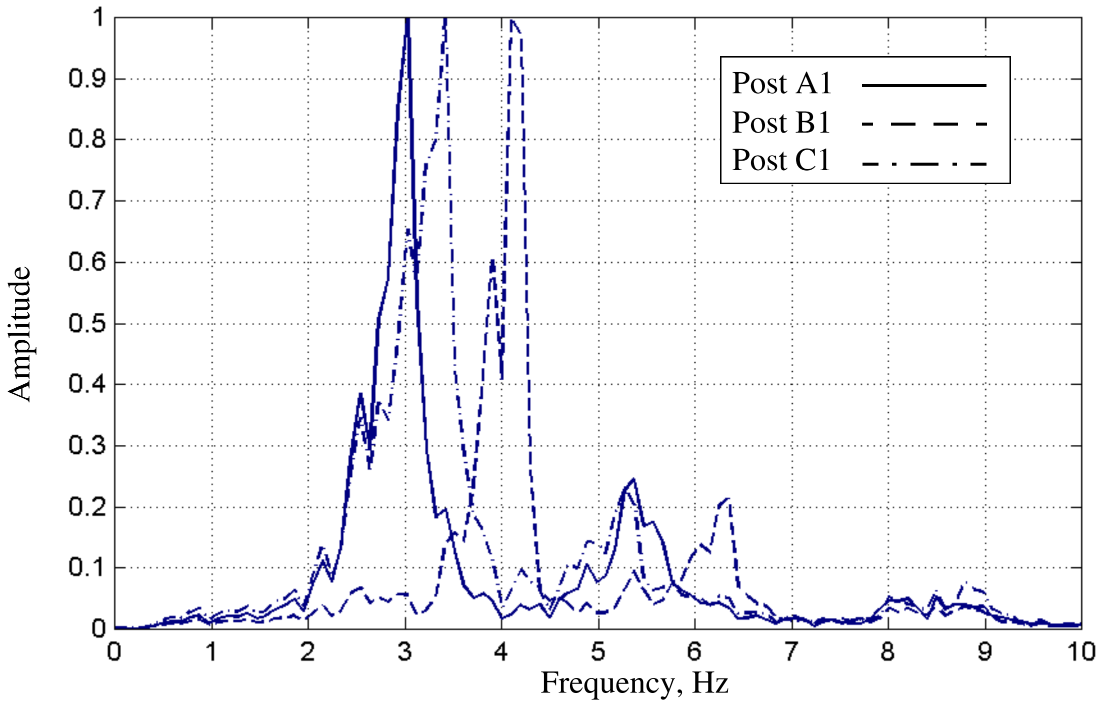

(a) *x*-direction

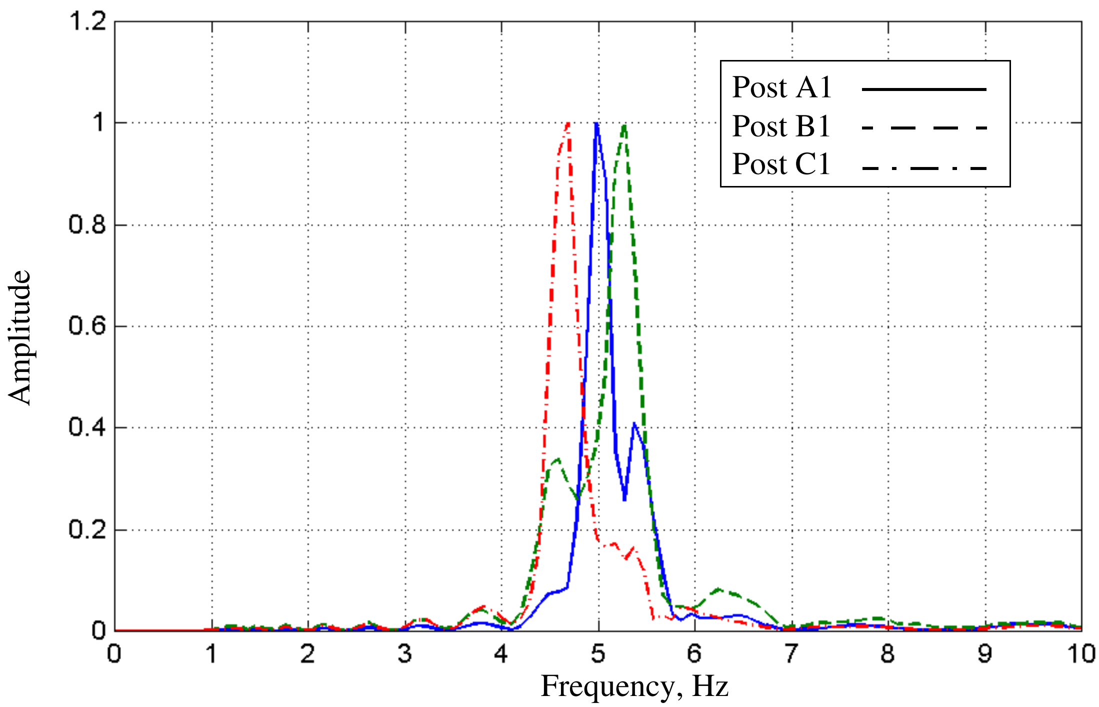

(b) *y*-direction

Figure 5-27 Power spectra for switch posts, closed blade, switch SW1 on the PEER frame

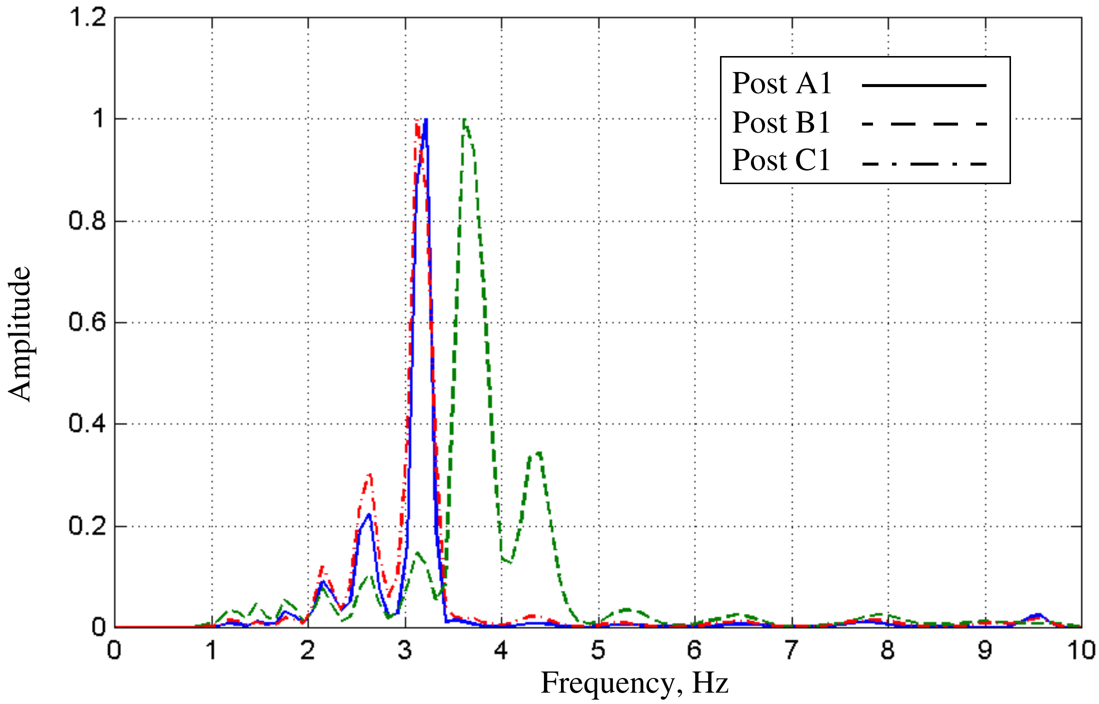

(a) *x*-direction

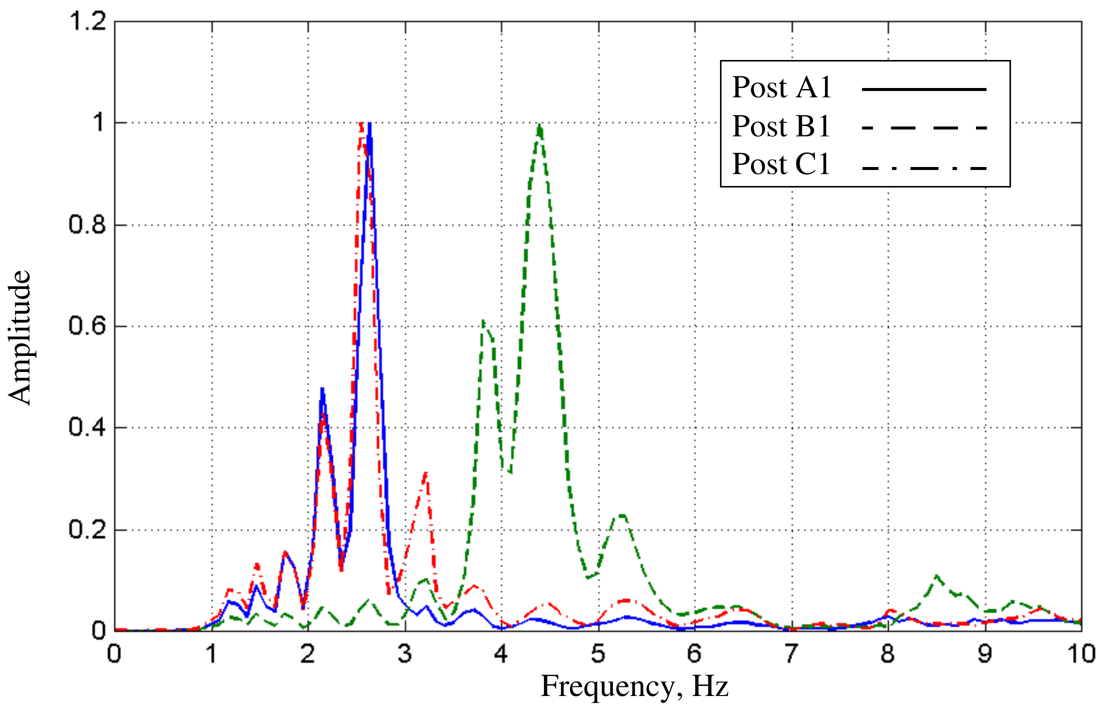

(b) *y*-direction

Figure 5-28 Power spectra for switch posts, open blade, switch SW1on the PEER frame

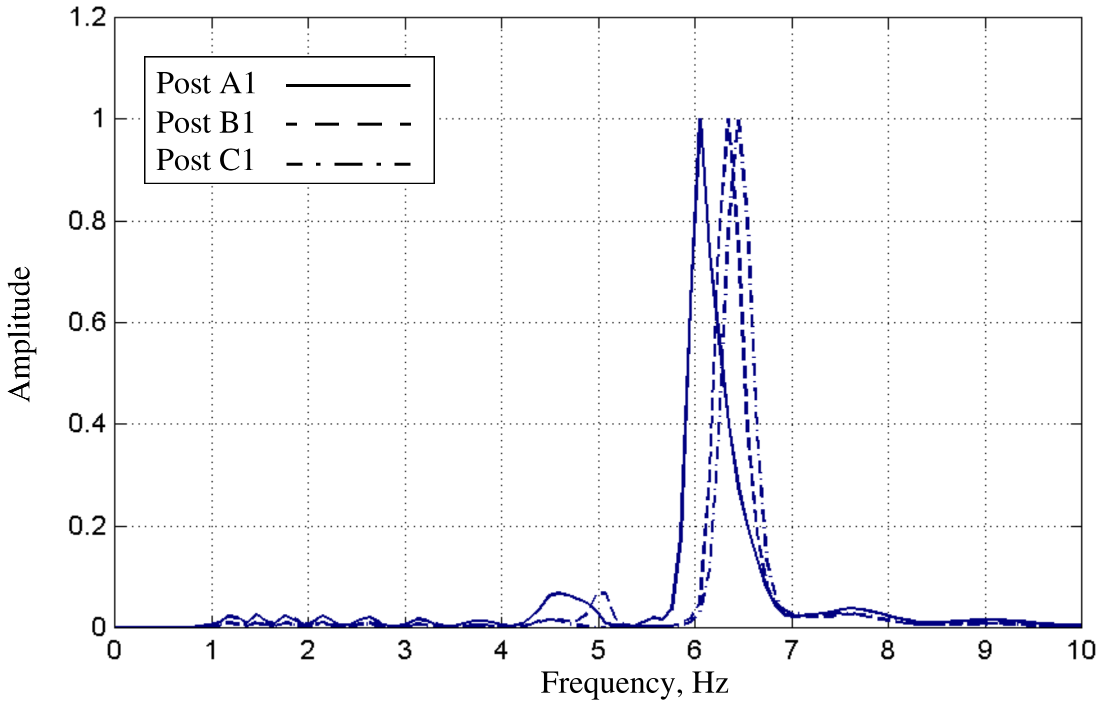

(a) *x*-direction

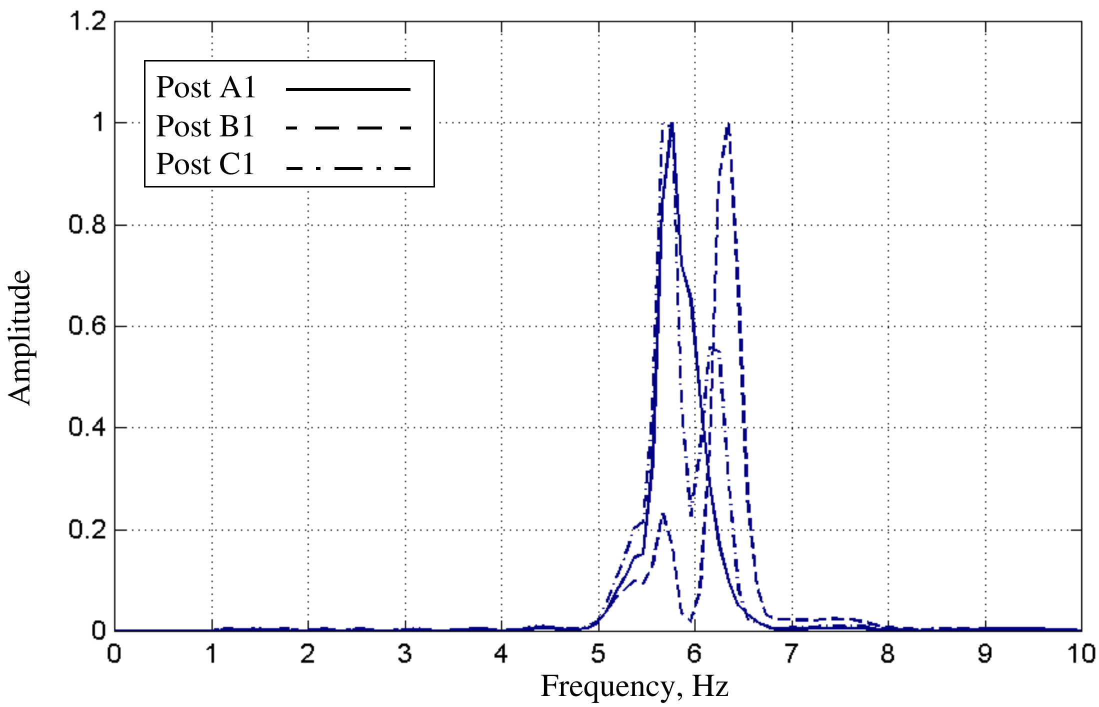

(b) *y*-direction

Figure 5-29 Power spectra for switch posts, closed blade, switch SW2 on the PEER frame

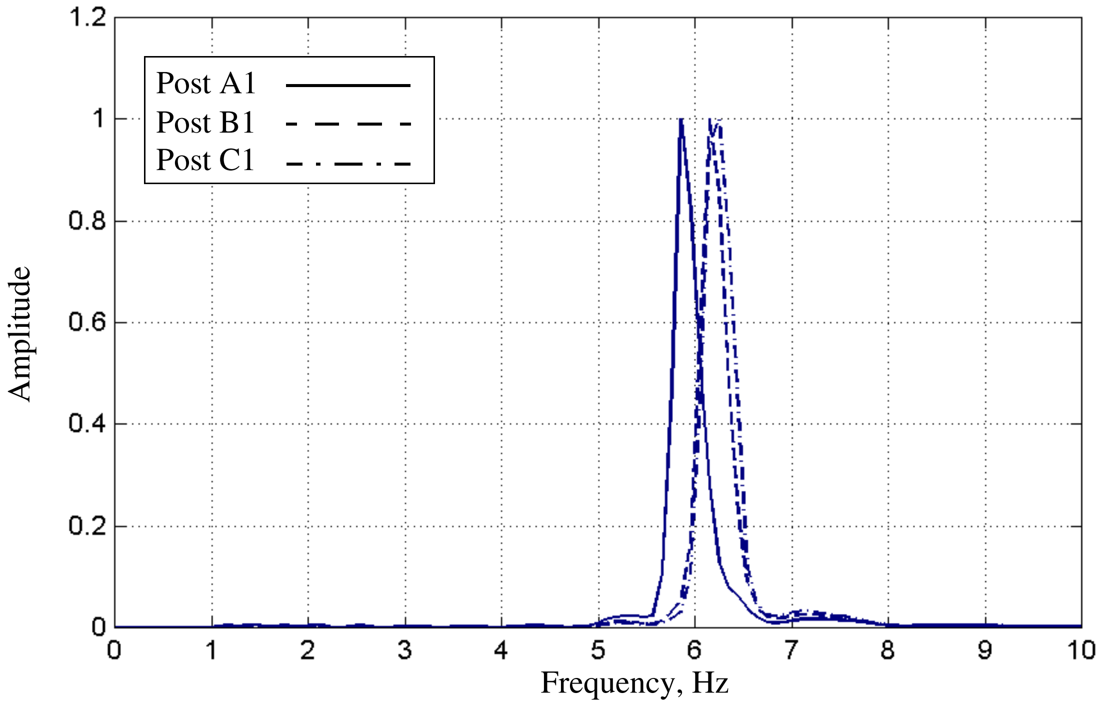

(a) *x*-direction

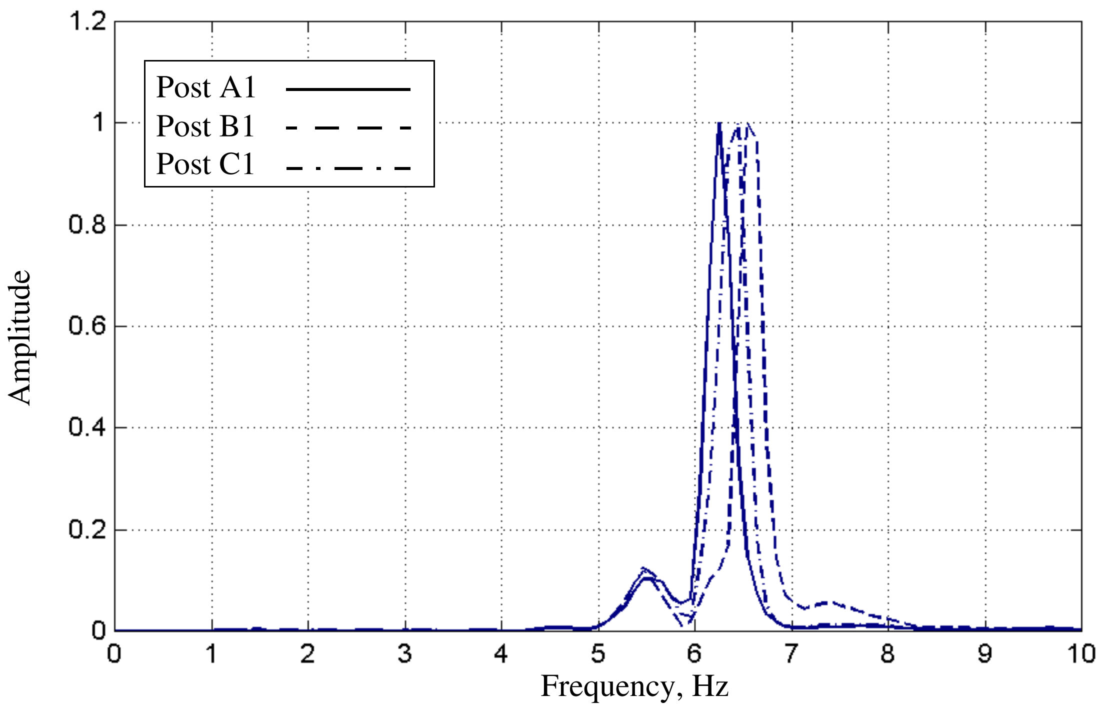

(b) *y*-direction

Figure 5-30 Power spectra for switch posts, open blade, switch SW2 on the PEER frame

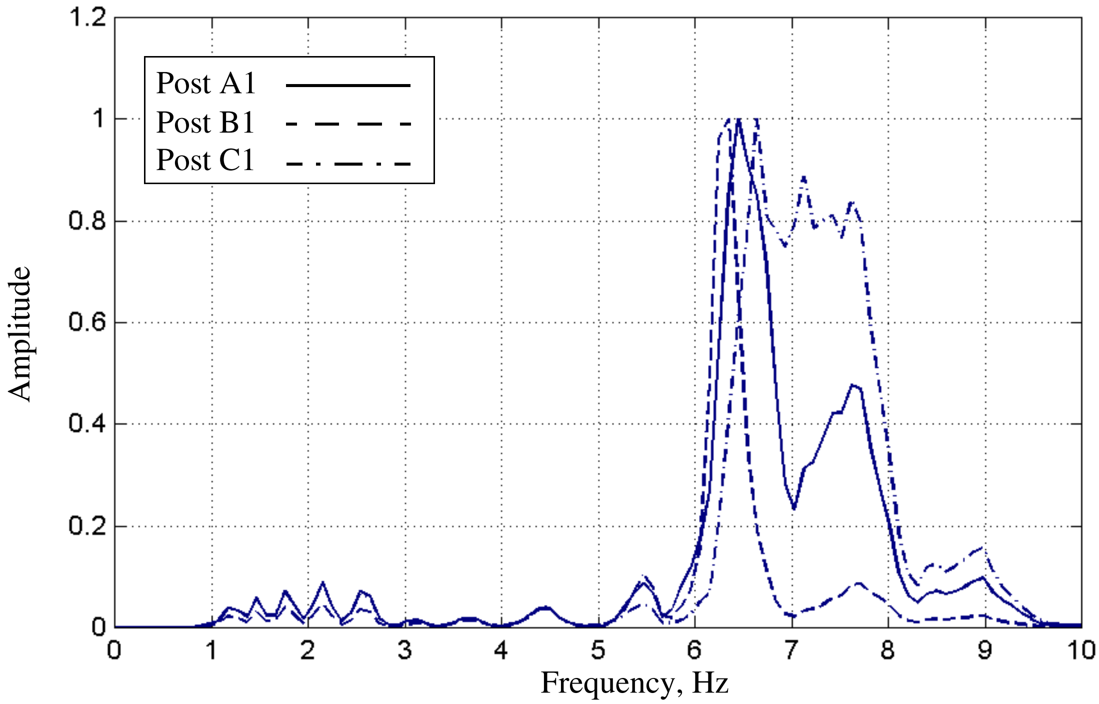

(a) *x*-direction

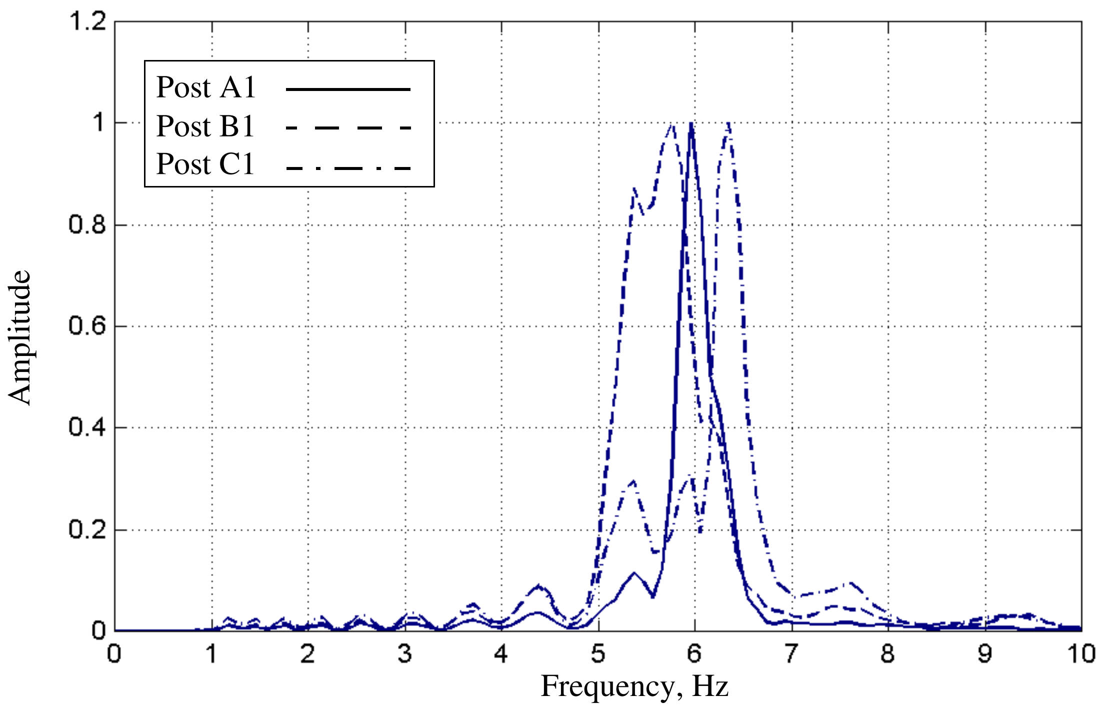

(b) *y*-direction

Figure 5-31 Power spectra for switch posts, closed blade, switch SW2a on the PEER frame

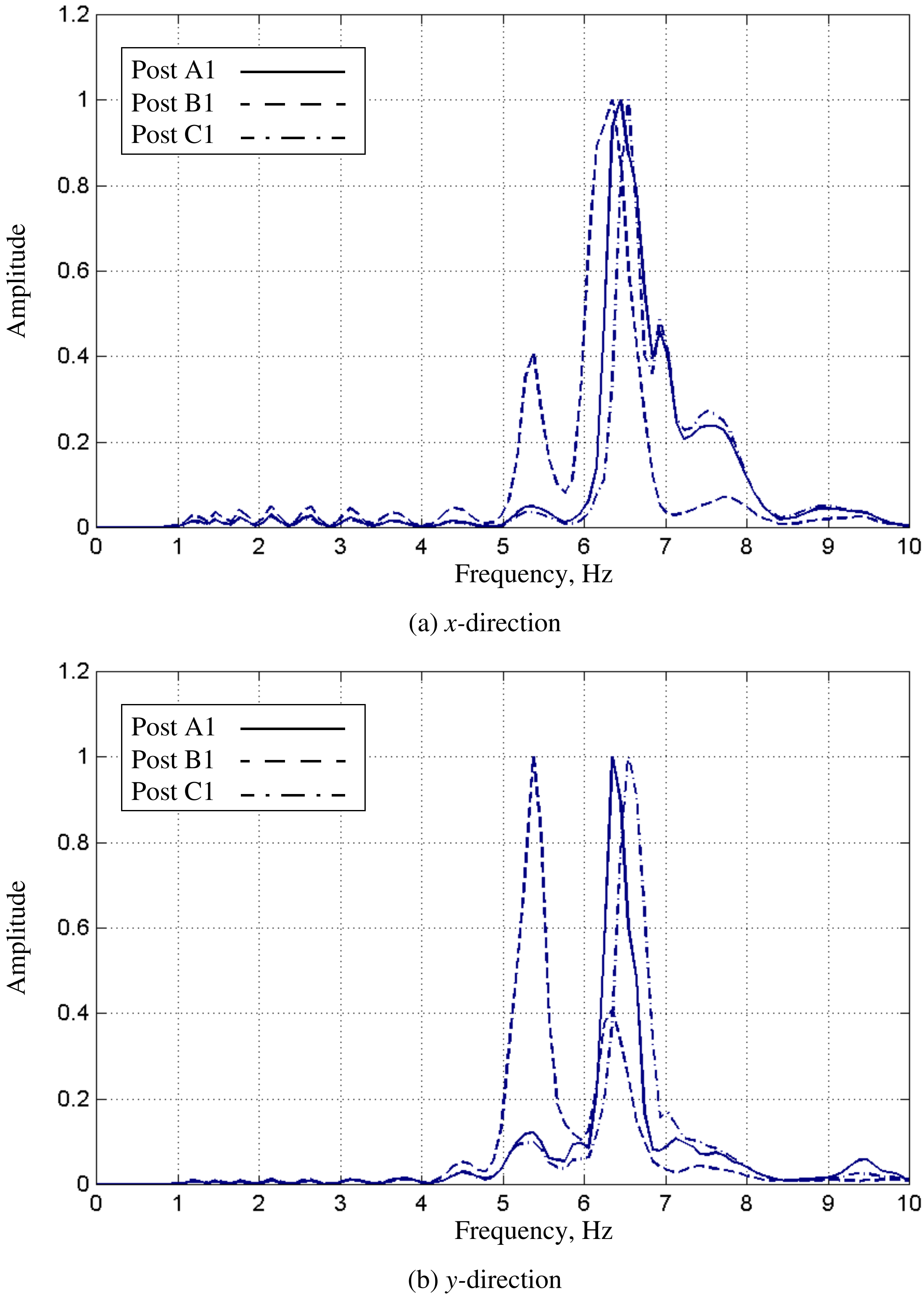

Figure 5-32 Power spectra for switch posts, open blade, switch SW2a on the PEER frame

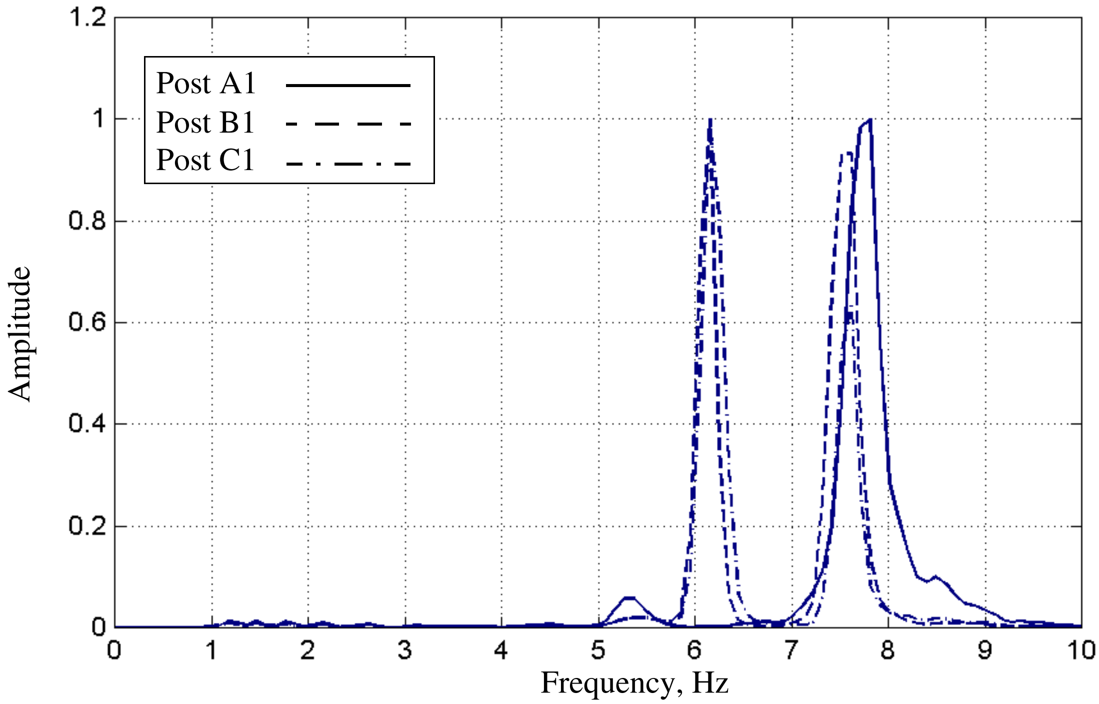

(a) *x*-direction

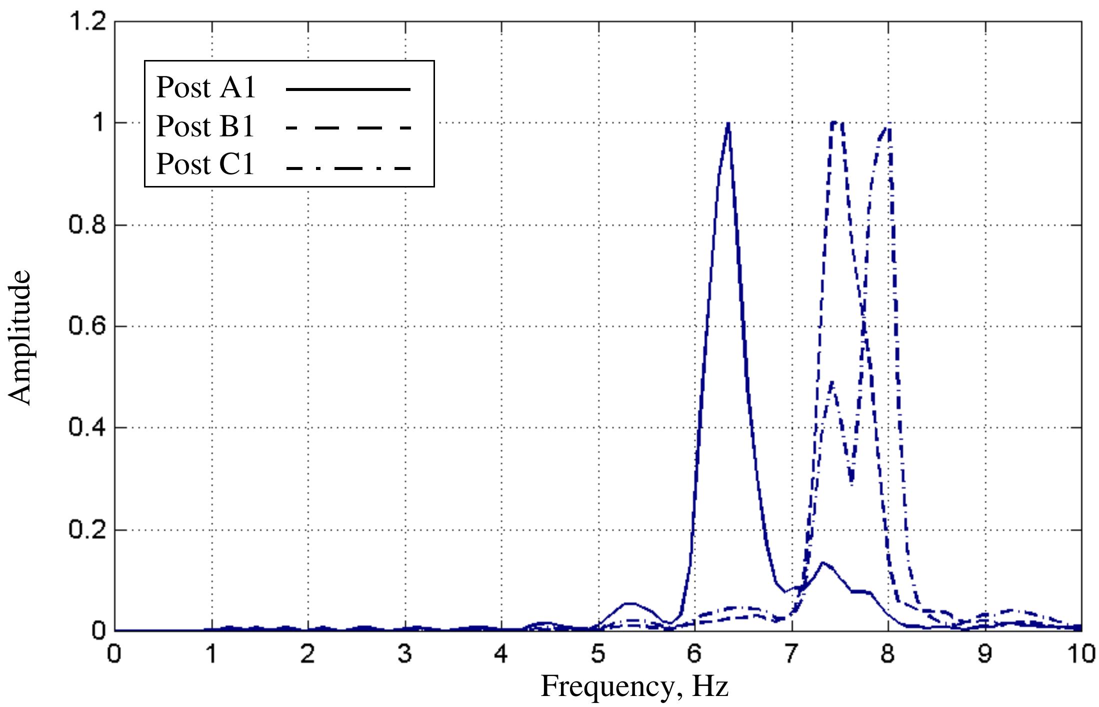

(b) *y*-direction

Figure 5-33 Power spectra for switch posts, closed blade, switch SW3 on the PEER frame

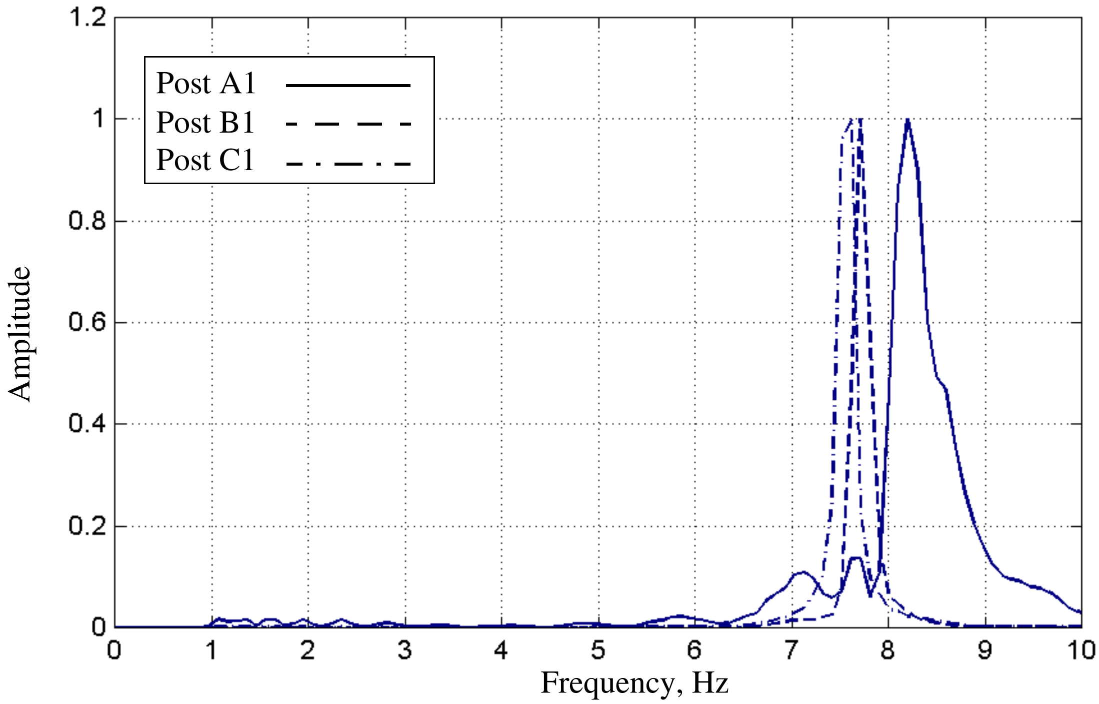

(a) *x*-direction

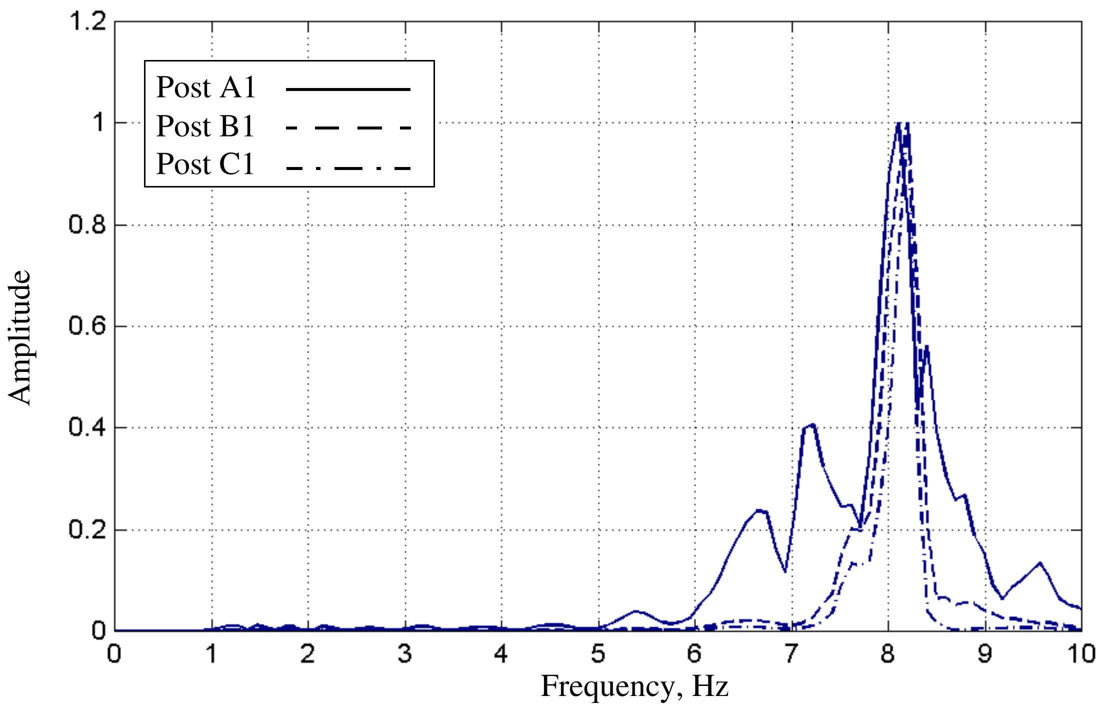

(b) *y*-direction

Figure 5-34 Power spectra for switch posts, open blade, switch SW3 on the PEER frame

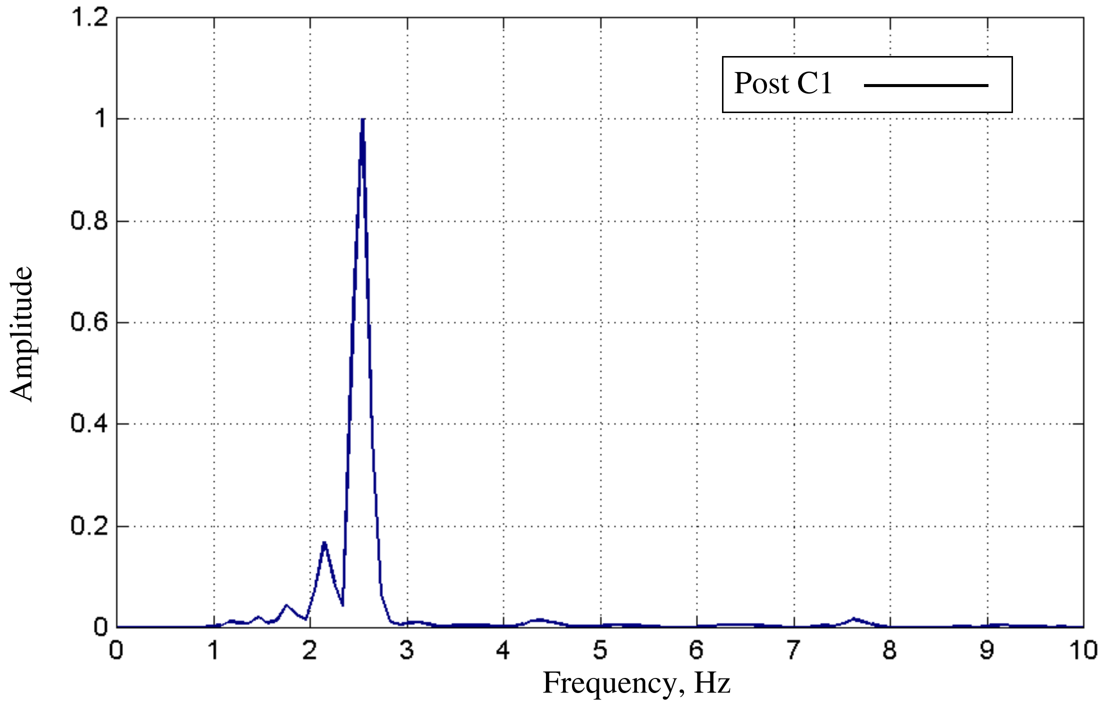

(a) *x*-direction

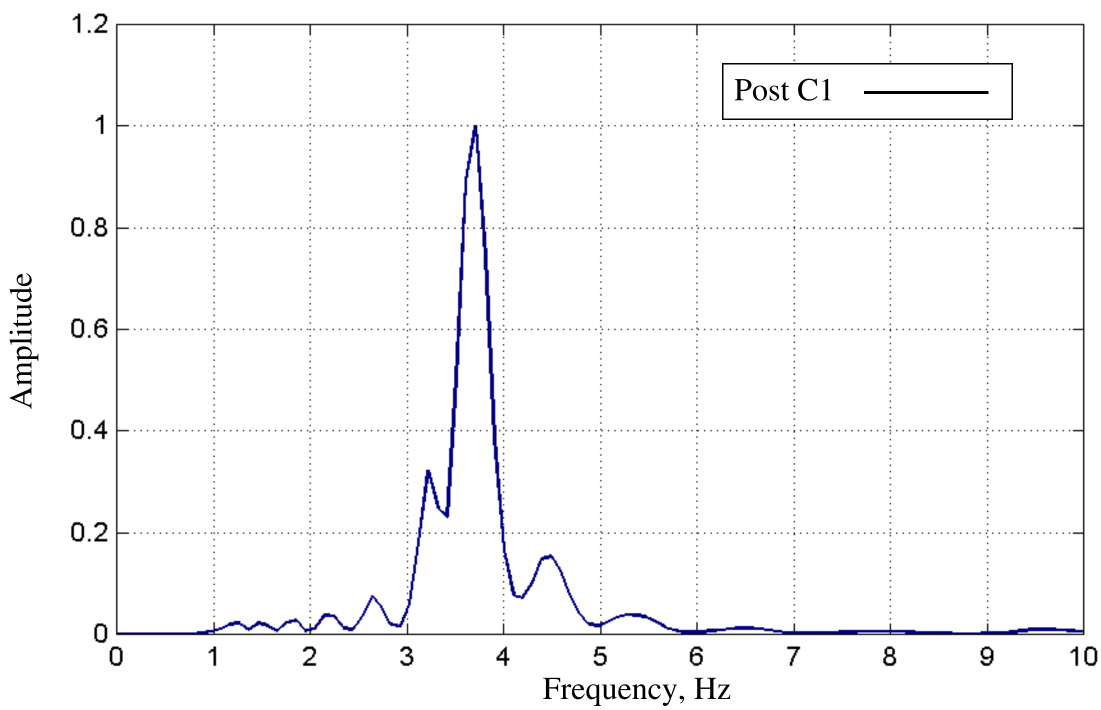

(b) *y*-direction

Figure 5-35 Power spectra for switch posts, closed blade, switch SW4 on the PEER frame

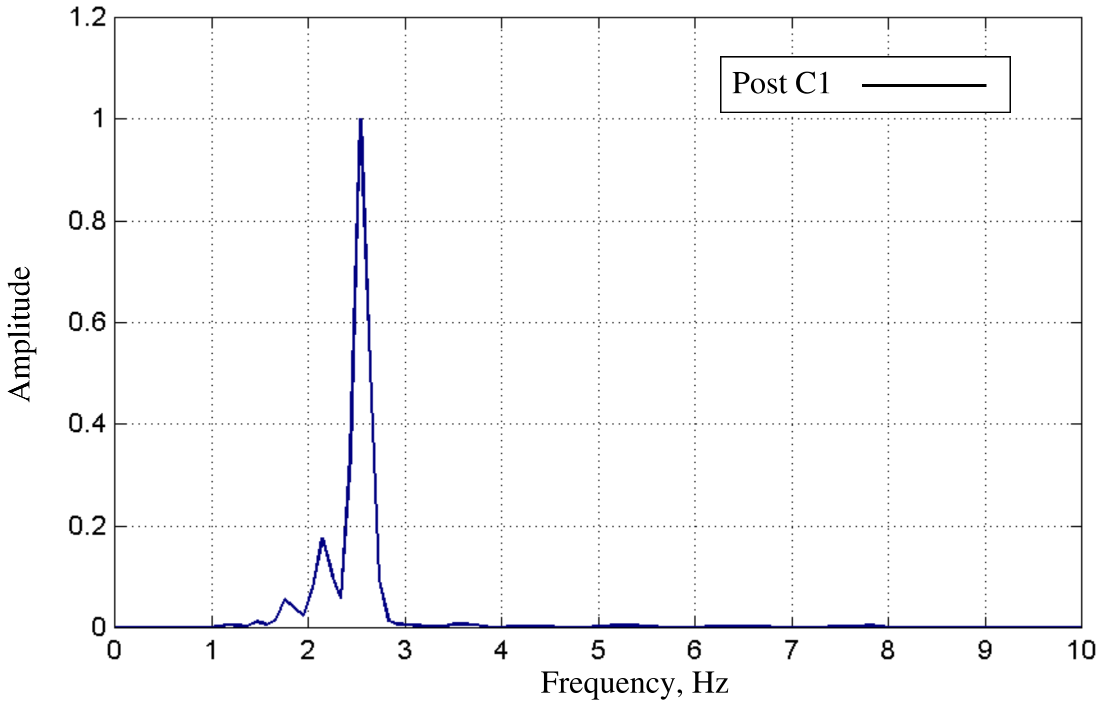

(a) *x*-direction

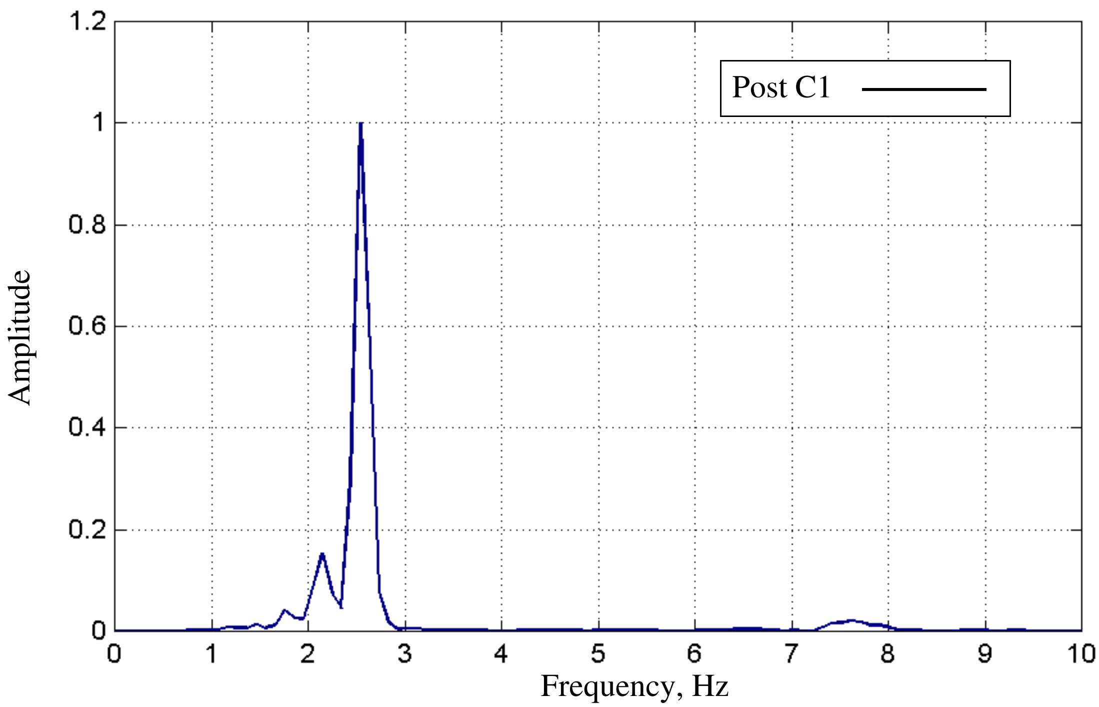

(b) *y*-direction

Figure 5-36 Power spectra for switch posts, open blade, switch SW4 on the PEER frame

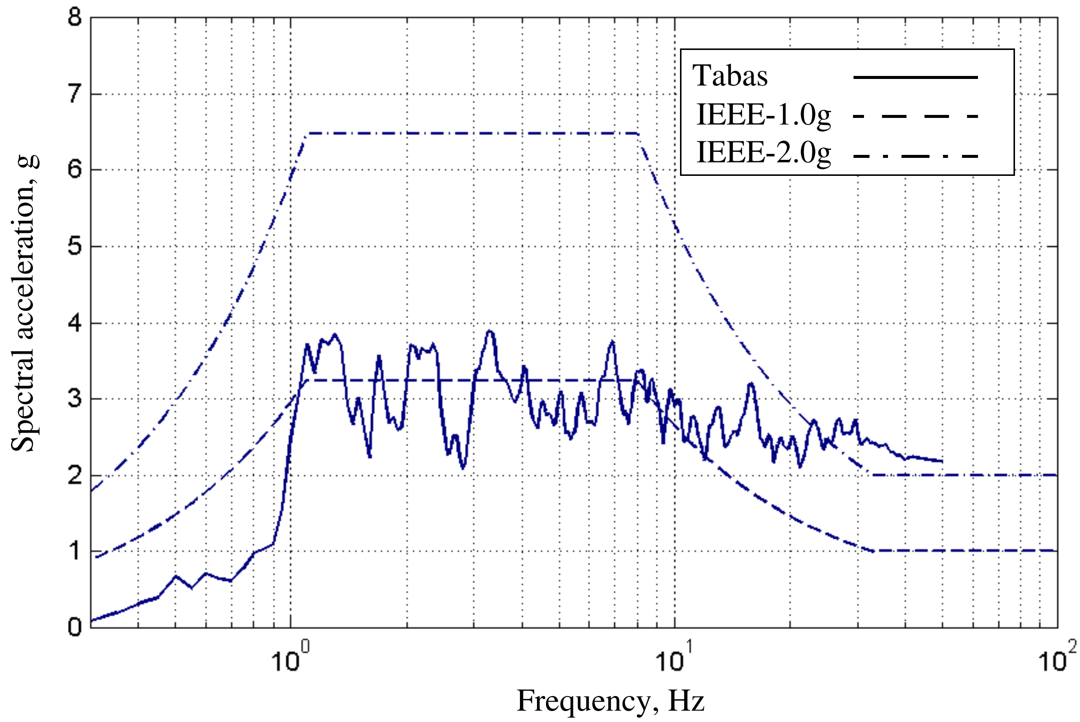

(a) *x*-direction

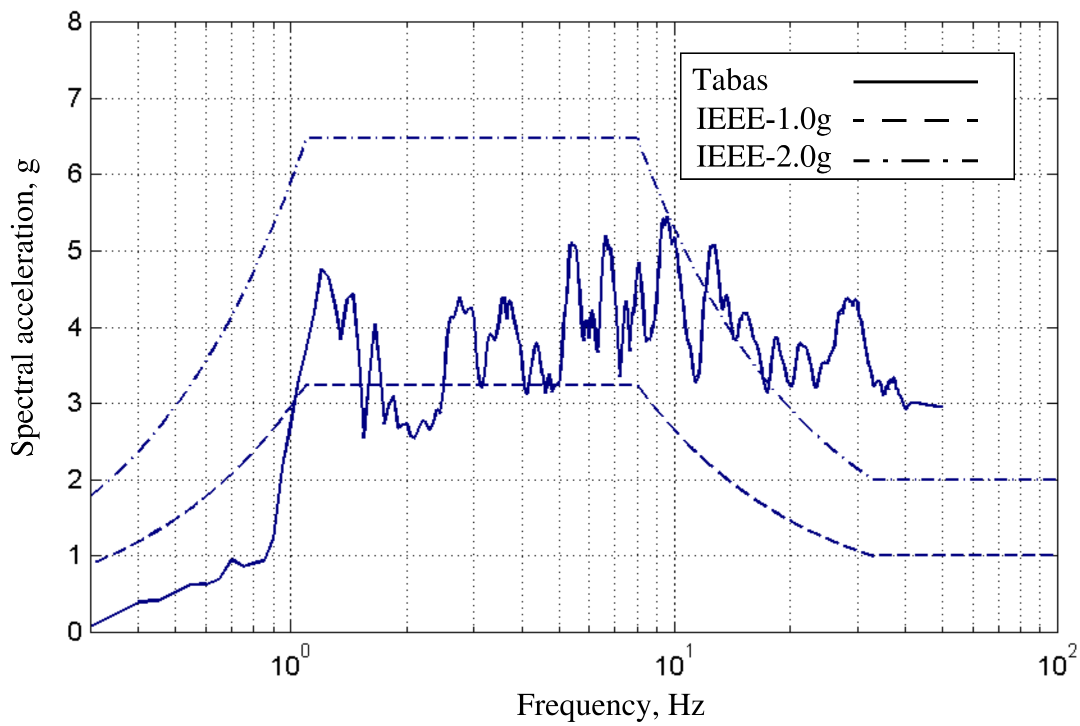

(b) *y*-direction

Figure 5-37 Response spectra for SW1 (2-percent damped, closed switch, Tests 21 and 22, target PGA equal to 1.0g)

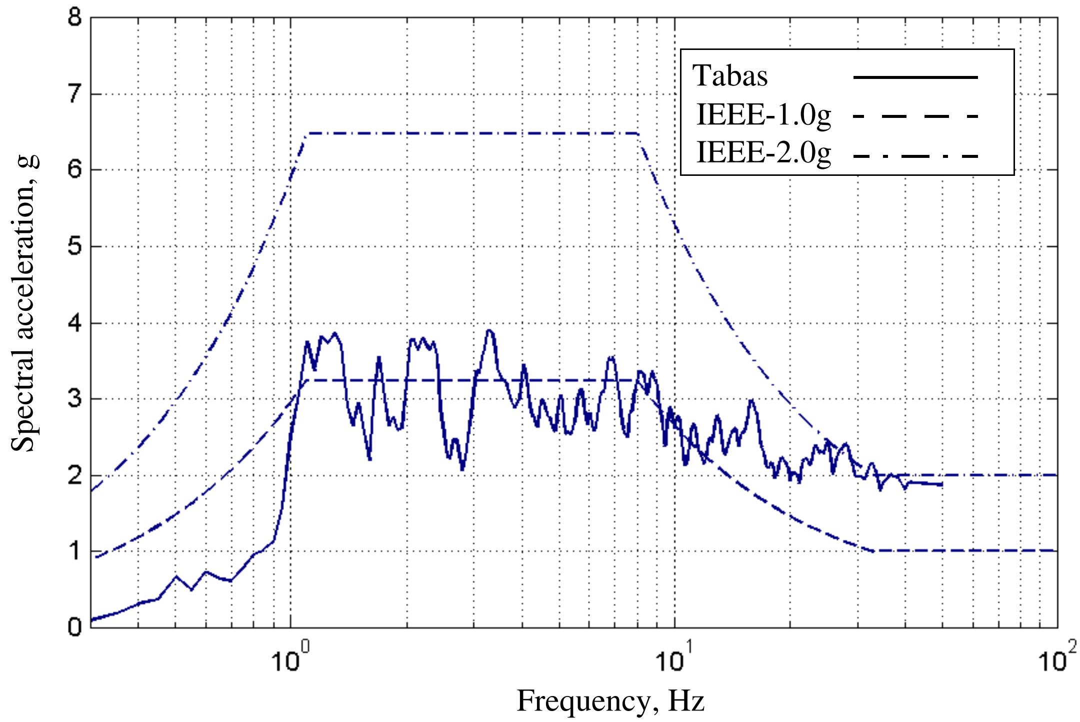

(a) *x*-direction

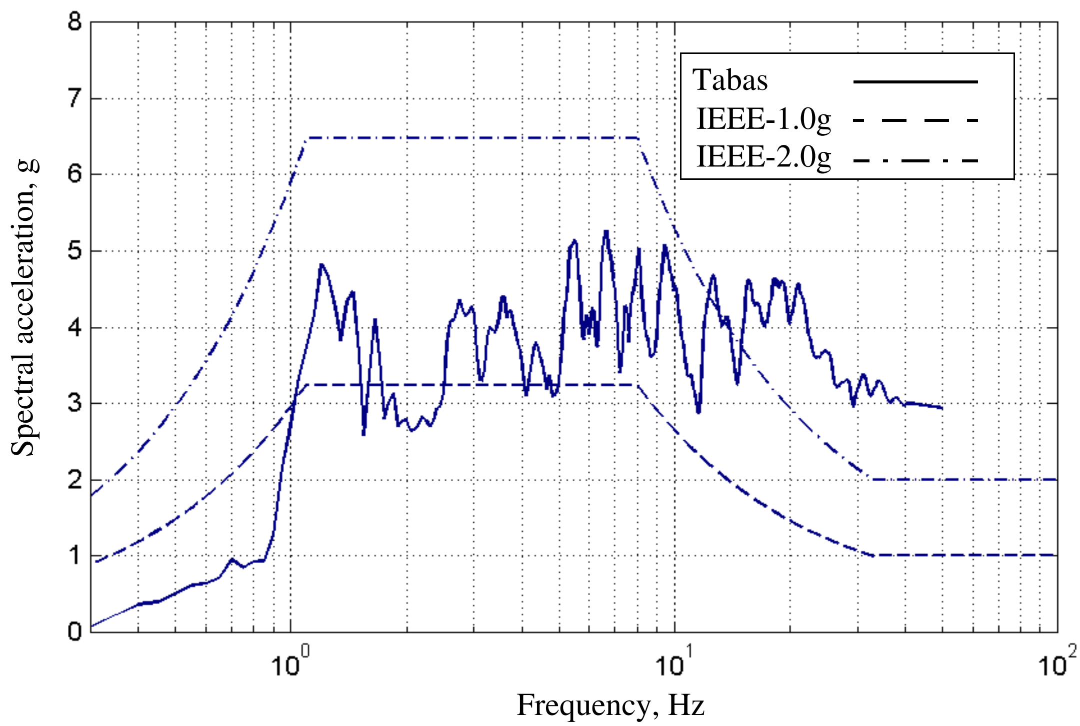

(b) *y*-direction

Figure 5-38 Response spectra for SW1 (2-percent damped, open switch, Tests 23 and 24, target PGA equal to 1.0g)

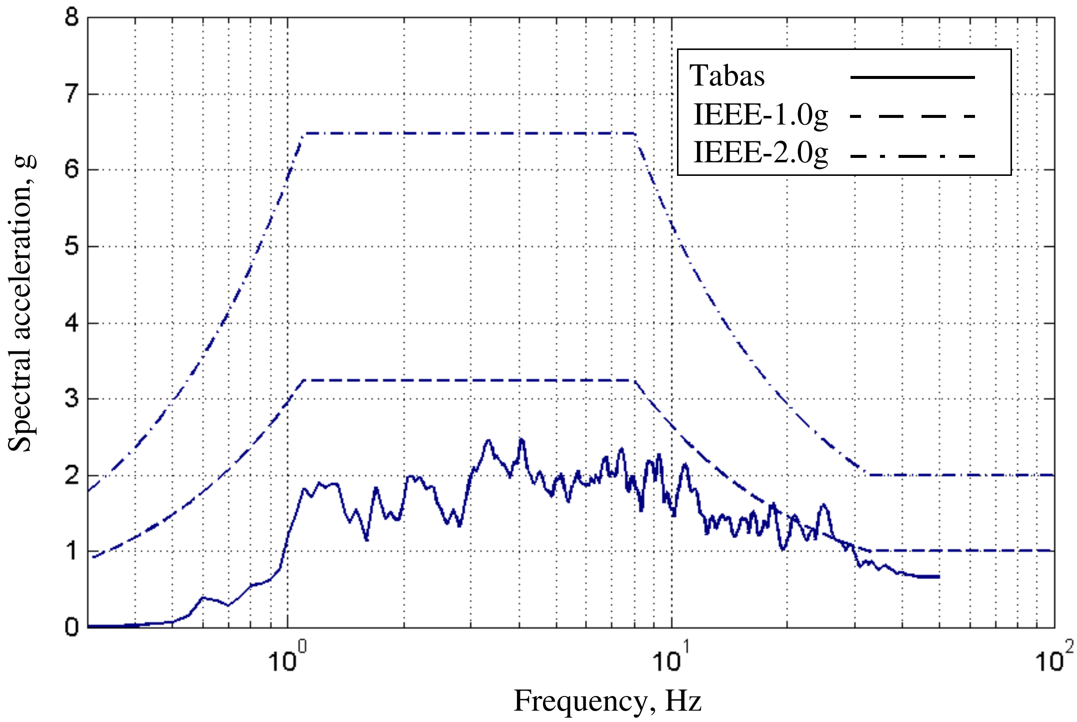

(a) *x*-direction

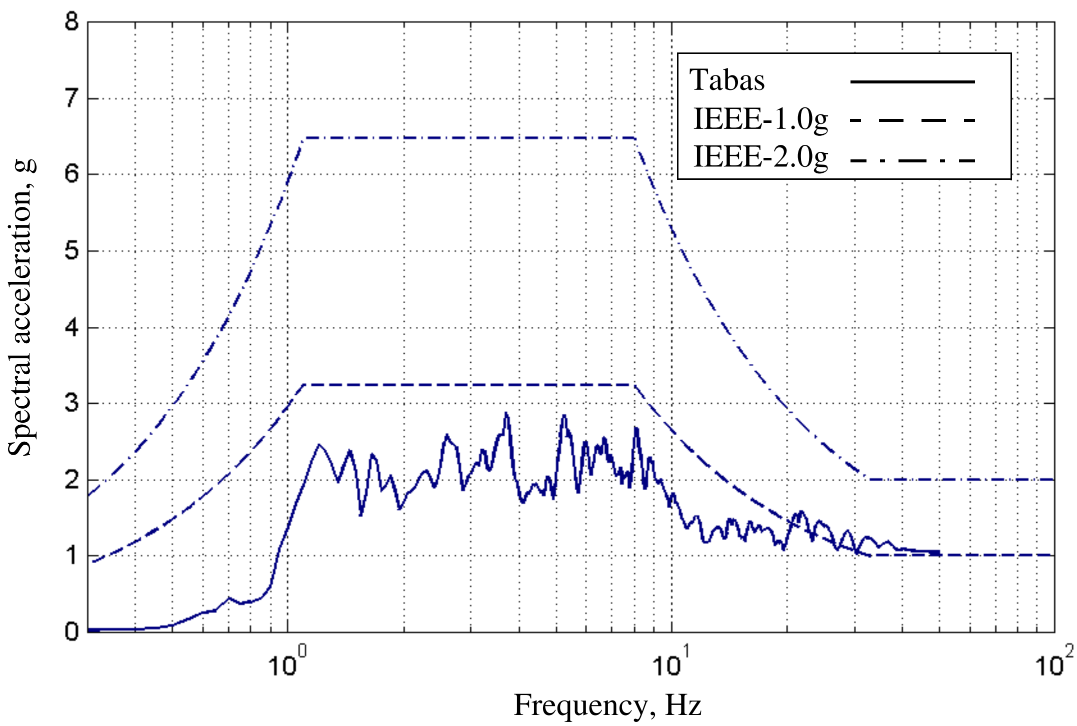

(b) *y*-direction

Figure 5-39 Response spectra for SW2 (2-percent damped, closed switch, Tests 7 and 8, target PGA equal to 0.5g)

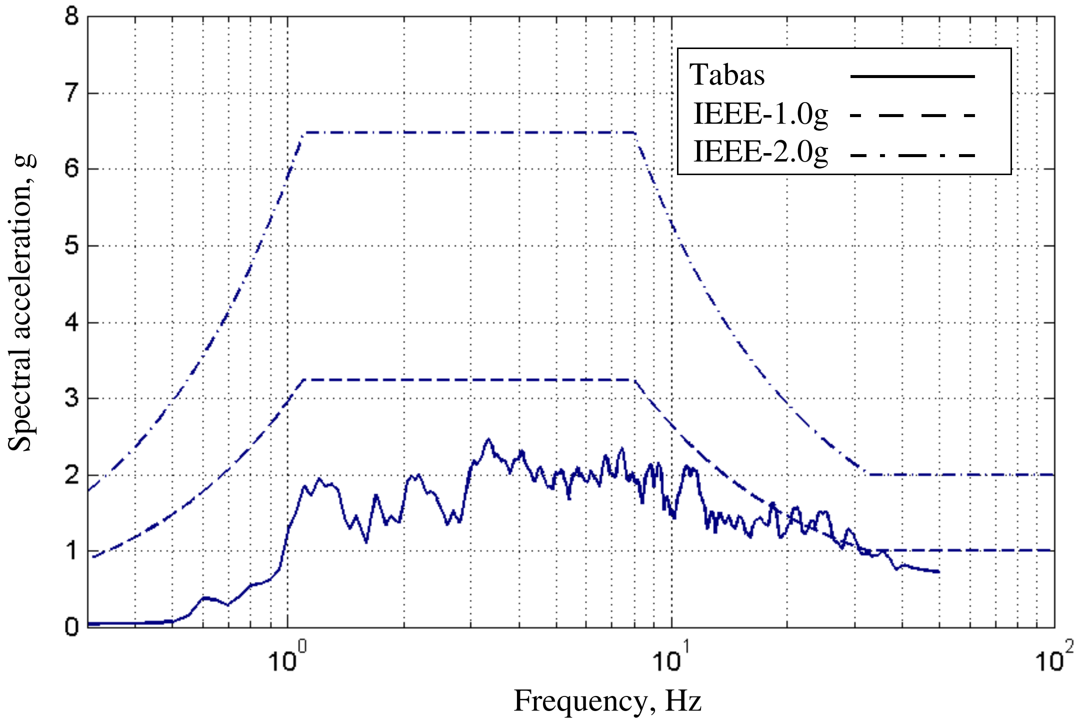

(a) *x*-direction

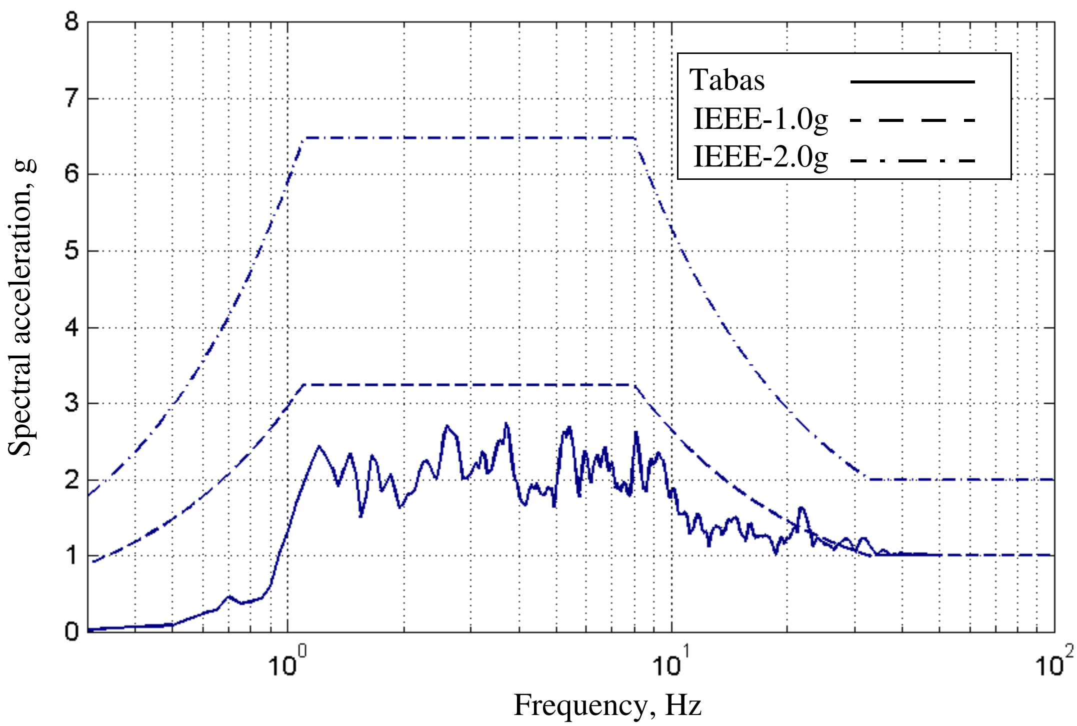

(b) *y*-direction

Figure 5-40 Response spectra for SW2 (2-percent damped, open switch, Tests 17 and 18, target PGA equal to 0.5g)

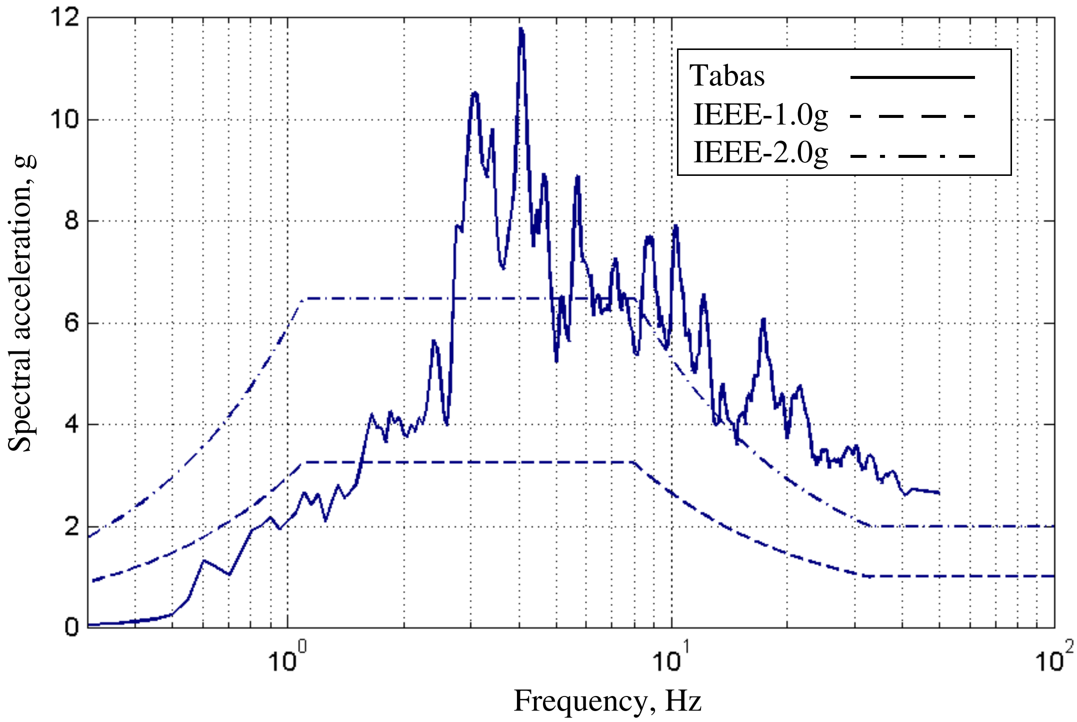

(a) *x*-direction

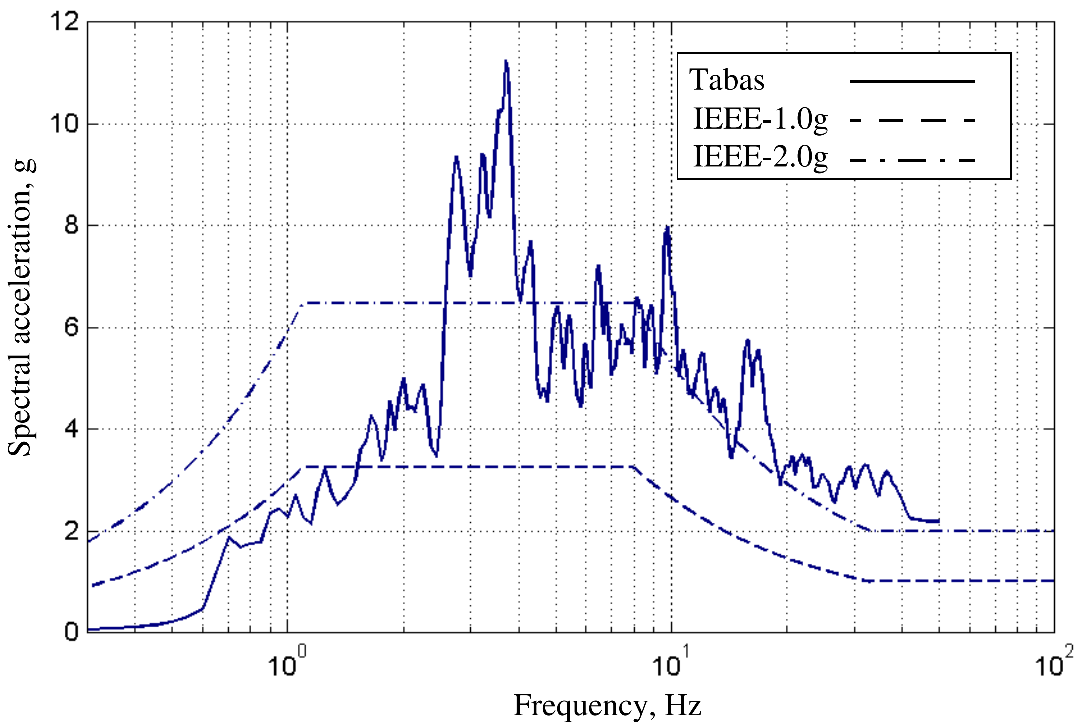

(b) *y*-direction

Figure 5-41 Response spectra for SW2a (2-percent damped, closed switch, Tests 50 and 51, target PGA equal to 2.0g)

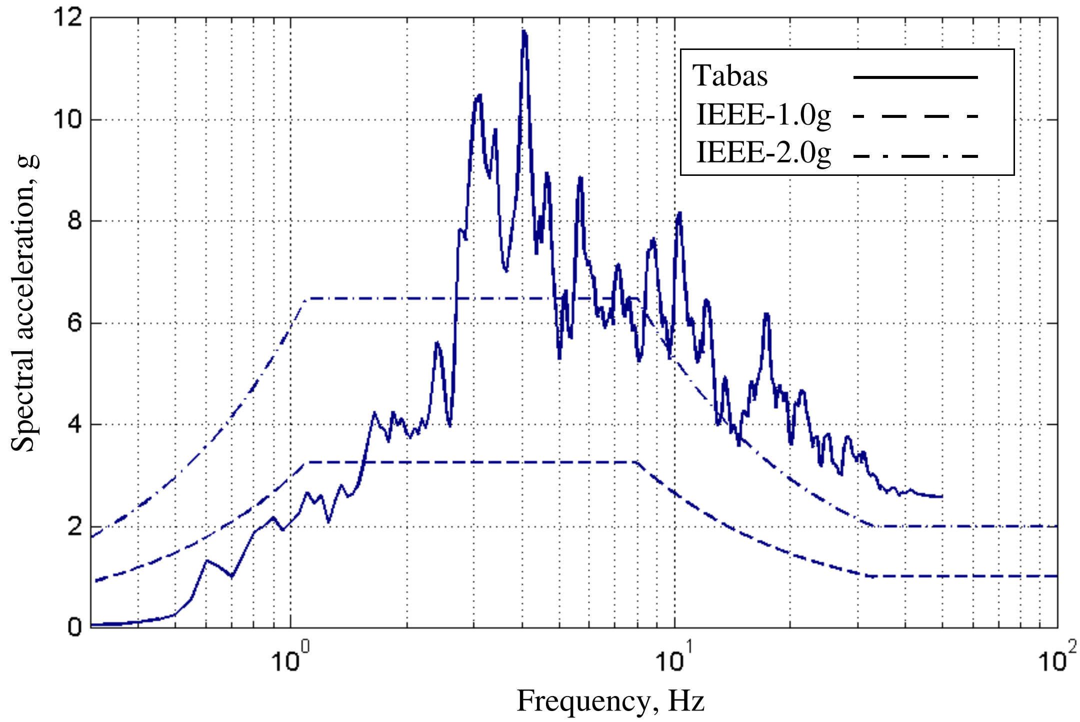

(a) *x*-direction

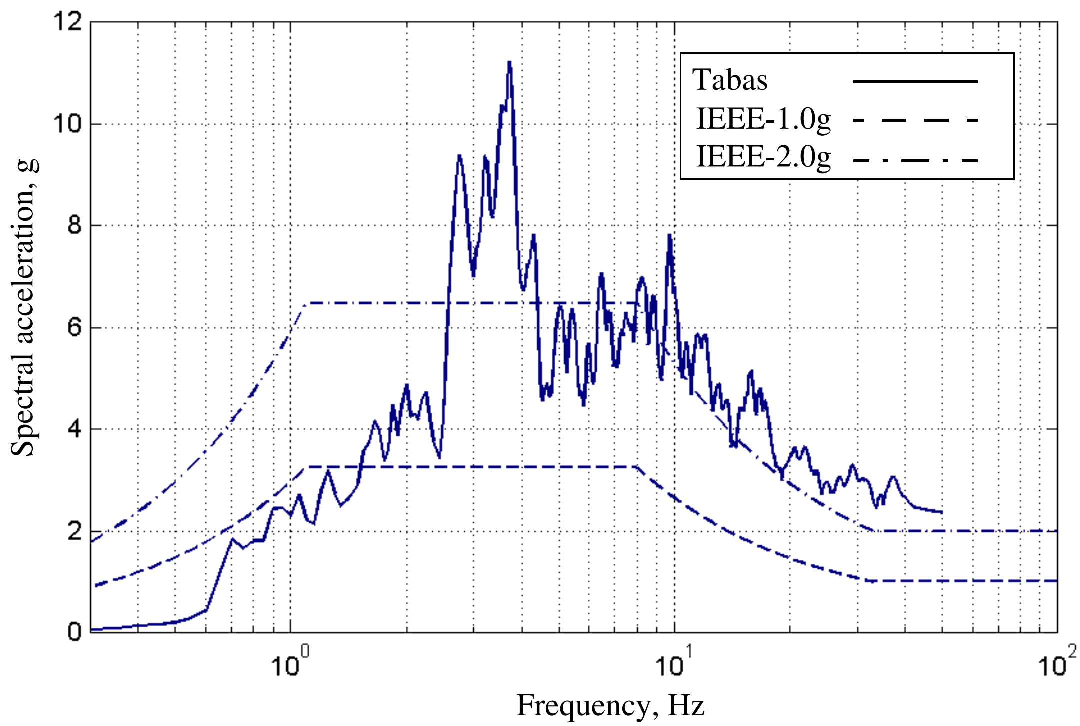

(b) *y*-direction

Figure 5-42 Response spectra for SW2a (2-percent damped, open switch, Tests 52 and 53, target PGA equal to 2.0g)

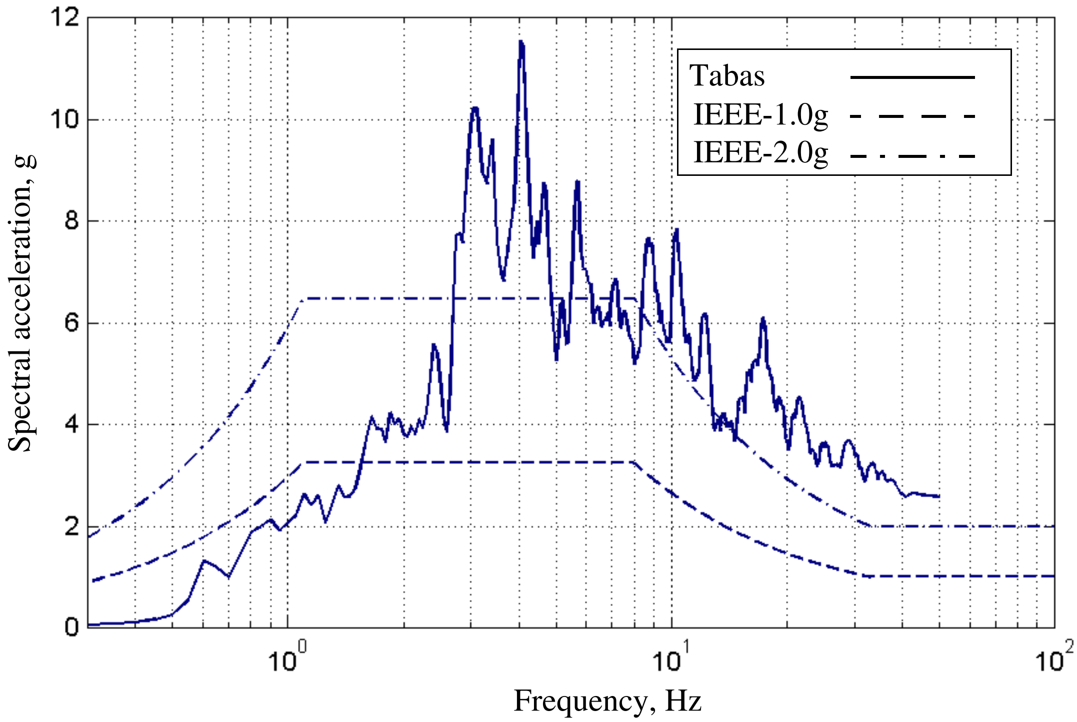

(a) *x*-direction

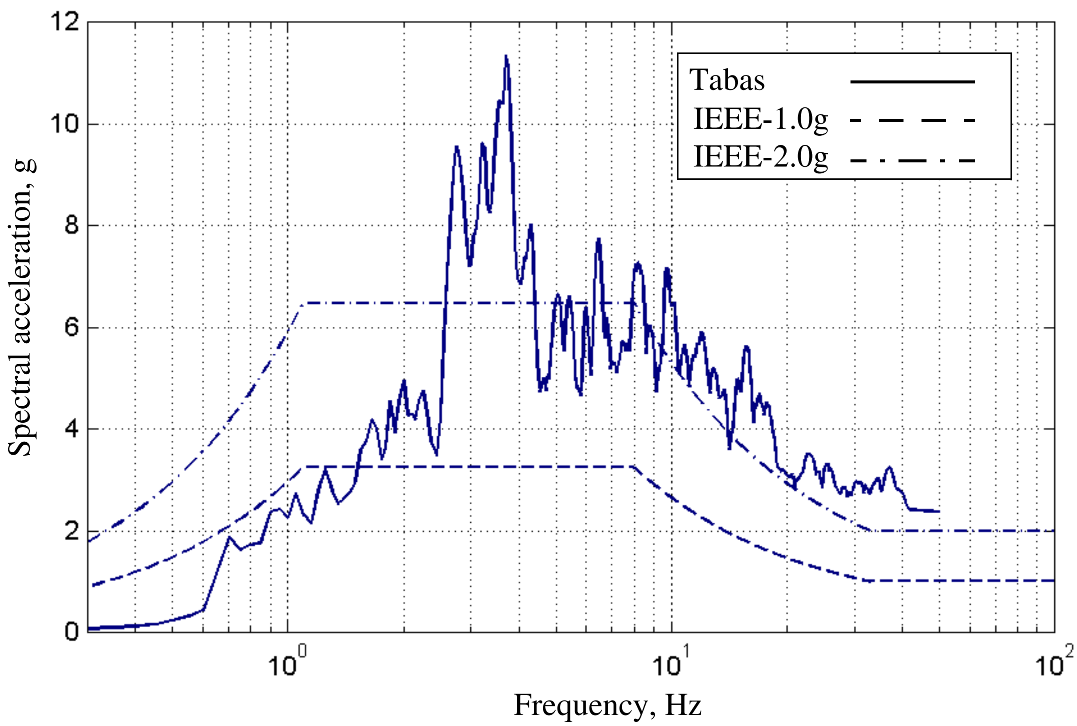

(b) *y*-direction

Figure 5-43 Response spectra for SW3 (2-percent damped, closed switch, Tests 55 and 56, target PGA equal to 2.0g)

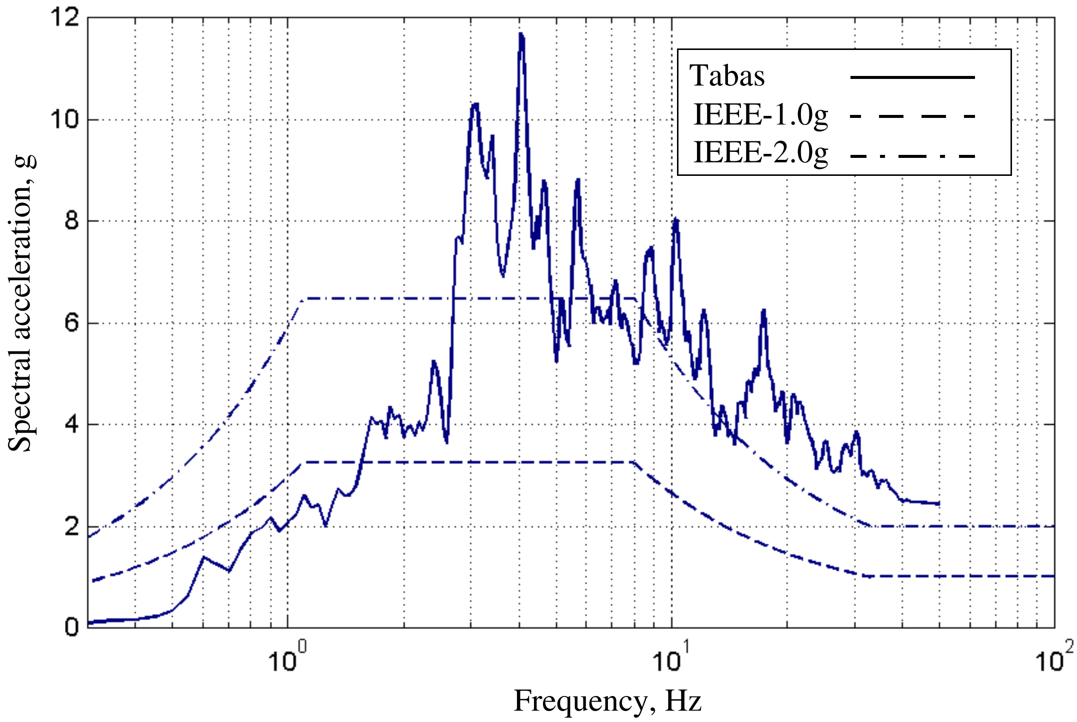

(a) *x*-direction

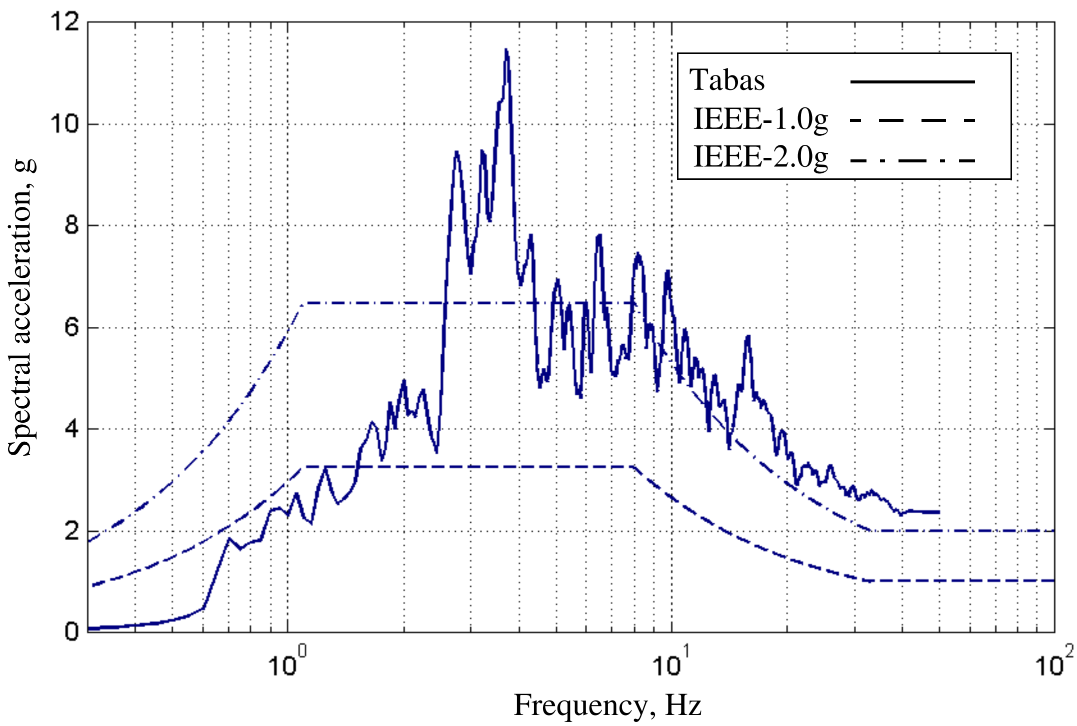

(b) *y*-direction

Figure 5-44 Response spectra for SW3 (2-percent damped, open switch, Tests 57 and 58, target PGA equal to 2.0g)

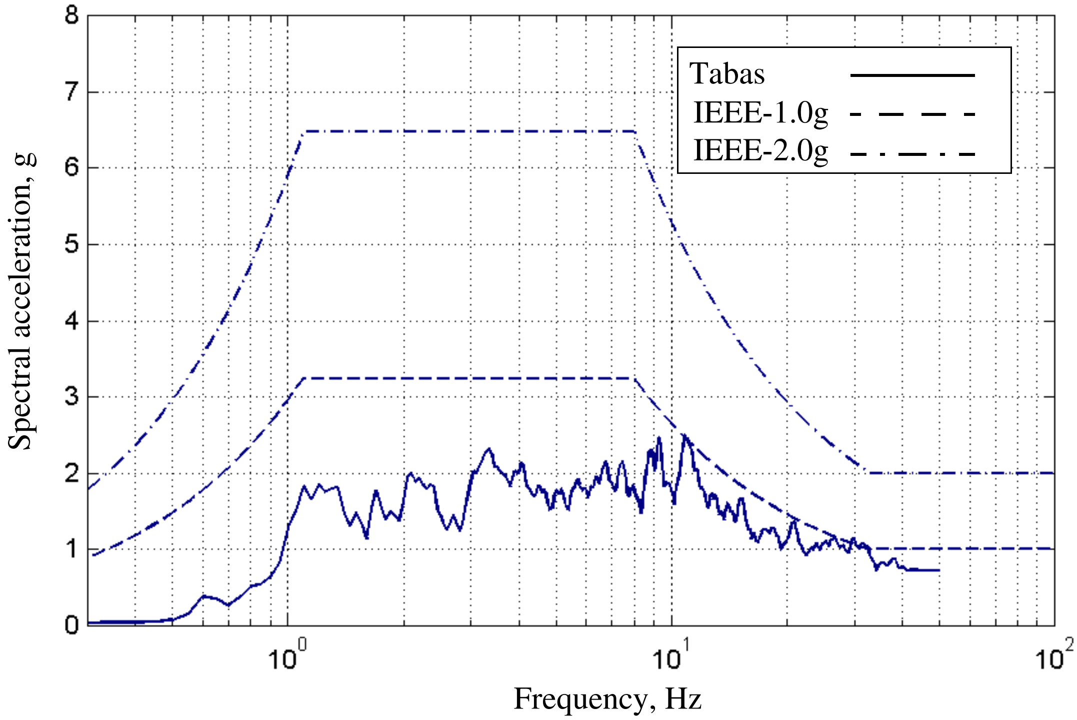

(a) *x*-direction

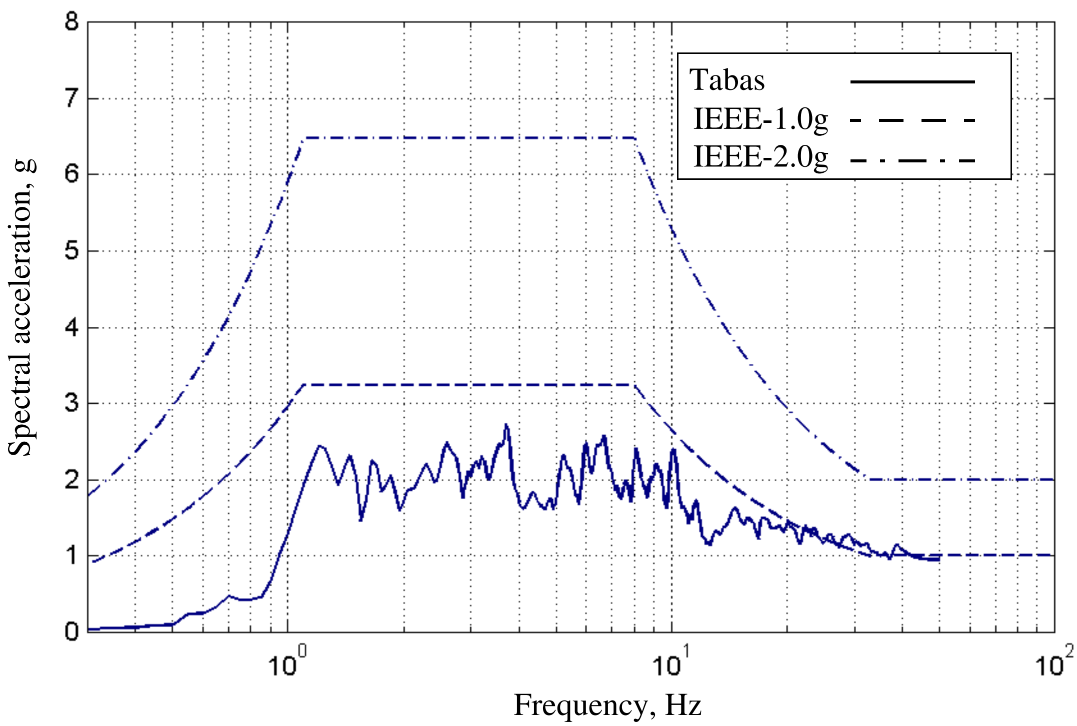

(b) *y*-direction

Figure 5-45 Response spectra for SW4 (2-percent damped, closed switch, Tests 20 and 21, target PGA equal to 0.5g)

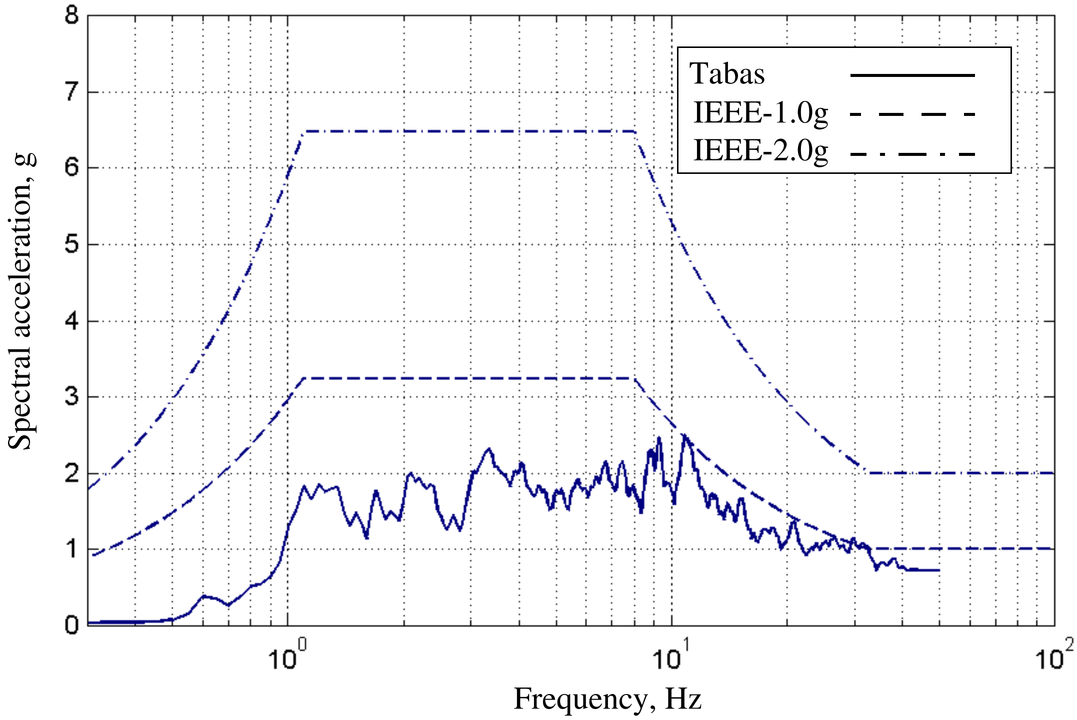

(a) *x*-direction

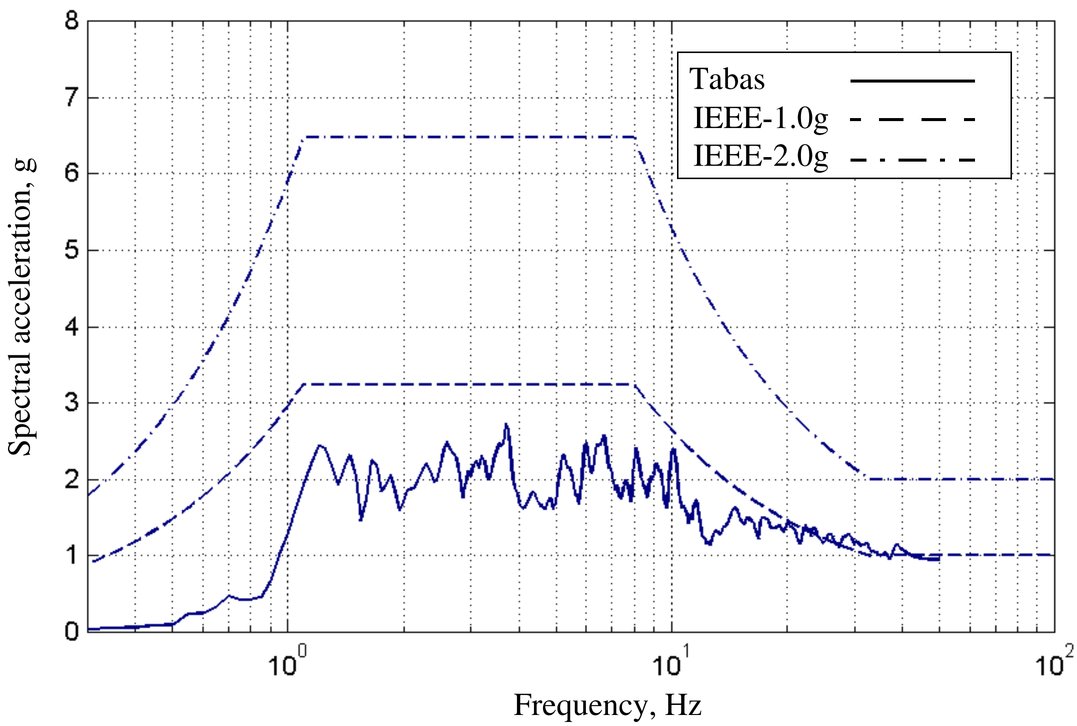

(b) *y*-direction

Figure 5-46 Response spectra for SW4 (2-percent damped, open switch, Tests 22 and 23, target PGA equal to 0.5g)

6 Mathematical Modeling of Switches

6.1 Introduction

One of the objectives of the studies described in this report was to characterize the response of switches mounted on elevated structures or frames by analysis. This work involved two tasks: (1) preparation of mathematical models for the switches and (2) analysis of switches mounted on the frames using the mathematical models. The first task is discussed in this chapter and the second task in Chapter 7.

The mathematical models of the switch posts were developed using their measured dynamic properties. Each pole of the switch comprised either two (horizontal-break) or three (vertical-break) posts. Figure 6-1 shows the vertical-break switch mounted on the PEER frame. The post designations are also shown in the figure. Each switch pole was modeled using two SDOF oscillators: P1 and P2. For the vertical-break switches, posts 2 and 3 were lumped together to obtain properties of oscillator P2. Figure 6-2 shows the mathematical model of the SDOF oscillators and the PEER frame. The designation for the SDOF oscillators (e.g., B-P1) used in this chapter and in Chapter 7 are also shown in the figure.

Response-history analysis using earthquake histories compatible with the IEEE 693-1997 spectrum for High Level qualification was used for validation studies. The SDOF oscillators described above were incorporated in the mathematical model of the PEER frame for analysis. Response quantities (displacements and accelerations) computed at the top of the post as a generalized SDOF oscillator were compared with the similar quantities measured during the tests of switches mounted on the PEER frame.

Section 6.2 presents a summary of experimental data pertinent to this chapter. Section 6.3 introduces the SDOF oscillators. Section 6.4 presents the results of the validation studies.

6.2 Properties of Switch Posts

6.2.1 Weight and height of posts

The weight and height of the switch posts were measured prior to the experimental program and are listed in Table 6-1. For all the posts, the tabulated weights include the weight of the base hardware, the insulators, the attachments at the tip of insulators, and the switch blade. The height is the distance between the bottom of double-channel beams and the top of the blade.

Table 6-1 Properties of switch posts

Switch	*Post 1*		*Post 2*		*Post 3*	
	Weight (kN)	*Height (m)*	*Weight (kN)*	*Height (m)*	*Weight (kN)*	*Height (m)*
SW1	1.4	2.5	1.4	2.5	-	-
SW2	1.4	2.6	1.5	2.6	1.5	2.6
SW3	0.6	2.6	0.7	2.6	0.7	2.6

6.2.2 Dynamic properties of the switches

The dynamic properties (frequencies, damping ratios, and mode shapes) of the switch posts were computed using the data from the tests of single poles of switches mounted directly on the simulator platform. The flexibility and damping in the earthquake simulator hydraulic system reduce the frequencies and increase the damping of the switch posts. Although the frequencies and mode shapes of the posts will likely not be noticeably changed by the flexibility of the simulator, the damping ratios will be overestimated especially when the acceleration of the earthquake simulator platform is large.

The fundamental frequencies of the posts are listed in Table 6-2. For all the posts, a damping ratio of approximately 5 percent of critical was computed from tests using the Tabas-1 histories with a target peak acceleration of 1.0g. The mode shapes for the switches were computed using the accelerometers placed at the base, midheight, and top of the posts and at the tip of the blades. Figures 6-3 through 6-5 show the mode shapes of switches SW1, SW2, and SW3, respectively.

Table 6-2 Modal frequency (Hz) of switch posts

		Closed Blade		*Open Blade*	
Switch	*Post*	*x-direction*	*y-direction*	*x-direction*	*y-direction*
SW1	1	3	5	3	3
	2	3	5	3	3
SW2	1	6	6	6	6
	2 or 3	5	6	5	6
SW3	1	7	8	7	8
	2 or 3	6	8	6	8

6.3 SDOF Models of Switch Posts

6.3.1 Introduction

A generalized SDOF model for each switch post was prepared following the procedures described in Appendix B. The effective mass and effective height of these oscillators were computed from:

$$\bar{m} = \Gamma \int m(s)\psi(s)dx \tag{6-1}$$

$$\bar{h} = \frac{\Gamma}{\bar{m}} \int h(s)m(s)\psi(s)dx \tag{6-2}$$

where, *m(s), h(s)*, and $\psi(s)$ are the mass distribution, height above the base, and the shape function (mode shape) of the post, respectively, and Γ is a scaler that transfers the results from the coordinates of the oscillator to those of the post:

$$\Gamma = \frac{\int m(s)\psi(s)ds}{\int m(s)\psi^2(s)ds} \tag{6-3}$$

A SDOF oscillator with a mass $\bar{m}$, height $\bar{h}$, and fundamental frequency *f* will have the same base shear and overturning moment as the switch post.

6.3.2 Properties of SDOF oscillators

The effective masses and effective heights of the SDOF oscillators were computed using Equations 6-1 and 6-2. The mass distribution, *m(s)*, for each post are described in Appendix B. The mode shapes of the poles (see Figures 6-3 through 6-5) were used as the shape functions ψ in these equations. Table 6-3 lists the computed effective mass and height for the posts P1 and P2 of the oscillators.

The normalized effective mass (with respect to the post mass of Table 6-1) and normalized effective height (with respect to the post height of Table 6-1) are presented in Table 6-4. For all the posts, the effective mass and height of the SDOF isolators are between 70 and 90 percent of the mass of the post and between 70 and 80 percent of the height of the post, respectively.

Table 6-3 Properties of the equivalent SDOF oscillators

Switch	*Post*	*Closed Blade*				*Open Blade*			
		x- direction		*y- direction*		*x- direction*		*y- direction*	
		$\bar{m}$ (kg)	$\bar{h}$ (m)	$\bar{m}$ (kg)	$\bar{h}$ (m)	$\bar{m}$ (kg)	$\bar{h}$ (m)	$\bar{m}$ (kg)	$\bar{h}$ (m)
SW1	P1	112	2.0	133	2.0	112	1.9	133	1.9
	P2	133	2.0	122	2.0	122	1.9	133	1.9
SW2	P1	102	1.8	112	1.8	102	1.8	102	1.8
	P2	234	1.8	214	1.8	224	1.9	224	1.9
SW3	P1	41	2.0	51	2.0	41	1.8	41	1.8
	P2	92	2.1	92	2.1	92	2.1	92	2.1

Table 6-4 Normalized properties of the equivalent SDOF oscillators

Switch	*Blade*	*Post*	*Normalized effective mass*		*Normalized effective height*
			x- direction	*y-direction*	*x- or y- direction*
SW1	Closed	P1	0.8	0.9	0.8
		P2	0.9	0.9	0.8
	Open	P1	0.8	0.9	0.8
		P2	0.9	0.9	0.8
SW2	Closed	P1	0.7	0.8	0.7
		P2	0.8	0.8	0.7
	Open	P1	0.7	0.7	0.7
		P2	0.8	0.8	0.8
SW3	Closed	P1	0.7	0.8	0.8
		P2	0.7	0.7	0.8
	Open	P1	0.7	0.7	0.7
		P2	0.7	0.7	0.8

For analysis, the SDOF oscillators were modeled as fixed-base cantilever columns of height $\bar{h}$. The rigidity of the beam-column elements (*EI*) was computed as:

$$EI = \frac{\bar{h}^3 k}{3} = \frac{(2\pi)^2}{3}\bar{h}^3\bar{m}f^2 \qquad (6\text{-}4)$$

where, k and f are the flexural stiffness and frequency of the oscillator, respectively.

6.4 Validation Studies

6.4.1 Mathematical model

SAP-2000 (CSI 1996) was used to validate the SDOF models of the switch posts. The PEER frame (see Figure 2-3) was modeled using nominal section properties and centerline dimensions. Oscillators P1 and P2 were modeled as described in Section 6.3.2. The switch operation hardware (including the inter-pole links) were not modeled. Figure 6-2 presents the mathematical model of the PEER frame and the SDOF oscillators. Only the switch response with the closed blade was studied. For this condition, the responses of oscillators P2 were constrained to equal those of oscillators P1 in the y-direction (coinciding with the longitudinal axis of the blade). Recorded accelerations of the simulator platform from the tests using the Tabas-1 histories with a target PGA of 1.0g were used as input histories to the mathematical model.

6.4.2 Analytical results

Due to the symmetry of the mathematical model, the responses of oscillators B-P1 and C-P1 were similar to that of A-P1, and the response of oscillators B-P2 and C-P2 were similar to that of A-P2. As such, only results for oscillators A-P1 and A-P2 are presented herein.

Figures 6-6 through 6-8 present the displacement history of the top of oscillator A-P1, relative to the PEER frame, transformed by Γ to the tip of the post. For all three switches, the analytical models predict the general shape and amplitude of the measured histories reasonably well.

The peak responses of switches (total acceleration and displacement relative to the PEER frame) are presented in Table 6-5. The maximum deformation responses of the SDOF oscillators were within 30% of the measured peak deformations, but the measured accelerations were substantially underestimated because the SDOF models could not account for higher mode effects and the complicated dynamics of the switch pole assemblies mounted on the flexible channels. Figure 6-9 presents a 3-sec segment of the displacement- and acceleration-response histories for post A-P2 of switch SW3. The analytical and measured displacement histories of Figure 6-9a have similar periodicity and amplitudes. Higher modes of response are clearly evident in the measured acceleration history of Figure 6-9b.

In summary, the SDOF oscillators can be used to estimate relative deformation in posts of vertical- and horizontal-break switches and thus maximum shear forces and bending moments, but likely will underestimate the maximum acceleration of switch posts. In the following chapter, the SDOF oscillators established in this chapter are used to estimate the response of switch posts mounted on tall and short, and braced and unbraced frames for the purpose of characterizing the likely performance of switch posts mounted on in-service or proposed frames.

Table 6-5 Experimental and analytical peak response of switches[1]

		Experimental (A1 and A2)				*Analytical (A-P1 and A-P2)*			
		Acceleration, g		*Displacement, mm*		*Acceleration, g*		*Displacement, mm*	
Switch[2]	*Post*[3]	*x-component*	*y-component*	*x-component*	*y-component*	*x-component*	*y-component*	*x-component*	*y-component*
SW1	A1 (A-P1)	3.9	6.5	51	51	2.1	3.8	38	40
	A2 (A-P2)	6.5	7.2	39	49	3.0	3.8	44	40
SW2	A1 (A-P1)	3.6	4.5	29	37	5.4	3.9	34	28
	A2 (A-P2)	5.6	4.9	87	33	6.7	3.9	76	28
SW3	A1 (A-P1)	3.8	6.5	21	37	3.8	4.8	21	36
	A2 (A-P2)	5.5	6.9	46	41	3.5	4.9	40	37

1. Results are for tests with closed blade using the Tabas-1 motion with a target PGA equal to 1.0g (Test 21 for SW1, Test 21 for SW2, and Test 23 for SW3)
2. SW1 = horizontal-break switch with porcelain insulators; SW2 = vertical-break switch with porcelain insulators; SW3 = vertical-break switch with composite insulators.
3. Refer to Figures 6-1 and 6-2 for identification of posts and SDOF oscillators, respectively.

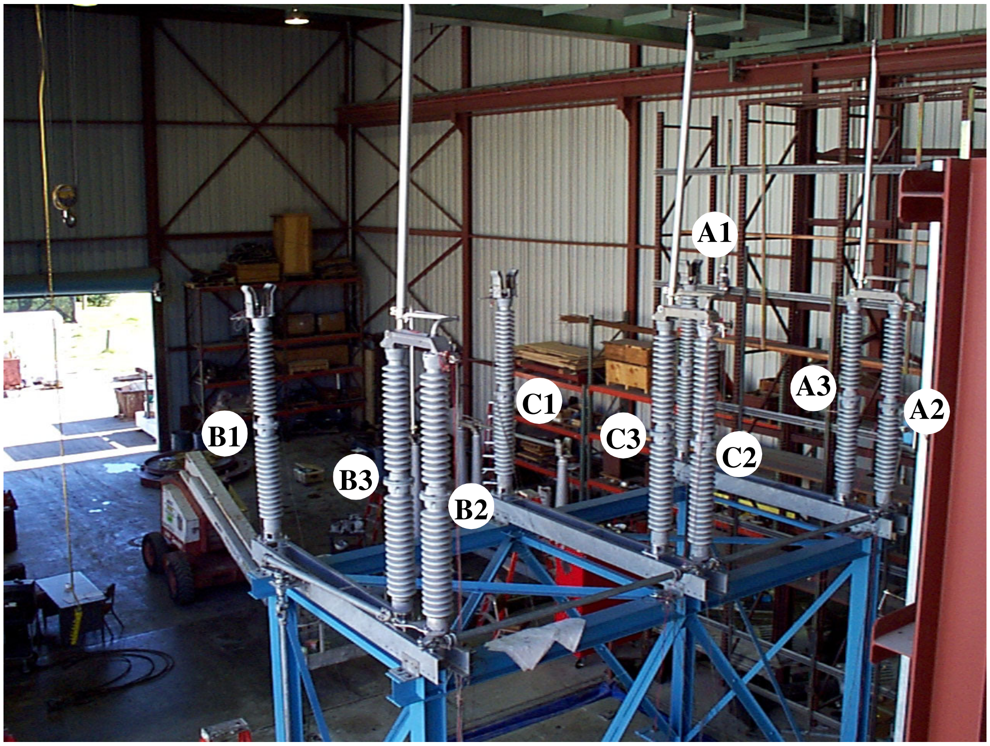

Figure 6-1 Vertical-break switch mounted on the PEER frame

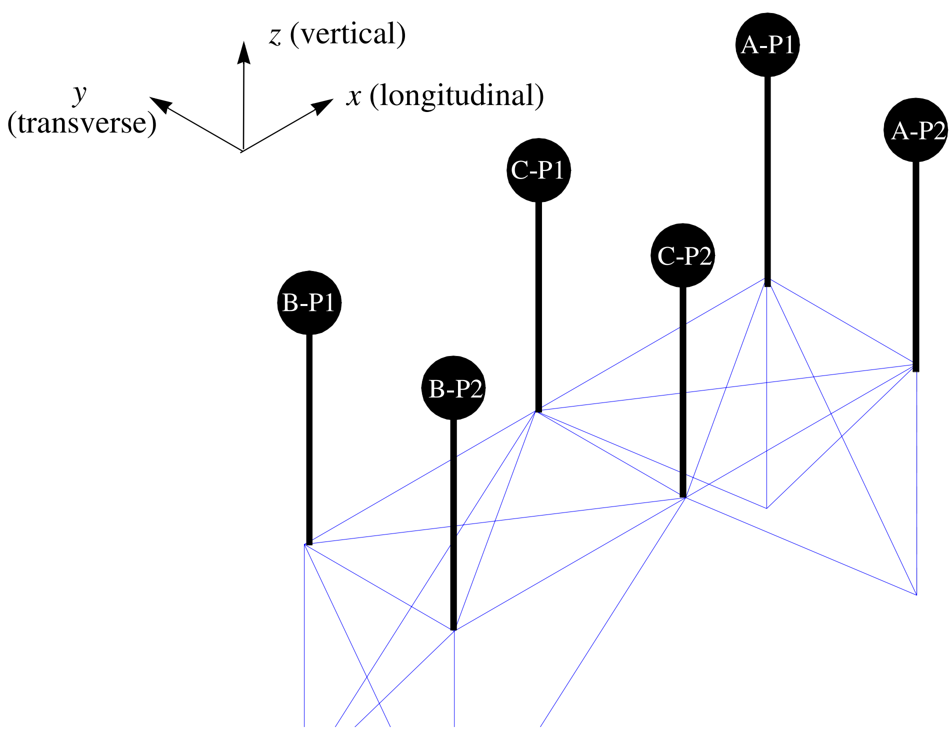

Figure 6-2 Mathematical model of the SDOF oscillators and the PEER frame

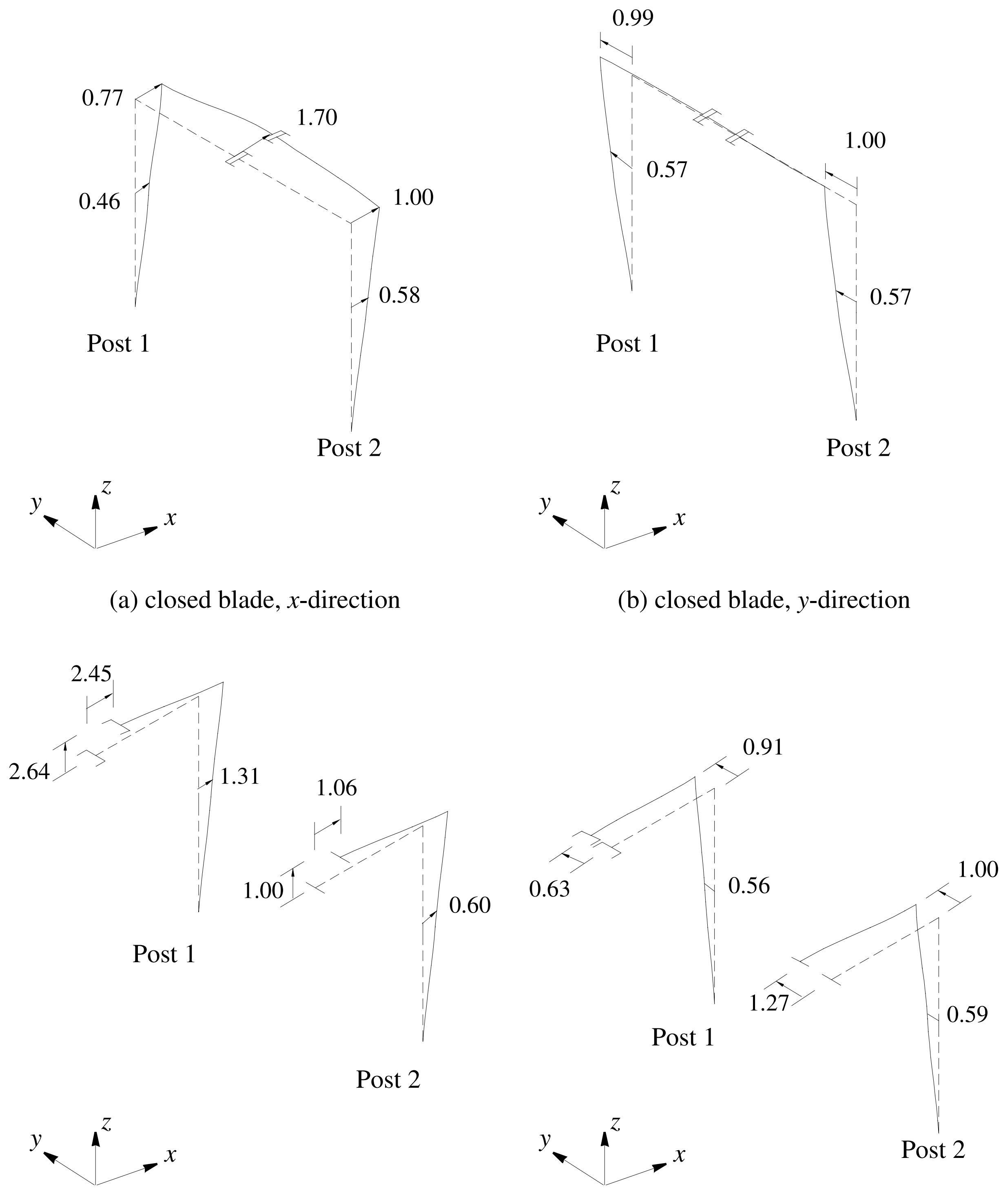

(a) closed blade, *x*-direction

(b) closed blade, *y*-direction

(c) open blade, *x*-direction

(d) open blade, *y*-direction

Figure 6-3 Mode shapes of horizontal-break switch SW1

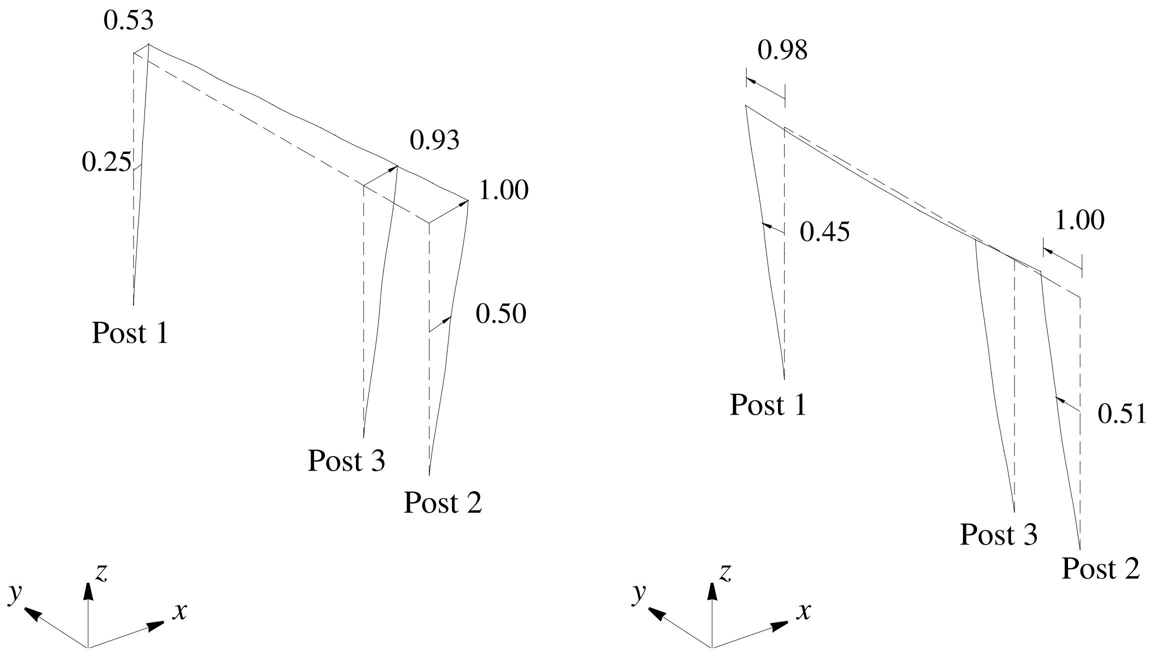

(a) closed blade, *x*-direction (b) closed blade, *y*-direction

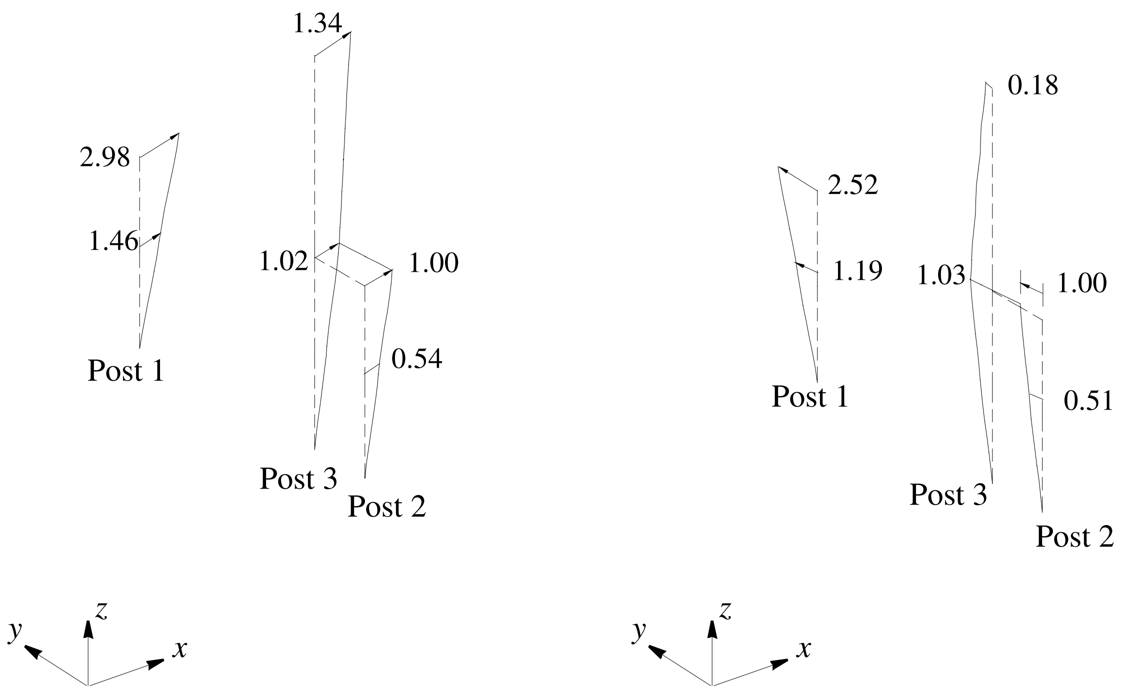

(c) open blade, *x*-direction (d) open blade, *y*-direction

Figure 6-4 Mode shapes of vertical-break switch SW2

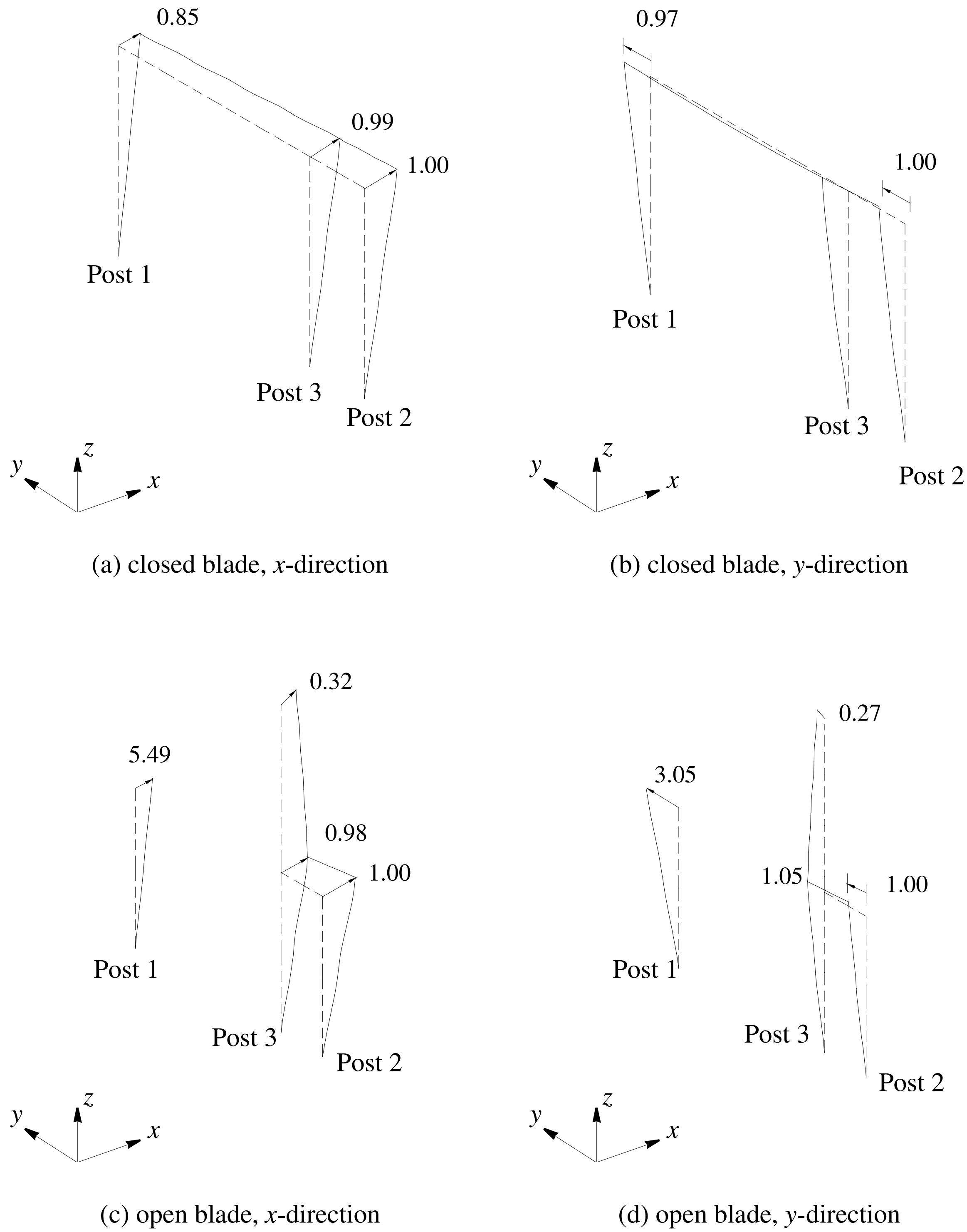

Figure 6-5 Mode shapes of vertical-break switch SW3

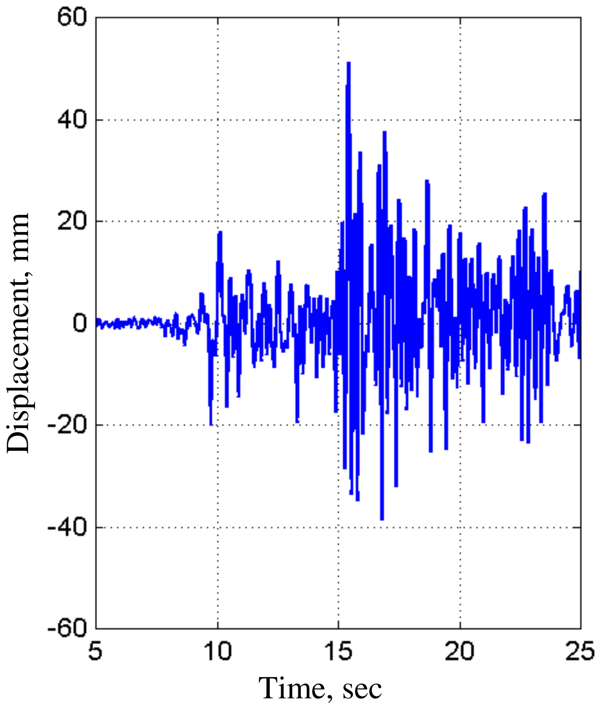

(a) *x*-component, experimental

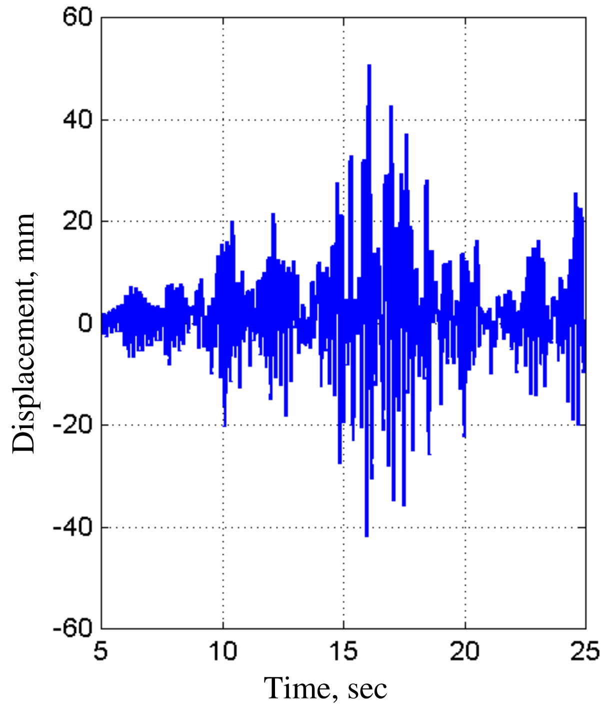

(b) *y*-component, experimental

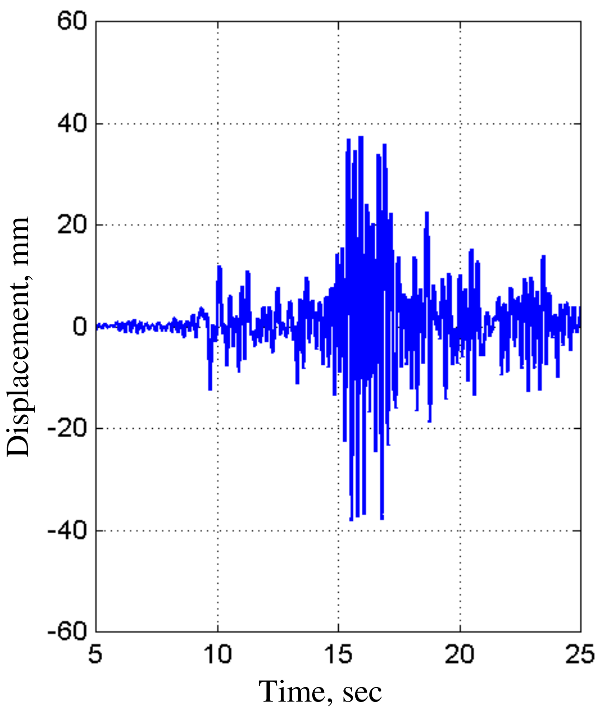

(c) *x*-component, analytical

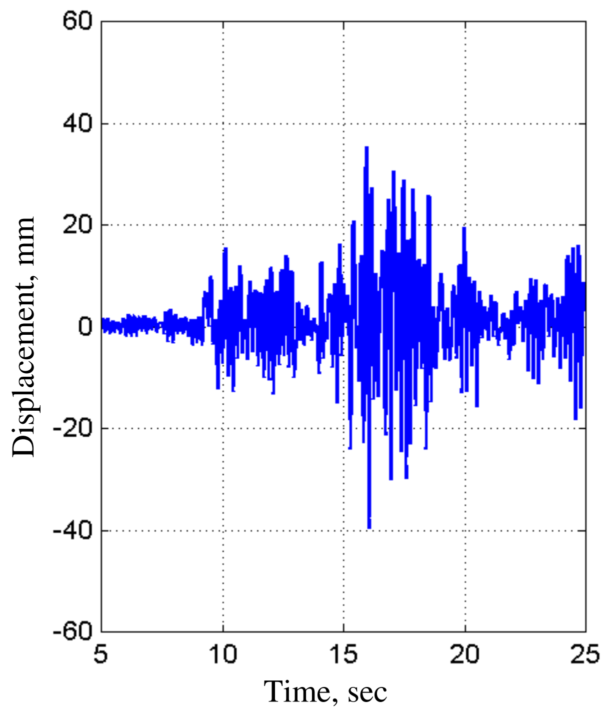

(d) *y*-component, analytical

Figure 6-6 Displacement response of post A1 and oscillator A-P1 relative to the PEER frame, switch SW1, closed blade, Tabas-1, target PGA equal to 1.0g

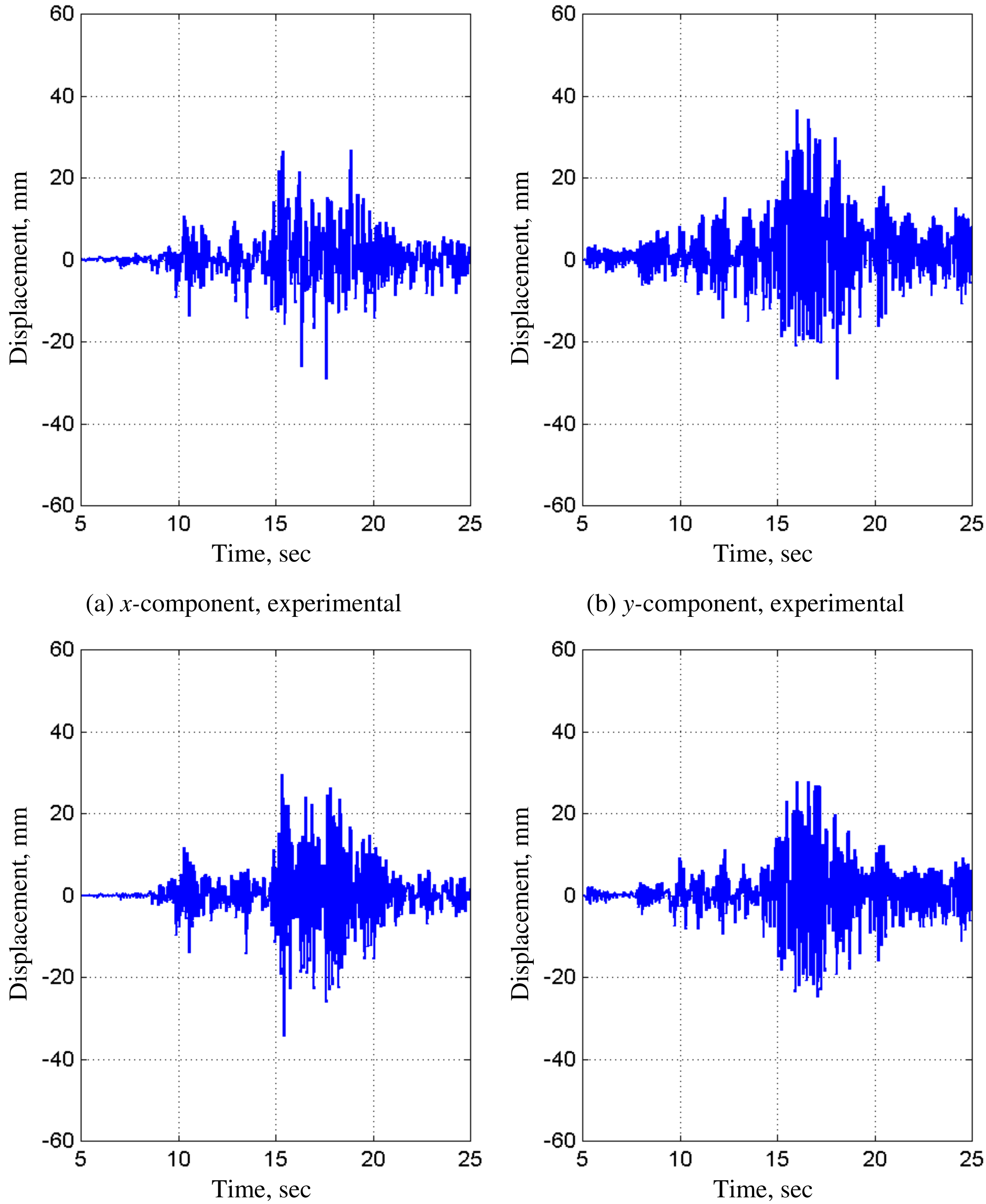

(a) *x*-component, experimental

(b) *y*-component, experimental

(c) *x*-component, analytical

(d) *y*-component, analytical

Figure 6-7 Displacement response of post A1 and oscillator A-P1 relative to the PEER frame, switch SW2, closed blade, Tabas-1, target PGA equal to 1.0g

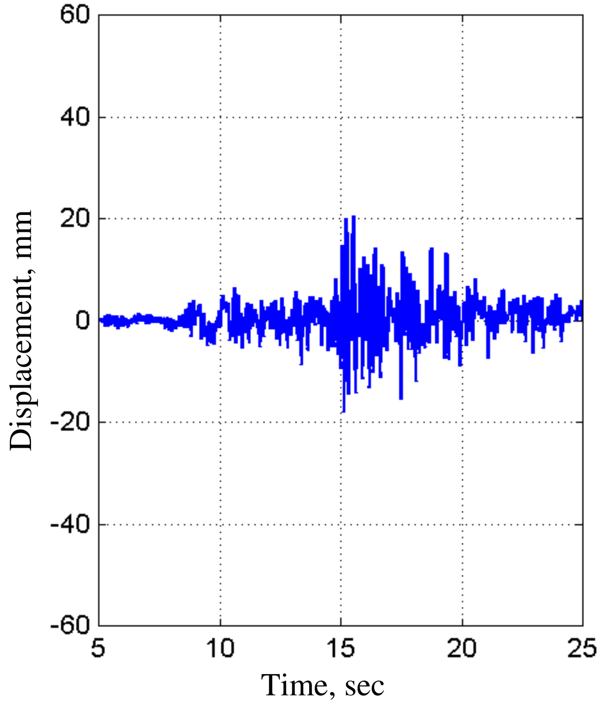

(a) *x*-component, experimental

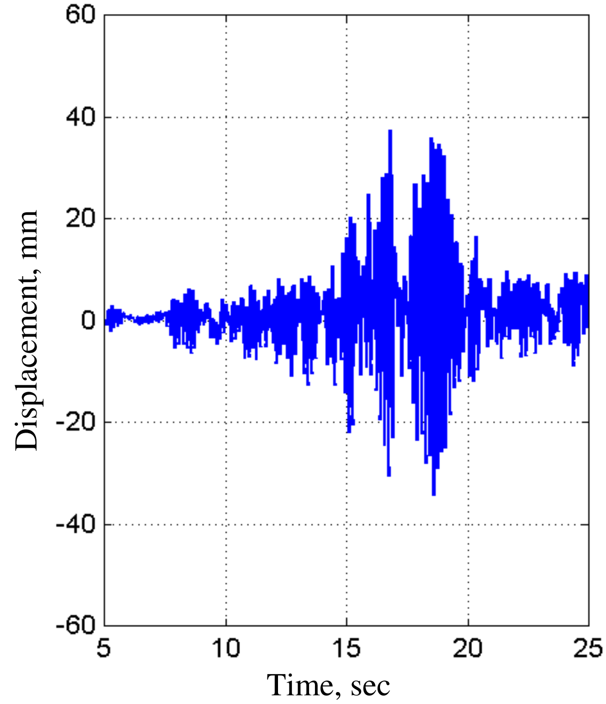

(b) *y*-component, experimental

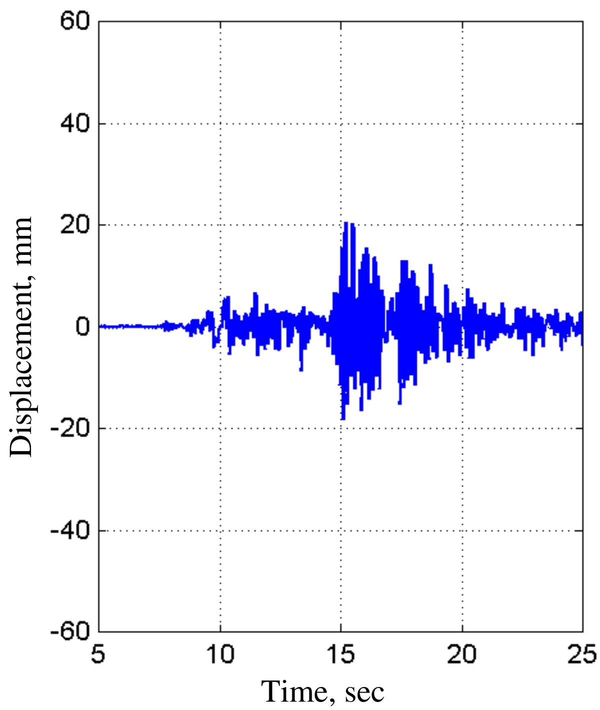

(c) *x*-component, analytical

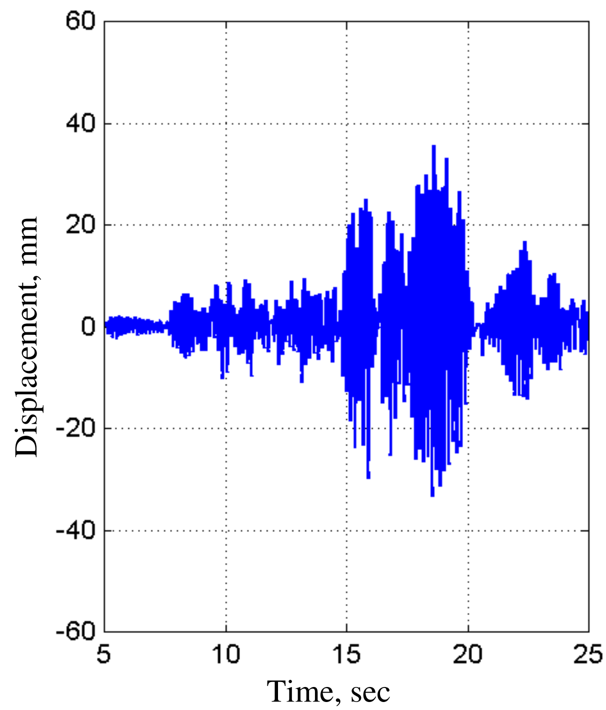

(d) *y*-component, analytical

Figure 6-8 Displacement response of post A1 and oscillator A-P1 relative to the PEER frame, switch SW3, closed blade, Tabas-1, target PGA equal to 1.0g

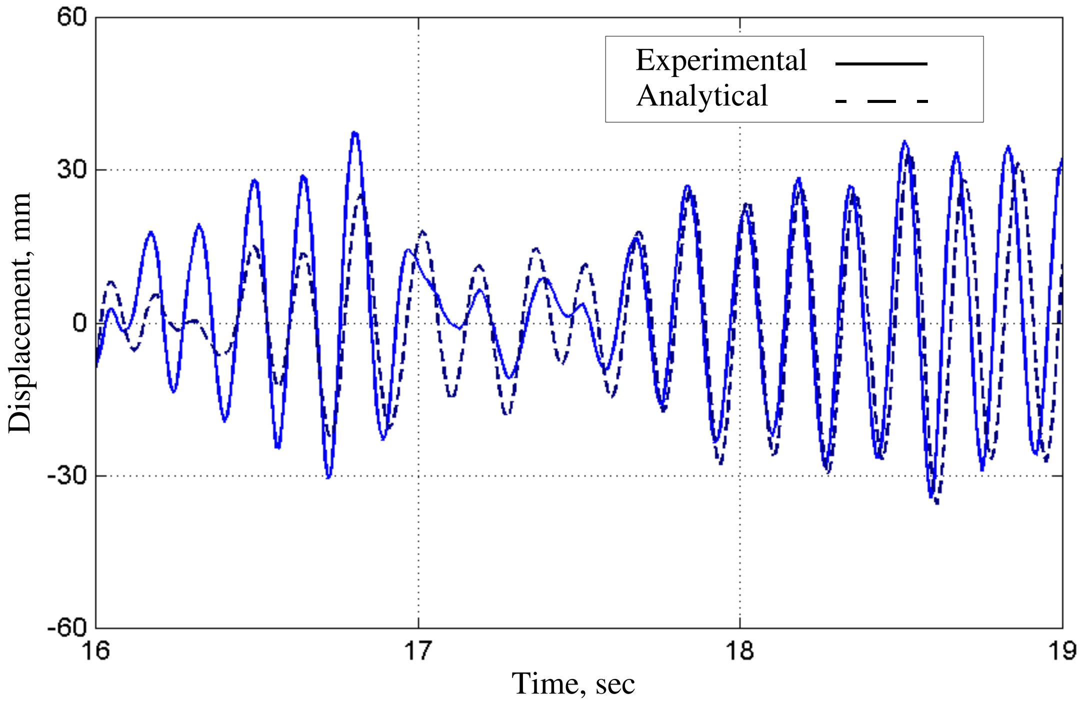

(a) Displacement response

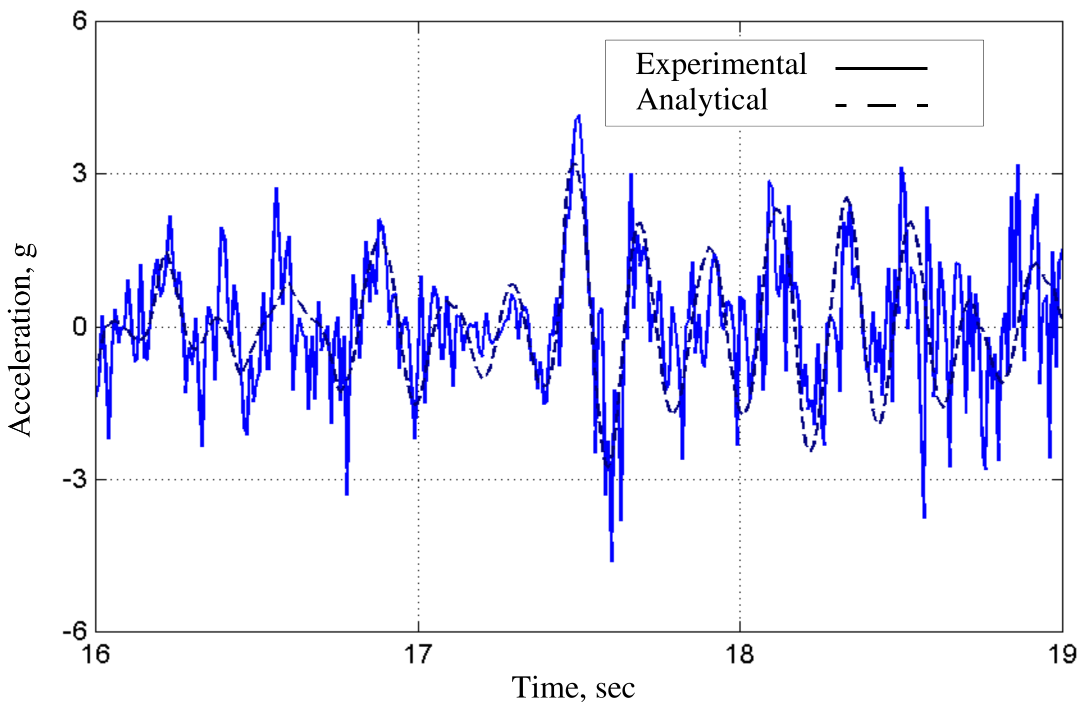

(b) Acceleration response

Figure 6-9 Analytical (A-P2) and experimental (A2) response of switch SW3

7 Response of Frame-Mounted Switches

7.1 Introduction

In the field, disconnect switches are typically mounted on elevated structures or frames. These structures are commonly between 3 m and 17 m in height, might be braced, and use various structural steel members. The dynamic properties of these lightly damped frames vary widely, which complicates the seismic qualification of frame-mounted switches for two reasons. First, IEEE 693-1997 writes that switches must be qualified on frames that are representative of those in service. Because of the large number and variety of frames in the Pacific Gas & Electric (PG&E) inventory, qualification of each switch on each type of frame would be overly onerous and prohibitively expensive. Second, most of the frames that are either in service or proposed for use are too large to be tested using existing earthquake simulators in the United States.

The primary objective of the work presented in this chapter was to characterize the degree to which stiff and flexible frames amplify earthquake ground motion from the base of the frame to the base of the switch poles to enable others to improve procedures for the seismic qualification of switches. Four frames were examined in an analytical study: two short or low-profile, and two tall or high-profile. Two of the frames, one short and one tall, were representative of frames in service at this time. The other two frames are proposed for future use in PG&E substations.

Two SDOF oscillators were used to represent each pole of each switch. The properties of these oscillators are listed in Chapter 6 for each switch. The oscillators were incorporated in the mathematical models of the four frames to study the response of the oscillators and to compare these responses with those of the oscillators mounted on a rigid base. Response-history analysis using earthquake histories compatible with the IEEE 693-1997 spectrum for High Level qualification was used for the analytical studies.

The remaining sections in this chapter present the results of the studies. Section 7.2 describes the four frames used in the study. Section 7.3 provides a brief description of the mathematical models of the switch posts and the earthquake histories used for the response-history analysis. Section 7.4 presents the results of the analysis and Section 7.5 identifies the key conclusions of the analytical studies. Comments on the likely seismic performance of the vertical-break switches SW2 and SW3 are presented in Section 7.5.

7.2 PG&E Frame Structures

7.2.1 Introduction

Four support structures were used for analysis: 01, 02, 03, and 04. Frame 01 is a low-profile braced frame that will be used for new construction. Frame 01 was referred to as the PG&E frame in Chapter 2 and was used for the earthquake simulator studies of Chapter 5. Frame 02 is a low-profile frame that is in service in the PG&E inventory at this time. The double-channel beams at the base of switch poles are bolted to the tube steel beams of Frame 02 and serve as the transverse members in the frame. Frame 03 is a high-profile frame that is proposed for use in new construction. Frame 04 is a high-profile frame that is in use at this time. Analysis was also performed with the switches mounted on a fictitious, infinitely rigid frame that was designated as Frame 00. Results of the analysis using Frame 00 were used to normalize the response of the switches mounted on Frames 01 through 04 and to calculate the amplification of the response of the switch posts due to flexibility in the frames.

Table 7-1 lists information on these frames. Figures 7-1 through 7-4 are line drawings of the frames. The dimensions, member sizes, and the coordinate system adopted for studies reported in this chapter are shown in the figures.

Table 7-1 Frame properties

Frame	*Height*[1] *(m)*	*Weight (kN)*	*Height Classification*	*Braced*	*Usage*[2]	*PG&E Designation*
Frame 00	NA[3]	NA	NA	NA	NA	NA
Frame 01	3.6	21	short (low-profile)	Yes	B	374657
Frame 02	5.5	13	short (low-profile)	No	A	456555
Frame 03	16.8	150	tall (high-profile)	Yes	B	Not assigned
Frame 04	16.8	65	tall (high-profile)	No	A	439941

1. Denotes the maximum height for this type of frame; frames may be shorter.
2. A = in-service; B = proposed for new construction.
3. NA = not applicable

7.2.2 Modal frequencies of the frames

The modal frequencies of the frames calculated by analysis are listed in Table 7-2 for the frame alone and for switch SW1 (closed blade) mounted on the frame. Frame 01, the PG&E frame, is by far the stiffest frame. The other frames, which are either unbraced or tall have much lower frequencies. The fundamental frequencies of Frames 02 through 04 range between 1 to 10 Hz: a range that envelopes the frequencies of the switches. Figures 7-5 through 7-8 show the longitudinal (x-), transverse (y-), vertical (z-), and torsional (rotation about z- axis) mode shapes of the four frames.

Table 7-2 Modal frequency of frames by analysis

Frame	*Frequency (Hz)*							
	Longitudinal (x)		*Transverse (y)*		*Vertical (z)*		*Torsional (x-y plane)*	
	Frame alone	*Frame plus switch*[1]	*Frame alone*	*Frame plus switch*[1]	*Frame alone*	*Frame plus switch*[1]	*Frame alone*	*Frame plus switch*[1]
Frame 00	∞	NA	∞	NA	∞	NA	∞	NA
Frame 01	45	43	24	24	54	49	63	56
Frame 02	4	3	4	3	8	7	6	4
Frame 03	1	1	8	8	4	3	10	10
Frame 04	4	3	5	3	15	12	7	7

1. Modal frequencies computed with switch SW1 (closed blade) mounted on frame.

7.3 Modeling and Input Histories

7.3.1 Mathematical models

SAP 2000 (CSI 1996) was used to estimate the response of switches mounted on Frames 00 through Frame 04. The frames were assumed to be fixed at the base. Nominal section and centerline dimensions were used to construct the models.

SDOF models of switch posts were prepared using the effective masses and effective heights of Table B-5. A damping ratio of 2 percent of critical was assumed for all switch posts. Such a value is a conservative estimate based on the resonant-search and static test data of Chapter 6. Figure 7-9 shows the mathematical model of a typical switch and frame. Note the locations of the SDOF oscillators, A-P1, A-P2, B-P1, B-P2, C-P1, and C-P2, that were used to represent the three poles of the switches (A, B, and C). The SDOF oscillators had different properties in the *x*- and *y*-directions and these properties varied depending on whether the blade was open or closed. When the blade was closed, the displacements of the SDOF models were constrained as described in Chapter 6.

Although the inter-pole links and other switch operation hardware (see Figure 2-18) can affect the response of frame-mounted switches, they were not included in the mathematical models because the links and related hardware vary widely in practice and results from the analysis of a specific configuration could not be easily extrapolated to cover other configurations.

7.3.2 Earthquake histories

The recorded near-field motions from the 1978 Tabas earthquake were used to prepare input histories for the analysis of the frame-mounted switches. Acceleration histories, power spectra, and response spectra of the recorded histories are shown in Figures 3.3 through 3.5. The Abrahamson spectrum-matching algorithm (Abrahamson 1996) was used to generate histories with spectra compatible with IEEE 693-1997 spectra for High Level qualification. For the two horizontal components, a 2-percent damped spectrum anchored to a peak ground acceleration (PGA) of 1.0g was used for the IEEE spectrum. The vertical earthquake history was selected as 80 percent of the horizontal *y*-component to match the IEEE vertical spectrum for High Level qualification. Unlike the histories used for experimentation for which the input histories were only part spectrum-compatible, the histories used for the analytical studies matched the entire IEEE spectrum. Figure 7-10 shows the two horizontal acceleration histories. Figure 7-11 presents the acceleration response spectra for these histories and the target IEEE spectrum.

7.4 Analysis Results

7.4.1 Introduction

Posts A-P1, A-P2, B-P1, and B-P2 are mounted directly above columns in all four support frames as depicted in Figure 7-9. Due to symmetry, the response of posts A-P1 and A-P2 were similar to those of posts B-P1 and B-P2, respectively. As such, only results for posts A-P1, A-P2, C-P1, and C-P2 are presented below for the analysis of the switches mounted on Frames 01 through 04. For the analysis using Frame 00, results are presented for A-P1 and A-P2 only because all posts are fixed to a rigid base.

Two quantities were used to characterize the response of the switches: (1) absolute acceleration at the tip of the posts, and (2) deformation of the posts. For both quantities, the results from the dynamic analysis were transformed from the SDOF coordinate system to the actual coordinate system of the switches. For example, let y denote the computed displacement at the tip of the SDOF oscillator (B-P2) of post B2. The displacement, u, at the tip of the post B2 is related to the displacement of the SDOF oscillators, y, as:

$$u = \frac{L}{M}y \tag{7-1}$$

where L and M are the effective excitation and effective mass, respectively, and are defined in Appendix B. A drawing of the transformation is shown in Figure 7-12a.

The total displacement at the tip of each post consists of three components as shown in Figure 7-12b: u_1 is the lateral displacement of the top of the frame, u_2 is the lateral displacement at the tip of the switch post due to the rotation of the frame at the base of the post, and u_3 is the deformation of the switch post. For Frame 00, u_1 and u_2 are zero. Displacement component u_3 is of greatest interest because the bending moment and shear force at the base of the switch post are directly related to u_3.

7.4.2 Benchmark switch post response on Frame 00

The maximum acceleration and displacement response of the switches mounted on Frame 00 are presented in Table 7-3.

Table 7-3 Analytical response of switches mounted on Frame 00

Switch	*Blade*	*Post Acceleration (g)*				*Post Deformation (mm)*			
		A-P1		A-P2		A-P1		A-P2	
		x-dir[1]	*y-dir*	*x-dir*	*y-dir*	*x-dir*	*y-dir*	*x-dir*	*y-dir*
SW1	Closed	3.1	4.6	3.9	4.6	74	46	97	46
	Open	4.2	4.9	4.2	4.4	99	147	107	101
SW2	Closed	4.1	4.4	4.4	4.5	28	28	57	28
	Open	4.1	4.5	4.3	4.3	28	31	44	30
SW3	Closed	3.9	3.5	4.2	3.6	21	15	32	15
	Open	3.9	4.1	4.1	3.9	21	16	26	15

1. See Figure 7-9 for the coordinate system.

Examination of the data in Table 7-3 shows that the deformations in the posts of the horizontal-break switch SW1 are substantially larger than those of the vertical-break switches SW2 and SW3. Larger deformations are expected in SW1 because the frequencies of this switch are less than those of SW2 and SW3.

7.4.3 Response of switches mounted on Frames 01 through 04

The maximum acceleration and deformation (u_3) response of the switch posts mounted on Frames 01 through 04 are presented in Tables 7-4 through 7-6 for SW1, SW2, and SW3, respectively. The values listed in these tables are normalized by the response of the switches mounted on the rigid Frame 00 (see Table 7-3). Values of less than 1.0 appear in a few cells in Tables 7-4 through 7-6 because the spectra of the earthquake histories used for analysis did not exactly match the target spectrum, and at certain frequencies fell below the target ordinates. As such, shifts in the frequency of the switch posts due to frame flexibility led to reductions in response in a few cases.

7.4.4 Switch SW1 (horizontal-break)

The normalized maximum accelerations and displacements of posts A-P1, A-P2, C-P1, and C-P2, for switch SW1 are presented in Table 7-4. The short braced frame proposed for future use, Frame 01, does not substantially amplify the acceleration or displacement responses of the switch posts. The remaining three frames, including the tall braced Frame 03 that is proposed for future use and the short unbraced Frame 02 that is currently in service, substantially increase the response of the switch posts.

Displacement histories for posts C-P1 and C-P2 of switch SW1 in the *x*- and *y*- directions are presented in Figures 7-13 through 7-16 for the closed blade condition and in Figures 7-17 through 7-20 for the open blade condition. The effect of frame flexibility is clearly evident in the response histories. The increase in the displacement response from the stiffest frame, Frame 00, to the more flexible frames (Frames 02 through 04) is also clearly evident.

7.4.5 Switch SW2 (vertical-break)

The normalized maximum accelerations and displacements of posts A-P1, A-P2, C-P1, and C-P2, for switch SW2 are presented in Table 7-5. The short braced frame proposed for future use, Frame 01, does not substantially amplify the acceleration or displacement responses of the switch posts. The remaining three frames, including the tall braced Frame 03 that is proposed for future use, substantially increase the response of the switch posts.

Displacement histories for posts C-P1 and C-P2 of switch SW1 in the *x*- and *y*- directions are presented in Figures 7-21 through 7-24 for the closed blade condition. The effect of frame flexibility is clearly evident in the response histories.

7.4.6 Switch SW3 (vertical-break)

The normalized maximum accelerations and displacements of posts A-P1, A-P2, C-P1, and C-P2, for switch SW3 are presented in Table 7-6. The short braced frame proposed for future use, Frame 01, does not substantially amplify the acceleration or displacement responses of the switch posts. The remaining three frames, including the tall braced Frame 03 that is proposed for future use and the short unbraced Frame 02 that is currently in service, substantially increase the response of the switch posts.

Displacement histories for posts C-P1 and C-P2 of switch SW1 in the *x*- and *y*- directions are presented in Figures 7-25 through 7-28 for the closed blade condition. The effect of frame flexibility is evident in the response histories. The amplification of the displacement response from the stiffest frame, Frame 01, to the more flexible frames (Frames 02 through 04) can be seen in Figures 7-26 and 7-28.

7.5 Concluding Remarks

Single-degree-of-freedom (SDOF) models of poles of disconnect switches were developed in Chapter 6 for the purpose of analyzing the response of switches on framed structures. Four frames, two in-service at this time and two proposed, were selected for study. Mathematical models of these frames were prepared for eigen analysis and response-history analysis using earthquake histories compatible with the IEEE spectra for High Level qualification. The SDOF models of the switch posts were incorporated into the mathematical models of four frames. The key conclusions of the studies described in this chapter are:

1. Frame 01, also termed the PG&E frame in this report, is a stiff braced frame that does not significantly amplify earthquake shaking from the base of the frame to the base of switches mounted on the frame. Switches of similar sizes and weights to SW1, SW2, and SW3 that have been qualified on a stiff or rigid frame should be considered to be qualified for

installation on the PG&E frame.

2. The two in-service frames analyzed in this chapter, the short unbraced Frame 02 and the tall braced Frame 04, substantially amplified the response of disconnect switches with frequencies similar to those of switches SW1, SW2, and SW3. Amplification factors of 2 and 3 were reported for Frames 02 and 04, respectively. Switches of similar sizes and weights to SW1, SW2, and SW3, that have been qualified on a stiff or rigid frame may not qualify if installed and tested on either Frames 02 and 04.

3. The tall braced Frame 03 that PG&E may use in future construction substantially amplified the response of the disconnect switches SW1, SW2, and SW3. Amplification factors in excess of 3 were calculated. The longitudinal, transverse, and vertical frequencies of this frame were 1 Hz, 8 Hz, and 4 Hz, respectively. Qualification of switches for use on this frame may not be possible because (a) the frame is too large to be tested on the largest simulator in the United States and (b) simulators in the United States, cannot impose the triaxial acceleration histories calculated at the base of the switch posts on a switch mounted directly on the simulator platform. PG&E should consider redesigning Frame 03 to substantially increase its stiffness and modal frequencies using braced steel columns and beams of tubular geometry supplemented with post-tensioned cables to provide stiffness in the longitudinal direction (see Figure 7-7 for orientation).

4. The vertical-break switches, SW2 and SW3, were qualified to the High Level on the stiff PEER frame when welded steel spacers were used in lieu of the more common cast aluminium spacers. The PEER frame, like the PG&E frame, was stiff and did not substantially amplify the earthquake shaking from the base of the frame to the base of the switches. As such, SW2 and SW3 should be considered to be qualified for installation on the PG&E frame.

5. IEEE 693-1997 writes that disconnect switches must be qualified on frames representative of those in service. This requirement is unrealistic given the wide variety of frames either in service or proposed for future construction. Given the physical limitations of earthquake simulators in the United States at this time, an alternate procedure for the seismic qualification and installation of switches is proposed that combines analysis and experimentation. First, switches mounted directly on an earthquake simulator or a stiff frame would be tested using a level of shaking that is twice that required for the desired level of qualification (e.g., 2 times 1.0g for qualification at the High Level). Second, mathematical models of the switch posts would be constructed using resonant-search and static test data. Such work would be undertaken by the hardware manufacturers. Third, the utilities would analyze and design frames using the SDOF models of the switch posts provided by the manufacturers with the objective of limiting the amplification of the response of the switches to 2.0 or less compared with the fixed-base condition. The factor of 2.0 is somewhat arbitrary but was chosen here because 2.0 is the value used in IEEE 693-1997 to characterize the amplification of motion in components supported on transformer tanks.

6. Analysis data similar to that presented in this chapter could be used to estimate the performance of a switch mounted on a support structure provided that (a) robust mathematical models, and (b) acceleration and deformation limits of the components of the switch

(including insulators, blades, base hardware, and cranking mechanism) were available. mathematical models could be prepared using resonant-search and static-test data similar to that presented in Chapter 5 and analytical procedures similar to those outlines in Chapter 6. Acceleration and deformation limits of the components of the switch would be established using static and dynamic testing. response-history analysis of the switches mounted on the support structures could be used to estimate the response of all components of the switch. The switch accelerations and deformations calculated by analysis would then be compared with the limiting values established by testing to judge the likely performance of the elevated switch. (Additional studies would be needed to characterize the acceleration and deformation limits of the switches described in Chapters 4 and 5. Mathematical models more detailed than those presented in Chapter 6 would be needed to characterize the acceleration response of the switch posts, assuming that the crank mechanism could be isolated from the switch).

Table 7-4 Normalized analytical response of frame-mounted switch SW1[1]

Switch[2]	*Blade*	*Frame*[3]	*Post Acceleration*								*Post Deformation*[4]							
			A-P1		A-P2		C-P1		C-P2		A-P1		A-P2		C-P1		C-P2	
			x-[5]	*y*-	*x*-	*y*-	*x*-	*y*-	*x*-	*y*-	*x*-	*y*-	*x*-	*y*-	*x*-	*y*-	*x*-	*y*-
SW1	Closed	Frame 01	1.2	1.1	1.1	1.0	1.4	1.1	1.1	0.9	1.0	0.9	1.0	0.9	1.0	0.9	1.0	0.9
		Frame 02	1.7	1.3	1.8	1.3	1.6	1.4	1.7	1.4	1.7	1.4	1.7	1.4	1.6	1.5	1.6	1.5
		Frame 03	2.2	1.5	2.3	1.5	1.7	2.6	1.5	2.6	2.3	1.3	2.2	1.3	1.8	2.6	1.7	2.6
		Frame 04	2.5	1.9	2.5	1.9	2.4	1.7	2.4	1.7	2.4	1.9	2.4	1.9	2.4	1.8	2.3	1.8
	Open	Frame 01	0.9	1.0	1.0	1.0	1.0	1.1	1.0	1.0	0.9	1.0	1.0	1.0	1.0	1.0	1.0	1.0
		Frame 02	1.6	1.4	1.8	1.3	1.5	1.7	1.8	1.3	1.5	1.5	1.8	1.2	1.4	1.8	1.8	1.3
		Frame 03	2.1	1.2	2.3	1.2	1.5	2.3	1.3	1.6	2.1	1.0	2.4	1.1	1.7	2.0	1.6	1.5
		Frame 04	2.5	2.1	2.2	1.7	2.4	2.0	2.2	1.7	2.3	2.0	2.2	1.5	2.2	2.0	2.2	1.6

1. All values are normalized by the response of the posts on the rigid frame; see Table 7-3.
2. See Table 2-4 for information on the switches
3. See Figures 7-1 through 7-4 for line drawings of the frames.
4. Denotes post deformation (u_3 of Figure 7-12b).
5. See Figures 7-1 for information on the coordinate system.

Table 7-5 Normalized analytical response of frame-mounted switch SW2[1]

Switch[2]	*Blade*	*Frame*[3]	*Post Acceleration*								*Post Deformation*[4]							
			A-P1		A-P2		C-P1		C-P2		A-P1		A-P2		C-P1		C-P2	
			x-[5]	*y*-	*x*-	*y*-	*x*-	*y*-	*x*-	*y*-	*x*-	*y*-	*x*-	*y*-	*x*-	*y*-	*x*-	*y*-
SW2	Closed	Frame 01	1.1	1.1	0.9	1.1	1.2	1.2	1.3	1.2	1.0	1.1	0.9	1.0	1.2	1.1	1.3	1.1
		Frame 02	1.7	1.2	1.3	1.2	1.1	1.5	1.1	1.5	1.8	1.5	1.4	1.4	1.2	1.8	1.3	1.7
		Frame 03	1.9	1.6	1.6	1.6	1.1	2.7	1.1	2.7	1.9	1.7	1.9	1.7	1.4	3.0	1.5	3.0
		Frame 04	1.6	1.6	1.9	1.6	1.5	1.7	1.8	1.7	1.7	1.9	2.1	1.7	1.6	1.9	2.0	1.7
	Open	Frame 01	1.0	1.0	0.9	1.0	1.2	1.0	1.2	1.0	1.0	1.0	0.9	1.0	1.2	1.0	1.2	1.0
		Frame 02	1.3	1.2	1.1	1.2	0.9	1.5	1.0	1.5	1.5	1.5	1.2	1.3	1.1	1.9	1.1	1.7
		Frame 03	2.2	1.4	1.5	1.4	1.1	2.7	1.1	2.6	2.2	1.4	1.6	1.4	1.4	2.7	1.3	2.6
		Frame 04	1.8	1.7	1.8	1.7	1.6	1.8	1.7	1.8	1.8	1.9	1.9	1.7	1.6	2.0	1.9	1.7

1. All values are normalized by the response of the posts on the rigid frame; see Table 7-3.
2. See Table 2-4 for information on the switches
3. See Figures 7-1 through 7-4 for line drawings of the frames.
4. Denotes post deformation (u_3 of Figure 7-12b).
5. See Figures 7-1 for information on the coordinate system.

Table 7-6 Normalized analytical response of frame-mounted switch SW3[1]

Switch[2]	*Blade*	*Frame*[3]	*Post Acceleration*								*Post Deformation*[4]							
			A-P1		A-P2		C-P1		C-P2		A-P1		A-P2		C-P1		C-P2	
			x-[5]	*y-*	*x-*	*y-*	*x-*	*y-*	*x-*	*y-*	*x-*	*y-*	*x-*	*y-*	*x-*	*y-*	*x-*	*y-*
SW3	Closed	Frame 01	1.1	1.2	1.0	1.1	1.1	1.2	1.2	1.2	1.0	1.2	1.0	1.1	1.1	1.2	1.2	1.2
		Frame 02	2.0	1.6	1.4	1.6	1.1	1.5	1.2	1.5	2.2	2.0	1.5	1.8	1.4	1.9	1.4	1.9
		Frame 03	3.0	3.7	1.7	3.7	1.1	3.8	1.0	3.7	3.2	4.0	1.9	3.8	1.4	4.3	1.3	4.0
		Frame 04	1.5	2.5	1.6	2.5	1.4	2.4	1.5	2.3	1.8	2.8	1.8	2.5	1.6	2.7	1.7	2.3
	Open	Frame 01	1.0	1.1	1.0	1.2	1.1	1.1	1.1	1.2	1.1	1.1	1.0	1.2	1.1	1.2	1.1	1.2
		Frame 02	1.9	1.3	1.6	1.3	1.2	1.3	1.1	1.3	2.1	1.7	1.8	1.5	1.4	1.8	1.4	1.5
		Frame 03	2.9	2.8	1.9	3.0	1.1	2.7	1.1	3.2	3.1	3.0	2.0	3.3	1.4	3.2	1.3	3.7
		Frame 04	1.6	2.4	1.8	2.3	1.4	2.1	1.6	2.1	1.8	3.0	1.9	2.4	1.7	2.7	1.7	2.2

1. All values are normalized by the response of the posts on the rigid frame; see Table 7-3.
2. See Table 2-4 for information on the switches
3. See Figures 7-1 through 7-4 for line drawings of the frames.
4. Denotes post deformation (u_3 of Figure 7-12b).
5. See Figures 7-1 for information on the coordinate system.

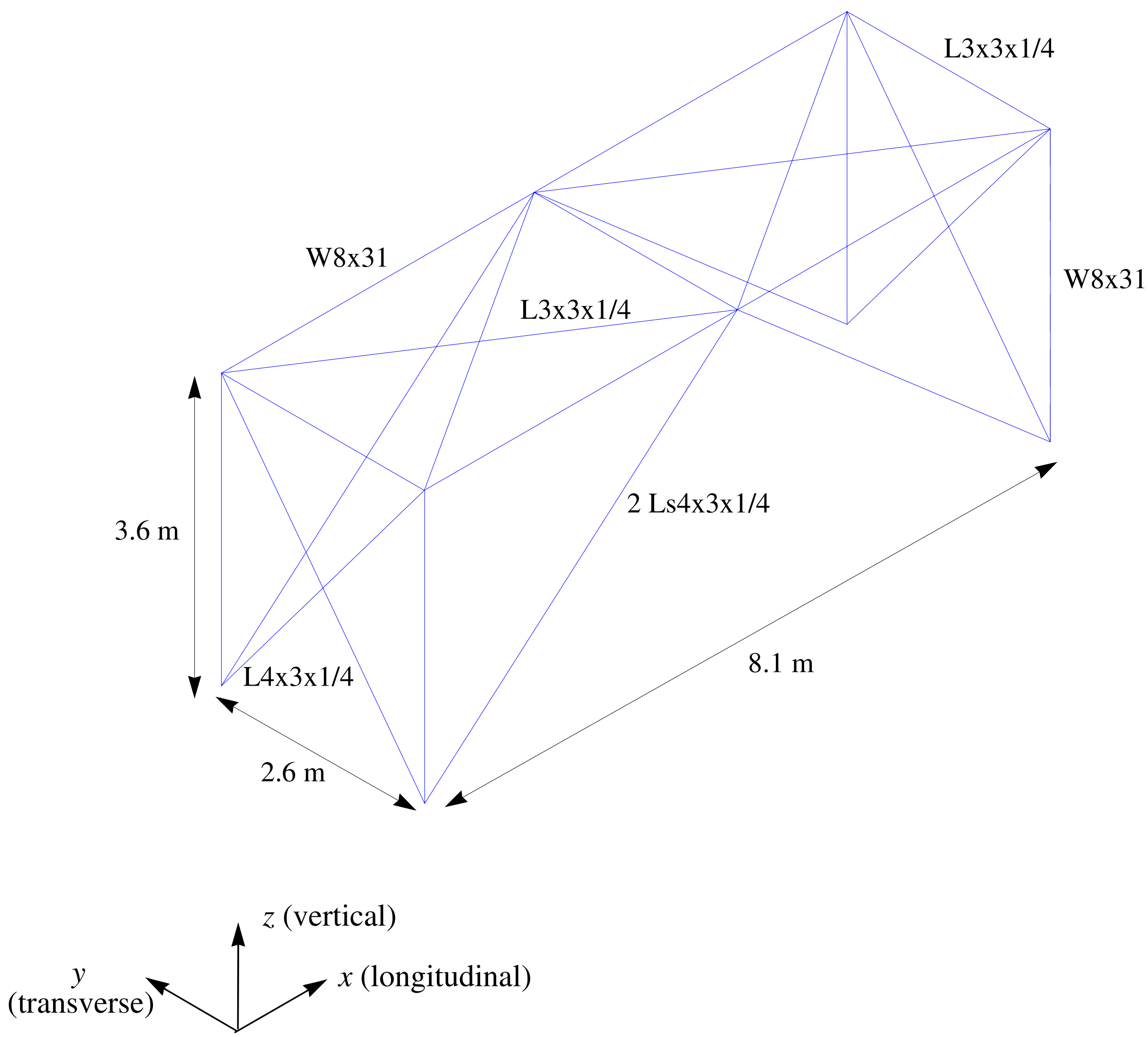

Figure 7-1 Line drawing of Frame 01

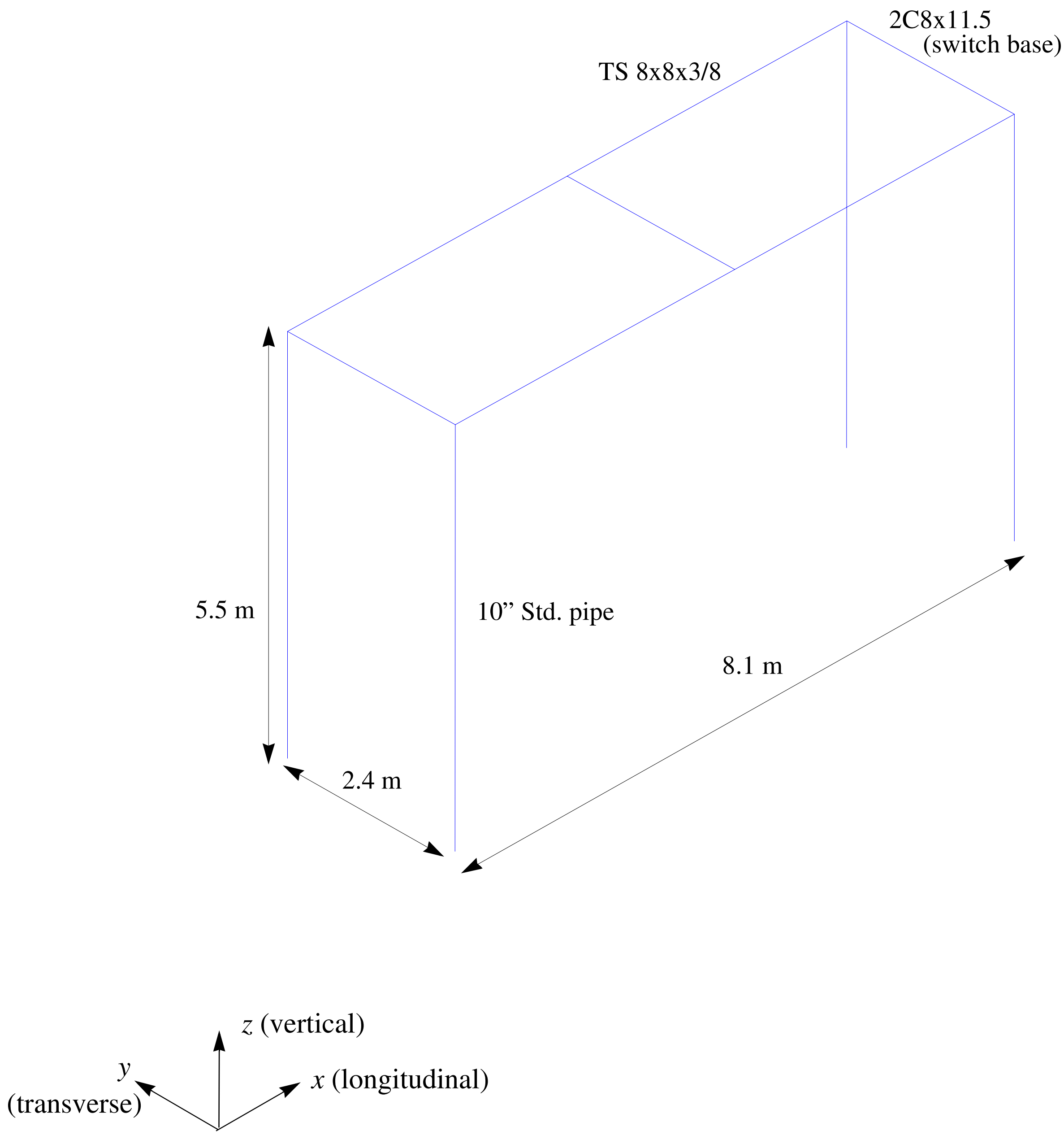

Figure 7-2 Line drawing of Frame 02

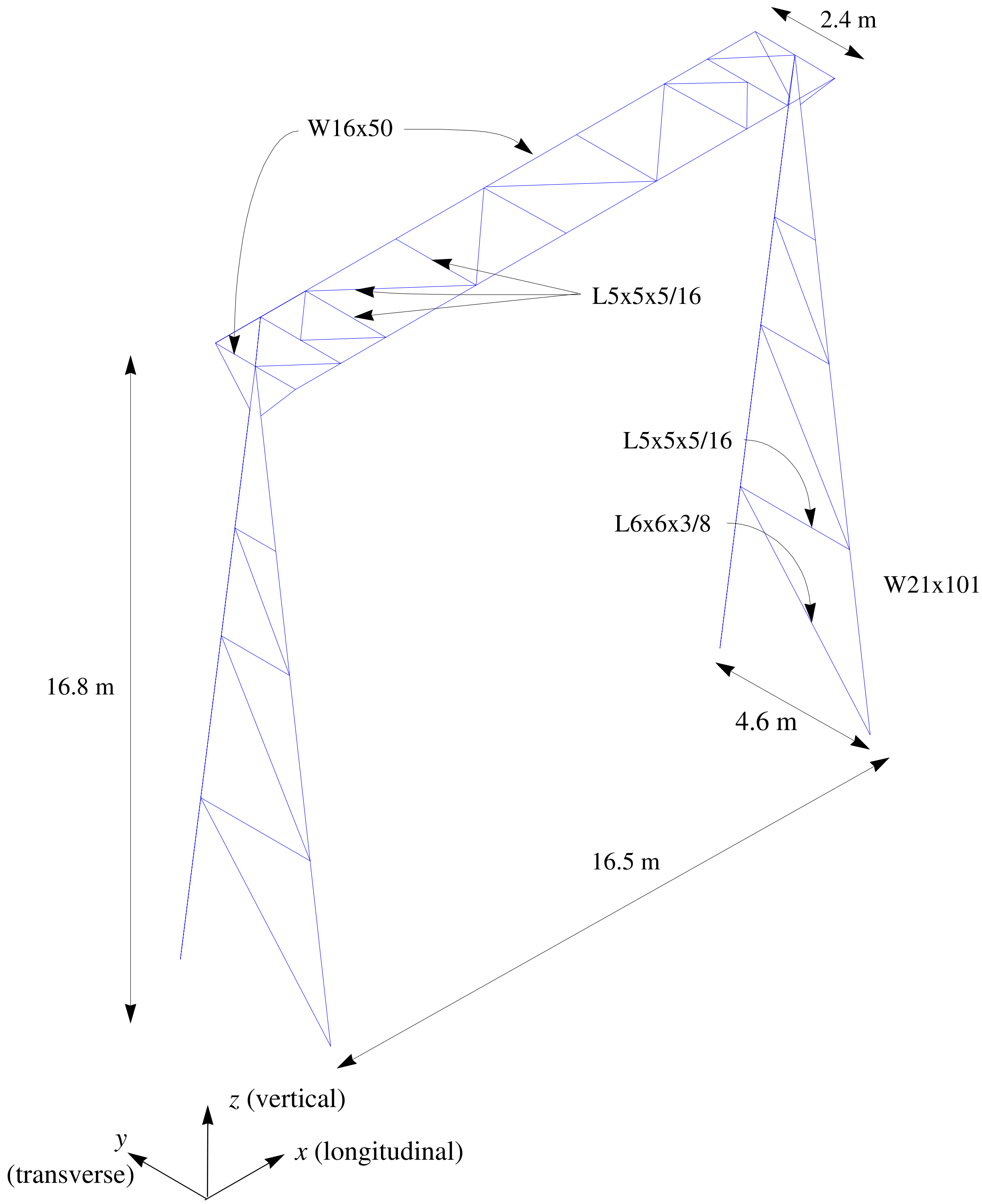

Figure 7-3 Line drawing of Frame 03

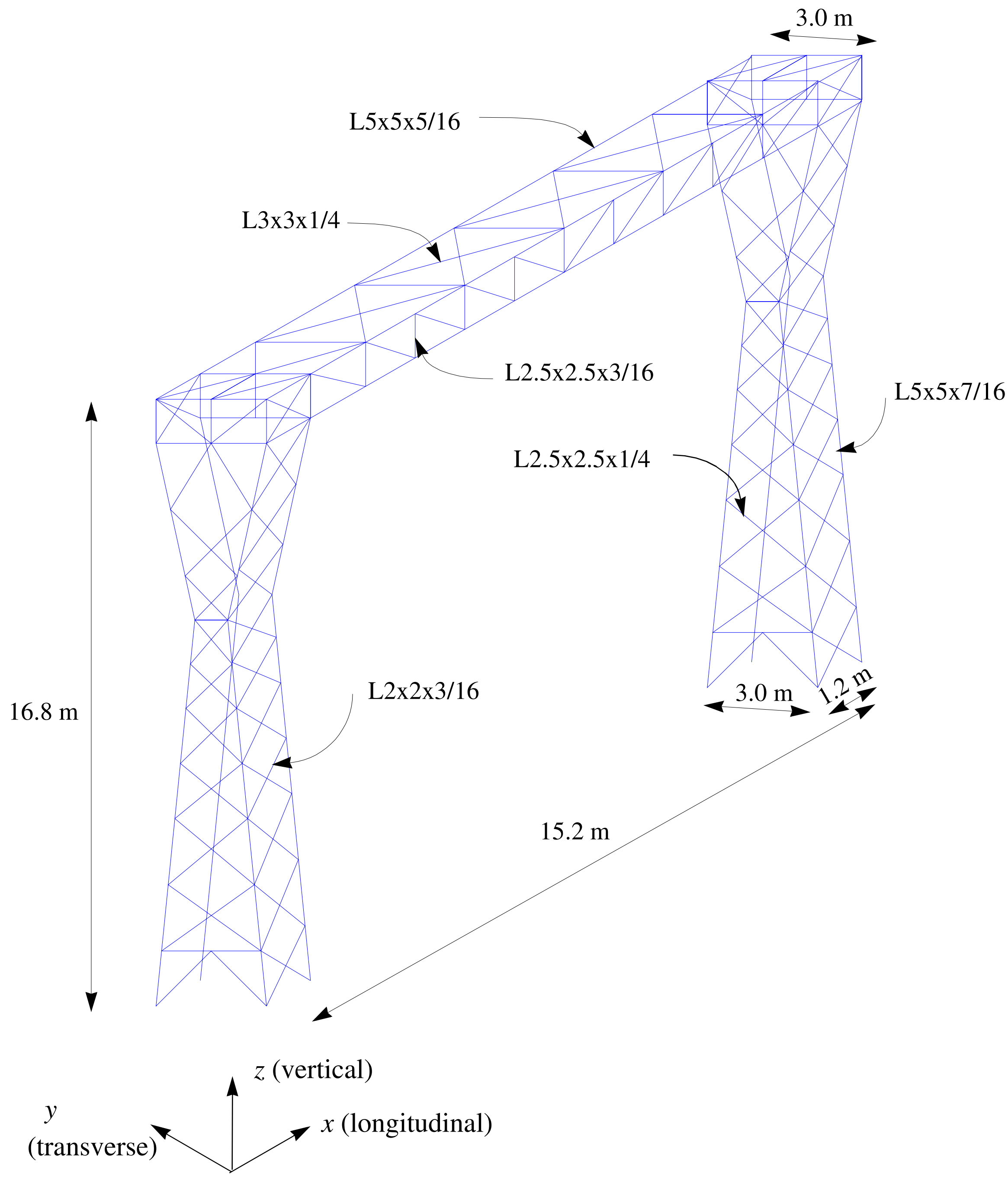

Figure 7-4 Line drawing of Frame 04

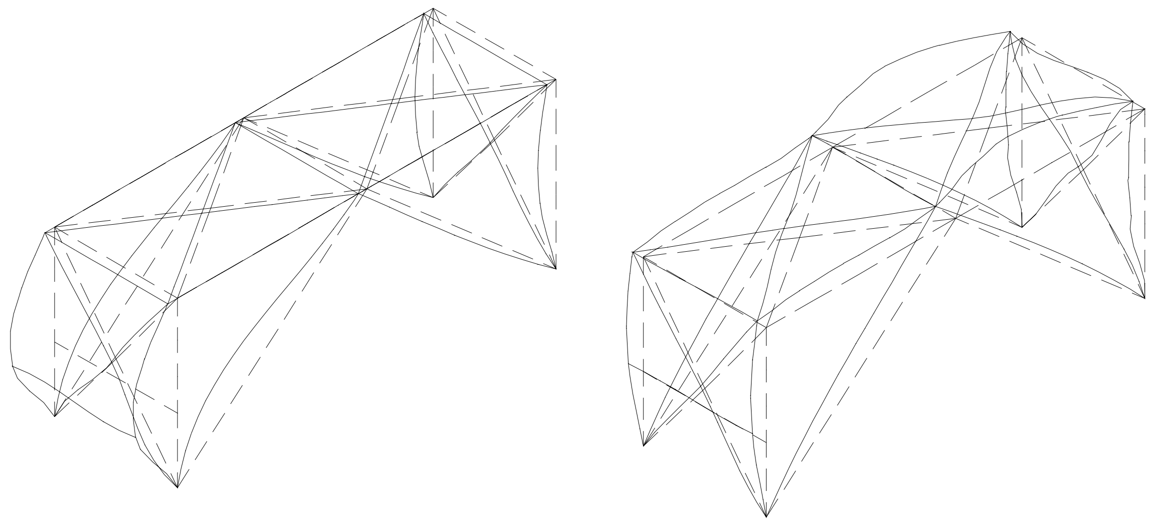

(a) Longitudinal mode (f = 45 Hz) (b) Transverse mode (f = 24 Hz)

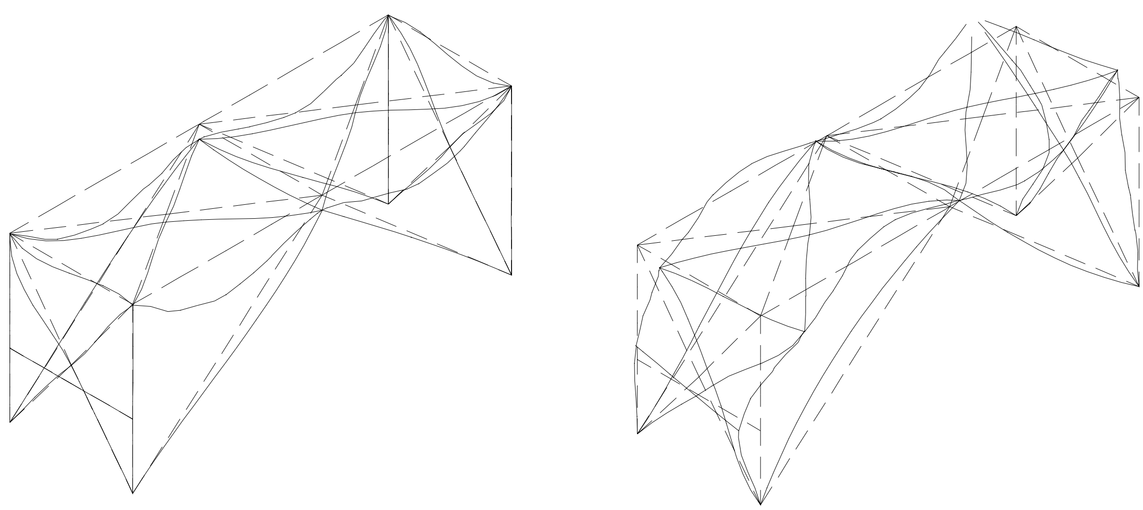

(c) Vertical mode (f = 54 Hz) (d) Torsional mode (f = 63 Hz)

Figure 7-5 Mode shapes of Frame 01

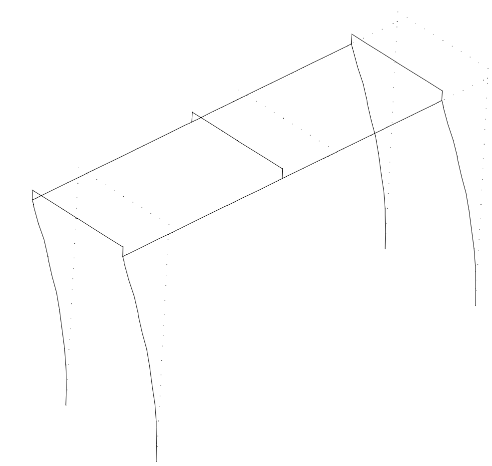

(a) Longitudinal mode (f = 4Hz)

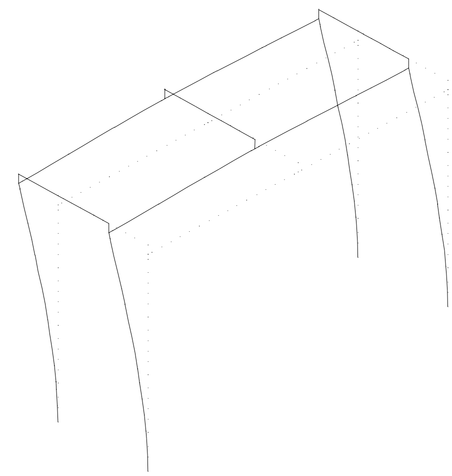

(b) Transverse mode (f = 4Hz)

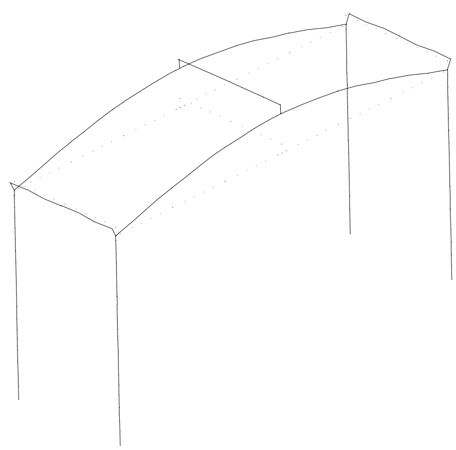

(c) Vertical mode (f = 8 Hz)

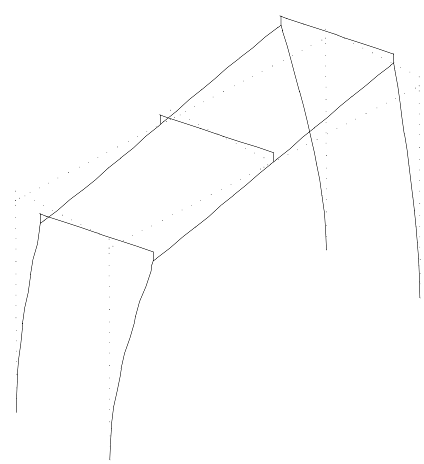

(d) Torsional mode (f = 6 Hz)

Figure 7-6 Mode shapes of Frame 02

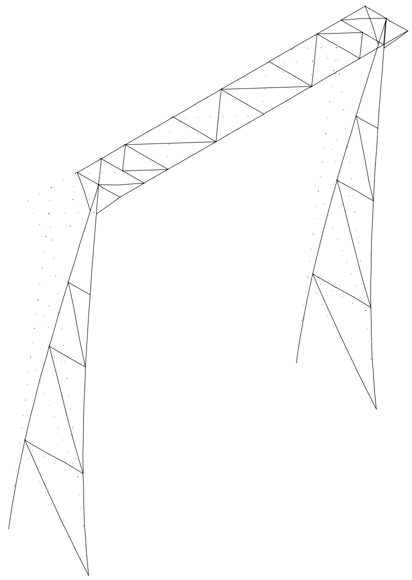

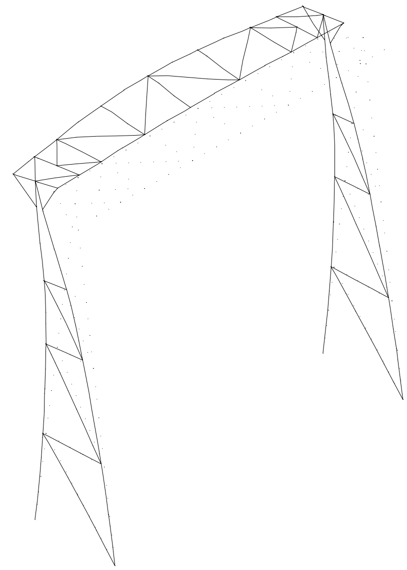

(a) Longitudinal mode ($f = 1$ Hz) (b) Transverse mode ($f = 8$ Hz)

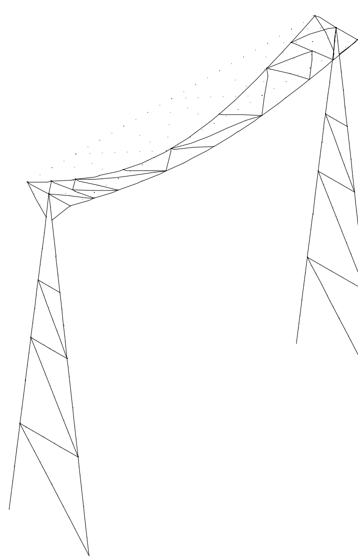

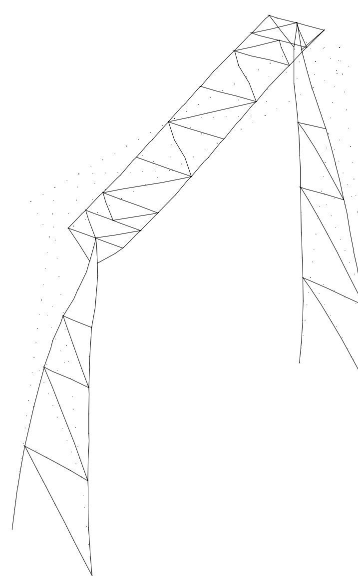

(c) Vertical mode ($f = 4$ Hz) (d) Torsional mode ($f = 10$ Hz)

Figure 7-7 Mode shapes of Frame 03

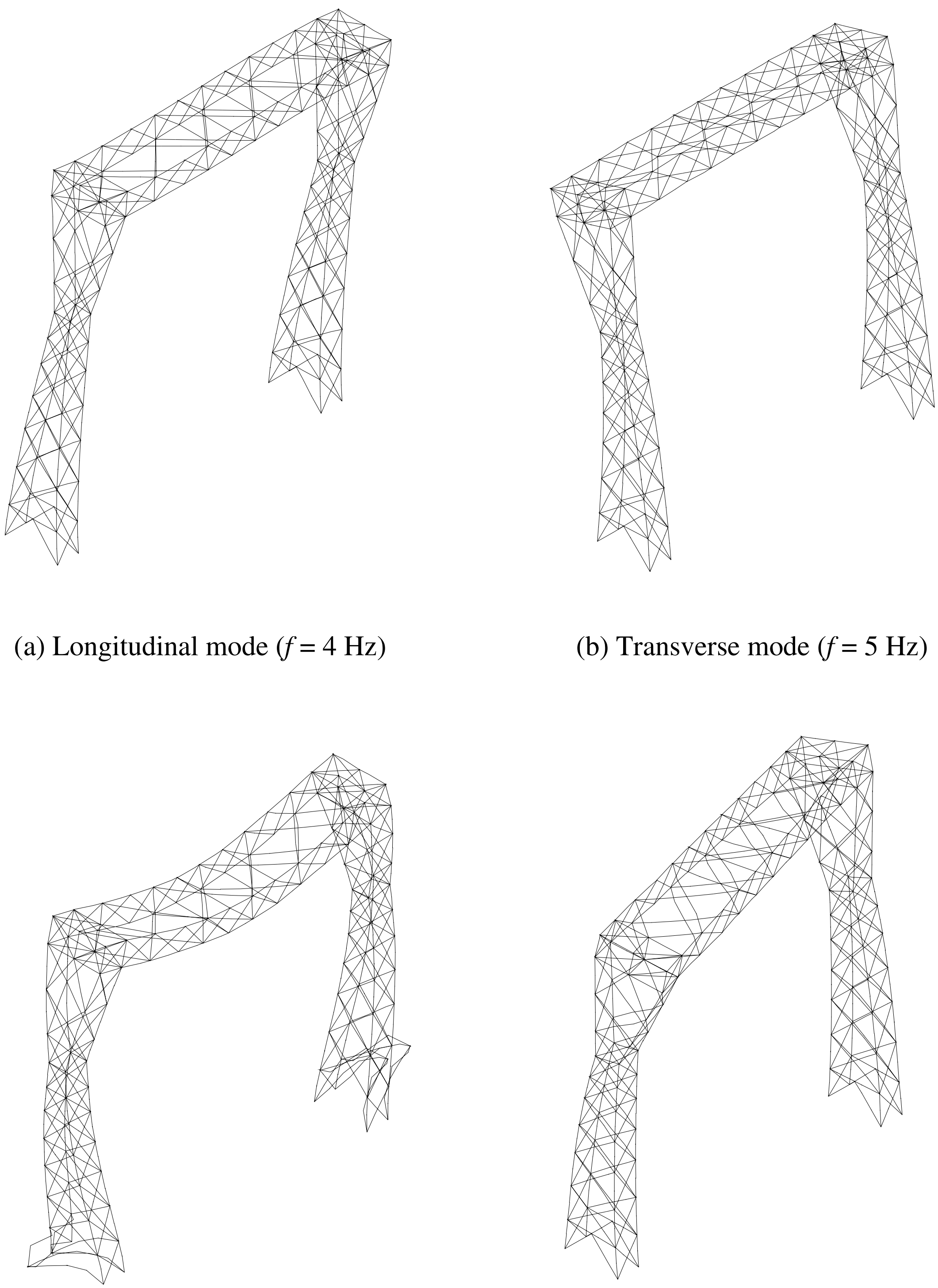

(a) Longitudinal mode ($f = 4$ Hz) (b) Transverse mode ($f = 5$ Hz)

(c) Vertical mode ($f = 15$ Hz) (d) Torsional mode ($f = 7$ Hz)

Figure 7-8 Mode shapes of Frame 04

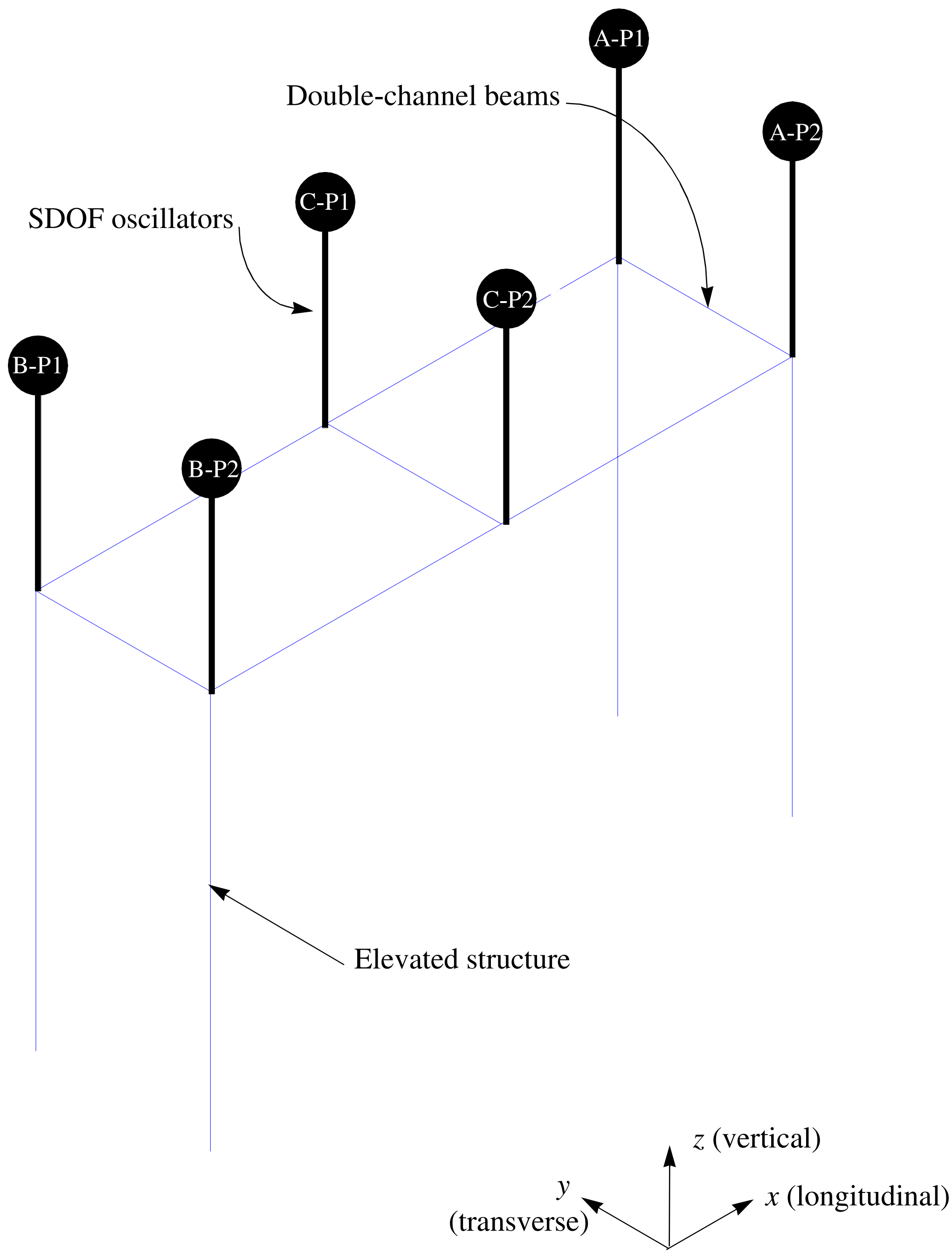

Figure 7-9 Analytical model of switch posts on the frame

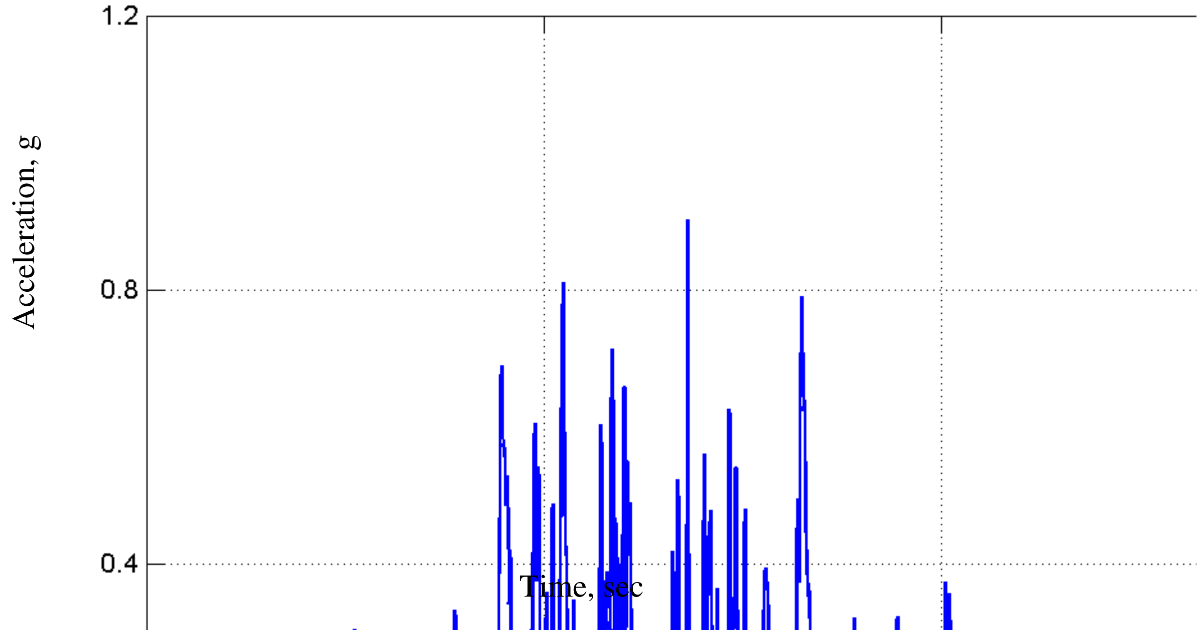

(a) Longitudinal (*x*-direction)

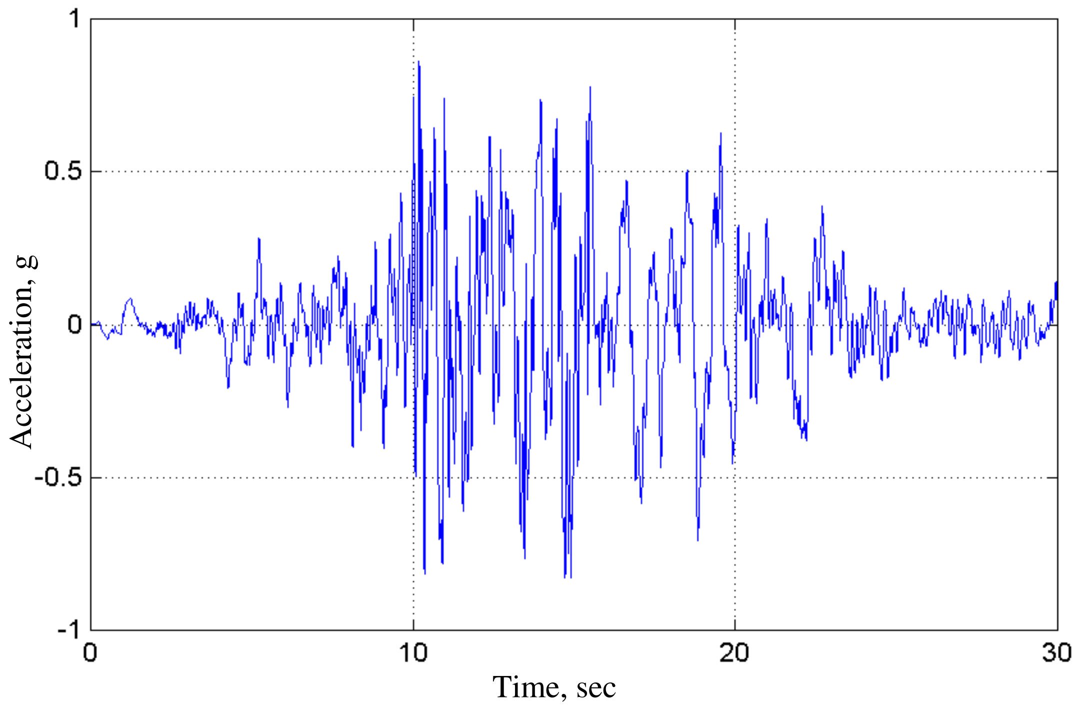

(b) Transverse (*y*-direction)

Figure 7-10 Acceleration histories used for analysis

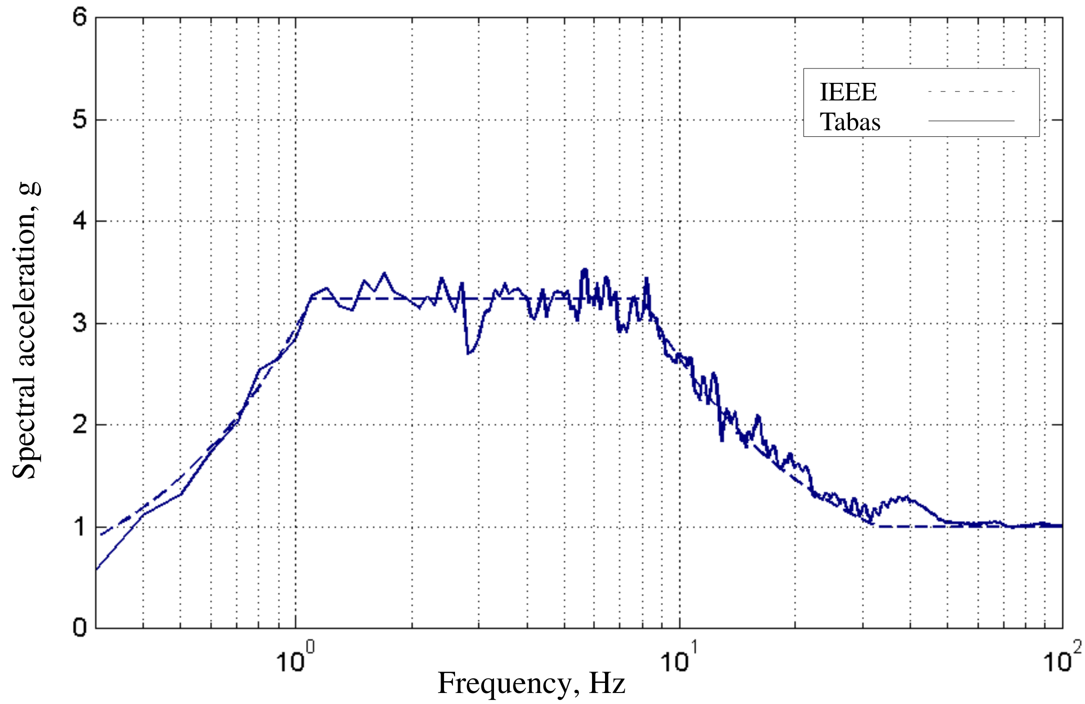

(a) Longitudinal (*x*-direction)

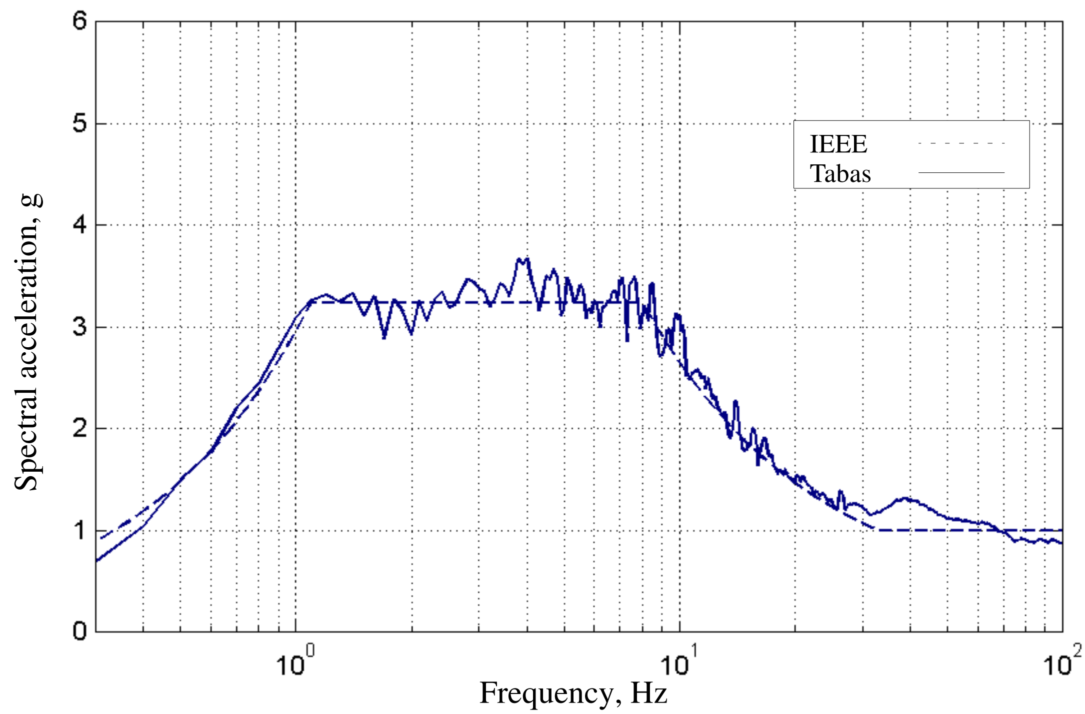

(b) Transverse (*y*-direction)

Figure 7-11 Acceleration response spectra for the earthquake histories

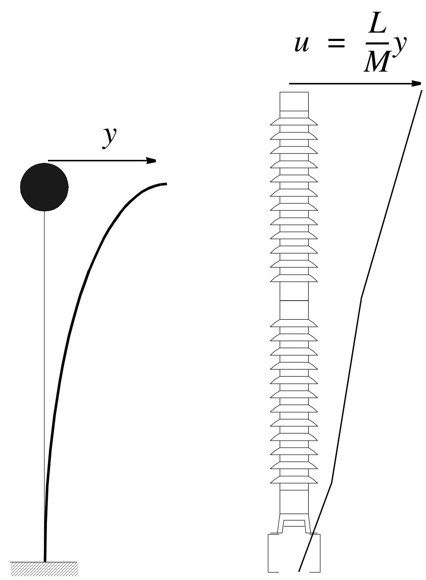

(a) Transformation to the switch tip

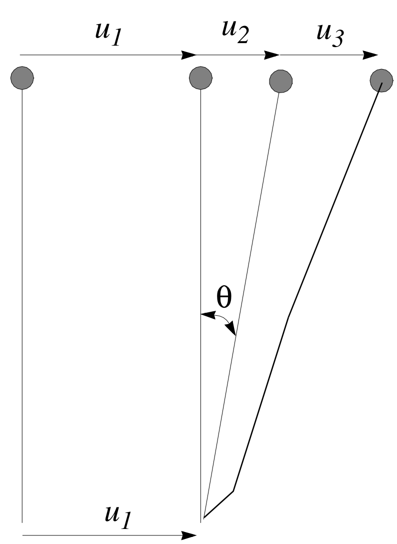

(b) Components of deformation

Figure 7-12 Coordinate transformation and components of switch deformation

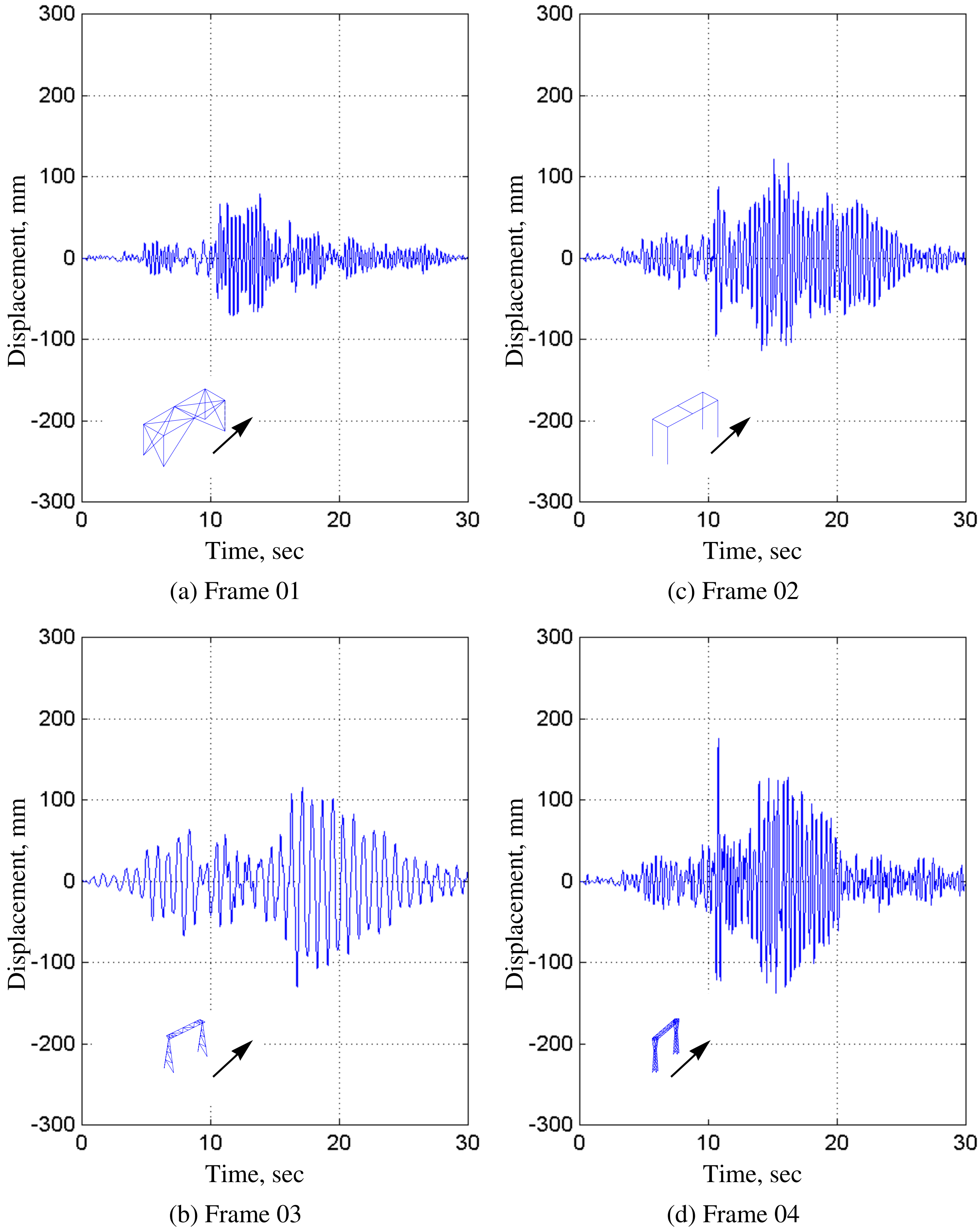

Figure 7-13 Deformation (u_3) of post tip relative to the frame, *x*-direction, switch SW1, closed blade, post P-C1, Tabas history, target PGA equal to 1.0g

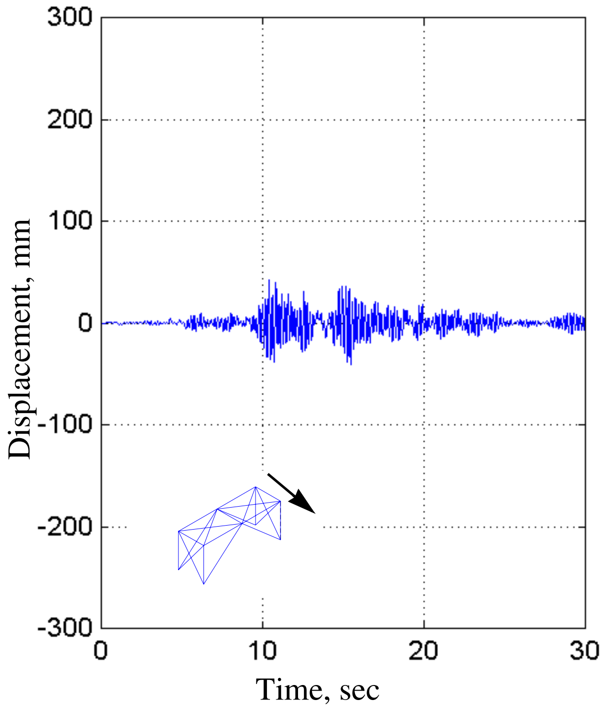

(a) Frame 01

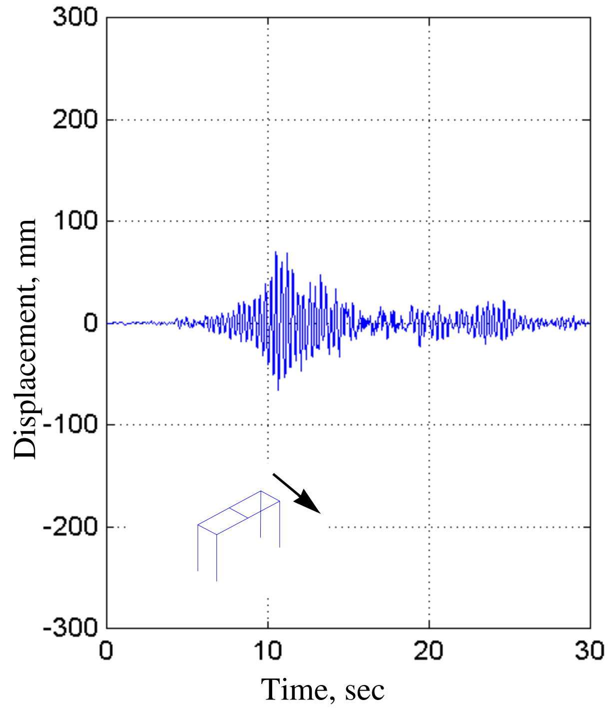

(c) Frame 02

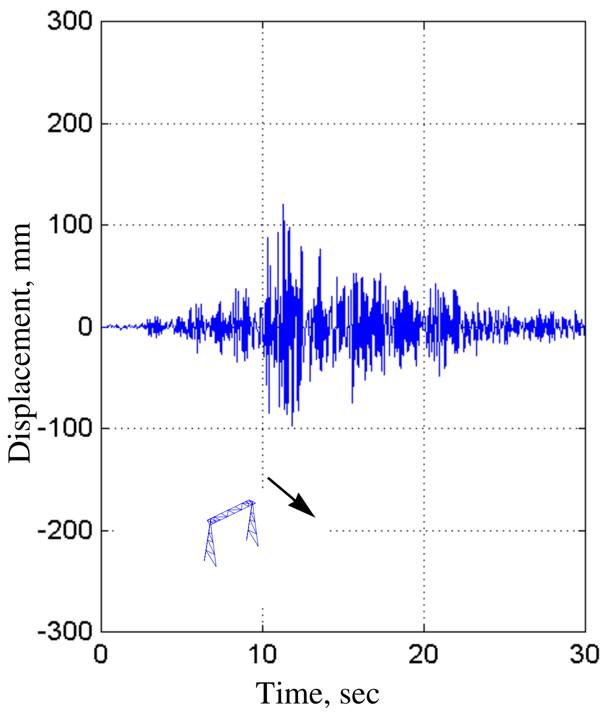

(b) Frame 03

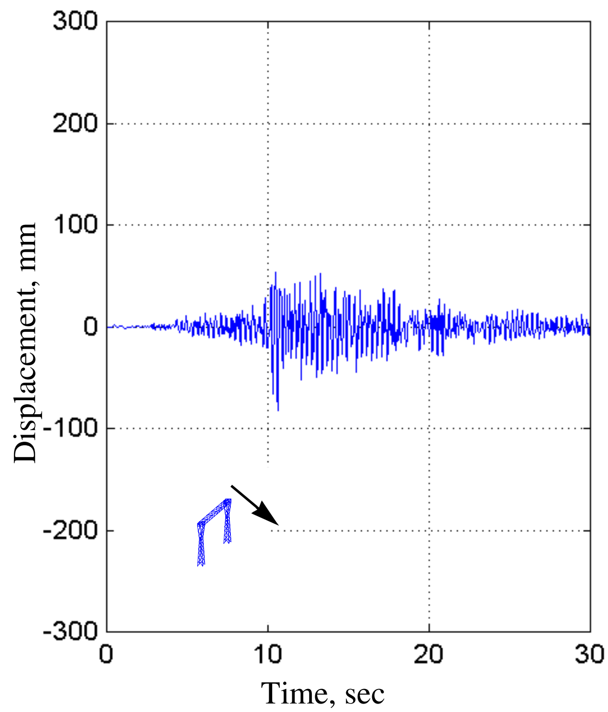

(d) Frame 04

Figure 7-14 Deformation (u_3) of post tip relative to the frame, *y*-direction, switch SW1, closed blade, post P-C1, Tabas history, target PGA equal to 1.0g

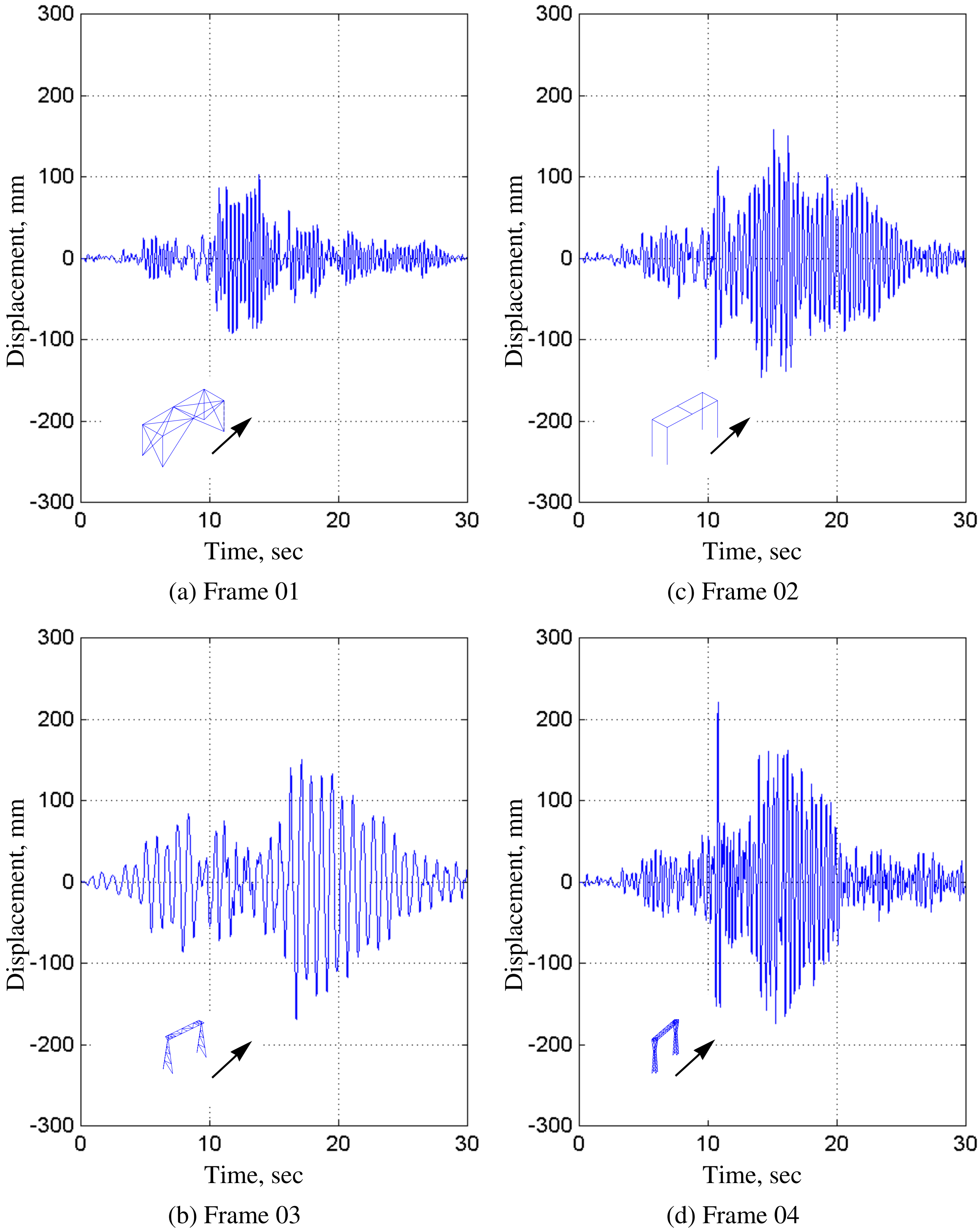

Figure 7-15 Deformation (u_3) of post tip relative to the frame, *x*-direction, switch SW1, closed blade, post P-C2, Tabas history, target PGA equal to 1.0g

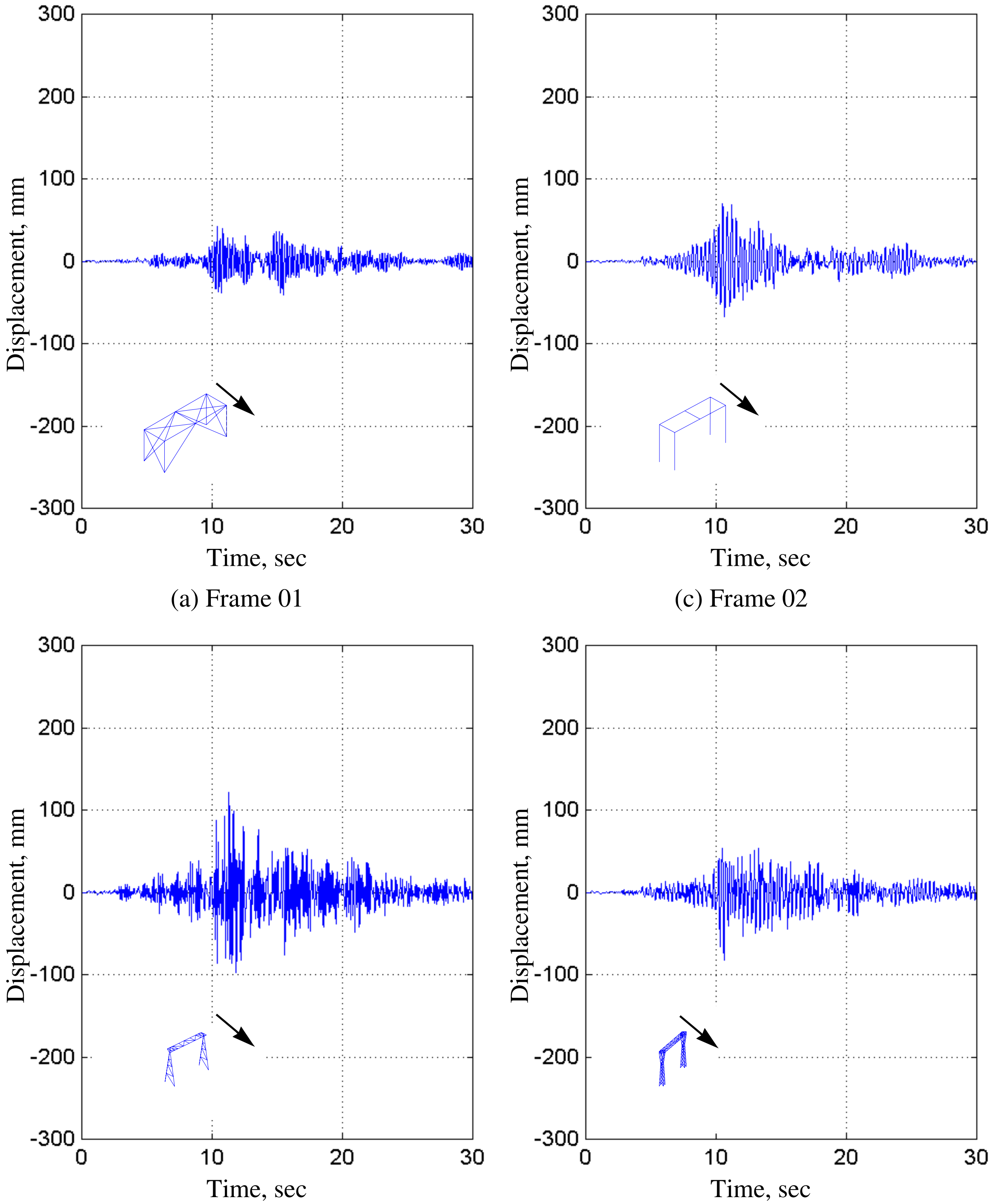

(a) Frame 01

(c) Frame 02

(b) Frame 03

(d) Frame 04

Figure 7-16 Deformation (u_3) of post tip relative to the frame, *y*-direction, switch SW1, closed blade, post P-C2, Tabas history, target PGA equal to 1.0g

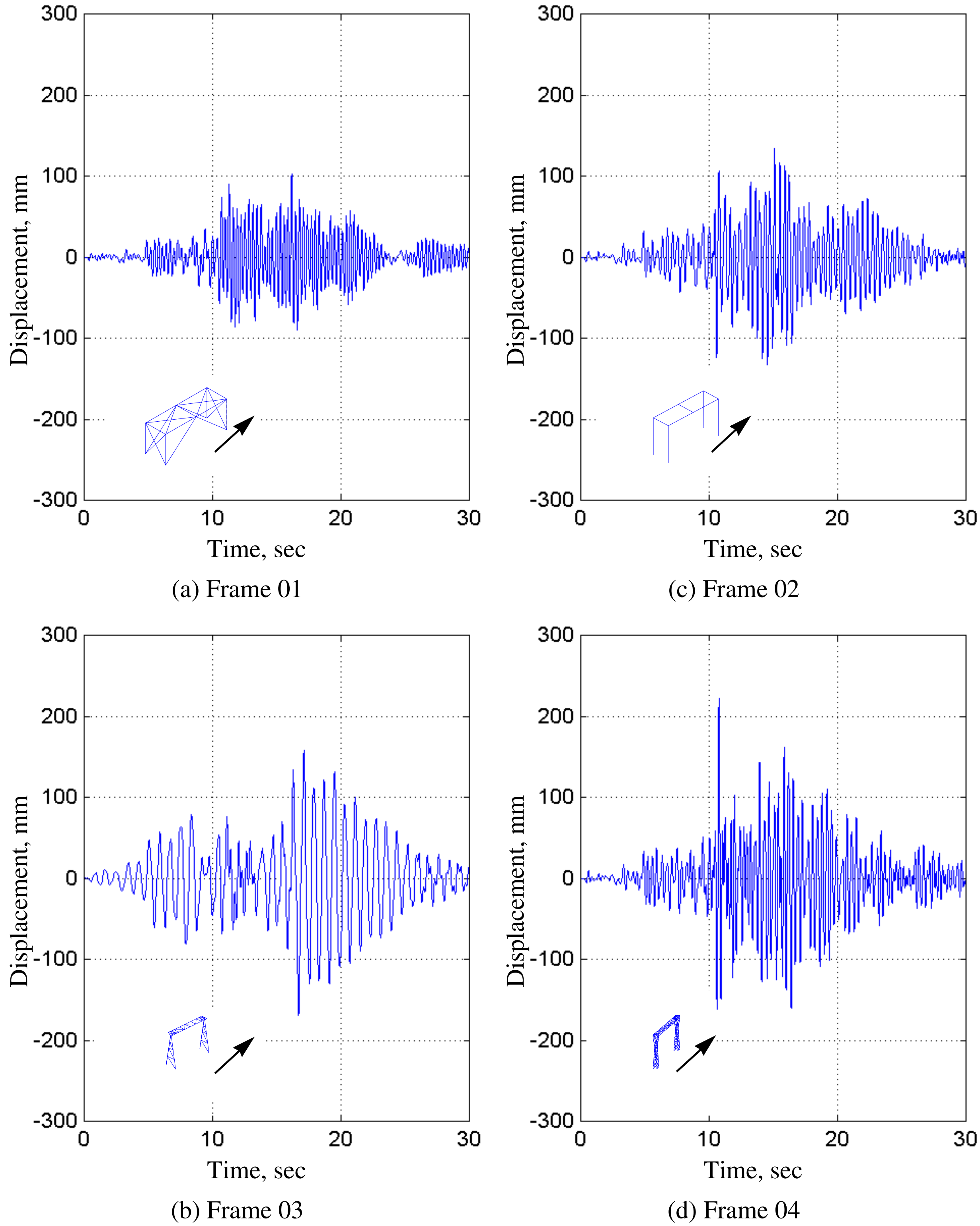

Figure 7-17 Deformation (u_3) of post tip relative to the frame, *x*-direction, switch SW1, open blade, post P-C1, Tabas history, target PGA equal to 1.0g

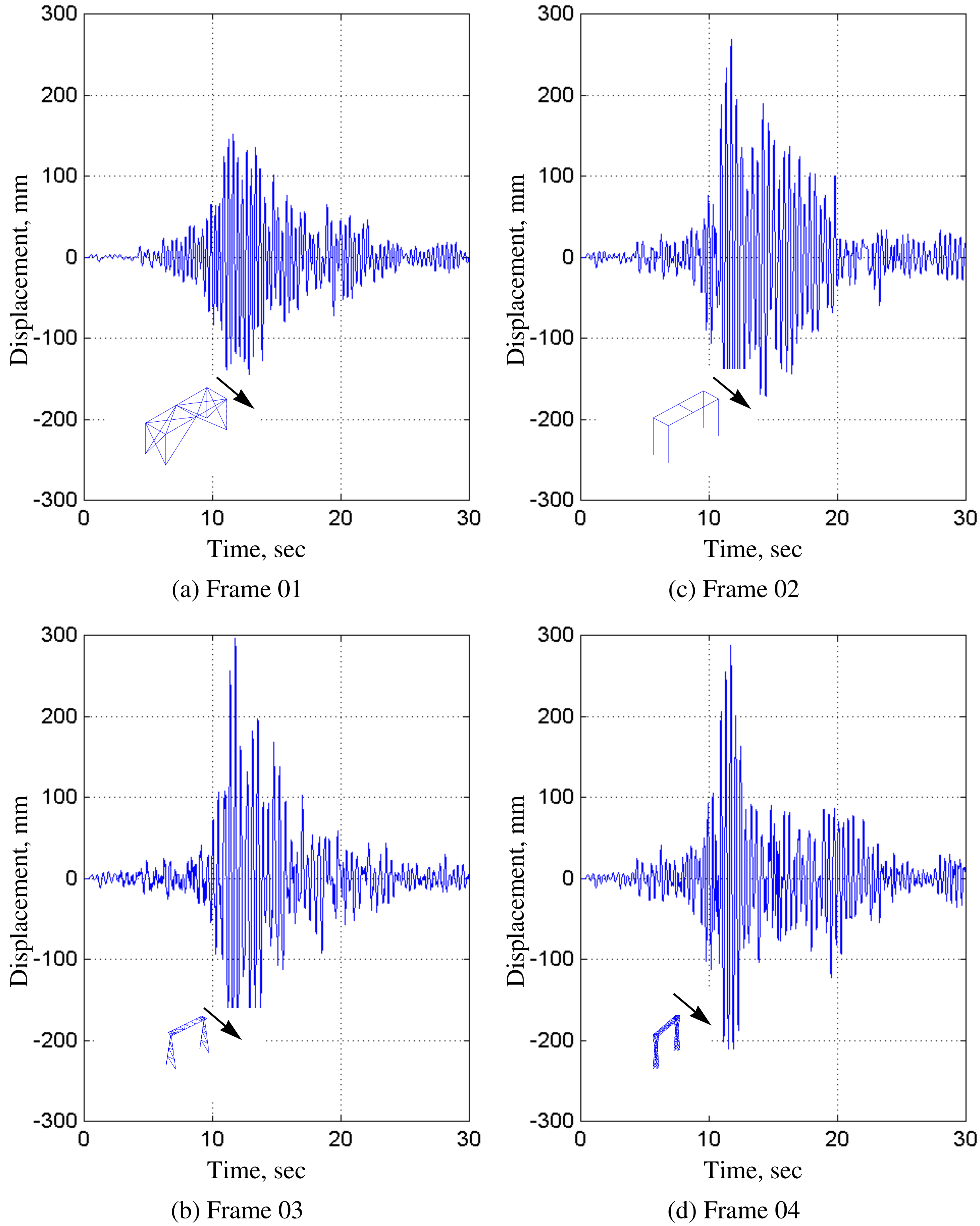

Figure 7-18 Deformation (u_3) of post tip relative to the frame, y-direction, switch SW1, open blade, post P-C1, Tabas history, target PGA equal to 1.0g

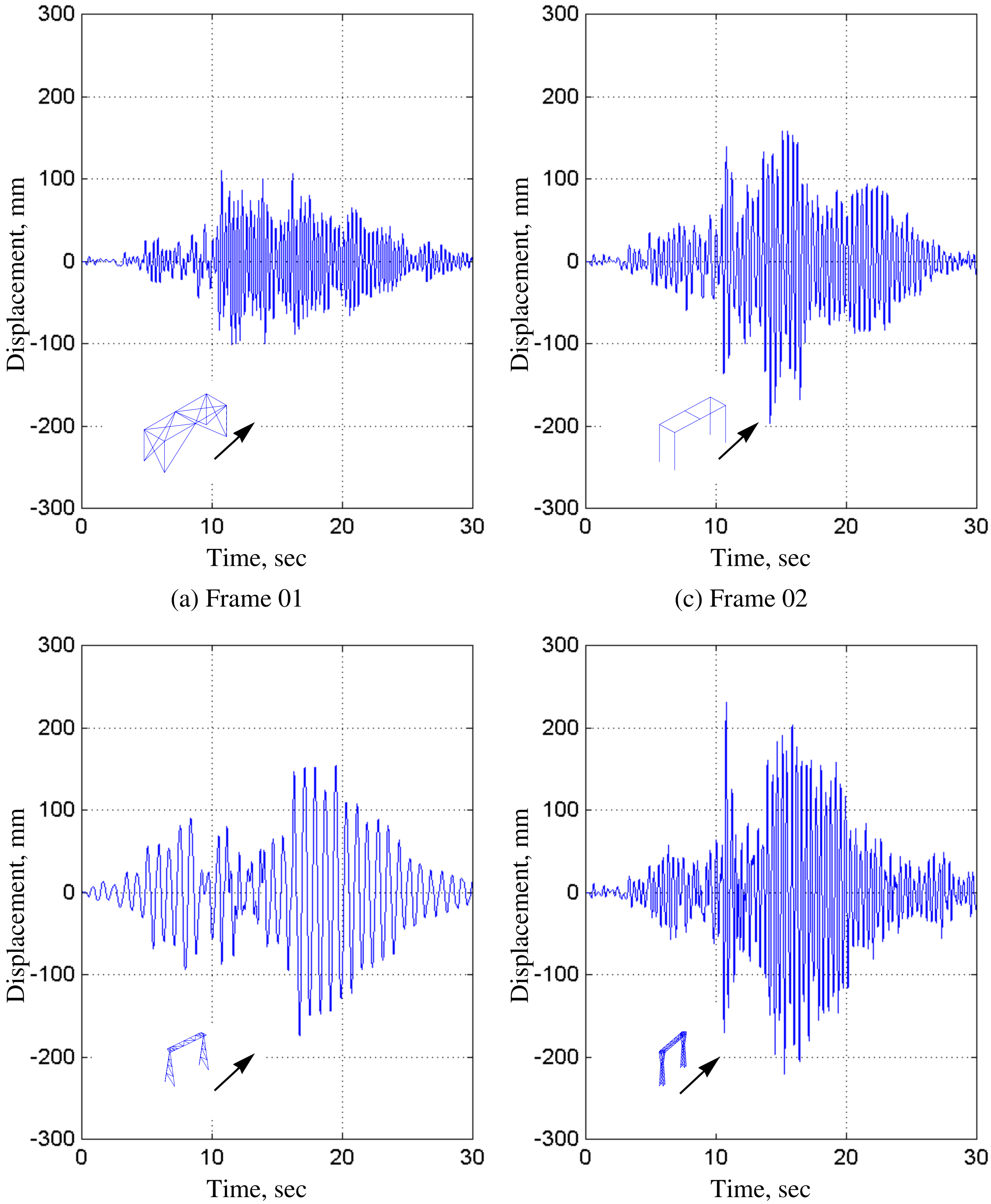

(a) Frame 01

(c) Frame 02

(b) Frame 03

(d) Frame 04

Figure 7-19 Deformation (u_3) of post tip relative to the frame, x-direction, switch SW1, open blade, post P-C2, Tabas history, target PGA equal to 1.0g

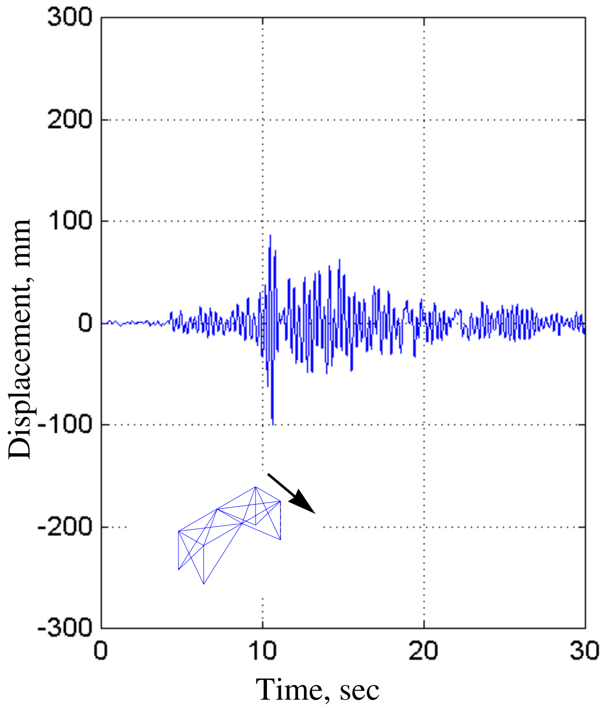

(a) Frame 01

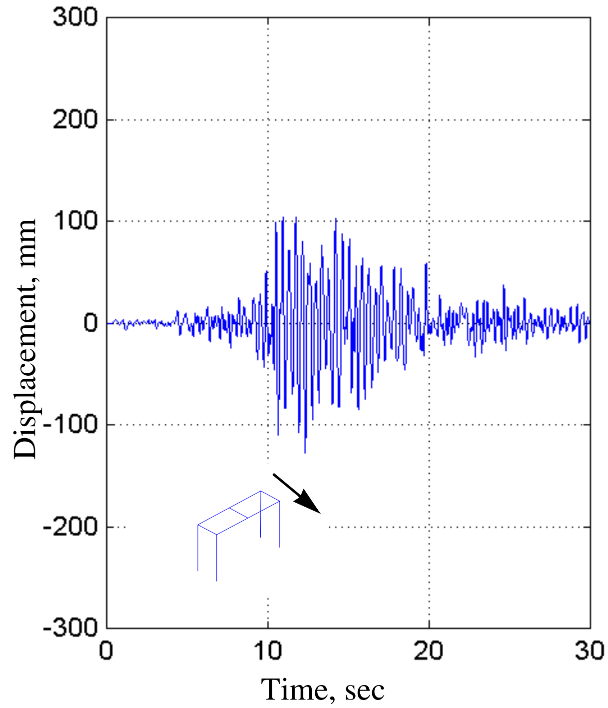

(c) Frame 02

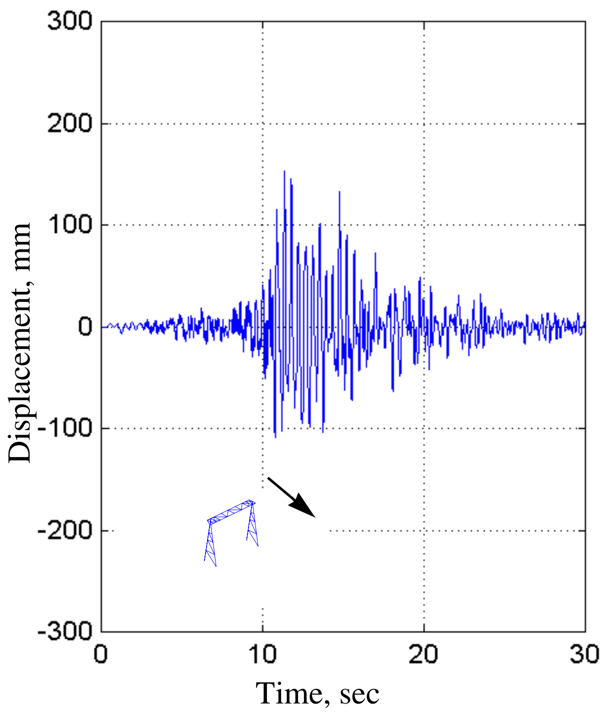

(b) Frame 03

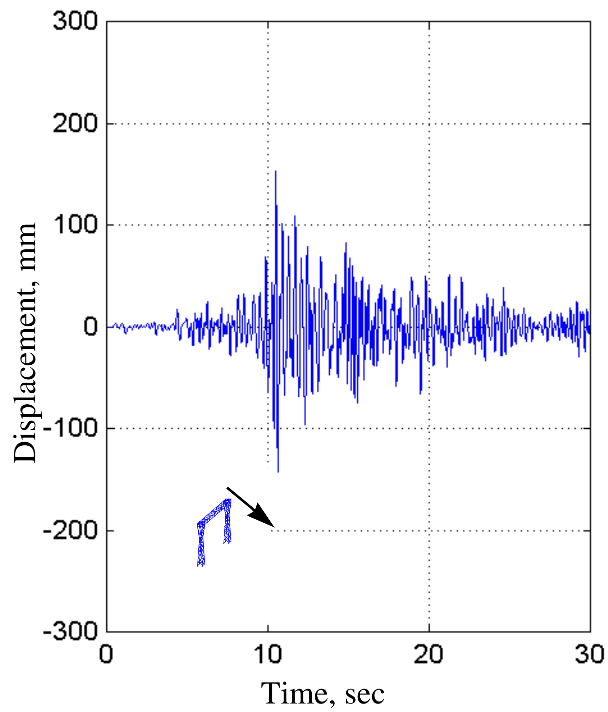

(d) Frame 04

Figure 7-20 Deformation (u_3) of post tip relative to the frame, *y*-direction, switch SW1, open blade, post P-C2, Tabas history, target PGA equal to 1.0g

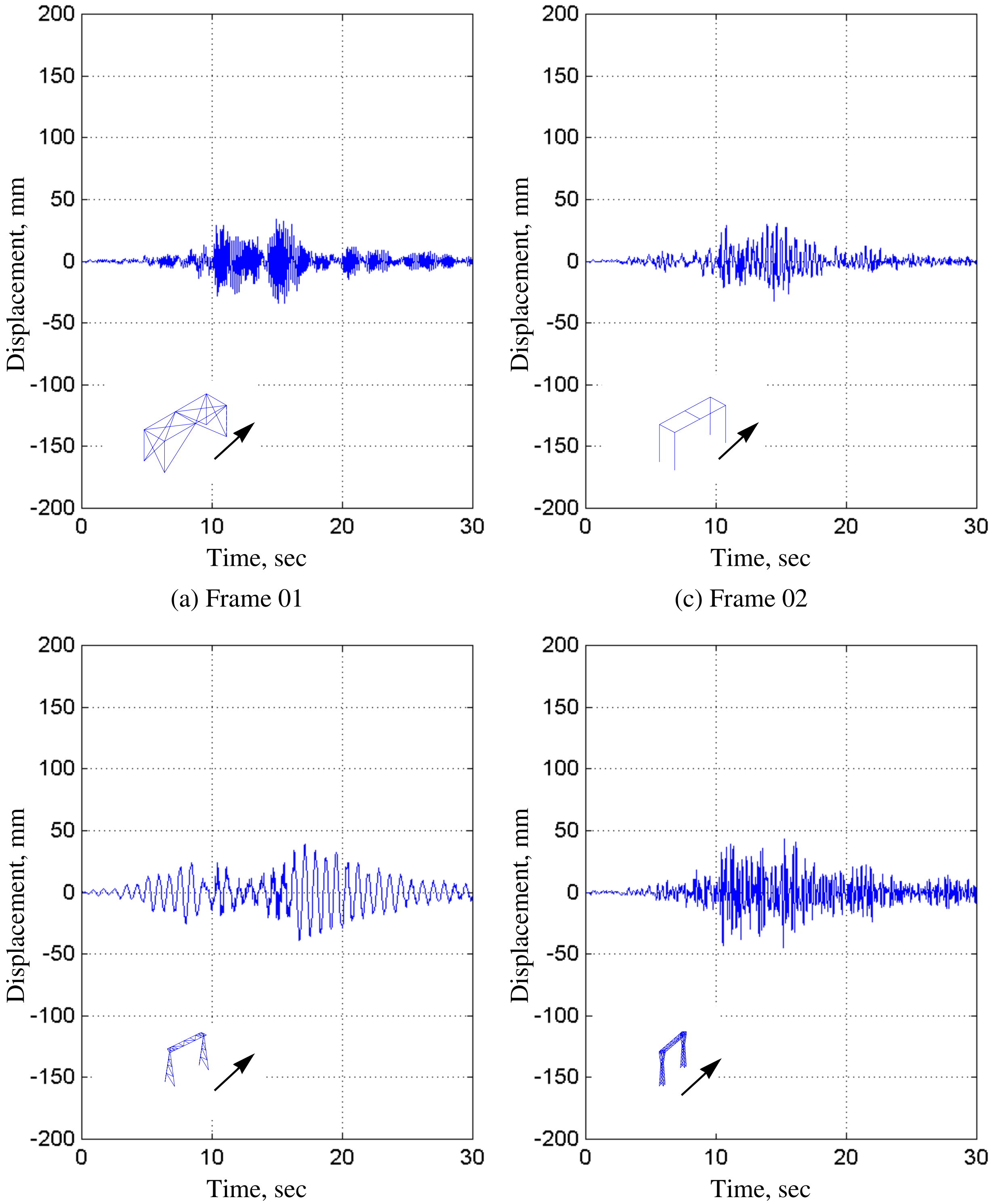

(a) Frame 01

(c) Frame 02

(b) Frame 03

(d) Frame 04

Figure 7-21 Deformation (u_3) of post tip relative to the frame, *x*-direction, switch SW2, closed blade, post P-C1, Tabas history, target PGA equal to 1.0g

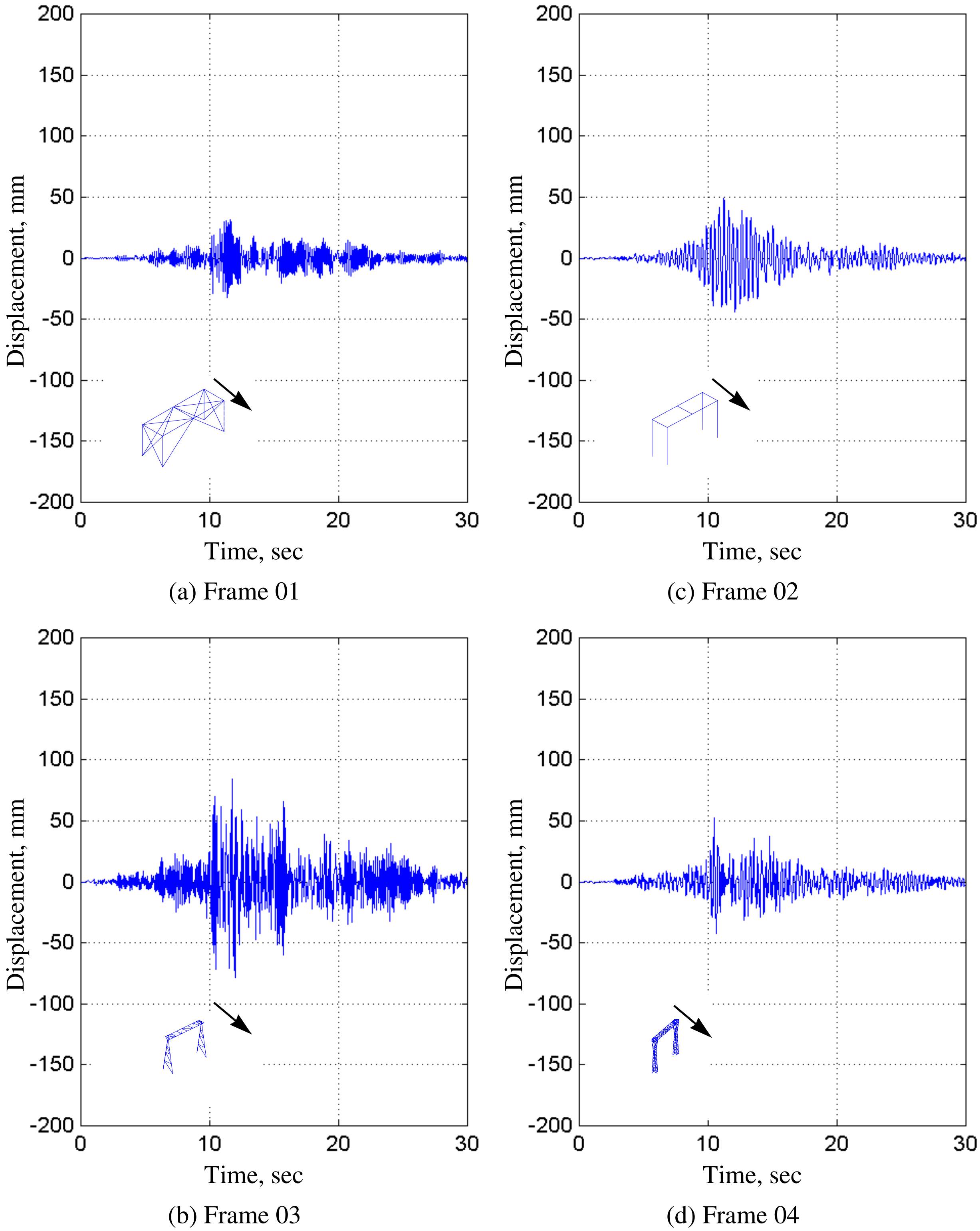

(a) Frame 01

(c) Frame 02

(b) Frame 03

(d) Frame 04

Figure 7-22 Deformation (u_3) of post tip relative to the frame, *y*-direction, switch SW2, closed blade, post P-C1, Tabas history, target PGA equal to 1.0g

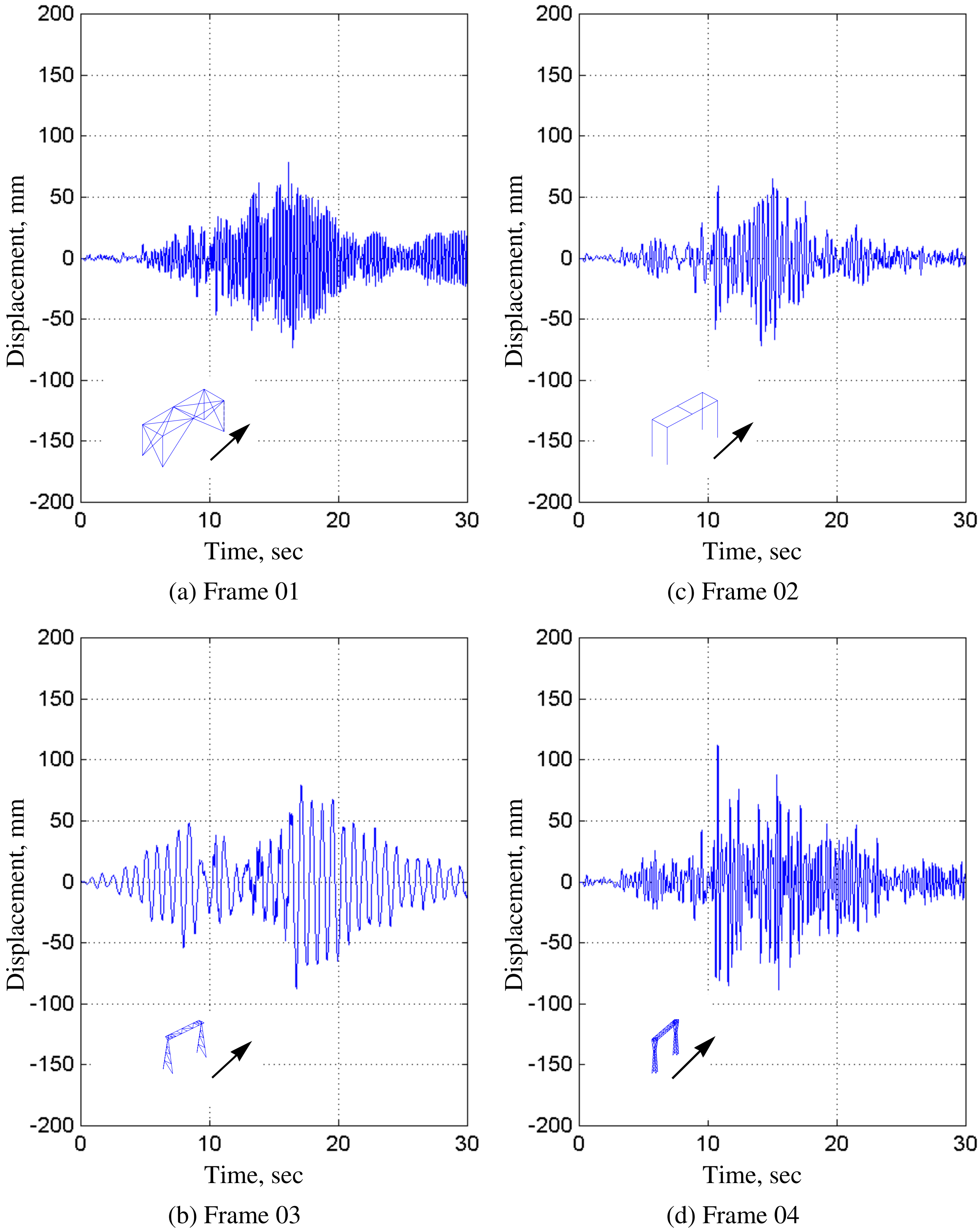

Figure 7-23 Deformation (u_3) of post tip relative to the frame, *x*-direction, switch SW2, closed blade, post P-C2, Tabas history, target PGA equal to 1.0g

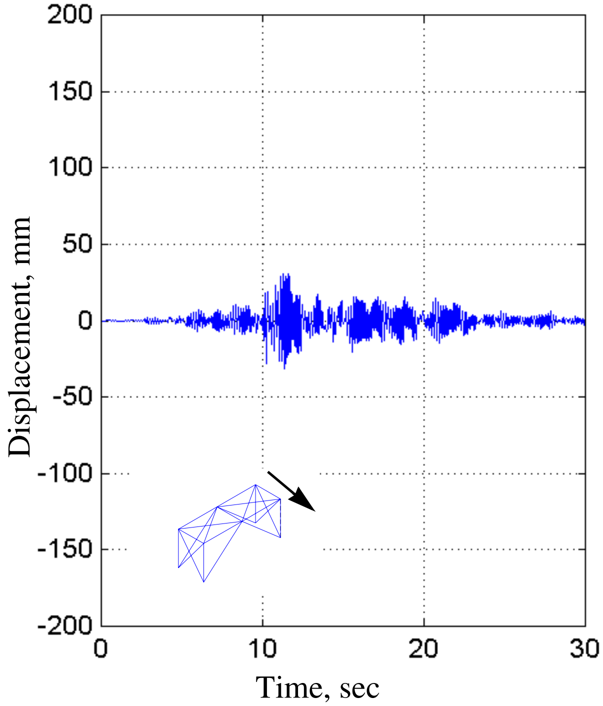

(a) Frame 01

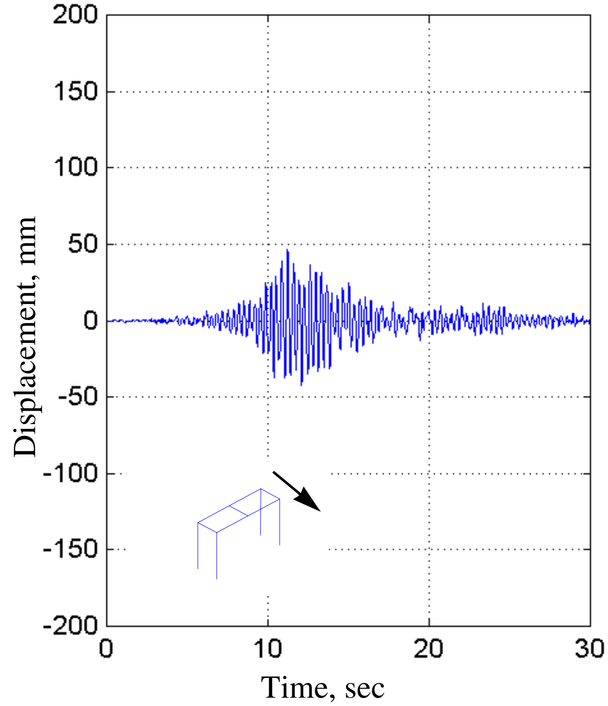

(c) Frame 02

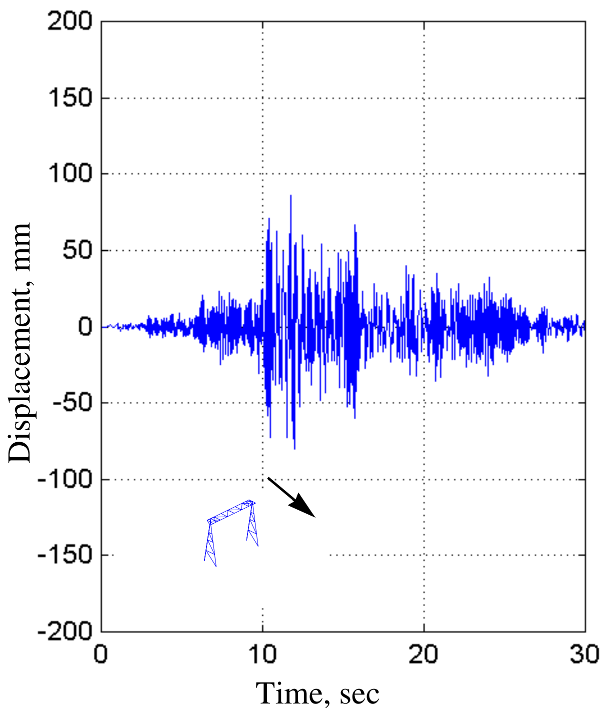

(b) Frame 03

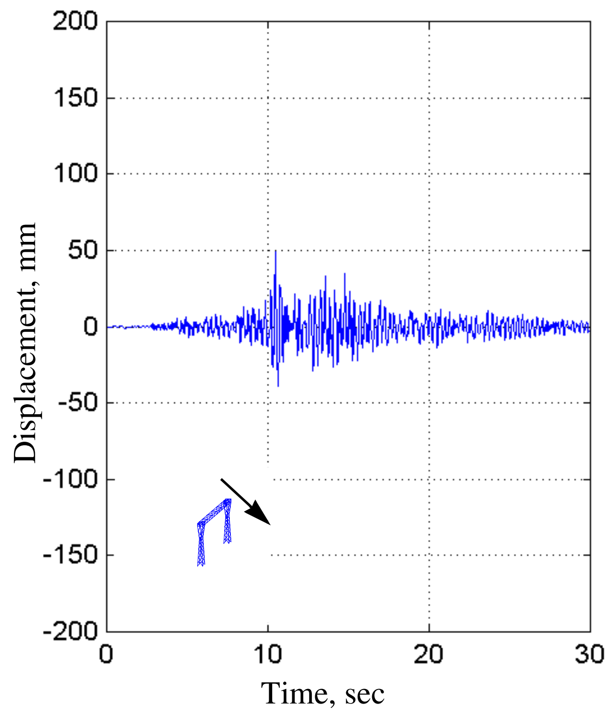

(d) Frame 04

Figure 7-24 Deformation (u_3) of post tip relative to the frame, *y*-direction, switch SW2, closed blade, post P-C2, Tabas history, target PGA equal to 1.0g

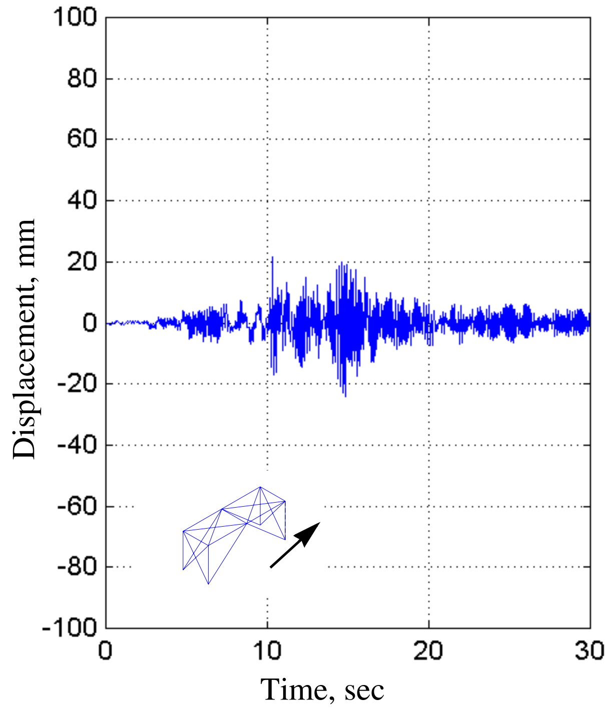

(a) Frame 01

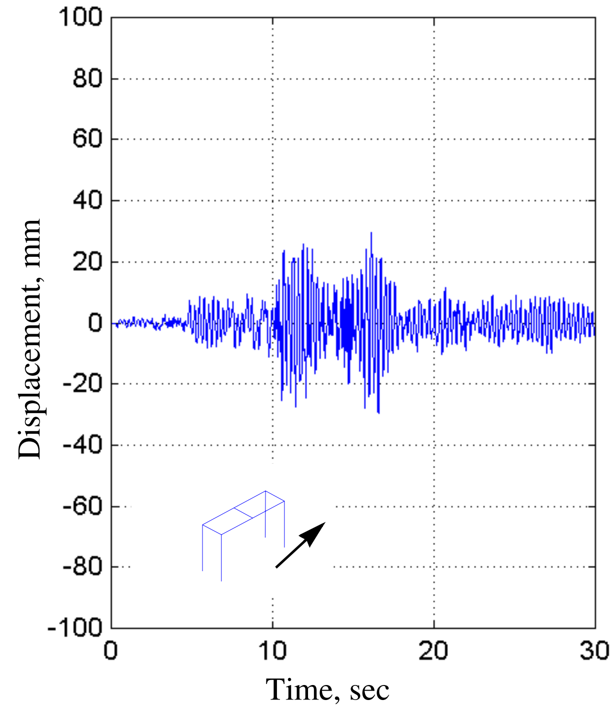

(c) Frame 02

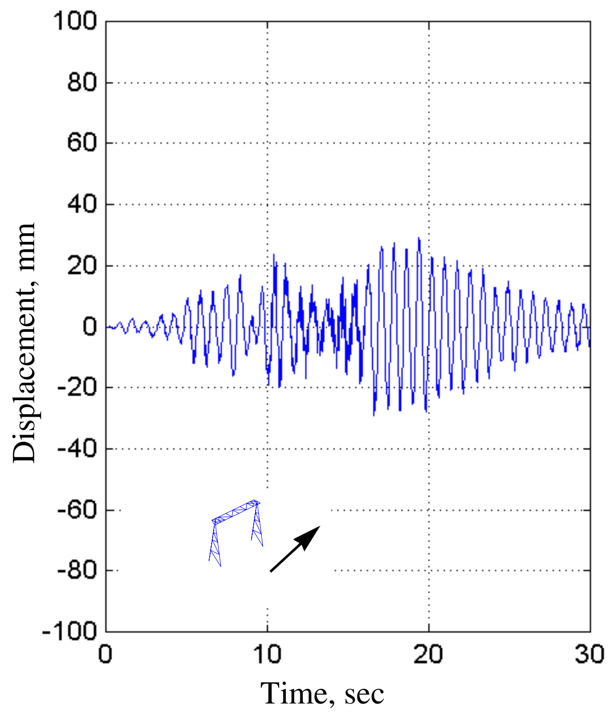

(b) Frame 03

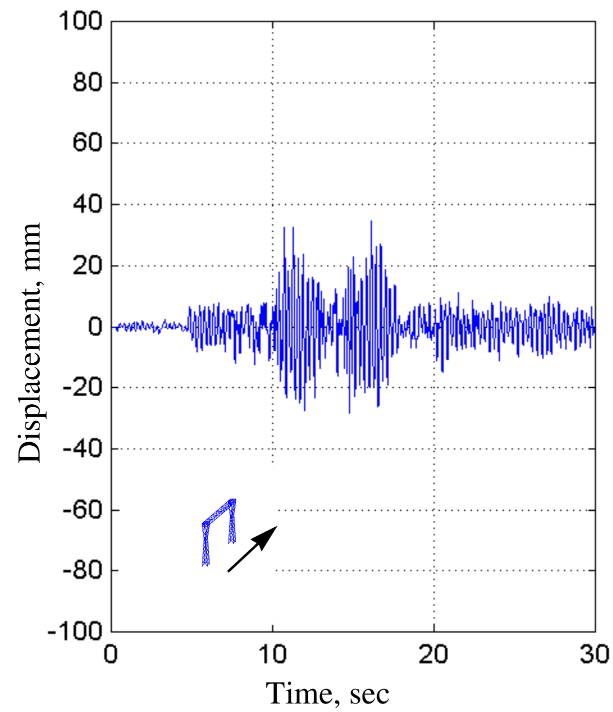

(d) Frame 04

Figure 7-25 Deformation (u_3) of post tip relative to the frame, *x*-direction, switch SW3, closed blade, post P-C1, Tabas history, target PGA equal to 1.0g

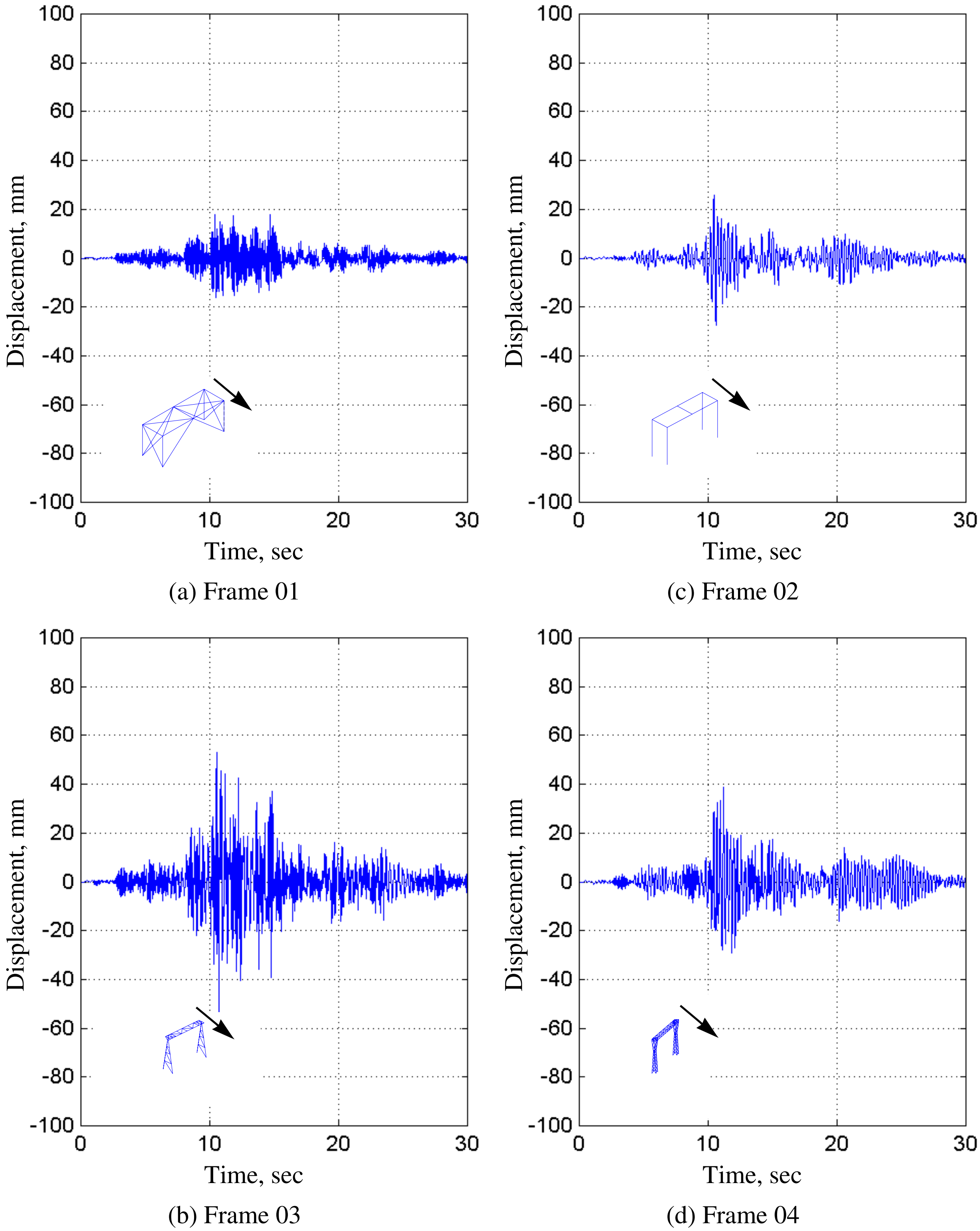

(a) Frame 01

(c) Frame 02

(b) Frame 03

(d) Frame 04

Figure 7-26 Deformation (u_3) of post tip relative to the frame, *y*-direction, switch SW3, closed blade, post P-C1, Tabas history, target PGA equal to 1.0g

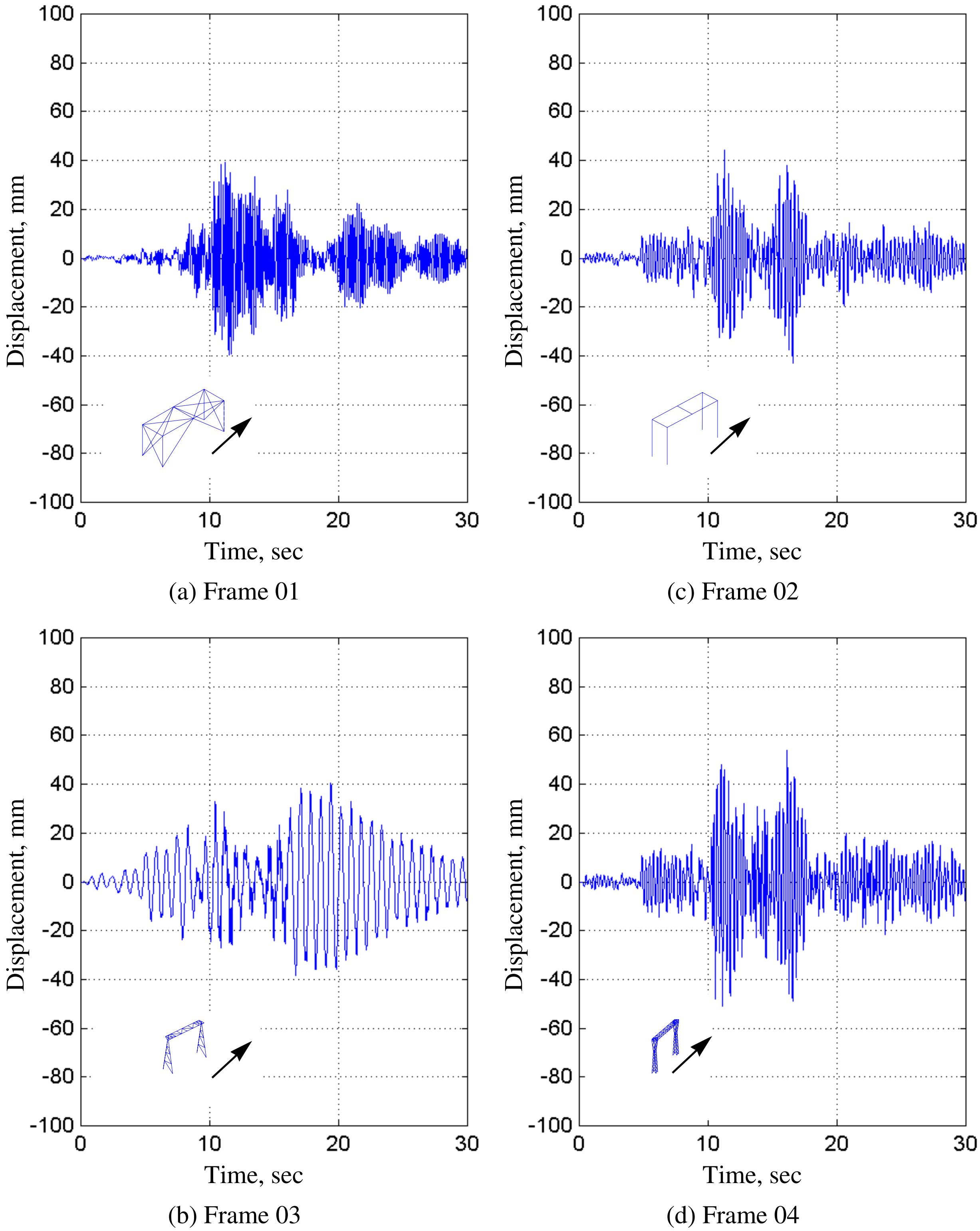

Figure 7-27 Deformation (u_3) of post tip relative to the frame, x-direction, switch SW3, closed blade, post P-C2, Tabas history, target PGA equal to 1.0g

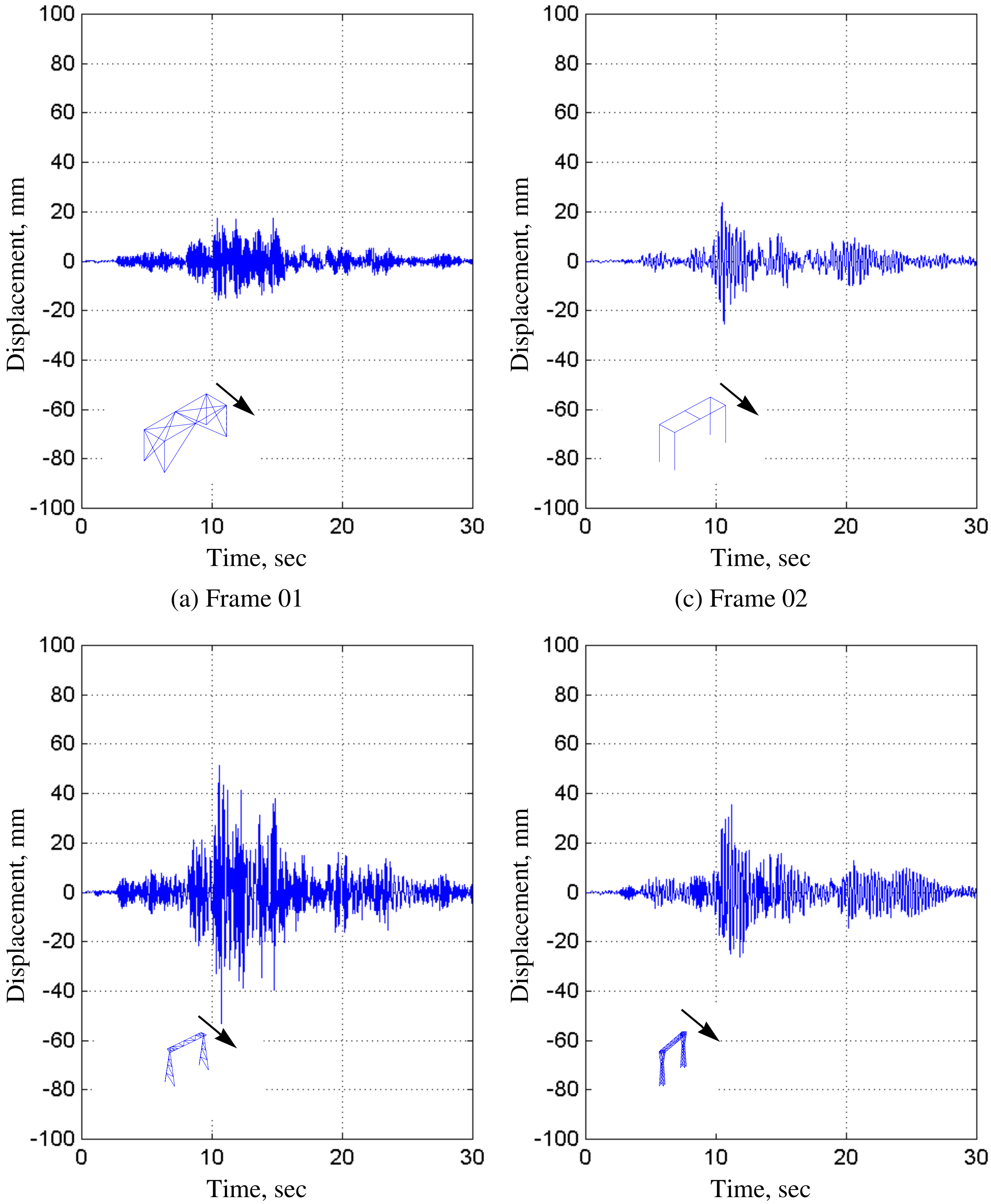

(a) Frame 01 (c) Frame 02

(b) Frame 03 (d) Frame 04

Figure 7-28 Deformation (u_3) of post tip relative to the frame, *y*-direction, switch SW3, closed blade, post P-C2, Tabas history, target PGA equal to 1.0g

8 Summary and Conclusions

8.1 Summary

8.1.1 Introduction

Disconnect switches are a key component of power transmission and distribution systems and are used to control the flow of electricity between high-voltage lines and transformer bushings and are used to isolate all types of substation equipment for maintenance. Switches consist of three poles of two or three posts each. Each post of the type tested consists of porcelain or composite insulators mounted on cast aluminum or steel base hardware attached to double-channel beams. The switch blade mounted at top of the posts provides the electrical connection between the switch terminals, which are attached to the top of insulator posts. A crank and inter-pole linkage operate the blade and synchronize the operation of the three poles. Switches are typically mounted on elevated structures or frames. The frames are classified by the utilities as either short (typical height of 12 ft or 4 m) or tall (typical height of 60 ft or 18 m). Mounting frames in service at the time of this writing are typically not braced and some frames rely on the channel at the base of the disconnect switches to provide stiffness in the short direction of the frame.

Porcelain disconnect switches have suffered structural and functional damage in past earthquakes but the literature contains virtually no information on the seismic performance of switches. This lack of information motivated the research project described in this report. The five objectives of the research project were: (1) develop earthquake ground motion records suitable for the seismic evaluation, qualification, and fragility testing of 230-kV disconnect switches; (2) conduct resonant-search and triaxial earthquake tests of single poles of disconnect switches mounted directly on the simulator platform to determine the dynamic properties of the poles and to evaluate the seismic response of the poles; (3) conduct resonant-search and triaxial earthquake tests of switches mounted on an elevated structure to determine the dynamic properties of the switches, to qualify the switches to the High Level if possible, and to determine modes of failure for the switches; (4) analyze the data acquired from the earthquake-simulator tests to develop simple mathematical models for switch poles; and (5) estimate the response of switches mounted on elevated support frames of different flexibility, using the switch models of item 4.

Five disconnect switches were evaluated by analysis and experimentation in this project. Switches SW1 and SW4 were ABB Type DR9 porcelain horizontal-break 230-kV switches. The insulator posts were approximately 90.5 in. (2.3 m) long and spaced 94 in. (2.4 m) apart; each pole was composed of two posts (designated as posts 1 and 2). Each post consisted of two porcelain insulator segments. The insulator posts were mounted on welded steel spacers that in turn were bolted to cast aluminum rotor bearing housings that were bolted to a C8x11.5 double-channel beam. Switches SW2, SW2a, and SW3 were ABB Type TTR-8 vertical-break 230-kV switches. The insulator posts were approximately 95.5 in. (2.4 m) long and each pole was composed of three posts (designated as posts 1, 2, and 3). A counterweight was attached at the tip of posts 2 and 3 to which the blade arm was attached. Each post of porcelain switches SW2 and SW2a consisted of two porcelain insulator segments. The posts for switch SW3 were single hollow core composite polymer insulators, 80 in. (2.0 m). The insulators for posts 1 and 3 were mounted on spacers. For switch SW2, cast aluminum spacers were used; for switch SW2a, welded steel spacers were used. Both aluminum and steel spacers were used for switch SW3. Post 2 of all switches was attached to a cast aluminum rotor bearing housing. All posts were bolted to C8x11.5 double-channel beams.

The earthquake histories used for the qualification and fragility testing of the 230-kV bushings were developed using the three-component set of near-field earthquake motions recorded during the 1978 Tabas earthquake. To obtain histories compatible with the IEEE 693-1997 spectrum with frequency contents representative of recorded ground motions only a segment of IEEE spectrum can be matched with individual histories. Two independent sets of three earthquake histories (Tabas-1 and Tabas-2) were generated to envelope collectively the entire IEEE spectrum. IEEE 693-1997 specifies that the disconnect switches must be qualified on frames similar to those used for field installation. Since it is impractical to qualify the switches on all possible mounting frames, a low-profile braced frame, termed the PEER frame, was used for testing. To indirectly account for the flexibility of taller and unbraced frames and the consequent amplification of the response of the switches, the ordinates of the target spectrum were doubled for qualification on a flexible frame. The process of qualification therefore involved the use of two sets of earthquake histories (Tabas-1 and Tabas-2) and two blade positions (open and closed).

8.1.2 Experimental studies

The experimental program for the disconnect switches consisted of tests of individual poles of SW1, SW2, and SW3 mounted directly on the simulator platform, followed by tests of complete switches SW1, SW2, SW2a, SW3, and a single pole of SW4 mounted on a stiff frame, termed the PEER frame.

Sine-sweep and white-noise tests were used to calculate the modal frequencies and damping ratios for the poles. The fundamental frequencies ranged between 3 Hz and 8 Hz for the switches with blades in the open and closed positions. Damping ratios ranged between 2 percent and 4 percent of critical.

Single poles from switches SW1, SW2, and SW3 were attached directly to the earthquake-simulator platform and tested using the Tabas-1 and Tabas-2 histories with amplitudes consistent with the IEEE 693-1997 spectrum for High Level qualification (target PGA equal to 1.0g). No structural damage was observed and electrical connectivity was maintained during these tests of the switch poles.

Switches SW1, SW2, SW2a, SW3, and a single pole of SW4 were installed on the PEER frame and subjected to increasing levels of earthquake shaking using the Tabas-1 and Tabas-2 set of earthquake histories. Switch SW1 was damaged during tests with target peak accelerations exceeding 1.5g. The damage included fracture of the post-blade connection and some of the cast aluminum rotor bearing housings. Switch SW2 was damaged during earthquake testing with a target peak acceleration of 1.0g. A cast aluminum spacer at the base of post B3 cracked during this test. The spacer was replaced and the switch was retested using earthquake histories with a target peak acceleration of 1.0g. The spacers beneath posts B3 and C3 fractured during these tests. All of the aluminum spacers were then replaced by welded steel spacers and the switch was retested (and designated as SW2a). Switch SW2a was subjected to increasing levels of shaking using the Tabas-1 and Tabas-2 histories and survived testing with target peak accelerations of 2.0g with no structural damage while maintaining electrical connectivity. Switch SW3 was subjected to 58 tests with increasing levels of earthquake shaking. Electrical connectivity was maintained during tests with target peak accelerations of 2.0g. Post-test inspection of the aluminum and steel spacers identified damage in the aluminum spacers only. Switch SW4 was damaged during a test with a target peak acceleration of 1.0g. The post-blade connection fractured during this test.

For all five switches, the maximum acceleration and deformation of the posts were recorded at pole B to which the crank and operational hardware were attached. Damage was most often observed to posts in pole B. Substantial reductions in accelerations and deformations in pole B, and thus damage for a given level of earthquake shaking in pole B, could be realized if the crank and operational hardware were effectively isolated from the poles. Such isolation would also substantially simplify mathematical models of switches and potentially permit part of the qualification process to be achieved by analysis as discussed in Section 7.5.

The earthquake testing served to identify the vulnerable components of horizontal- and vertical-break switches. For the horizontal-break switches, the welded blade-post connections and the cast aluminum rotor bearing housings were the most vulnerable components. Improved materials, quality control, and fabrication inspection could lead to enhanced performance of the horizontal-break switches. For the vertical-break switches, the cast aluminum spacers at the base of posts 2 and 3 were the most vulnerable components. Replacement of the cast aluminum spacers with welded steel spacers proved to be an effective strategy for improving the robustness of the switches. The double-channel beams and attachment angles at the base of the posts in the horizontal- and vertical-break switches were a significant source of flexibility in the switches. At high levels of earthquake shaking, substantial deformation in the flanges of the beams and severe damage to the bolts in the connections were observed. Changes to these structural components and connection details could lead to substantial improvements in the response of disconnect switches.

8.1.3 Analytical studies

Analytical studies were undertaken to build on the results obtained from the experimental studies and to garner an understanding of the likely performance of switches mounted on frames of different flexibility than that used for the experimental program.

Single-degree-of-freedom (SDOF) models of posts of switch poles were prepared using data from the tests of poles mounted directly on the earthquake simulator. Models were prepared for switches SW1, SW2, and SW3. Each switch pole was modeled using two SDOF oscillators and each switch was modeled using six oscillators. For the vertical break switch SW1, posts 1 and 2 were modeled separately. For switches SW2 and SW3, post 1 was modeled as one SDOF oscillator and posts 2 and 3 were combined in another SDOF oscillator. The accuracy of the SDOF representations of the switch posts was checked using data from tests of the three switches mounted on the PEER frame. The SDOF models reproduced the maximum switch deformations reasonably well but underestimated the peak accelerations. However, because damage is more a function of deformation rather than acceleration, the SDOF models were deemed acceptable for the characterization of the response of frame-mounted switches.

Four frames were selected for analysis and evaluation. These frames were selected to be representative of both in-service frames and frames proposed for future construction. Construction details were provided by PG&E. Frame 01 is a low-profile braced frame and designated by PG&E for new construction. Frame 02 is a low-profile unbraced frame that is in-service at this time; the double-channel beams at the base of switch poles serve as the transverse members for this frame. Frame 03 is a new high-profile braced steel frame that is proposed for future construction. Frame 04 is a high-profile, in-service frame. Mathematical models of each of the frames were prepared for eigenvalue and response-history analysis. Frame 01 was by far the stiffest of all the frames. Frames 02 through 04 have frequencies between 1 and 10 Hz which is a range that brackets the fundamental frequencies of all five switches. To facilitate the evaluation of the effects of frame flexibility on the response of disconnect switches and to provide a linkage between the analytical and experimental studies, the switches were analyzed assuming that they were supported on an infinitely rigid frame: Frame 00. Because the PEER frame was very stiff and did not substantially amplify the earthquake shaking to the base of the switches, observations from tests using the PEER frame were assumed to be representative of tests conducted on switches mounted directly on the simulator. (Note that poles of individual switches and not complete switches with cracks and operational hardware were tested on the simulator.) SDOF models of the switches were incorporated into the mathematical models of the frames. The resulting models were analyzed using one set of earthquake histories that were compatible with IEEE 693-1997 spectrum for High Level qualification. The set of histories was developed using the near-field motions recorded during the 1978 Tabas, Iran, earthquake.

Analysis results were normalized by the responses of the switch posts when mounted on the rigid Frame 00. Frame 01 did not significantly amplify earthquake shaking from the base of the frame to the base of switches mounted on the frame. The two in-service frames, the short unbraced Frame 02 and the tall braced Frame 04, substantially amplified the response of disconnect switches with frequencies similar to those of switches SW1, SW2, and SW3. Amplification factors of 2 and 3 were reported for Frames 02 and 04, respectively. The tall braced Frame 03 that PG&E may use in future construction substantially amplified the response of the disconnect switches SW1, SW2, and SW3. Amplification factors in excess of 3 were calculated. Stresses in Frames 01 through 04 were not checked because such checking was not the intent of this study.

8.2 Conclusions

8.2.1 Seismic response of 230-kV disconnect switches

Five 230-kV disconnect switches were mounted and tested on the stiff PEER frame. The two horizontal-break switches (SW1 and SW4) were damaged during tests with earthquake histories whose spectral ordinates fell below the IEEE 693-1997 spectrum for High Level qualification (peak acceleration equal to 1.0g). The vertical-break switches that were mounted on welded steel spacers (SW2a and SW3) survived tests with earthquake histories whose spectral ordinates equaled or exceeded the IEEE 693-1997 spectrum for High Level qualification (peak acceleration equal to 1.0g). Because the PEER frame is of similar stiffness to the low-profile braced Frame 01 that is proposed for new construction, SW2a and SW3 should be considered to be qualified to the High Level for use on Frame 01.

The earthquake simulator could not generate shaking whose spectral ordinates equaled or exceeded two times the IEEE 693-1997 spectrum for High Level qualification. As such, neither SW2a nor SW3 were qualified to the High Level for use on flexible frames.

The most vulnerable components in all five switches were the cast aluminum rotor bearings and spacers and the welded blade-to-post connections. Changes in construction practice and the use of different materials could substantially improve the robustness of disconnect switches.

8.2.2 Switch operation mechanism

The switch operation hardware and its attachments to pole B result in higher accelerations and larger displacements in the posts of pole B. Most of the damage observed during the earthquake tests was in the posts of pole B. Isolation of this hardware and its attachments could both substantially improved the seismic performance of switches and enable the switch manufacturers to develop robust mathematical models of switch posts that could be used to qualify switches by analysis.

8.2.3 Flexibility of base hardware

The double-channel beams at the base of the posts in each pole are a significant source of flexibility in the pole and must be included in the characterization and qualification of posts, poles, and switches. Greater attention to these structural components and improved connection details could lead to substantial improvements in the seismic performance of disconnect switches.

8.2.4 Elevated support frames

Frame 01 is a stiff braced frame that does not significantly amplify earthquake shaking from the base of the frame to the base of switches mounted on the frame. Switches of similar sizes and weights to SW1, SW2, and SW3 that have been qualified on a stiff or rigid frame should be considered to be qualified for installation on the PG&E frame. The two in-service frames, the short unbraced Frame 02 and the tall braced Frame 04, substantially amplified the response of disconnect switches with frequencies similar to those of switches SW1, SW2, and SW3. Switches of similar sizes and weights to SW1, SW2, and SW3 that have been qualified on a stiff or rigid frame may not qualify if installed and tested on either Frames 02 and 04.

The tall braced Frame 03 that PG&E may use for future construction substantially amplified the response of the disconnect switches SW1, SW2, and SW3. Amplification factors in excess of 3 were calculated. Qualification of switches for use on this frame may not be physically possible using earthquake simulator testing. PG&E should consider redesigning Frame 03 to substantially increase its stiffness and modal frequencies using braced steel columns and beams of tubular geometry supplemented with post-tensioned cables to provide stiffness in the longitudinal direction.

8.2.5 Procedures for seismic qualification

IEEE 693-1997 writes that disconnect switches must be qualified on frames representative of those in service. This requirement is unrealistic given the wide variety of frames either in service or proposed for future construction. Given the physical limitations of earthquake simulators in the United States at this time, an alternate procedure for the seismic qualification and installation of switches is proposed that combines analysis and experimentation. This procedure is preliminary and mutable. First, switches (including the base beams and switch-operation hardware) mounted directly on the earthquake simulator would be tested using a level of shaking that is twice that required for the desired level of qualification (i.e., 2 times PL or 2 times 1.0g) for qualification at the High Level). Second, mathematical models of the switch posts would be constructed in a manner similar to that described in Chapter 6 using resonant-search and static test data from the simulator tests. Such work would be undertaken by the equipment manufacturers. Third, the utilities would analyze and design frames using the SDOF models of the switch posts provided by the manufacturers with the objective of limiting the amplification of the response of the switches to 2.0 or less compared with the fixed base condition. The factor of 2.0 is somewhat arbitrary but was chosen here because 2.0 is the value used in IEEE 693-1997 to characterize the amplification of motion in components supported on transformer tanks.

References

AAI 2000. *Aluminum Design Manual*: *Allowable stress design specifications.* Washington D.C.: The Aluminum Association, Inc.

Abrahamson, N., 1996. *Nonstationary response-spectrum matching.* Unpublished paper.

AISC 1995. *Manual of steel construction: Allowable stress design.* Chicago, Il.: American Institute of Steel Construction, Inc.

Clough R. W. and Penzien J. 1993. *Dynamics of structures.* New York: McGraw-Hill, Inc.

Chopra, A. 1995. *Dynamics of structures: theory and application to earthquake engineering.* Englewood Cliffs, N.J.: Prentice Hall, Inc.

Computers and Structures, Inc., 1996. *SAP2000, Integrated finite element analysis and design of structures.* Version 6.1 Berkeley, Calif.

Der Kiureghian, A., Keshishian, P., and Hakobian, A. 1997. *Multiple support response spectrum analysis of bridges including the site-response effect & the MSRS code.* EERC 97/02 Berkeley, Calif.: Earthquake Engineering Research Center, University of California.

Gilani, A. S., Chavez, J. W., Fenves, G. L., and Whittaker, A. S. 1998. *Seismic evaluation of 196 kV porcelain transformer bushings.* PEER 98/02 Berkeley, Calif.: Pacific Earthquake Engineering Research Center, University of California.

IEEE, 1998. *IEEE Standard 693-1997, Recommended practices for seismic design of substations*. Piscataway, N.J.: IEEE Standards Department.

Mathworks. 1999. *The language of technical computing*. Natick, Mass.: The Mathworks, Inc.

Thornberry, L. R. and Hardy, R. 1997. *Seismic simulation test program on type CGCB-G 230kV disconnect switch.* Report No. 45998-1 Huntsville, Ala.: Wyle Laboratories.

UBC 1997. *1997 Uniform Building Code*, *Volume 2: Structural engineering design provisions* Whittier, Calif.: International Conference of Building Officials.

Appendix A IEEE 693-1997 Standard for Seismic Testing of Disconnect Switches

A.1 Introduction

The document IEEE 693-1997 (IEEE 1998) entitled *Recommended Practices for Seismic Design of Substations* is used in the United States for the seismic qualification and fragility testing of high-voltage electrical substation equipment such as disconnect switches. This document provides qualification requirements for substation equipment and supports manufactured from steel, aluminum, porcelain, and composite materials. Procedures for equipment qualification using analytical studies (static analysis, static coefficient analysis, and response-spectrum analysis) and experimental methods (response-history testing, sine-beat testing, and static pull-testing) are described. The objective of the document is "... to secure equipment such that it performs acceptably under reasonably anticipated strong ground motion."

IEEE 693-1997 identifies eleven methods for experimental testing. The most rigorous method is earthquake simulation using earthquake ground motion records, the spectral ordinates of which equal or exceed (envelop) those of a Required Response Spectrum (RRS). Categories of earthquake-simulator testing include uniaxial (one horizontal), biaxial (horizontal and vertical), multiaxial (two horizontal, no vertical) , and triaxial (two horizontal and vertical) testing.

Section 9 of IEEE 693-1997 titled "Seismic performance criteria for electrical substation equipment" describes seismic performance criteria for electrical substation equipment. Information on three seismic qualification levels (Low, Moderate, and High), Performance Levels (PL), the Required Response Spectrum (RRS), the relation between PL and RRS, and acceptance criteria are provided.

The studies described in the body of this report employed triaxial earthquake simulator testing for the qualification and fragility testing of 230-kV disconnect switches as described in Annex A (Standard clauses) and Annex E (Disconnect and ground switches) of IEEE 693-1997. IEEE 693-1997 writes text on seven key topics related to the seismic qualification of disconnect switches:

1. Performance level and performance factor
2. Performance level qualification

3. Support frame
4. Qualification procedure
5. Testing procedures
6. Instrumentation
7. Acceptance criteria

Each of these topics is elaborated upon in the following sections.

A.2 Performance Level and Performance Factor

A Performance Level (PL) for substation equipment is represented in IEEE 693-1997 by a response spectrum. The shape of this spectrum represents a broadband response that envelopes earthquake effects in different areas considering site conditions that range from soft soil to rock. Three values of equivalent viscous damping are specified: 2 percent, 5 percent, and 10 percent. The PL shape brackets the vast majority of substations site conditions, and in particular provides longer period coverage for soft soil. However, very soft sites and hill sites may not be adequately covered by the spectral shapes.

Three seismic performance levels are identified in IEEE 693-1997: High, Moderate, and Low. In California, the relevant performance levels are High and Moderate. Equipment that is shown to perform acceptably in ground shaking consistent with the High Seismic Performance Level (see Figure A-1) is said to be seismically qualified to the High Level. Equipment that is shown to perform acceptably in ground shaking consistent with the Moderate Seismic Performance Level (see Figure A-2) is said to be seismically qualified to the Moderate Level.

IEEE 693-1997 states that it is often impractical or not cost effective to test to the High or Moderate PL because (a) laboratory testing equipment might be unable to attain the necessary high accelerations, and/or (b) damage to ductile components at the PL, although acceptable in terms of component qualification, would result in the component being discarded following testing. For these reasons, equipment may be tested using accelerations that are 50 percent of the PL. The reduced level of shaking is called the Required Response Spectrum (RRS). The ratio of PL to RRS, termed the performance factor in IEEE 693-1997, is equal to 2. The High and Moderate RRSs are shown in Figures A-3 and A-4, respectively. The shapes of the RRS and the PL are identical, but the ordinates of the RRS are one-half of the PL.

Equipment tested or analyzed using the RRS is expected to have acceptable performance at the PL. This assumption is checked by measuring the stresses obtained from testing at the RRS, and by (a) comparing the stresses to 50 percent (equal to the inverse of the performance factor) of the ultimate strength of the brittle (e.g., porcelain, cast aluminum, and other) components, (b) using a lower factor of safety against yield combined with an allowance for ductility of steel and other ductile materials, and (c) checking the composite components for damage.

A.3 Performance Level Qualification

Procedures for selecting the appropriate seismic qualification level for a site are presented in IEEE 693-1997. Qualification levels are directly related to site-specific peak acceleration values calculated using a 2-percent probability of exceedance in 50 years. If the peak ground acceleration is less than 0.1g, the site is classified as Low. If the peak ground acceleration exceeds 0.5g, the site is classified as High. If the peak ground acceleration ranges in value between 0.1g and 0.5g, the site is classified as Moderate. Sites in California are classified as either Moderate or High.

A.4 Support Frame for Disconnect Switches

IEEE 693-1997 writes that disconnect switches 169-kV and larger must be qualified using earthquake-simulator testing. The specifications state that the equipment shall be tested in its equivalent in-service configuration, including pedestal or other support structure. For the disconnect switches tested on mounting frames similar to in-service configuration, the amplification of earthquake motion due to the influence of the flexibility in the support is included in the test setup, and as such the acceleration ordinates of the Test Response Spectrum (TRS) are equal to the ordinates of the Required Response Spectrum (RRS).

A.5 Qualification Procedures for Disconnect Switches

IEEE 693-1997 writes that the switch, structure, and operating mechanism be installed on the earthquake simulator and mechanically adjusted. Correct operation (full opening and full closing) must be verified prior to testing, and tests must be performed with the switch both open and closed.

A.6 Testing Procedures for Disconnect Switches

A.6.1 Introduction

One type of static and three types of earthquake-simulator testing are identified in IEEE 693-1997 for the seismic qualification of switches and components: (1) composite polymer load tests, (2) frequency resonant-search tests, (3) sine-beat test, and (4) earthquake ground motions tests. Static testing involves applying a horizontal static load of 50% of the specified mechanical load or SML at the top of the composite insulator and measuring the resulting deflection. Such a test precedes shake-table tests. Resonant-search tests and earthquake ground motion tests (termed *time-history shake table tests* in IEEE 693-1997) are mandatory. Additional information on these two types of tests follow.

A.6.2 Resonant-search tests

Sine-sweep or broadband white noise tests are used to establish the dynamic characteristics (natural frequencies and damping ratios) of disconnect switches. These so-called *resonant-search* tests are undertaken using unidirectional excitation along each principal axis of the earthquake simulator platform. IEEE 693-1997 specifies that the input level for the resonant-search tests shall be between 0.05g and 0.1g.

If sine-sweep tests are used, IEEE 693-1997 specifies that the resonant search be conducted at a rate not exceeding one octave per minute in the range for which the equipment has resonant frequencies. Resonant-search tests below 1 Hz or above 33 Hz are not required. Modal damping is calculated using the half-power bandwidth method.

A.6.3 Earthquake ground motion tests

Triaxial earthquake simulator testing is mandated for the seismic qualification of switches rated at or above 169 kV. The Test Response Spectrum (TRS) for each horizontal earthquake motion must match or exceed the target spectrum. The TRS for the vertical earthquake motion shall be no less than 80 percent of target spectrum. Earthquake motions can be established using either synthetic or recorded histories. IEEE 693-1997 recommends that 2-percent damping be used for spectral matching and requires at least 20 sec of strong motion shaking be present in each earthquake record.

A.7 Instrumentation of Disconnect Switches

IEEE 693-1997 states that disconnect switches must be instrumented to record the following response quantities:

1. maximum vertical and horizontal accelerations at the top of the insulator, the end of the blade, and at the top of the earthquake-simulator platform
2. maximum displacement of the top of the insulator and at the end of the blade
3. maximum stresses at the base of porcelain insulator, at the base of the switch arm hinge, and at base of two opposite diagonal legs of the supporting frame
4. electrical continuity across the main disconnect switch when the switch is closed

A.8 Acceptance Criteria for Disconnect Switches

IEEE 693-1997 writes that a disconnect switch is considered to have passed the qualification tests if all the criteria tabulated below related to general performance, allowable stresses, and operation are met. The data obtained from testing using ground motions compatible with the Test Response Spectrum are used to assess general performance and allowable stresses.

A.8.1 General requirements :

The general requirements for porcelain slip, operation, and deflection follow:

1. *Porcelain slip*. No observable offset of porcelain on its base.
2. *Operational state*. The disconnect switch shall be operational during testing. When tested in the closed position, the switch shall stay closed throughout the test. When tested in the open position, it shall stay open throughout the test.
3. *Deflections.* For the shake-table tests, the measured deflections shall be within the design limits of the disconnect switch.

A.8.2 Component response:

The requirements for maximum response in components are:

1. *Brittle components*. The total stress in porcelain and the seismic stresses in cast aluminum or other brittle components must be less than 50 percent of the ultimate value.
2. *Ductile components*. For steel and ductile aluminum, the total stresses must be less than 50 percent of the allowable stresses specified in the latest editions of the AISC: *Manual of Steel Construction* (AISC 1995) and the AAI: *Aluminum Design Manual* (AAI 2000), respectively.
3. *Composite components.* (a) Composite components are not damaged during earthquake tests; (b) the insulator shall return to its pre-deflection position within 5-percent of its measured deflection for static tests.

A.8.3 Functional requirements:

Disconnect switches tested on an earthquake simulator shall pass the following tests to ensure its functionality:

1. *Millivolt drop test*. Circuit resistance before and after the shake table test.
2. *Continuity test*. Electrical continuity across the main disconnect switch when the switch is closed.
3. *Mechanical operating test.* Correct operation, full opening, and full closing shall be verified.

A.8.4 Special requirements for composite switches

In addition to meeting the qualification requirements stated above, a shed seal test is performed on composite polymer insulators. This is a test of the ability of the sheath-shed to prevent the entrance of water. After completion of shake-table testing, the equipment is immersed in either ambient-temperature water for 7 days or in boiling water for 42 hours. The specified functional test shall be performed and compared to the tests done prior to shake table tests. The sealing method will be considered acceptable if the post functional tests are within acceptable limits specified for these functions and have not changed appreciably, and if there is no indication of water migration past the outside surface of the sheds.

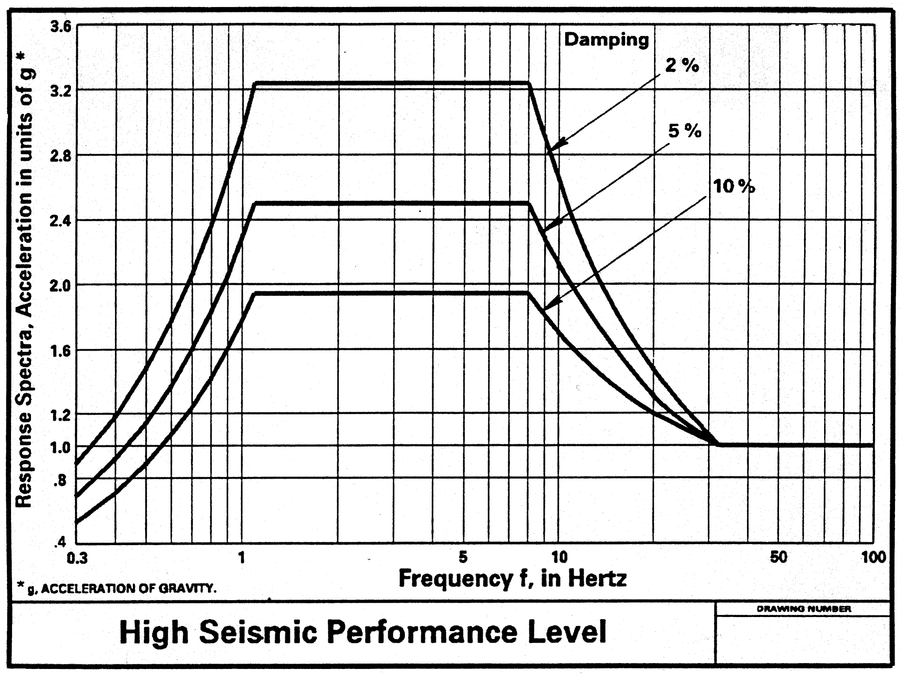

Figure A-1 Spectra for High Seismic Performance Level (IEEE 1998)

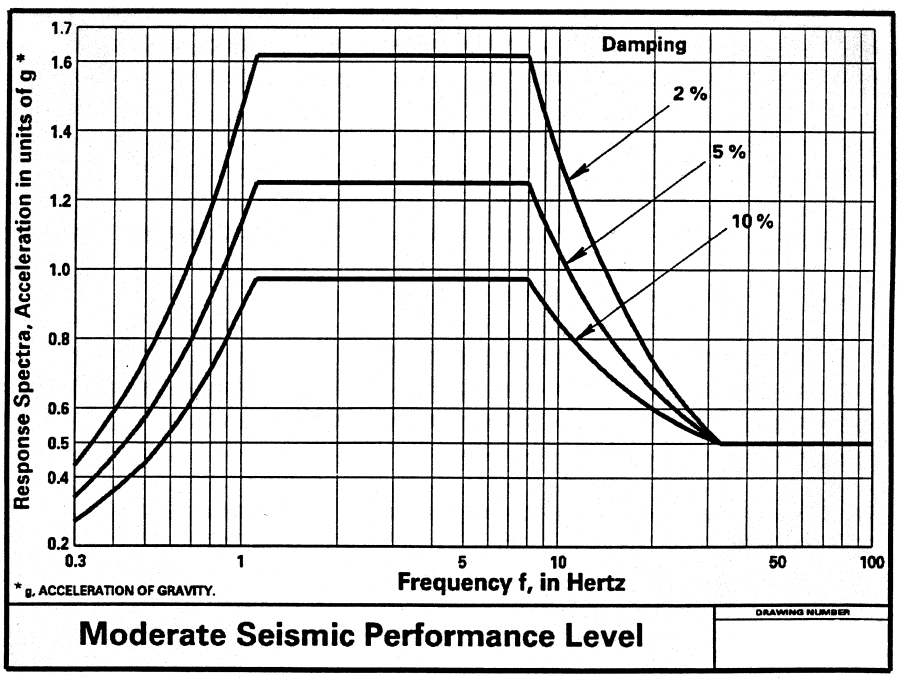

Figure A-2 Spectra for Moderate Seismic Performance Level (IEEE 1998)

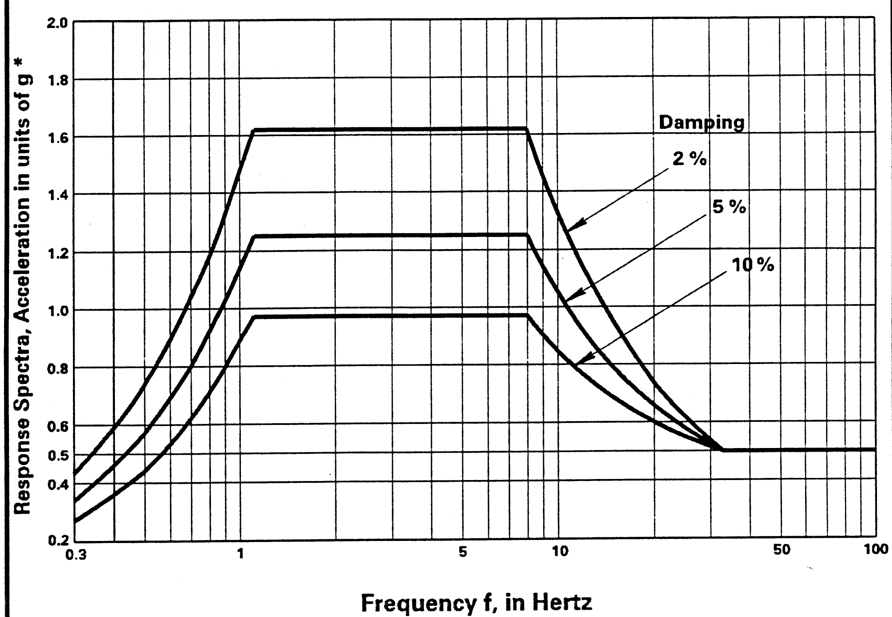

THE ABOVE REQUIRED RESPONSE SPECTRA ARE DERIVED FROM THE FOLLOWING:

f is in Hertz

$\beta = [3.21 - 0.68 \ln(D)] / 2.1156$

D = Percent of Critical Damping Expressed as 1, 2, 5, 10, etc

0 - 1.1Hz = $1.144 \beta f$

1.1 - 8Hz = 1.25β

8 - 33Hz = $(13.2 \beta - 5.28) \frac{1}{f} - 0.4 \beta + 0.66$

33Hz and over = 0.5g

0.5g

*g, ACCELERATION OF GRAVITY.

DRAWING NUMBER

High Required Response Spectrum

Figure A-3 Spectra for High Level Required Response Spectrum (IEEE 1998)

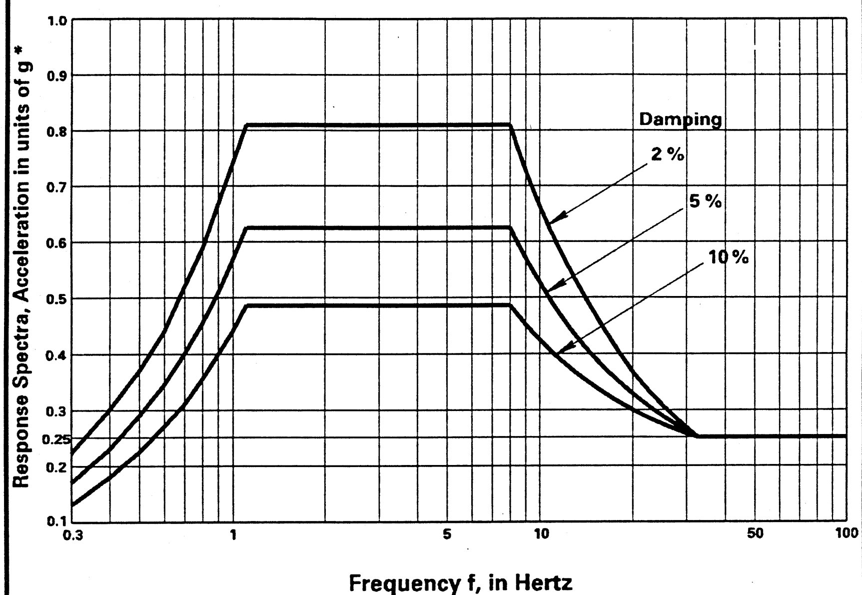

THE ABOVE REQUIRED RESPONSE SPECTRA ARE DERIVED FROM THE FOLLOWING:

f is in Hertz

$\beta = [3.21 - 0.68 \ln(D)] / 2.1156$

D = Percent of Critical Damping Expressed as 1, 2, 5, 10, etc

0 - 1.1Hz = $0.572\beta f$

1.1 - 8Hz = 0.625β

8 - 33Hz = $(6.6\beta - 2.64)\frac{1}{f} - 0.2\beta + 0.33$

33Hz and over = 0.25g

0.25g

* g, ACCELERATION OF GRAVITY.

Moderate Required Response Spectrum

DRAWING NUMBER

Figure A-4 Spectra for Moderate Level Required Response Spectrum (IEEE 1998)

Appendix B SDOF Models of Switch Posts

B.1 Introduction

In the studies described in Chapters 6 and 7, single-degree-of-freedom (SDOF) models of switch posts were used for analysis and evaluation. In this appendix, the procedure used to develop these models is presented. Section B.2 provides the theoretical background used to develop the SDOF oscillators. The step-by-step procedure used to prepare one SDOF oscillator is presented in Section B.3. The computed properties for all the oscillators are listed in Section B.3.

B.2 Introduction

The governing equation of motion for a linear elastic system with distributed mass, stiffness, and loading can be written as:

$$m(s)\ddot{u}(s,t) + c(s)\dot{u}(s,t) + k(s)u(s,t) = -m(s)r(s)\ddot{u}_g(t) \tag{B-1}$$

where, u, $\dot{u}$, and $\ddot{u}$ are the displacement, velocity, and acceleration of the system relative to the ground, respectively, $\ddot{u}_g$ is the ground acceleration; m, c, and k are the mass, damping, and stiffness functions of the system, respectively, and r is the influence function. In this equation, time is denoted by t, and s designates the spatial coordinate (x, y, or z).

The linear system can be approximated by a generalized SDOF oscillator (Chopra 1995). If the displaced shape of the system can be described by a shape function $\psi(x)$, the equation of motion for the generalized SDOF oscillator can be written as:

$$\ddot{y}(t) + 2\omega\xi\dot{y}(t) + \omega^2 y(t) = \ddot{u}_g(t) \tag{B-2}$$

where y is the displacement of the generalized SDOF oscillator, and ω and ξ are the frequency and damping ratio of the SDOF oscillator, respectively. The displacements of the system with the distributed parameters are related to the displacements of the SDOF oscillator by:

$$u(s,t) = \Gamma\psi(s)y(t) \tag{B-3}$$

where, Γ is equal to the generalized excitation (L) divided by the generalized mass (M) of the SDOF oscillator, where

$$M = \int m(s)\psi^2(s)ds \tag{B-4}$$

$$L = \int m(s)\psi(s)r(s)ds \tag{B-5}$$

The distribution of elastic forces (f_s) acting on the distributed parameter system can be computed as:

$$f_s(s, t) = k(s)u(x, t) = k(s)\Gamma\psi(s)y(t) \tag{B-6}$$

where, k is the stiffness function of the distributed parameter system. If the distributed parameter system is subjected to a ground acceleration history that has a spectral acceleration of S_a for a frequency of f and a damping ratio of ξ, maximum elastic force can be computed from:

$$f_{s_0}(s) = \Gamma m(s)\psi(s)S_a(f, \xi) \tag{B-7}$$

The maximum base shear (V_b) and overturning moment (M_o) for the distributed parameter system can be approximated by:

$$V_b = S_a(f, \xi)\Gamma\int m(s)\psi(s)ds \tag{B-8}$$

and

$$M_o = S_a(f, \xi)\Gamma\int m(s)\psi(s)h(s)ds \tag{B-9}$$

where, $h(s)$ represents the height (along the z-axis) above the base. The maximum base shear and overturning moment for the SDOF oscillator with mass $\overline{m}$ and height $\bar{h}$ are:

$$V_b = \overline{m}S_a(f, \xi) \tag{B-10}$$

and

$$M_o = \overline{m}\bar{h}S_a(f, \xi) \tag{B-11}$$

The SDOF oscillator and the distributed parameter system will have the same maximum base shear and overturning moment if the mass and height of the SDOF oscillator are selected as:

$$\bar{m} = \Gamma \int m(s)\psi(s)ds \tag{B-12}$$

$$\bar{h} = \frac{\Gamma}{\bar{m}} \int h(s)m(s)\psi(s)ds \tag{B-13}$$

The maximum displacement at the top of the system ($s = L$) is

$$u_{max}(L) = \Gamma\psi(L)S_d(f, \xi) \tag{B-14}$$

where

$$S_d(f, \xi) = \frac{S_a(f, \xi)}{(2\pi f)^2} \tag{B-15}$$

B.3 Computation of Properties of SDOF Oscillators

B.3.1 Introduction

The objective of the study described in this section was to represent the switch post of Figure B-1a by the SDOF oscillator of Figure B-1c using the mode shape (or shape function) of Figure B-1b. The displaced shape of Figure B-1b is consistent with the observations made in Chapter 4 regarding the deformed shape of switch poles, namely, that the double-channel beams and the attachment hardware at the base of the posts are the significant source of the flexibility in the posts, and that the insulators can be assumed to be rigid. The flexibility at the base of the posts and the large stiffness of the insulator are included in the model by assuming a rotational spring at the base of the SDOF oscillator and infinitely rigid insulators.

Each switch pole was modeled as two SDOF oscillators (P1 and P2). Figure B-2 shows a pole of a horizontal and vertical-break switch, and the SDOF oscillators used to model them. Each post of a horizontal-break pole was modeled as a SDOF oscillator (Figure B-2a). For the vertical-break pole of Figure B-2b, the post without the blade (post 1) was modeled as a SDOF oscillator (P1) and posts 2 and 3 were combined as the second oscillator (P2). Such an approach was considered reasonable because posts 2 and 3 were connected at the tops with a rigid blade counterweight, and it was assumed that the displacements were constrained to be equal.

The mode shapes of Figures 6-1 through 6-3 were used as the shape functions, $\psi(s)$, to compute the properties of the SDOF oscillators. The mode shape (shape function) of a typical post is shown in Figure B-3. The undeformed and deformed shapes are shown as dashed and solid lines, respectively. In this figure, the switch post consists of three components with distributed mass (component *1-2* or the lower insulator, component *2-3* or the upper insulator, and component *3-4* or the blade) and one component with concentrated mass (component *3* attached to the top insulator). In the figure, h is the elevation (z-ordinate) of a point above the base of the double-channel beams; l is the length of the blade; m is the mass per unit length, M is the concentrated mass at top of the upper insulator; and δ is the ordinate of the deformed shape (shape function). Subscripts 1 through 4 were used to designate the base, midheight, and top of the post, and tip of the blade respectively. For example, m_{23} is the mass per unit length of the upper insulator (component *2-3*), and δ_3 is the ordinate of the shape function at the top of upper insulator.

For the horizontal-break switch, there was no component with concentrated mass. Such components were present for the vertical-break switches (the counterweight at the top of posts 2 and 3 and the attachment at the top of posts 1). For switches SW1 and SW2, each post consisted of two porcelain insulators. The upper insulator was smaller than the lower insulator, but both were cylindrical and had uniform mass per unit length. Each post of switch SW3 had a single composite insulator in the shape of a truncated cone; this insulator was assumed to have a linear mass distribution over its length.

B.3.2 Property of switch posts

Prior to assembling the switch poles, the height and mass of each component was measured. Where possible, the measured values were compared with the specification data provided by the manufacturer. The measured and specified data were found to be in good agreement. The measured data of Table B-1 were used to compute the mass and height properties of the SDOF oscillators.

Table B-1 properties of switch posts

Switch	*Post*	*Bottom Insulator*		*Top insulator*		*Blade*		M^1 *(N)*	$h_1{}^2$ *(m)*
		Weight (N)	*Length (m)*	*Weight (N)*	*Length (m)*	*Weight (N)*	*Length (m)*		
SW1	1	700	1.0	560	1.0	190	1.3	-	0.53
	2	700	1.0	560	1.0	170	1.2	-	0.53
SW2	1	700	1.0	560	1.0	-	-	100	0.40
	2	700	1.0	560	1.0	120	2.9	300	0.40
	3	700	1.0	560	1.0				0.40
SW3	1	480	2.0	-	-	-	-	100	0.40
	2	480	2.0	-	-	120	2.9	300	0.40
	3	480	2.0	-	-				0.40

1. Denotes the mass of the blade counterweight at the top of posts for the vertical-break switches.
2. Denotes the combined height of the double-channel beams and other base hardware; see Figures B-3.

B.3.3 Computation of generalized mass and excitation

Equations B-4 and B-5 were used to compute the generalized mass and generalized excitation for the switch posts. For the switch posts, *r(s)* is equal to unity. The generalized mass and excitation of the post were computed by summing the contributions from the different components of the post. For example, the contributions of the top insulator (with a mass per unit length m_{23}) and the blade counterweight (with a concentrated mass M_3) to the generalized mass and excitation are:

$$M_{2-3} = \int_{h_2}^{h_3} m_{23}(s)\left(\delta_2 + \frac{\delta_3 - \delta_2}{h_3 - h_2}(s - h_2)\right)^2 ds \tag{B-16}$$

$$L_{2-3} = \int_{h_2}^{h_3} m_{23}(s)\left(\delta_2 + \frac{\delta_3 - \delta_2}{h_3 - h_2}(s - h_2)\right) ds \tag{B-17}$$

$$M_3 = M_3(\delta_3)^2 \tag{B-18}$$

$$L_3 = M_3\delta_3 \tag{B-19}$$

This procedure is demonstrated more completely by computing the generalized mass and generalized excitation for the SDOF oscillator of post P2 of switch SW1 in the *y*-direction with an open blade. The mode shape (shape function) for this post is shown in Figure 6-1d and is reproduced in Figure B-4. For this switch, the mass per unit length of each insulator and the blade is constant. As such Equations B-16 and B-17 can be simplified to:

$$M_{2-3} = \frac{m_{23}}{3}(h_3 - h_2)(\delta_3^2 + \delta_2^2 + \delta_2\delta_3) \tag{B-20}$$

$$L_{2-3} = \frac{m_{23}}{2}(\delta_3 + \delta_2)(h_3 - h_2) \tag{B-21}$$

The generalized mass and excitation for this post can be computed by summing the contribution of the various components. The calculations are tabulated in Table B-2

The generalized mass and excitation for the posts P1 and P2 of switches SW1, SW2, and SW3 were computed in a similar manner to that presented above for post P2 of switch SW1. The generalized mass and excitation for posts were normalized with respect to the mass of the posts to obtain dimensionless quantities. These normalized values are presented in Table B-3.

Table B-2 Generalized mass and excitation for post P2 of switch SW1, in y-direction, open blade

Component	m *(kg/m)*	$(h_j-h_i)^1$ *(m)*	$\delta_i^{\,1}$	$\delta_j^{\,1}$	M *(kg)*	L *(kg-m)*
Lower insulator	70.9	1.02	0.25	0.59	13.5	30.4
Upper insulator	57.1	1.02	0.59	1.00	37.4	46.3
Blade	13.4	1.22	1.00	1.27	20.9	17.8
Total	-	-	-	-	71.6	94.4

1. Note: h_i and h_j are the elevation above the base at the beginning and end of the component; δ_i and δ_j are the ordinates of the shape function measured at the beginning and end of the component .

Table B-3 Normalized generalized mass and excitation of switch posts[1]

Switch	*Blade*	*Post*	*x-direction*			*y-direction*		
			M	L	Γ	M	L	Γ
SW1	Closed	P1	0.46	0.60	1.29	0.44	0.61	1.37
		P2	0.47	0.62	1.32	0.42	0.59	1.39
	Open	P1	0.44	0.59	1.34	0.45	0.65	1.45
		P2	0.47	0.63	1.34	0.49	0.65	1.35
SW2	Closed	P1	0.36	0.51	1.44	0.37	0.52	1.42
		P2	0.41	0.64	1.57	0.35	0.51	1.45
	Open	P1	0.35	0.51	1.45	0.34	0.50	1.44
		P2	0.45	0.58	1.29	0.40	0.55	1.37
SW3	Closed	P1	0.33	0.46	1.41	0.41	0.2	1.25
		P2	0.38	0.49	1.32	0.42	0.53	1.26
	Open	P1	0.32	0.46	1.42	0.32	0.46	1.42
		P2	0.37	0.50	1.37	0.39	0.52	1.33

1. The generalized mass and excitation are normalized with respect to the post mass. The post mass is computed as sum of the component masses listed Table B-1.

B.3.4 Computation of effective mass and effective height

Equations B-12 and B-13 were used to compute the effective mass and effective height of the switch posts. The integrals in these equations were replaced by summing the contributions of various components. The effective mass and effective height for the entire post is calculated as :

$$\overline{m} = \sum \overline{m}_{ij} \tag{B-22}$$

and

$$\bar{h} = \frac{1}{\bar{m}}\sum \bar{m}_{ij}\bar{h}_{ij} \tag{B-23}$$

where, $\bar{m}_{ij}$ and $\bar{h}_{ij}$ are the effective mass and the height of the component *i-j* (see Section B.3.1 for definition of post components) of the post. For the components whose deformed shape was linear, the displaced shape was divided into two parts (one constant and one triangular) for the calculation.

The application of this procedure to the SDOF oscillator P2 of switch SW1 in the *y*-direction with an open blade is presented here and illustrated in Figure B-5. For example, the contribution from the triangular part of the displaced shape to the effective mass of the top insulator, $\bar{m}_{23_{tr}}$, is equal to:

$$\bar{m}_{23_{tr}} = \frac{1}{2}(\delta_3 - \delta_2)m_{23}(h_3 - h_2)\Gamma = \frac{1}{2}(1.0 - 0.59)(58)1.39 = 15.9 \tag{B-24}$$

where the ordinates of the shape function are obtained from Figure B-4, the mass and length of the insulator are taken from Table B-1, and Γ is listed in Table B-3. This portion of the effective mass acts 1.7 m above the base of bottom insulator, or 2.2 m above the base of the double-channel beams.

Table B-4 Effective mass and effective height for post P2, switch SW1, *y*-direction, open blade

Component	*Displaced shape*	$\bar{m}_i = \sum \bar{m}_{ij}$ *(kg)*	$\bar{h}_i$ *(m)*	$\bar{m}_i\ \bar{h}_i$ *(kg-m)*	$\bar{h} = \frac{1}{\bar{m}}\sum \bar{m}_{ij}\bar{h}_{ij}$ *(m)*
Bottom insulator *(1-2)*	constant	24.0	1.04	25.0	
	triangular	16.3	1.2	19.6	
Top insulator *(2-3)*	constant	45.8	2.05	93.9	
	triangular	15.9	2.22	35.3	
Blade *(3-4)*	linear	24.9	2.56	63.7	
Total	-	127.0	-	237.5	1.88

The effective mass and effective height of the posts P1 and P2 for switches SW1, SW2, and SW3 were computed in a similar manner to that described above and are presented in Table B-5. For the purpose of analysis, only a single value of effective height can be used in *x*- and *y*- directions for a given switch and a given blade position. For example, post P2 of switch SW1 with an open blade has to have identical effective heights in both *x*- and *y*- directions. Consequently, the effective heights listed in Table B-5 are the average of the computed values in *x*- and *y*- directions.

Table B-5 Properties of the equivalent SDOF oscillators

Switch	Post	*Closed Blade*				*Open Blade*			
		x- direction		*y- direction*		*x- direction*		*y- direction*	
		$\overline{m}$ (kg)	$\bar{h}$ (m)	$\overline{m}$ (kg)	$\bar{h}$ (m)	$\overline{m}$ (kg)	$\bar{h}$ (m)	$\overline{m}$ (kg)	$\bar{h}$ (m)
SW1	P1	112	2.0	133	2.0	112	1.9	133	1.9
	P2	133	2.0	122	2.0	122	1.9	133	1.9
SW2	P1	102	1.8	112	1.8	102	1.8	102	1.8
	P2	234	1.8	214	1.8	224	1.9	224	1.9
SW3	P1	41	2.0	51	2.0	41	1.8	41	1.8
	P2	92	2.1	92	2.1	92	2.1	92	2.1

For analysis of the switches mounted directly on a rigid frame, the effective heights of the posts P1 and P2 were taken as the values listed in Table B-5. The mathematical models of the frame described in Chapters 6 and 7 included the double-channel beams at the bases of the switch poles. As such, the effective heights of oscillators P1 and P2 were reduced by the depth of the beams (equal to 8 in. or 200 mm) for the analysis of P1 and P2 on the support frames. The reduction in the effective mass of oscillators P1 and P2 was neglected for such analysis.

For switch SW1, SDOF isolators P1 and P2 have similar effective weights and heights because the posts 1 and 2 of the switch use similar insulators and blades. For this switch, the blade opens in the horizontal plane and as such, the effective height of the SDOF isolator is not sensitive to blade position. For the vertical-break switches SW2 and SW3, the effective mass of SDOF oscillator P2 is larger than that of P1 because two switch posts (posts 2 and 3) are included in P2 (see Figure B-2). For these switches, the blade opens in the vertical plane and is hinged at the base so that only bending moment about the x-axis is transferred to the insulator (see Figure 2-13). Accordingly, when the blade is open, the effective height of post P2 is unchanged in the y-direction but increases in the x-direction. The normalized effective mass (with respect to the post mass) and normalized effective height (with respect to the post height) are presented in Table B-6. For all the posts, the effective mass and height of the SDOF isolators are between 70 and 90 percent of the mass of the post and between 70 and 80 percent of the height of the post, respectively.

Table B-6 Normalized properties of the equivalent SDOF oscillators

Switch	*Blade*	*Post*	*Normalized effective mass*		*Normalized effective height*
			x- direction	*y-direction*	*x- or y- direction*
SW1	Closed	P1	0.8	0.9	0.8
		P2	0.9	0.9	0.8
	Open	P1	0.8	0.9	0.8
		P2	0.9	0.9	0.8
SW2	Closed	P1	0.7	0.8	0.7
		P2	0.8	0.8	0.7
	Open	P1	0.7	0.7	0.7
		P2	0.8	0.8	0.8
SW3	Closed	P1	0.7	0.8	0.8
		P2	0.7	0.7	0.8
	Open	P1	0.7	0.7	0.7
		P2	0.7	0.7	0.8

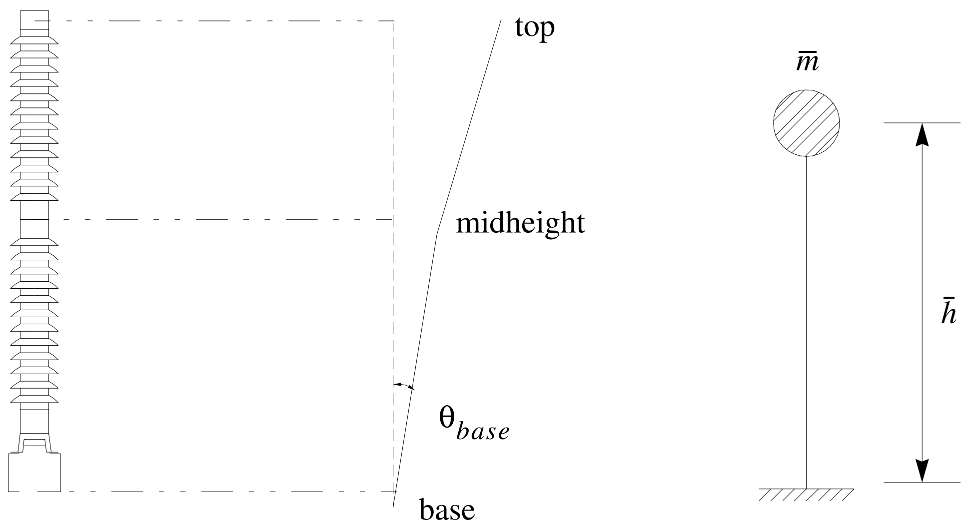

(a) switch post (b) assumed mode shape (c) SDOF oscillator

Figure B-1 Single-degree-of-freedom model of a switch post

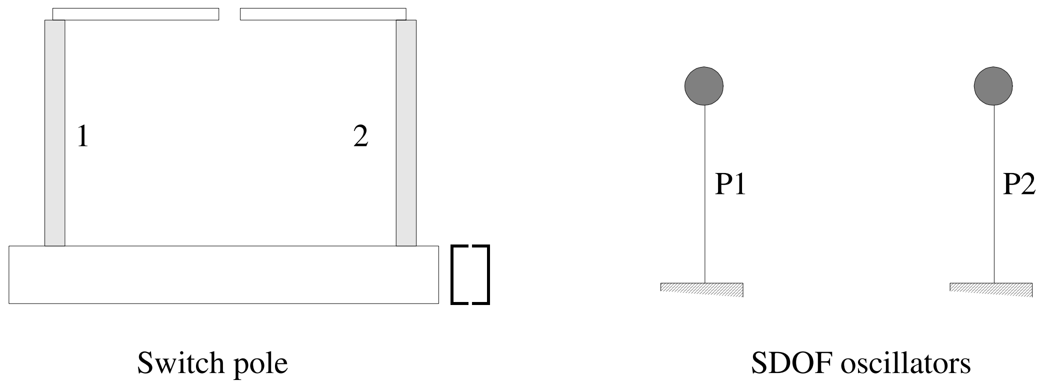

(a) Horizontal-break switch pole

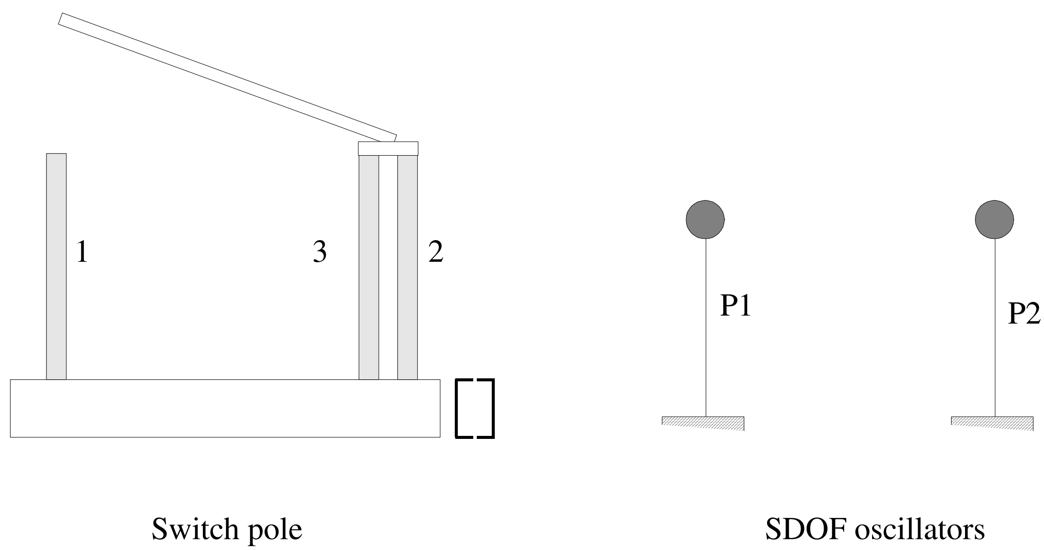

(b) vertical-break switch pole

Figure B-2 Representation of switch poles as SDOF oscillators

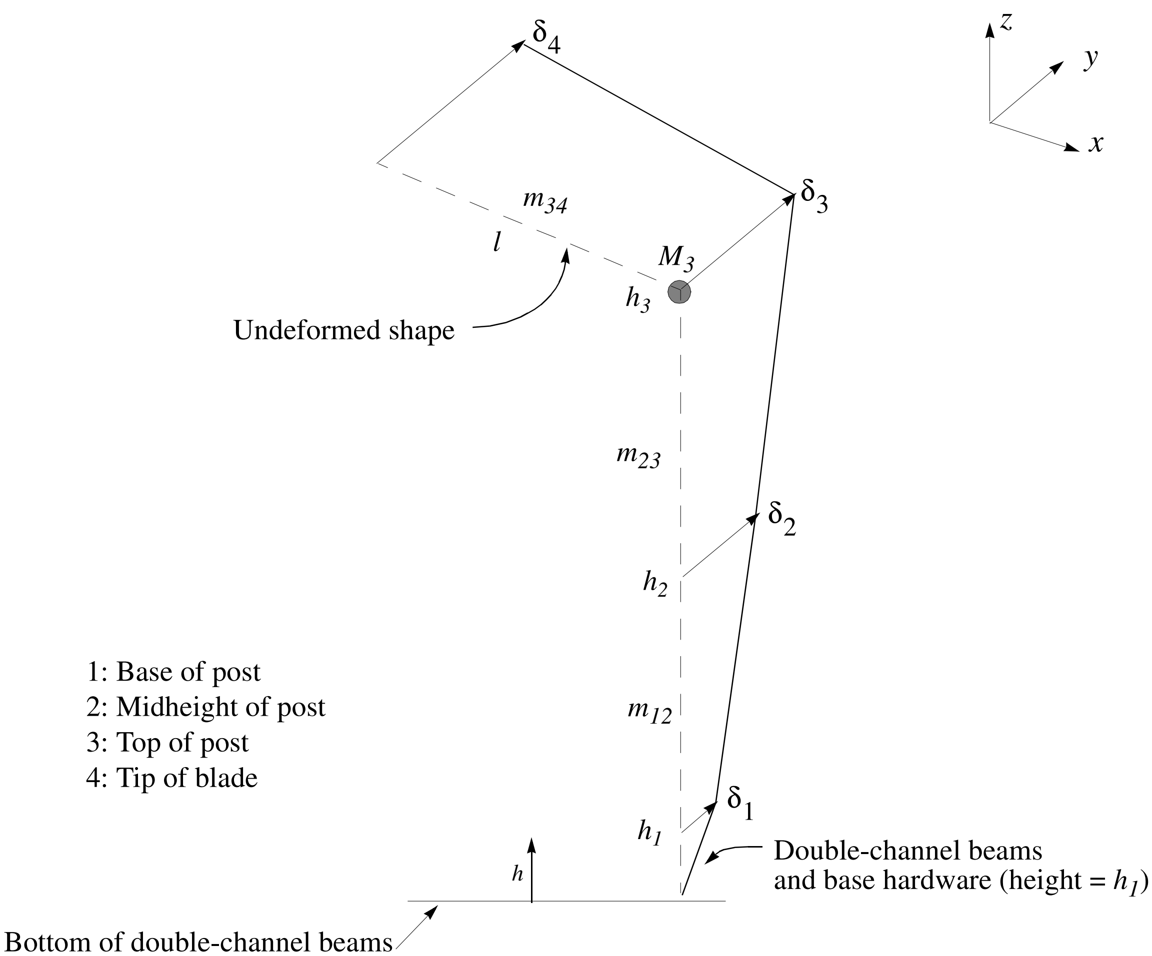

Figure B-3 Deformed shape for a switch post

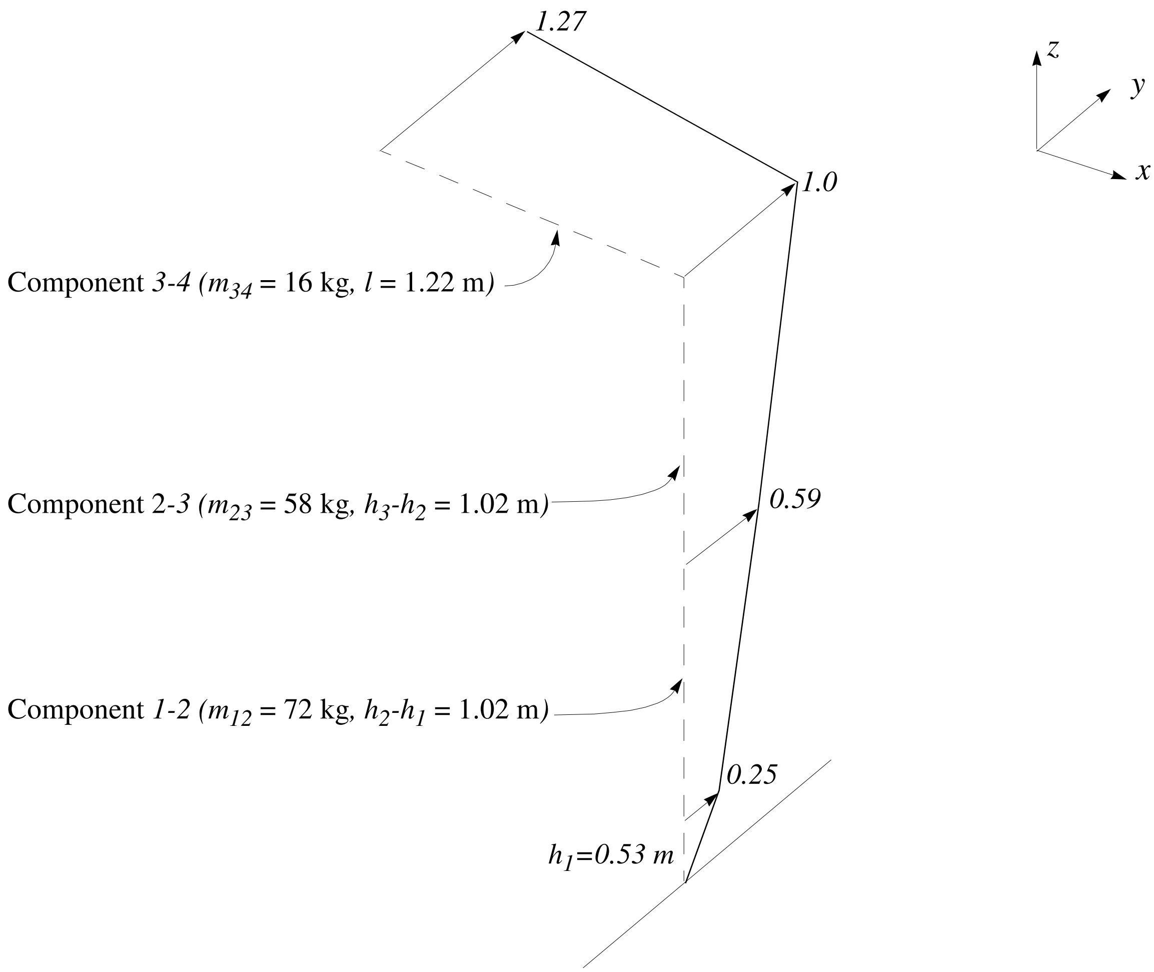

Figure B-4 Shape function and components of post P2 of switch SW1, y-direction, open blade

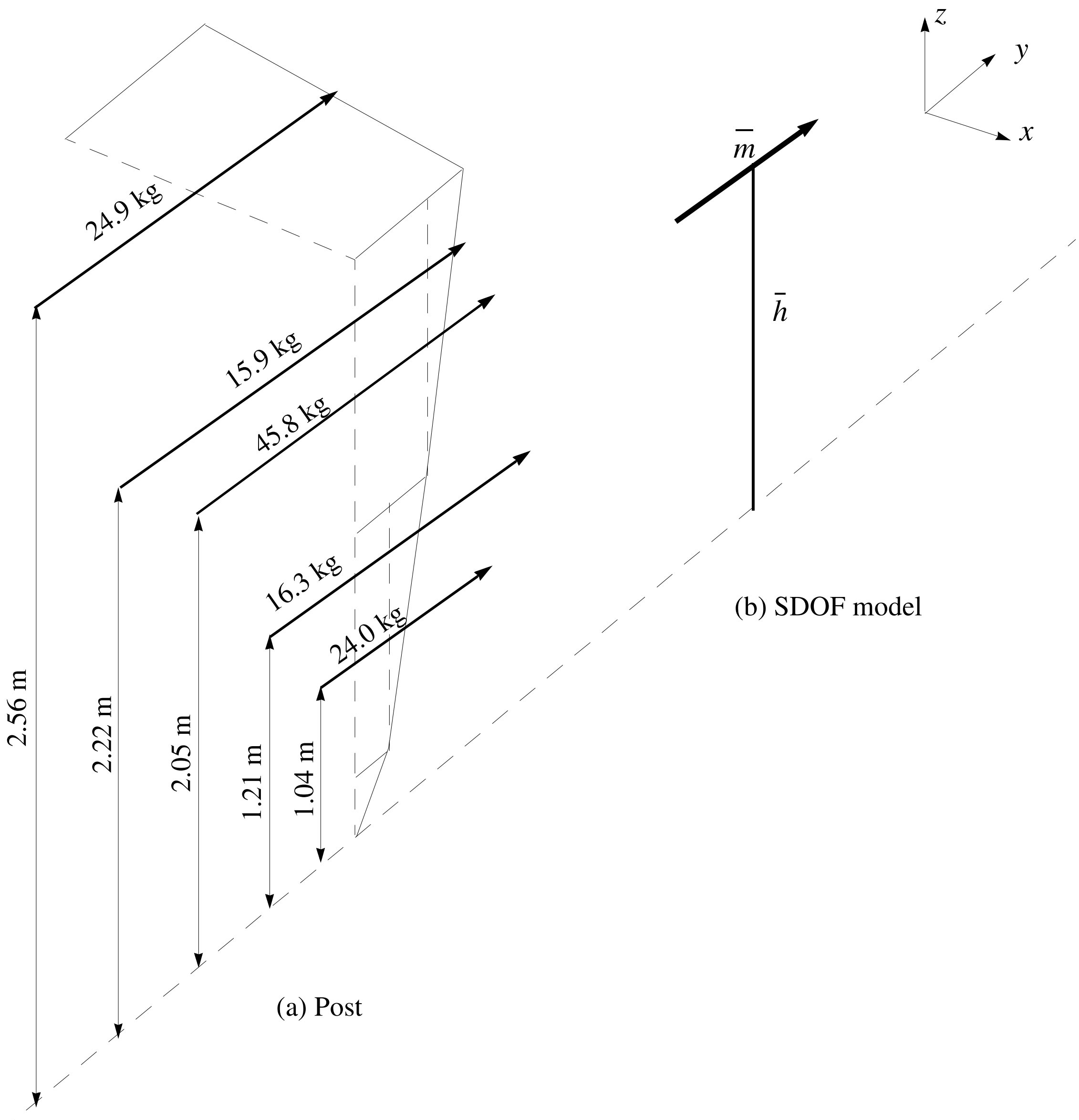

Figure B-5 Computation of effective mass and height for post P2 of switch SW1, *y*-direction, open blade